IRD 64-36

Research programme on magnetoplasmadynamic power generation. Technical summary report 1 December 1962 to 31 March 1964

Part 3: Theoretical

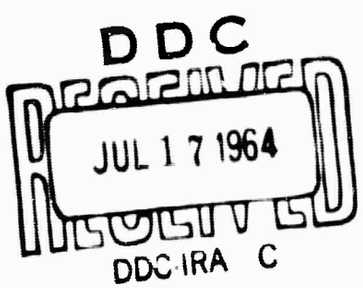

INTERNATIONAL RESEARCH & DEVELOPMENT CO LTD

Fossway, Newcastle upon Tyne 6, England

DISCLAIMER NOTICE

THIS DOCUMENT IS THE BEST QUALITY AVAILABLE.

COPY FURNISHED CONTAINED A SIGNIFICANT NUMBER OF PAGES WHICH DO NOT REPRODUCE LEGIBLY.

RESEARCH PROGRAMME ON

MAGNETOPLASMADYNAMIC POWER GENERATION

Contract N62558-3127

TECHNICAL SUMMARY REPORT

1 December 1962 to 31 March 1964

PART 3 . THEORETICAL

Advanced Research Projects Agency
Order No. 209-62, Amendment No. 2
Contract period : 1 December 1961 to 31 July 1964
Contract amount : £382,500
Contractor : International Research & Development Co Ltd
Principal Investigator : Dr. B.C. Lindley

International Research & Development Co Ltd
Newcastle upon Tyne 6
England

RESEARCH PROGRAMME ON MAGNETOPLASMADYNAMIC POWER GENERATION

TECHNICAL SUMMARY REPORT

1 December 1962 to 31 March 1964

SUMMARY

CONTENTS TO PART 3

AUTHORS' NOTE

The investigations reported in Chapters 21 to 30 (excluding Chapter 26) have been carried out at different times during the contract period. The most recent calculations incorporate the most recent data and more refined techniques based on the earlier work; consequently in certain cases apparent contradictions may exist where two different techniques or numerical values have been used for essentially the same calculation.

The valuable contributions made by Miss N.A. Cooper*, Mr. C.A. Robinson†, Mr. W. Simpson‡, Mr. R. Sheehan‡ and Mr. R. Tunnicliffe** in the investigations reported here is gratefully acknowledged.

* Present address Mathematics Department, Birmingham University

† Present address Sidney Sussex College, Cambridge University

‡ Computing section, IRD

** Theoretical section, IRD.

BLANK PAGE

CHAPTER 21

VISCOSITY OF MPD WORKING FLUIDS

by

I.R. McNab

21.1 GENERAL INTRODUCTION

Considerable and increasing use of alkali metals is currently being made in devices concerned with the generation of electrical power by unconventional means (thermionic diodes[1] and magnetoplasmadynamic generators (MPD)[2,3]) and electrostatic propulsion[4]. The attractiveness of the alkali metals follows from their low ionization potentials and the consequent ease with which they may be ionized. Few attempts have been made to calculate or measure their thermodynamic and transport properties (other than electrical conductivity) and the effect of ionization on such properties[5].

The element cesium is of particular interest in closed cycle MPD electrical power generation since, although it has a high capital cost, it has the lowest ionization potential of the group. Base-load MPD-steam stations envisage the use of a small atomic percentage of alkali metal in an inert gas, such as helium or argon, since it is with seeding fractions of about one atomic percent that the maximum electrical conductivity is obtained. For space power generation, radiator size and weight considerations may necessitate the use of a Rankine cycle with a pure alkali metal.

In the present calculations, the viscosity of pure cesium has been evaluated theoretically and the part played by ionization assessed. (Under given temperature and pressure conditions ionization effects are most noticeable in cesium because of the low ionization potential) The viscosity is of particular interest at the present time since consideration of 'second order' effects in MPD generators includes a study of the boundary layers in such generators. Recent studies[6-8] indicate that the power loss arising from reverse currents in the boundary layers may reduce the power output of an MPD generator by a factor of four.

Following this calculation, which is appropriate to a Rankine cycle MPD generator using pure cesium as the working fluid, the viscosity of cesium-helium

mixtures has been investigated, the effects of seeding fraction being of particular interest in this case which applies to terrestrial base-load power generation.

The general behaviour of the viscosity of binary mixtures is then examined, special regard being paid to the occurrence of maxima in the viscosity and their dependence on temperature for a large number of gases.

21.2* VISCOSITY OF PARTIALLY-IONIZED GASEOUS CESIUM

21.2.1 INTRODUCTION

To calculate the viscosity of a gas, it is necessary to determine the velocity distribution function $f(\underline{r}, \underline{v}, t)$ for each species of particle present. This function is defined such that

$$f_j(\underline{r}, \underline{v}, t)\, dx\, dy\, dz\, dv_x\, dv_y\, dv_z\, dt \qquad \ldots\ldots (21.1)$$

is the number of particles of species j which have position co-ordinates between x and $x + dx$, y and $y + dy$, z and $z + dz$, and which have components of velocity between v_x and $v_x + dv_x$, v_y and $v_y + dv_y$, v_z and $v_z + dv_z$. If the dependence of f upon the variation of flow velocity with position in the gas is known, the viscosity can be calculated. Unfortunately, the Boltzmann - Fokker - Planck equation, which according to the statistical mechanics of ionized gases gives f to a good approximation for charged particles[9,10], is mathematically intractable. Data concerning the velocity distribution function can be obtained from the simpler Boltzmann equation, although the use of this equation involves the assumption that the time during which two particles are in contact (this is, a collision) is infinitesimal compared with the time between collisions; this assumption is doubtful when charged particles are present[9,11]. The use of an approximate solution of the Boltzmann equation developed by Chapman[12] and Enskog[13] is discussed in section 21.2.4.

The only other feasible approach seems to be that of elementary kinetic theory, in which viscosity is treated as a 'free path phenomenon'. The coefficient of viscosity can be calculated very roughly by assuming a simple form for the velocity distribution function, and evaluating the momentum transported across unit area in the gas by the thermal motions of the particles. This method is developed in section 21.2.3 to determine the nature of the effect of ionization on viscosity; it is too approximate to yield a great deal of useful information.

---

* Based on IRD 63-10 'The viscosity of gaseous cesium at temperatures up to 3000°K' C.A. Robinson and I.R. McNab, and, 'Viscosity of partially ionized gaseous cesium' C.A. Robinson and I.R. McNab. J.App.Phys. June 1964.

21.2.2 The viscosity of an ionized gas

Viscosity, the development of shear stresses in a moving fluid, is due to the transport of momentum from point to point by the random thermal motions of the molecules. In simple kinetic theory, viscosity is known as a 'free path phenomenon', since the free path is the distance a particle travels between collisions which change its momentum. In more rigorous theory the connection with the free path becomes more obscure.

A monatomic gas in which a small percentage of the atoms are thermally ionized will contain not only charged particles and neutral atoms in the ground state, but also a considerable number of excited particles, with the result that inelastic and superelastic collisions will occasionally take place. The effect of these excited particles is very complicated to analyse and has been neglected in this treatment. It also appears from considerations of elementary kinetic theory that the momentum transported by electrons in a 1 per cent ionized gas will be at most 10^{-3} of that carried by neutrals, owing to the small mass and large charge/mass ratio of the electron. Accordingly, the momentum transport due to electrons has been neglected, as has the small effect of collisions with electrons on the motions of the heavy particles. The plasma is thus reduced, as far as viscosity phenomena are concerned, to a binary mixture of positive ions and neutral atoms, with electrons present only to restore the macroscopic charge neutrality. The resultant simplification of the theory is considerable.

21.2.3 Approximate calculation of viscosity from elementary kinetic theory

An expression for the viscosity of a slightly ionized gas will be obtained from 'free path' considerations. Collisions between atoms and atoms, and between atoms and ions will be assumed to behave as encounters between rigid elastic spheres in which the distances of closest approach of the centres are respectively ρ and ρ'. The mean free path of an atom is therefore

$$\lambda_a = \frac{1}{\sqrt{2}\,\pi\,(n_a\rho^2 + n_i\rho'^2)} \qquad \ldots\ldots (21.2)$$

The force between two ions will be assumed to be that of Coulomb repulsion only, since it is unlikely that two ions in a plasma at the temperatures under consideration (1000° to 2500°K) will have sufficient kinetic energy to approach closely enough for the short-range quantum mechanical forces to be important. The evaluation of the mean free path of an ion is complicated by the fact that any one ion may at any instant be close enough to each of several others to interact with them, since the mean distance between ions may be considerably less than the Debye shielding distance:

$$h = \left(\frac{kT}{4\pi n_e e^2} \right)^{1/2} \qquad \ldots\ldots (21.3)$$

The mean distance an ion travels before its velocity is deflected through approximately 45^0 may be evaluated. This will be used as the mean free path of an ion among ions. The mean square change per second in the velocity of an ion in a direction perpendicular to its initial velocity is denoted by $\langle (\Delta v_\perp)^2 \rangle$. The time after which an ion has been deflected appreciably from its original direction by other ions, called by Spitzer[14] the deflection time, is

$$t_D = \frac{v^2}{\langle (\Delta v_\perp)^2 \rangle} \qquad \ldots\ldots (21.4)$$

During this time the ion will have travelled a distance which will be used as the mean free path of an ion among ions:

$$\frac{v^3}{\langle (\Delta v_\perp)^2 \rangle} \qquad \ldots\ldots (21.5)$$

Employing methods similar to those used by Rosenbluth et al[15]

$$\langle (\Delta v_\perp)^2 \rangle = \frac{8\pi n_i e^4 \ln \Lambda}{m_i^2 \sqrt{(v^2 + \overline{v^2})}} \qquad \ldots\ldots (21.6)$$

where $\Lambda = \dfrac{m_i \overline{v^2} h}{e^2}$

$$= \frac{3}{2e^3} \left(\frac{k^3 T^3}{\pi n_e} \right)^{1/2} \qquad \ldots\ldots (21.7)$$

The expression (21.5) now becomes

$$\frac{m_i^2 v^3 \sqrt{(v^2 + \overline{v^2})}}{8\pi n_i e^4 \ln \Lambda} \qquad \ldots\ldots (21.8)$$

which on substituting root mean square values becomes approximately

$$\frac{9\sqrt{2}\, k^2 T^2}{8\pi n_i e^4 \ln \Lambda} \qquad \ldots\ldots (21.9)$$

When the effect of collisions with atoms is taken into consideration, the mean free path of an ion in the plasma,

$$\lambda_i = \left[\sqrt{2}\, \pi \left(n_a \rho'^2 + \frac{4 n_i e^4 \ln \Lambda}{9 k^2 T^2} \right) \right]^{-1} , \qquad \ldots\ldots (21.10)$$

is obtained.

The coefficient of viscosity due to each species of particle is the momentum

transported by particles of that species in unit time across unit area in the gas per unit velocity gradient perpendicular to that area. If the velocity distribution is assumed everywhere locally Maxwellian, the approximate expression for the coefficient of viscosity is

$$\eta = \frac{2}{3} n\lambda \sqrt{\frac{2m\ kT}{\pi}} \quad . \qquad \ldots\ldots (21.11)$$

Summing over the two types of particle

$$\eta = \frac{2}{3}\sqrt{\frac{2kT}{\pi}}\left(n_a\lambda_a \sqrt{m_a} + n_i\lambda_i \sqrt{m_i} \right). \qquad \ldots\ldots (21.12)$$

Values for the mean free paths may now be substituted. Assuming $m_a = m_i$

$$\eta = \frac{2}{3}\sqrt{\frac{mkT}{\pi^3}}\left(\frac{1-\alpha}{\rho^2(1-\alpha) + \alpha\rho'^2} + \frac{\alpha}{(1-\alpha)\rho'^2 + \frac{4\alpha e^4 \ln\Lambda}{9k^2T^2}} \right) \ldots\ldots (21.13)$$

When the fractional ionization α is small, by far the greater part of the viscosity is due to the first term in the bracket. The Coulomb interactions enter the expression only through the term in $\ln\Lambda$, and their only effect is to reduce further the already small second term in the bracket. It may be inferred that the viscosity of a slightly ionized gas is almost entirely due to momentum transported by neutral atoms, and that the effect of ionization is slightly to reduce the viscosity, through the effects of Coulomb repulsion. The physical interpretation is that the long-range Coulomb forces reduce the momentum transported by ions by shortening the mean free path of the ions.

21.2.4 Theory based upon the Boltzmann equation

21.2.4.1 General theory

As stated in section 21.2.2, elementary kinetic theory calculations show that virtually all the viscosity of a slightly ionized monatomic gas will be due to momentum transport by atoms and ions; this results in considerable simplification of the calculation.

To compute the viscosity of a gas it is necessary to obtain information about the velocity distribution function of each species of particle present. This is usually done by solving the Boltzmann equation by the approximate method due to Chapman[12] and Enskog[13], which has been highly developed by Chapman and Cowling[11]. The distribution function is expanded as a series and a set of integral equations derived for coefficients describing the first order perturbation from the known equilibrium solution. These equations are solved by an expansion in orthogonal polynomials. Expressions are obtained for the transport coefficients, including viscosity of a pure gas or gas mixture, in

terms of the collision integrals, which depend on the interparticle forces through the angle of deflection χ produced when two particles collide with relative velocity g and impact parameter b. The results are expressed most conveniently in terms of the 'reduced' dimensionless variables:

impact parameter	$b^* = b/\sigma$
relative velocity	$g^* = (\mu g^2/2\epsilon)^{\frac{1}{2}}$
particle separation	$r^* = r/\sigma$
interparticle potential energy	$\phi^* = \phi/\epsilon$
temperature	$T^* = kT/\epsilon$
Debye length	$h^* = h/\sigma_i$

where σ is the critical separation and ϵ the critical energy of interaction of the colliding particles, and the Debye length is the characteristic Coulomb interaction distance, given by equation (21.3).

The collision integrals have been normalized in several ways, the notation followed here being that of Hirschfelder, Curtiss and Bird[16], thus:

$$\Omega^{(p,s)*}(T^*) = \frac{4}{\left\{1 - \frac{1}{2}\left[\frac{1+(-1)^p}{1+p}\right]\right\}(s+1)!\,T^{*s+2}} \times \int_0^\infty\int_0^\infty \exp\left(-\frac{g^{*2}}{T^*}\right) g^{*2s+3}\,(1-\cos^p\chi)\,b^*\,db^*\,dg^* \quad \ldots.(21.14)$$

where the deflection angle χ in a centre-of-mass frame of reference is given by classical mechanics:

$$\chi = \pi - 2b^*g^* \int_0^{(r^*_{min})^{-1}} (g^{*2} - b^{*2}u^{*2}g^{*2} - \phi^*)^{-1/2}\,du^* \quad \ldots\ldots\ (21.15)$$

in which $u = 1/r$.

The expression for the first approximation to the viscosity of a gas mixture involves only $\Omega^{(1,1)*}$ and $\Omega^{(2,2)*}$, higher approximations require evaluation of $\Omega^{(p,s)*}$ for larger p and s. The viscosity of a pure gas (to the first approximation) is[16]

$$\eta = 266.93\ 10^{-7}\,(MT)^{\frac{1}{2}}/\sigma^2\Omega^{(2,2)*}(T^*) \quad \ldots\ldots\ (21.16)$$

where η is in poise, σ in Å and T in °K. The viscosity of a binary mixture of components of the same molecular weight M (such as the mixture of atoms and ions here) is given in terms of the viscosities η_1 and η_2 of the separate components and a third quantity, η_{12}, expressing the atom-ion contribution:

$$\eta_{12} = 266.93\ 10^{-7}\,(MT)^{\frac{1}{2}}/\sigma_{12}^2\Omega_2^{(2,2)*}(T_{12}^*) \quad \ldots\ldots\ (21.17)$$

in which $\sigma_{12} = (\sigma_1+\sigma_2)/2$. The viscosity of a binary mixture of atoms and ions with fractional ionization α then becomes

$$\eta_{mix} = \frac{1 + Z}{X + Y} \qquad \ldots\ldots (21.18)$$

where

$$\left.\begin{aligned} X &= \frac{(1-\alpha)^2}{\eta_a} + \frac{2\alpha(1-\alpha)}{\eta_{ai}} + \frac{\alpha^2}{\eta_i} \\ Y &= \frac{3}{5} A^*_{ai}\left[\frac{(1-\alpha)^2}{\eta_a} + \frac{2\alpha(1-\alpha)\eta_{ai}}{\eta_a\eta_i} + \frac{\alpha^2}{\eta_i}\right] \\ Z &= \frac{3}{5} A^*_{ai}\left[(1-\alpha)^2 + 2\alpha(1-\alpha)\left(\frac{\eta_{ai}}{\eta_a} + \frac{\eta_{ai}}{\eta_i} - 1\right) + \alpha^2\right] \end{aligned}\right\} \qquad \ldots\ldots (21.19)$$

$$A^*_{ai} = \frac{\Omega_{ai}^{(2,2)*}}{\Omega_{ai}^{(1,1)*}} \qquad \ldots\ldots (21.20)$$

These formulae may be used to evaluate the viscosity when the appropriate collision integrals have been calculated from the interparticle potential functions.

21.2.4.2 Interparticle potential functions and collision integrals

In the absence of experimental data for the interaction potentials in cesium the following potential functions have been assumed.

Atom-atom

The Lennard-Jones (6-12) potential[17]

$$\phi_a(r) = 4\epsilon_a\left[\left(\frac{\sigma_a}{r}\right)^{12} - \left(\frac{\sigma_a}{r}\right)^{6}\right], \qquad \ldots\ldots (21.21)$$

which takes into account the inverse seventh power attractive (van der Waal's) forces and short range repulsive forces, has been used with considerable success in the past (see, for example, Ref. 16) and will be assumed here. The variation of $\phi_a(r)$ with r is shown in Fig. 21.1; the colision integral $\Omega^{(2,2)*}$ for this potential is tabulated in Ref. 16 and shown in Fig. 21.4.

Atom-ion

For this case the potential requires an inverse fourth power attractive component to account for the attraction between the ionic charge and the induced dipole moment in the atom, while the short range repulsive forces, which vary rapidly with distance, may conveniently be represented by an impenetrable core. The potential takes the form

$$\left.\begin{aligned} &\phi_{ai}(r) = \infty \text{ for } (r < \sigma_{ai}) \\ \text{and } &\phi_{ai}(r) = -\epsilon_{ai}\left(\frac{\sigma_{ai}}{r}\right)^4 \text{ for } (r > \sigma_{ai}) \ . \end{aligned}\right\} \qquad \ldots\ldots (21.22)$$

A graph of $\phi_{ai}(r)$ against r is shown in Fig. 21.2.

Writing equation (21.15) in the form

$$\chi = \pi - 2\theta \qquad \ldots\ldots (21.23)$$

and substituting the above potential, yields an elliptic integral of the first kind for θ. This can be reduced to standard form as shown in Appendix 21.A, and evaluated by references to tables or numerical integration. While no definite information is available for cesium, experimental polarizabilities for other monatomic gas molecules suggest that the interaction potential ϵ_{ai}/k will be of the order of 500°K. Since the range of gas temperature under consideration is 1000° to 3500°K all cases of practical interest here will be covered by a range of values of T^*_{ai} from 1 to 20. The required integrals $\Omega_{ai}^{(1,1)^*}$ and $\Omega_{ai}^{(2,2)^*}$ (Eq. 21.14) have been evaluated by mechanical quadrature on a Pegasus digital computer for several values in this range, and are shown in Table 21.1 and Fig. 21.5. This method of evaluation appears superior in this case to the approximate method suggested by Chapman and Cowling (see Ref. 11) which is mainly useful for potential functions of this form when the attractive component is very weak.

Ion-ion

The most precise form of potential to represent the ionic repulsion is the shielded Coulomb potential predicted by the Debye-Hückel theory:

$$\phi_i \propto r^{-1} e^{-r/h} .$$

However it has been shown by Liboff[18] that, even in the case of a highly ionized gas, only a very small error in viscosity computations is incurred by using an ordinary Coulomb potential with a cutoff at the Debye length instead. The use of this modification greatly simplifies calculation. The short range forces may again be represented by an impenetrable core, although it is very unlikely that, at the temperatures under consideration, the colliding pair of ions will have sufficient kinetic energy for this to be brought into action. The potential function then assumes the form (shown in Fig. 21.3):

$$\phi_i(r) = \infty \text{ for } (r < \sigma_i),$$

$$\phi_i(r) = \frac{e^2}{\sigma_i}\left(\frac{\sigma_i}{r}\right) \text{ for } (\sigma_i < r < h),$$

$$\text{and } \phi_i(r) = 0 \text{ for } (r > h).$$

Neglecting the few pairs of ions which approach as closely as the impenetrable core, the deflection angle becomes that given by classical mechanics for a Coulomb potential:

$$\chi = 2 \arcsin\left(4 g^{*4} b^{*2} + 1\right)^{-\frac{1}{2}}$$

This will be used for all ion-ion encounters in which the impact parameter is less than the Debye length; when the impact parameter is greater than h the deflection is zero. Using this value of χ in equation (21.14) and replacing the upper limit of integration over b* of ∞ by h* yields

$$\Omega_{ii}^{(2,2)*} = \frac{1}{4T_i^{*2}} \int_0^\infty \exp\left(-\frac{g^{*2}}{T_i^*}\right)\left(\frac{g^{*2}}{T_i^*}\right) \int_0^{h^{*2}} \left[\frac{4g^{*4}}{4g^{*4}b^{*2}+1} - \frac{4g^{*4}}{(4g^{*4}b^{*2}+1)^2}\right] \omega b^{*2} d\left(\frac{g^{*2}}{T_i^*}\right)$$

$$= \frac{1}{4T_i^{*2}} \int_0^\infty \exp\left(-\frac{g^{*2}}{T_i^*}\right)\left(\frac{g^{*2}}{T_i^*}\right) \left[\ln(1+4g^{*4}h^{*2}) - \frac{4g^{*4}h^{*2}}{1+4g^{*4}h^{*2}}\right] d\left(\frac{g^{*2}}{T_i^*}\right)$$

Hirschfelder, Curtiss and Bird[16] recommend that, since the term in square brackets varies comparatively slowly with g* it may be taken outside the integral sign, g^{*2} being replaced everywhere by mean value over all collisions, $2T_i^*$. If this be done the expression integrates immediately to give

$$\Omega_{ii}^{(2,2)*} = \frac{1}{4T_i^{*2}} \left[\ln(1 + 16T_i^{*2}h^{*2}) - \frac{16T_i^{*2}h^{*2}}{1+16T_i^{*2}h^{*2}}\right] \qquad \ldots\ldots (21.24)$$

The slight inaccuracy introduced through the last approximation is not important. An accurate evaluation of $\Omega_{ii}^{(2,2)*}$ should consider the variation of h* with temperature and ion density, approximate values of h* of practical interest here being in the range $10^2 \leq h^* \leq 10^4$. However, owing to the form of equations (21.18), (21.19) and (21.20), η_{mix} does not depend critically on the value of Ω_{ii}, provided this is large and the fractional ionization is ≤ 0.1, and thus h* may be assumed constant without appreciable loss of accuracy; this has been confirmed by numerical calculations. Fig. 21.6 shows the variation of $\Omega_{ii}^{(2,2)*}$ with T_i^* as given by equation (21.24) for $h^* = 10^2$, 10^3 and 10^4.

21.2.4.3 Results and discussion

From the values of $\Omega_{aa}^{(2,2)*}$ given in Ref. 16, of $\Omega_{ai}^{(1,1)*}$ and $\Omega_{ai}^{(2,2)*}$ computed by numerical integration and shown in Table 21.1, and $\Omega_{ii}^{(2,2)*}$ calculated from equation (21.24), the viscosity coefficient η_{mix} of the slightly ionized cesium may be calculated for any set of values of the force constants, fractional ionization, Debye length and temperature.

The values which have been used here are

$\sigma_a = \sigma_{ai} = \sigma_i = 3.5$Å, $\epsilon_a/k = 100^\circ$K, $\epsilon_{ai}/k = 500^\circ$K and $\epsilon_i/k = e^2/k\sigma_i = 4.77.10^4$ $^\circ$K

The fractional ionization (α), which depends on temperature and pressure, is obtained from Saha's equation[19]:

$$\log_{10}\left(\frac{\alpha^2}{1-\alpha^2}P\right) = -\frac{5041\ I}{T} + \frac{5}{2}\log_{10} T - 6.483, \qquad \ldots\ldots (21.25)$$

using the ionization potential of 3.893 V for cesium. A constant reduced Debye length (h^*) of 10^3 has been used.

Fig. 21.7 shows the resulting viscosity of ionized cesium (η_{mix}) for pressures of 10^{-2}, 10^{-3}, 10^{-4} and 10^{-5} atm and temperature in the range 1000° to 3500°K as found from equations (21.18) (21.19) (21.20), and the viscosity of un-ionized cesium (η_a) over the same temperature range, from equation (21.16). It is clear that, over the greater part of the temperature range, the viscosity increases with temperature; the viscosity of un-ionized cesium may be expressed as

$$\eta_a = 9.5\ 10^{-6}\ T^{2/3}\ g/cm\ sec$$

It is also clear that the effects of ionization are small until the fractional ionization is greater than 1%; at fractional ionizations of about 10% the reduction in viscosity due to ionization is over 20%. This drop in viscosity with increasing ionization may be explained by saying that the ions have, owing to their mutual Coulomb interactions, a much shorter mean free path than neutral atoms, and hence contribute little to the momentum transport process. It is doubtful whether the Enskog-Chapman solution of the Boltzmann equation can be used to evaluate transport coefficients for ionized gas having a fractional ionization greater than about 10%: solution of the Boltzmann-Fokker-Planch equation becomes the appropriate procedure[10].

The neglect of electrons, diatomic cesium and excited atomic states in the partially ionized gas introduces negligible error in the computed viscosity, as do the approximations made in deriving the ion-ion collision integral (equation 21.24) and the assumption of constant h^* in the numerical evaluation. The most likely sources of error are the critical interaction energies (ϵ), effective atomic diameters (σ) and the exact form of the interparticle potential functions (ϕ). It is clear that more accurate calculations of the viscosity of ionized cesium require experimental data on ϵ, σ and ϕ which is at present lacking.

In principle the above treatment may be applied to any partially ionized monatomic gas provided few excited and molecular particles are present and the appropriate potential functions and numerical quantities are employed.

21.3 THE VISCOSITY OF HELIUM-CESIUM MIXTURES

Detailed evaluation of the performance of an MPD generator using helium-cesium mixture as the working fluid requires, amongst other factors, basic physical data relating to the gas mixture. Few experimental results are available for such

mixtures, or even for the pure gases, over the temperature range required (about 1000° to 3000°K); thus theoretical estimates must be obtained. In this section the helium-cesium viscosity is evaluated as a function of temperature and cesium concentration. The viscosity is important for determining the flow parameters in an MPD generator and thus, for example, the power losses sustained through reverse currents in the boundary layers.

21.3.1 Evaluation of viscosity

The previous section has considered the effects of ionization on the viscosity of pure cesium and shown that, provided the fractional ionization is less than 1%, the presence of ions and electrons does not significantly alter the viscosity. Since the fractional ionization of a helium-cesium mixture in thermal equilibrium at the temperatures and pressures of most MPD generators is less than 1%, the effects of ionization will be neglected in the present evaluation of viscosity. (Note that the neglect of ionization may not be valid if non-thermal ionization occurs in the gas mixture; in this case the method of treating the problem will depend on the ionization level.) Thus the problem is reduced to evaluating the viscosity of a binary mixture of helium and cesium. The first approximation to the viscosity is then given by equation 21.18, where

$$X = \frac{(1-x_2)^2}{\eta_1} + \frac{2(1-x_2)x_2}{\eta_{12}} + \frac{x_2^2}{\eta_2} \qquad \ldots\ldots (21.26)$$

$$Y = \frac{3}{5} A_{12}^* \left\{ \frac{(1-x_2)^2}{\eta_1} \frac{M_1}{M_2} + (1-x_2)x_2 \left[\frac{(M_1+M_2)^2}{2M_1M_2} \right] \frac{\eta_{12}}{\eta_1\eta_2} + \frac{x_2^2}{\eta_2} \frac{M_2}{M_1} \right\} \qquad (21.27)$$

$$Z = \frac{3}{5} A_{12}^* \left\{ (1-x_2)^2 \frac{M_1}{M_2} + 2(1-x_2)x_2 \left[\left(\frac{(M_1+M_2)^2}{4M_1M_2} \right) \left(\frac{\eta_{12}}{\eta_1} + \frac{\eta_{12}}{\eta_2} \right) - 1 \right] + x_2^2 \frac{M_2}{M_1} \right\} \qquad \ldots\ldots (21.28)$$

$$\eta_1 = \frac{266.93 \times 10^{-7} (M_1 T)^{\frac{1}{2}}}{\sigma_1^2 \Omega_{11}^{(2,2)^*}(T_1^*)} \quad \text{gm/cm sec} \qquad \ldots\ldots (21.29)$$

$$\eta_2 = \frac{266.93 \times 10^{-7} (M_2 T)^{\frac{1}{2}}}{\sigma_2^2 \Omega_{22}^{(2,2)^*}(T_2^*)} \quad \text{gm/cm. sec} \qquad \ldots\ldots (21.30)$$

$$\eta_{12} = \frac{266.93 \times 10^{-7}}{\sigma_{12}^2 \Omega_{12}^{(2,2)^*}(T_{12})^*} \left[\frac{2M_1M_2T}{M_1+M_2} \right]^{\frac{1}{2}} \quad \text{gm/cm. sec} \qquad \ldots\ldots (21.31)$$

and $$A_{12}^* = \frac{\Omega_{12}^{(2,2)*}(T_{12}^*)}{\Omega_{12}^{(1,1)*}(T_{12}^*)} \quad \ldots\ldots (21.32)$$

In the above expressions, the subscripts 1 and 2 refer to helium and cesium respectively, and x_2 is the mole fraction of cesium, defined by

$$x_2 = \frac{n_2}{n_1+n_2} \quad \ldots\ldots (21.33)$$

Evaluation of η_{mix} requires values of the collision integrals $\Omega_{11}^{(2,2)*}$, $\Omega_{22}^{(2,2)*}$, $\Omega_{12}^{(1,1)*}$ and $\Omega_{12}^{(2,2)*}$ which are obtained from equations (21.14) and (21.15). Information on helium-helium interactions shows that the Lennard-Jones 6-12 potential reproduces experimental results very accurately for the present data above 10°C,[16] (p560); this potential has the form given in equation 21.21. No experimental data are available for the interaction potential for cesium-cesium encounters, while for cesium-helium collisions the interaction potential has the asymptotic form[21] of the van der Walls force:

$$\phi(r) \alpha -\frac{C}{r^6} \quad \ldots\ldots (21.34)$$

In this evaluation the Lennard-Jones 6-12 potential has been assumed for these interactions also. The collision integrals for this potential have been evaluated and are given in Hirschfelder et al[16] (Table 1M) as functions of the reduced temperature $T^* = kT/\epsilon$. Thus evaluation of T_1^*, T_{12}^* and T_2^* from the critical interaction energies ϵ_1, ϵ_{12} and ϵ_2 enables the collision integrals to be determined and, knowing the atomic diameters and masses, the viscosity of the binary mixture may then be obtained.

Information on ϵ_1 and σ_1 for helium-helium interactions is rather varied at present. According to Chapman and Cowling[11] (p.395):

$\epsilon_1/k = 6.03°$ $\sigma_1 = 2.70$ Å from viscosity measurements

and $\epsilon_1/k = 6.03°K$, $\sigma_1 = 2.63$ Å from virial coefficient measurements

while from Hirschfelder et al[16] (p.1110):

$\epsilon_1/k = 10.22°K$, $\sigma_1 = 2.576$Å from viscosity measurements

and $\epsilon_1/k = 10.22°K$, $\sigma_1 = 2.556$ Å (quantum calculation)
$\epsilon_1/k = 6.03°K$, $\sigma_1 = 2.63$ Å (classical calculation)
} from virial coefficient measurements

Initial calculations carried out here with $\epsilon_1/k = 10°K$ and $\sigma_1 = 2.6$Å gave theoretical values of η consistently less than those observed experimentally. A better fit with experimental values is obtained using $\epsilon_1/k = 10°K$ and σ=2.5 Å.

Although no information is available for cesium, examination of data for other monatomic elements shows that $\epsilon_2/k = 200^\circ K$ and $\sigma_2 = 4\text{Å}$ will not be unreasonable values. (The value of σ_2 used here will be more accurate than the 3.5Å used previously[22]. The conclusions reached by Robinson and McNab[22], namely that the effects of ionization are small, are not affected by this change.) Following the usual procedure of defining the interaction energy and effective diameter for helium-cesium encounters by geometric and arithmetic means of the values for the pure gases, that is

$$\epsilon_{12} = (\epsilon_1 \epsilon_2)^{\frac{1}{2}} \qquad \ldots\ldots (21.35)$$

$$\sigma_{12} = (\sigma_1 + \sigma_2)/2 \qquad \ldots\ldots (21.36)$$

yields $\epsilon_{12}/k = 45^\circ K$ and $\sigma_{12} = 3.25$ Å

For this interaction it is possible to determine the van der Waals constant C in equation (21.35) using the above values of ϵ_{12} and σ_{12}; thus from equation (21.21) and (21.35)

$$C_{12} = 4\epsilon_{12}\sigma_{12}^6 = 29.2 \times 10^{-60} \text{ cm}^6.$$

This value of C may be compared with those found experimentally. Rosin and Rabi and Estermann, Foner and Stern[21] using molecular techniques found $C_{12} = 29.4$ and 370×10^{-60} cm^6 respectively, while from measurements of the polarizabilities of alkali metals by Scheffers and Stark[21], and polarizabilities of rare gas atoms obtained from refractivity measurements a value of 44 is obtained. Thus the value of C_{12} used here is in excellent agreement with Rosin and Rabi's results and in fair agreement with polarizability measurements but is very different from the value obtained by Estermann et al.[21] Further measurements on this interaction are required to clarify the situation.

For the present calculation the values of ϵ_{12} and σ_{12} which gives $C_{12} = 29.2 \times 10^{-60}$ cm^6 have been used, together with the values of ϵ_1, ϵ_2, σ_1 and σ_2 previously quoted. With these values and equations (21.18) (21.26-33) the viscosity of the mixture has been obtained as a function of temperature and mole fraction of cesium x_2.

21.3.2 Results and discussion

The results of the calculations are presented graphically in Fig. 21.6, 7 and 8. Fig. 21.8 illustrates the variation of viscosity with temperature for pure helium ($x_2 = 0$), pure cesium ($x_2 = 1.0$) and binary mixtures with mole fractions of cesium (x_2) of 0.01, 0.1 and 0.5. The viscosity of pure cesium may be expressed as

$$\eta_2 = 6.8 \times 10^{-6} T^{0.66} \text{ gm/cm sec}$$

$$\eta_1 = 5.1 \times 10^{-6}\ T^{0.65}\ \text{gm/cm sec}$$

over the range 200° to 3000°K, T being in °K. A comparison between experimental results[11,23] and the present theoretical values (Fig. 21.9), shows that the agreement for helium is within about 6% over the range of measured values. Better choice of the form of the interparticle potential function may remove this discrepancy.

From Fig. 21.8 the addition of cesium to $x_2 = 0.01$ increases the viscosity by about 6% while for $x_2 = 0.10$ the viscosity is about 40% greater than that of pure helium above 2000°K. As the mole fraction of cesium is increased still further the viscosity of the mixture becomes greater than that of pure cesium, as exemplified by the curve $x_2 = 0.5$ of Fig. 21. According to Chapman and Cowling[11] (p.231) the explanation of this effect is as follows. The addition of a quantity of a heavy gas to itself causes two opposing effects (on the viscosity) - a reduction in the mean free path and an increase in the number of carriers of momentum - which just balance. If, however, a lighter gas is added to the heavy gas, the small additional transport of momentum by the lighter particles more than outweighs the decrease in the mean free path of the heavy particles caused by the addition. (The alteration in mean free path of the heavy particles by much lighter particles is very small.) Thus the viscosity of the mixture may be higher than that of either of the pure gases. This effect may be seen more clearly in Fig. 21.10. According to Chapman and Cowling[11] (p.233) the maximum in the binary viscosity should become less pronounced as the temperature increases, the viscosity of a hydrogen-hydrochloric acid mixture being given as an example. However, this does not occur for a cesium-helium mixture (Fig. 21.10); the maximum in fact becomes more pronounced.

21.4 VISCOSITY MAXIMA IN BINARY GAS MIXTURES

21.4.1 Introduction

The calculations reported in section 21.3, using the first approximation to the viscosity of a gas mixture, showed that for helium-cesium mixtures the viscosity of the mixture was higher than either of the individual components; that is, the addition of a light gas to a heavy gas increased the viscosity of the latter (in general, but not always, the viscosity of a heavy gas is greater than that of a light gas). The explanation of this effect, put forward by Chapman and Cowling[11], was outlined in section 21.3.2.

According to Chapman and Cowling[11] the maximum in the binary viscosity should become less pronounced as temperature increases, the viscosity of a hydrogen-hydrochloric acid mixture being given as an example. However the calculations reported in 21.3 showed that this was not true for helium-cesium mixtures - the maximum becomes more pronounced as temperature increases. In view of the doubt associated with the data used for cesium in these calculations, further work has been carried out on this effect for other gases for which more reliable data is available.

21.4.2 Theory

The effect of the introduction of a light gas into a heavy gas is most conveniently examined by the use of the 'impurity' approximation for the viscosity of a binary mixture given in Ref. 11. This expression is derived for the condition that only a small amount of impurity gas (the light gas in this case) is added to the main gas.

Writing Chapman and Cowling's impurity approximation in the nomenclature employed by Hirschfelder, Curtiss and Bird[16]:

$$\eta_{MIX} = \eta_2 + \frac{1-x_2}{x_2} \frac{\left\{ \frac{3}{5} A_{12}^* \frac{(M_1+M_2)^2}{2M_1M_2} \eta_{12} + 2\left(1-\frac{3}{5}A_{12}^*\right)\eta_2 - \frac{2\eta_2^2}{\eta_{12}} \right\}}{1 + \frac{3}{5} A_{12}^* \frac{M_1}{M_2}} \qquad (21.37)$$

The lighter gas is species 1, the heavier gas species 2.

It is apparent that the viscosity of gas 2 will be increased by the addition of the lighter gas only if

$$\Delta > 0 \qquad .....(21.38)$$

where

$$\Delta = \frac{3}{5} A_{12}^* \frac{(M_1+M_2)^2}{2M_1M_2} \eta_{12} + 2\left(1-\frac{3}{5} A_{12}^*\right)\eta_2 - \frac{2\eta_2^2}{\eta_{12}} \qquad .....(21.39)$$

21.4.3 Calculations and results

A Pegasus autocode computer programme has been used to investigate equations (21.38) and (21.39) for increasing temperatures for various gas mixtures. The viscosities η_2 and η_{12} have been evaluated assuming that the Lennard-Jones (6-12) potential is operative, thus an unequal interval interpolation routine, together with the data of Table 21.2 here and Table 1M of Ref. 16, was used to evaluate the appropriate collision integrals. (The data for the Lennard-Jones force constants in Table 21.2 is, with the exception of cesium, taken from Ref. 24).

The results (values of Δ at different temperatures) fall into three main

ategories:

mixtures which show no viscosity maximum;

mixtures which have a viscosity maximum at low temperatures which disappears as the temperature increases;

nd a third group of mixtures, unpredicted in Ref. 11, having a viscosity maximum hich, in general, becomes more pronounced as the temperature increases. These ixtures are shown in Table 21.3. In all these cases the first component is the ighter gas (species 1) and $\eta_2/\eta_1 > 1$. The mixtures in the first column are uoted in Ref. 24 as having no maximum and those in the other two columns, with he exception of A-Cs and He-Cs as having a maximum.

The quantity Δ has been evaluated over a wide range of temperature (200° to 000°K) and typical results for several gas mixtures in each group are shown in ig. 21.11. No account has been taken of dissociation, ionization, vibrational r rotational energy modes or chemical interactions in these calculations although hese effects will undoubtedly become important at high temperatures for some of ne gases. It is probable from this point of view that the results for the inert as mixtures will be the most reliable.

21.4.4 Discussion and conclusions

It has been found that for a number of binary gas mixtures the viscosity ows a maximum which becomes more pronounced as temperature increases. This is ontrary to the example quoted by Chapman and Cowling[11] (H_2-HCl). The criterion iven in equation (21.38) and (21.39) for a viscosity maximum is written by apman and Cowling in a rather different form:

$$\frac{E}{2\eta_2} + 2\left(\frac{2}{3} - A\right) > \frac{4A\,\eta_2}{3EM_1M_2} \qquad \ldots\ldots (21.40)$$

ere

$$E = \frac{2}{3} nm_o (D_{12})_1 \quad \text{and} \quad A = \frac{2}{5} A_{12}^* \qquad \ldots\ldots (21.41)$$

nce A is almost temperature independant the dominant temperature dependant term E/η_2.

r constant pressures:

$$E = \frac{2}{3} \frac{pm_o}{kT} (D_{12})_1$$

d, for hard sphere collisions, $(D_{12})_1 \propto T^{3/2}$, thus $E \propto T^{1/2}$. Typically riations of η_2 with temperature are approximately as $T^{0.65}$, thus $E/\eta_2 \propto 1/T^{0.15}$. rce if the inequality of equation (21.40) is true at a given temperature, as the mperature increases it will eventually cease to be true, that is, the viscosity ximum will vanish, as stated in Ref. 11.

However, the diffusion coefficient varies as $T^{3/2}$ only for hard sphere collisions. For unlike molecules repelling each other with a force varying inversely as the ν_{12}^{th} power of the distance, then for constant pressure

$$D_{12} \propto T^{1+S}$$

where

$$S = \frac{1}{2} + \frac{2}{\nu_{12}-1}$$

For hard spheres, $\nu_{12} = \infty$, $S = {}^{1}/_{2}$ and $D_{12} \propto T^{3/2}$, as given above. However ν_{12} is usually in the range 5 to 11 (Ref 11, p 249, 257). For $\nu_{12} = 9$, $S = 0.75$ and $D_{12} \propto T^{1.75}$ thus for $\eta_2 \propto T^{0.65}$ $E/\eta_2 \propto T^{0.1}$. Thus is the reverse case of that quoted above since, as the temperature increases the viscosity maximum becomes more pronounced.

A physical explanation has recently been put forward by Cowling[25]. To take further the comments in ref. 11 (p 269), there is a maximum in the viscosity only if the lighter gas has a smaller equivalent molecular radius than the heavier ($\sigma_1 < \sigma_2$); and the maximum disappears with increasing temperature only if the difference between the two molecular radii becomes smaller as the temperature increases. For gases with no maximum σ_1/σ_2 at 0°C (N.B. These σ are not those of Table 21.2) is greater than about ${}^{2}/3$, for gases with a maximum always σ_1/σ_2 is less than about 0.6; for gases with σ_1/σ_2 between these values the maximum may disappear with increasing temperature. It has therefore been shown that some gases exhibit a viscosity maximum which becomes more pronounced as temperature increases, contrary to the more usual cases where the maximum disappears. At the present time no experimental data is known which supports this conclusion.

REFERENCES

1 KAYE, J. and WELSH, J.A. (Eds) 'Direct conversion of heat to electricity' (J. Wiley and Son, Inc, New York and London, 1960) Part B

2 See for example 'Magnetoplasmadynamic Electrical Power Generation' (IEE Conference Report Series, No. 4, 1963)

3 MANNEL, C and MATHER, N.W. (Eds) 'Engineering Aspects of magnetohydrodynamics' (Columbia University Press, New York and London, 1962), Part 2.

4 LANGMUIR, D.B. STUHLINGER, E. and SELLEN, J.M. (Eds) 'Electrostatic propulsion' (Academic Press, New York and London, 1961)

5 An exception is the work of D.B. Clifton on the enthalpy and specific heat of cesium (Loss Alamos Scientific Laboratory Report LA 2419, August 1960)

6 BLACKMAN, V.H. JONES, M.S., and DEMETRIADES, A. Ref 3, p 180

7 WU, J.C. Ref 2, p 156

8 YEH, H. and SUTTON, G.W. Ref 2, p 159

9 COHEN, R.S., SPITZER, L. and McROUTLY, P. Phys. Rev. Vol.80, p 230, 1950

10 GASIONOWICZ, S., NEUMANN, M., and RIDDELL, R.J. Phys. Rev. Vol.101, p 922, 1956

11 CHAPMAN, S. and COWLING, T.G. 'The mathematical theory of non-uniform gases' 2nd Edition, Cambridge University Press, 1952

12 CHAPMAN, S. Phil. Trans. Roy. Soc. Vol.A216, p 279, 1916, Vol.A217, p 115, 1917

13 ENSKOG, D. 'The kinetic theory of phenomena in fairly rare gases'. Dissertation, Upsala, 1917

14 SPITZER, L. Jr. 'Physics of fully ionized gases' Interscience publishers. New York, 1956

15 ROSENBLUTH, M.N., McDONALD, W.M., and JUDD, D.L. Phys. Rev. Vol.107, p 1, 1957

16 HIRSCHFELDER, J.O. CURTISS, C.F. and BIRD, R.B. 'Molecular theory of gases and liquids' John Wiley and Sons, inc. New York 1954

17 LENNARD-JONES, J.E. Proc. Roy. Soc. (London) Vol.A106, p 441, 1924

18 LIBOFF, R.L. Phys. Fluids, Vol.2, p 40, 1959

19 SAHA, M.N. and SAHA, H.K. 'A treatise on Modern physics' (The Indian Press Ltd., Allahabad and Calcutta, 1934).

20 THOMSON, J.J. Phil Mag. Vol.47, p 342, 1924

21 MASSEY, H.S.W. and BURHOP, E.H.S. 'Electronic and ionic impact phenomena' Clarendon Press, Oxford, 1956 p 396

22 ROBINSON, C.A. and McNAB, I.R. 'The viscosity of gaseous cesium at temperatures up to 3000°K'. IRD Report 63-10, February 1963

23 KEYES, F.G. 'The heat conductivity, viscosity, specific heat and Prandtl numbers for thirteen gases' Technical report No. 37. Massachusetts Institute of Technology April 1952.

24 HIRSCHFELDER, J.C., TAYLOR, M.H., KIHARA, T and RUTHERFORD, R. 'Viscosity of two-component gaseous mixtures' Physics of Fluids, Vol.4, p 663, 1961

25 COWLING, T.G. Private communication (8.4.64)

APPENDIX 21-A

CALCULATION OF DEFLECTION ANGLE FOR ATOM-ION COLLISION

When the form of the potential ϕ_{ai} is substituted from (21.22), equations (21.15) and (21.23) give

$$\theta = b^* g^* \int_0^{(r_{min}^*)^{-1}} \frac{du^*}{(g^{*2} - b^{*2} g^{*2} u^{*2} + u^{*4})^{1/2}} \qquad \ldots\ldots (21.A.1)$$

If the force law were that of a simple attraction with no impenetrable core, the reduced distance of closest approach of the centres would be the reciprocal of the smallest root u_0^* of the equation

$$g^{*2} - b^{*2} g^{*2} u^{*2} + u^{*4} = 0 \qquad \ldots\ldots (21.A.2)$$

which has real roots if and only if $b^{*2} \geq \frac{2}{g^*}$. When the roots are real, the reduced distance of closest approach will be u_0^{*-1} or 1, whichever is greater, since under no circumstances can the pair approach more closely than σ_{ai}. Three cases in all may be distinguished:

(1) if $b^{*2} > 1 + \frac{1}{g^{*2}}$, equation (21.A.2) has real roots and $u_0^{*-1} > 1$. Thus $r_{min}^* = u_0^{*-1}$.

(2) if $\frac{2}{g^*} < b^{*2} < 1 + \frac{1}{g^{*2}}$, equation (21.A.2) has real roots and $u_0^{*-1} < 1$: therefore $r_{min}^* = 1$.

(3) if $b^{*2} < \frac{2}{g^*}$, equation (21.A.2) has no real roots, so $r_{min}^* = 1$.

In cases (1) and (2) the integral may be simplified by the substitution $u^* = u_0^* \sin\phi$ employed by Thomson[20]. In case (1) the result is

$$\theta = b^* u^* \int_0^{\pi/2} \frac{d\phi}{(1 - \frac{u_0^{*4}}{g^{*2}} \sin^2\phi)^{1/2}} \qquad \ldots\ldots (21.A.3)$$

while case (2) yields

$$\theta = b^* u_0^* \int_0^{\beta} \frac{d\phi}{(1 - \frac{u_0^{*4}}{g^{*2}} \sin^2\phi)^{1/2}} \qquad \ldots\ldots (21.A.4)$$

where $\beta = \text{arc sin}\,(u_0^{*-1})$. $\qquad \ldots\ldots (21.A.5)$

In case (3) the integral is reduced to standard form by the substitution

$$\tan^2\frac{\phi}{2} = \frac{u^{*2}}{g^*}$$

which gives $\theta = \frac{1}{2} b^* \sqrt{g^*} \int_0^{\gamma} \frac{d\psi}{\left(1 - \frac{2+b^{*2}g^*}{4} \sin^2 \psi\right)^{1/2}}$ ..... (21.A.6)

where $\gamma = 2 \arctan \left(\frac{1}{\sqrt{g^*}}\right)$ ..... (21.A.7)

Thus in all cases θ, and hence χ (eqn. (21.15)) can be expressed in terms of an elliptic integral of the first kind. Equations (21.A.3), (21.A.4) and (21.A.6) were used to obtain values of χ from which the collision integrals $\Omega_{ai}^{(1,1)^*}$ and $\Omega_{ai}^{(2,2)^*}$ given by equation (21.14) could be evaluated by Gaussian quadrature.

TABLE 21.1

COMPUTED COLLISION INTEGRALS ($\Omega_{ai}^{(1,1)*}$ AND $\Omega_{ai}^{(2,2)*}$)

FOR ATOM-ION INTERACTION

T_{ai}^*	$\Omega_{ai}^{(1,1)*}$	$\Omega_{ai}^{(2,2)*}$
1	1.230	1.230
3	1.080	1.065
5	1.055	1.038
10	1.036	1.019
15	1.030	1.012
20	1.027	1.009

TABLE 21.2

DATA USED IN VISCOSITY CALCULATIONS

GAS	ϵ/k^*	σ^{**}	M
H_2	36.7	2.958	2.016
He	6.03	2.63	4.004
CH_4	137	3.882	16.047
NH_3	320	2.60	17.036
Ne	33.74	2.756	20.177
CO	88.0	3.706	28.019
N_2	79.8	3.749	28.022
C_2H_4	205	4.232	28.063
C_2H_6	230	4.418	30.080
O_2	88.0	3.541	32.008
HCl	360	3.305	36.480
A	124	3.418	39.960
CO_2	213	3.897	44.024
C_3H_8	254	5.061	44.111
SO_2	252	4.290	64.671
Kr	166.67	3.682	83.830
Xe	225.3	4.070	131.341
Cs	250	4.1	132.95 +

* Units of ^{o}K

** Units of Angstroms

\+ Estimated.

TABLE 21.3

RESULTS

No. maximum	Maximum which disappears	Maximum always
CH_4-CO_2	H_2-HCl	H_2-C_2H_4
C_2H_4-A	H_2-CH_4	H_2-C_2H_6
C_2H_4-O_2	H_2-NH_3	H_2-SO_2
CO-O_2	H_2-CO_2	H_2-C_3H_8
N_2-O_2	H_2-Xe	He-A
H_2-O_2	A -Cs	He-Kr
H_2-Ne		He-Xe
		He-Cs

FIG. 1 LENNARD – JONES POTENTIAL

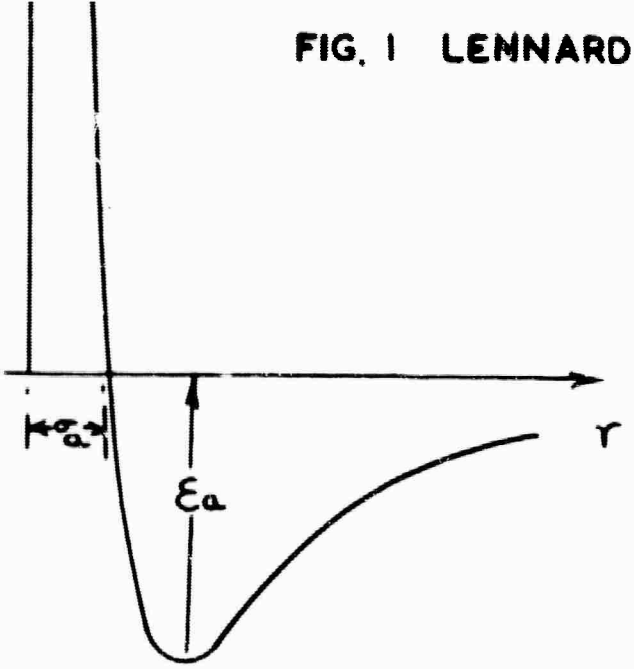

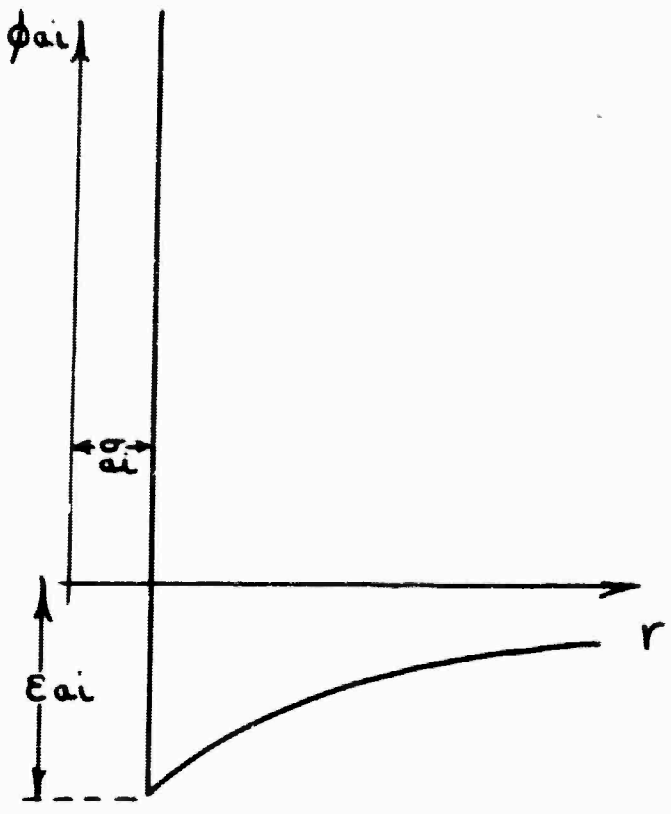

FIG.2 POTENTIAL FOR ATOM–ION INTERACTION

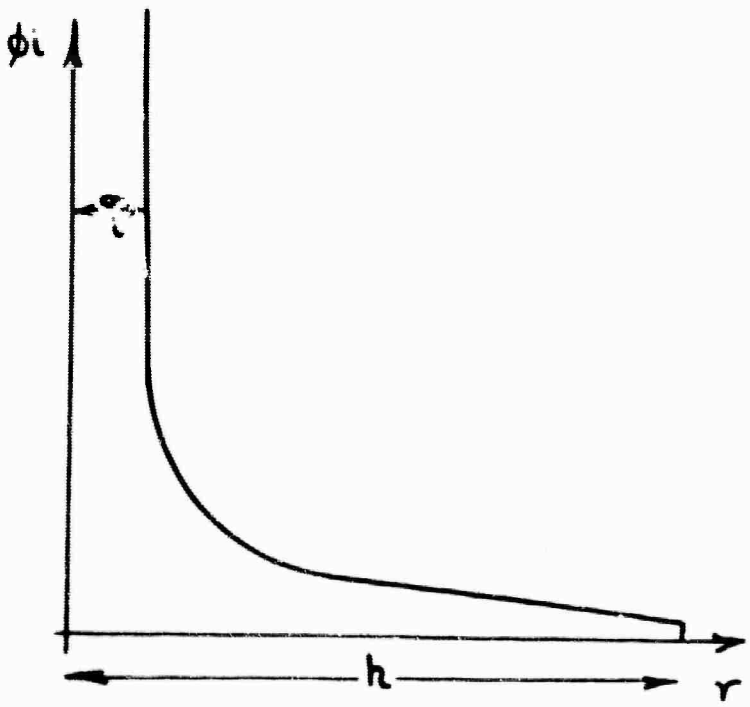

FIG. 3 POTENTIAL FOR ION–ION INTERACTION.

FIG 21·1,2 &3

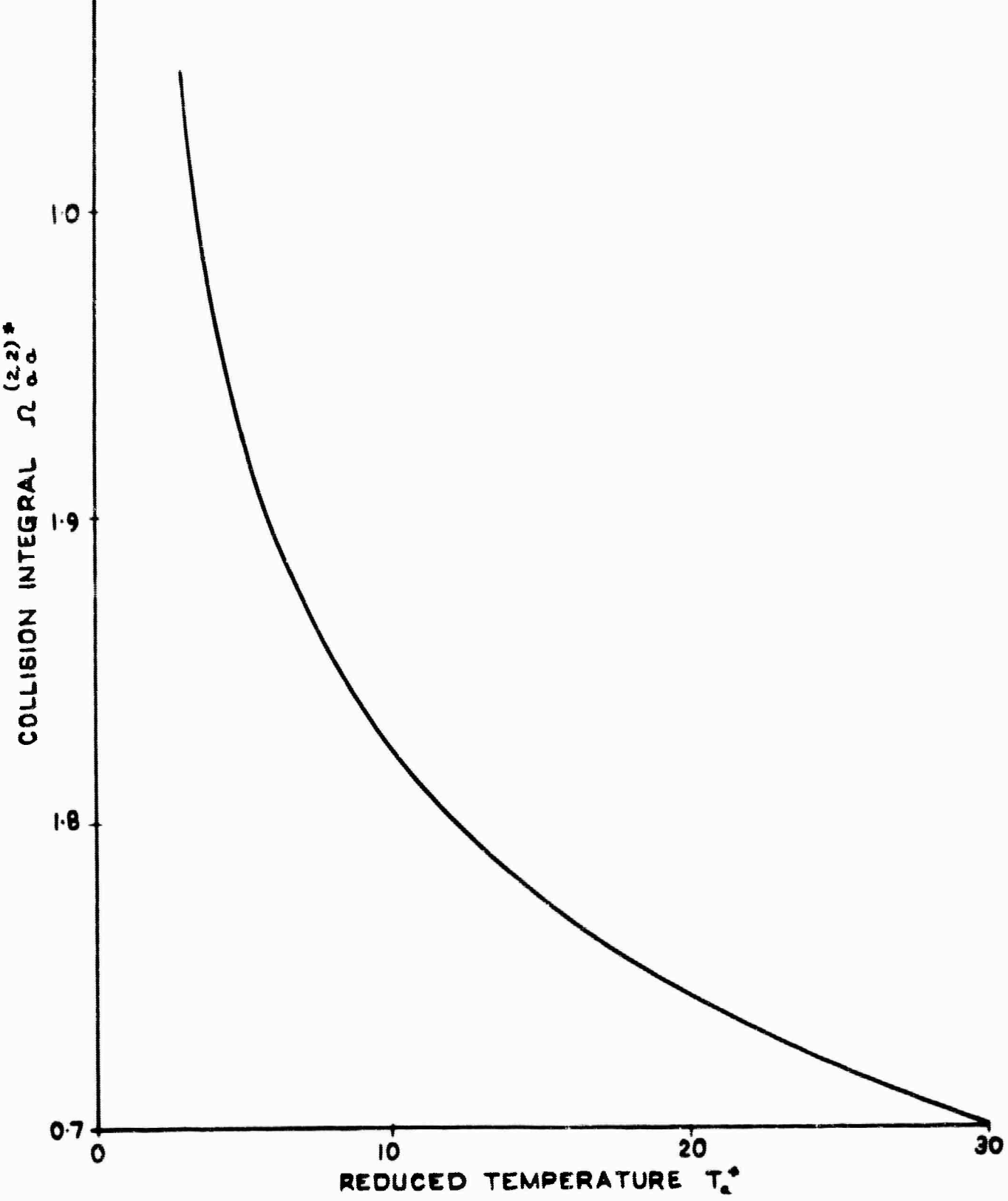

COLLISION INTEGRAL $\Omega_{a a}^{(2,2)*}$ AS A FUNCTION OF REDUCED TEMPERATURE T_a^* FOR LENNARD-JONES POTENTIAL

FIG 21·4

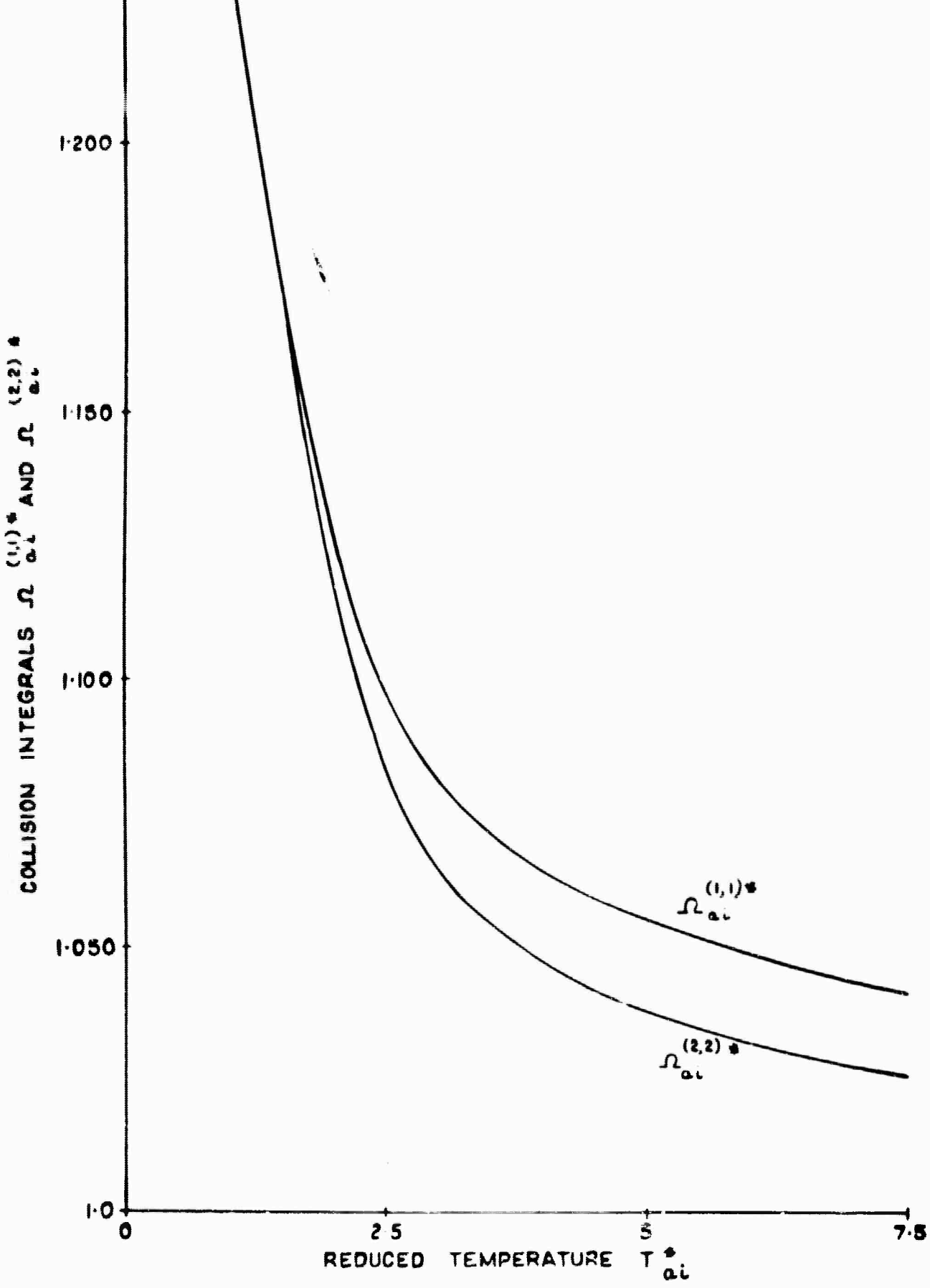

COLLISION INTEGRALS $\Omega_{ai}^{(1,1)*}$ AND $\Omega_{ai}^{(2,2)*}$ AS A FUNCTION OF REDUCED TEMPERATURE T_{ai}^{*} FOR ATOM-ION INTERACTION

FIG 21·5

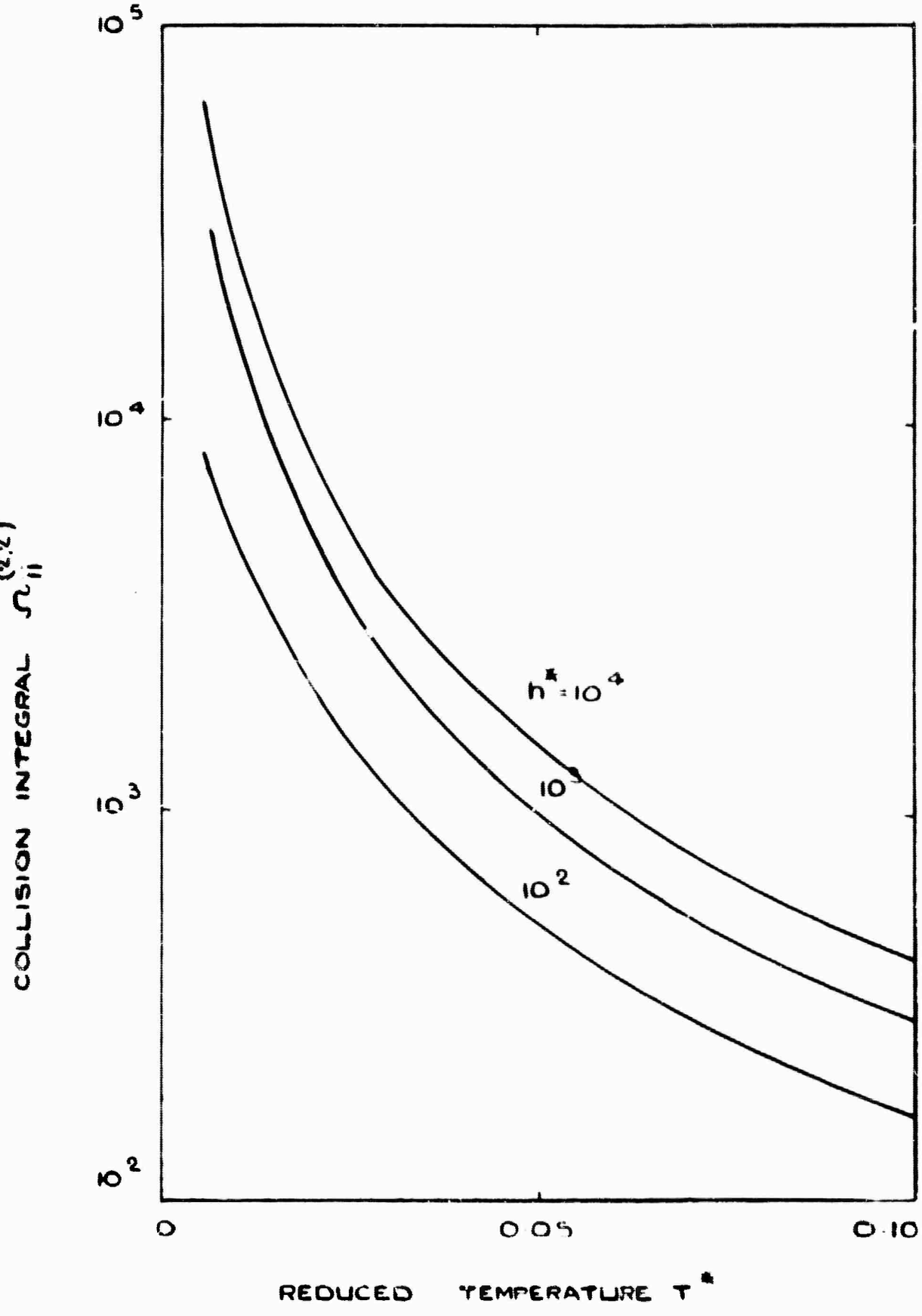

ION-ION COLLISION INTEGRAL AS A FUNCTION OF THE REDUCED TEMPERATURE

FIG. 21·6

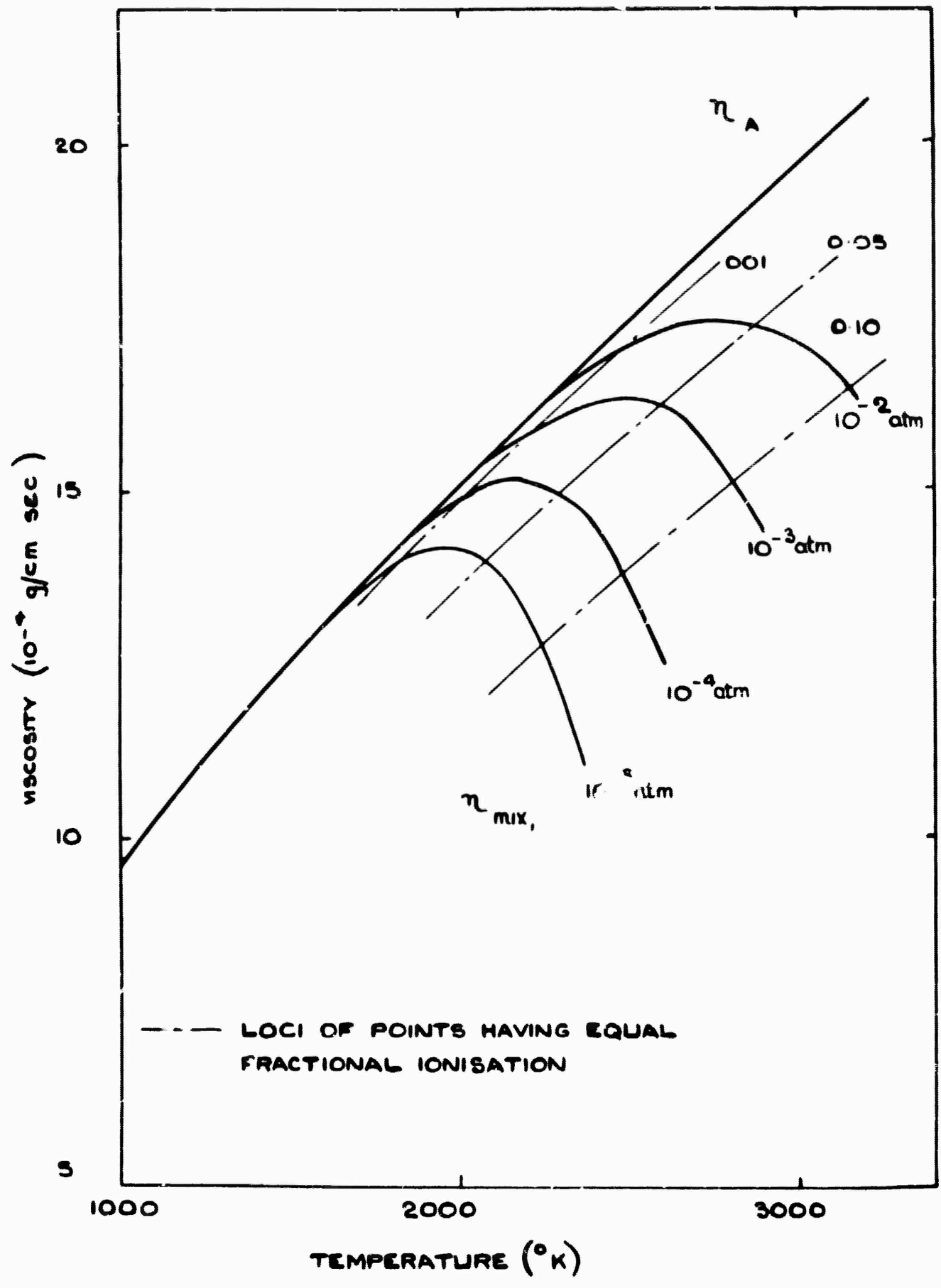

COSITY OF IONIZED CESIUM AS A FUNCTION OF TEMPERATURE

FIG 21·7

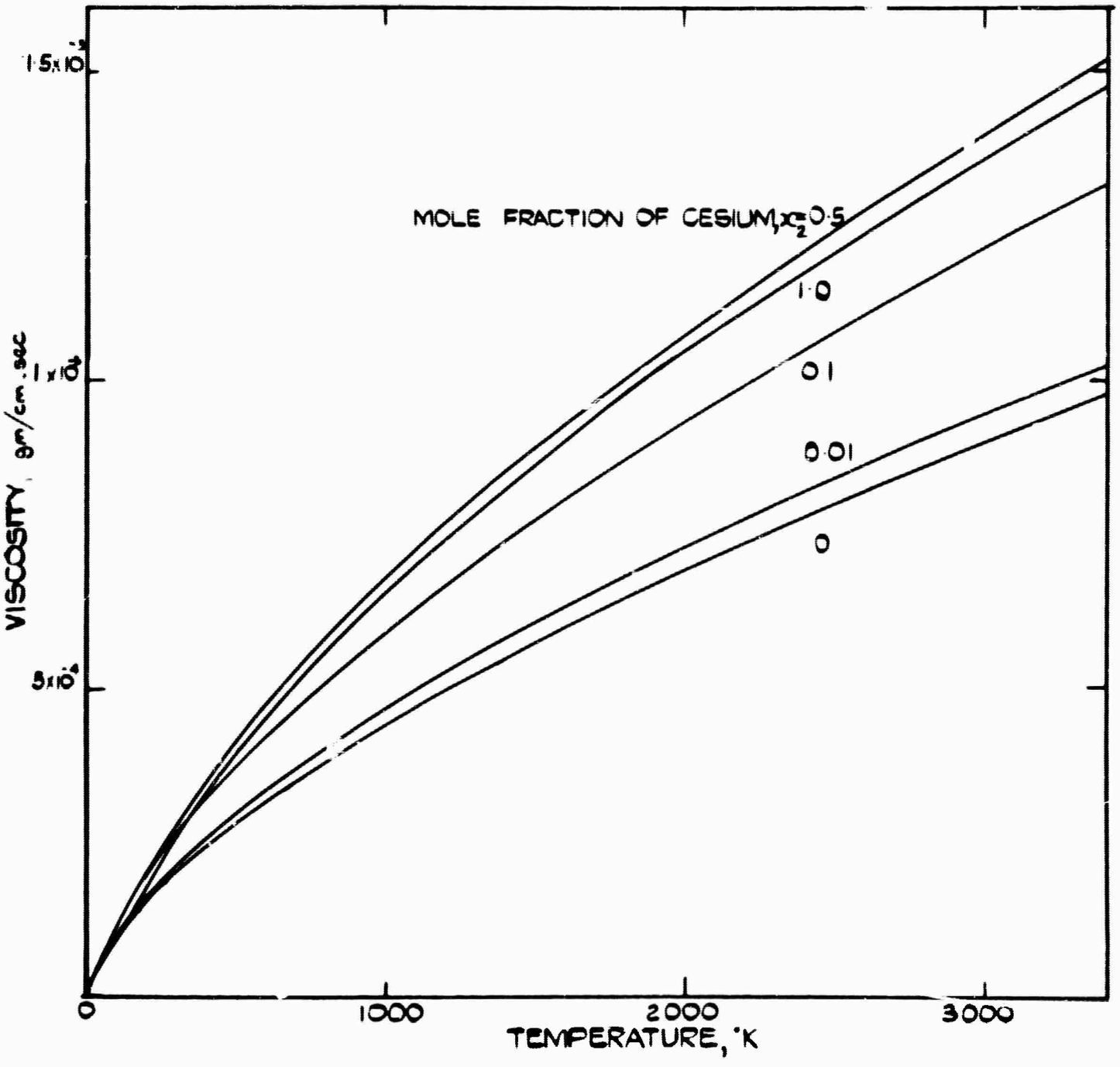

VISCOSITY AS A FUNCTION OF TEMPERATURE FOR HELIUM-CESIUM MIXTURES

FIG 21·8

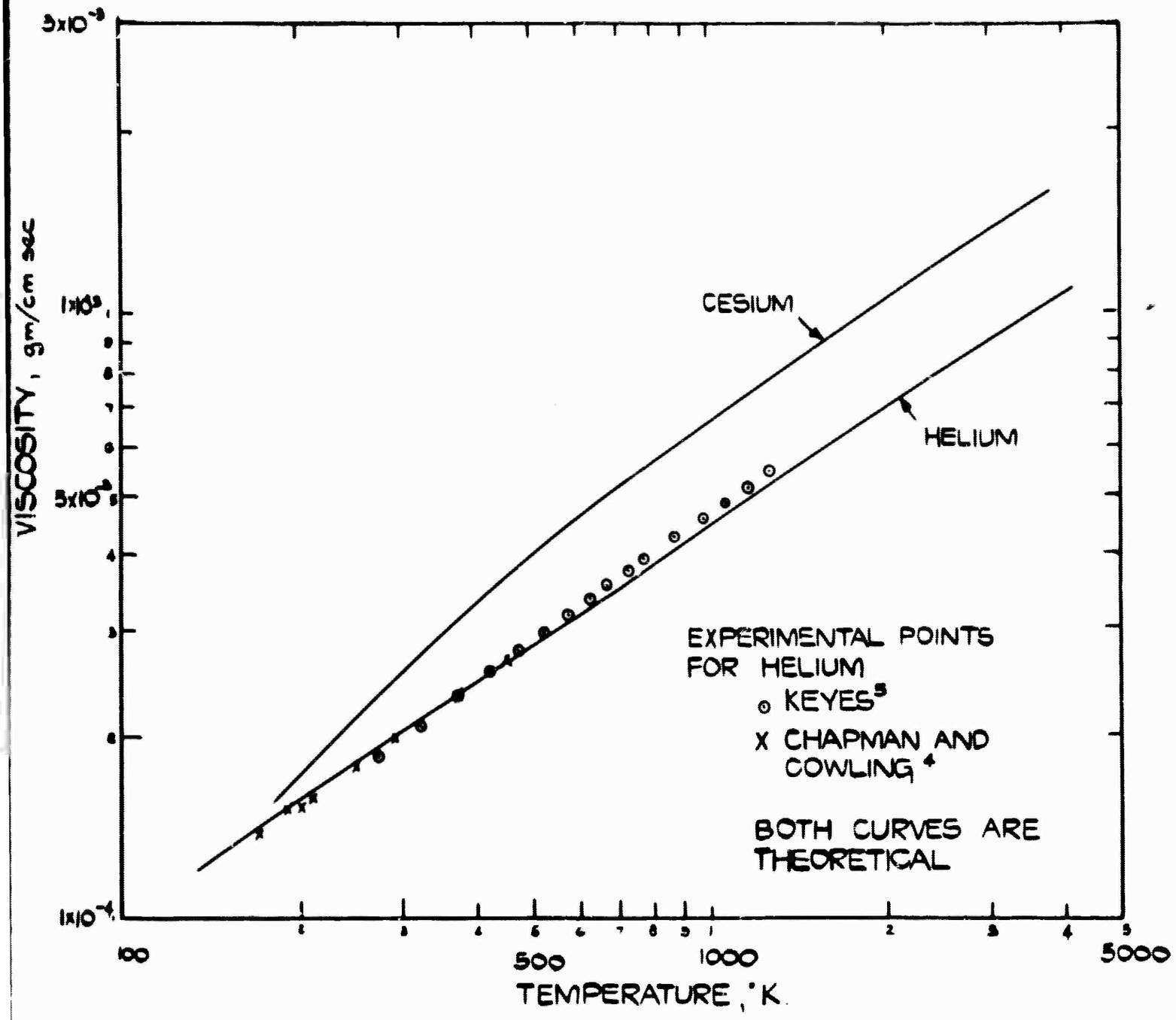

COMPARISON OF EXPERIMENTAL AND THEORETICAL VISCOSITIES

FIG 21·9

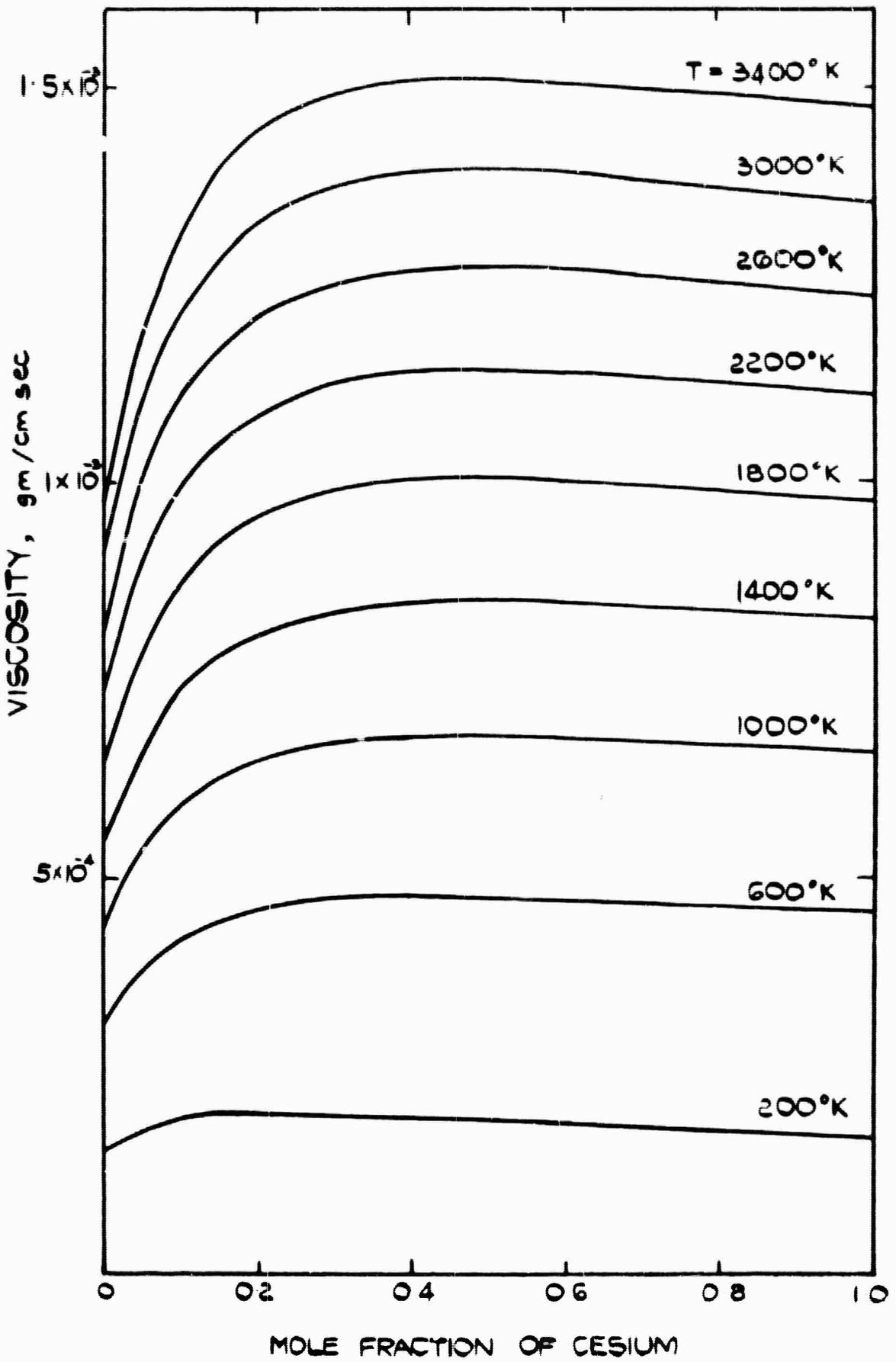

VISCOSITY AS A FUNCTION OF MOLE FRACTION OF CESIUM

FIG 21·10

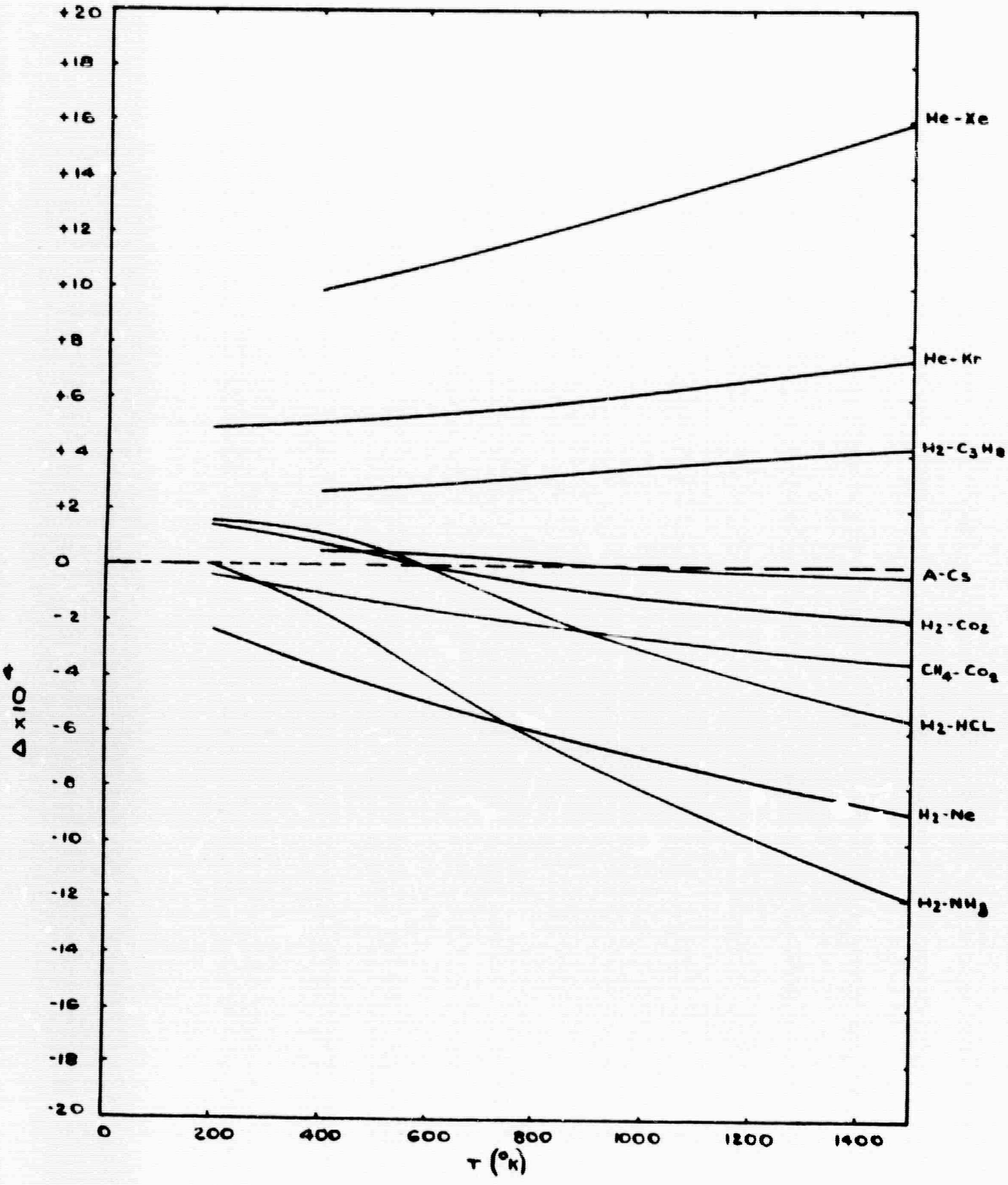

PARAMETER Δ AS A FUNCTION OF TEMPERATURE

FIG 21·11

A	Defined by equation (21.41)
A^*	coefficient defined in equation (21.20) or (21.32)
b	impact parameter
C	van der Waals constant
D_{12}	diffusion coefficient
E	defined by equation (21.41)
e	electron charge
f	velocity distribution function
g	relative velocity
h	Debye length
I	ionization potential
k	Boltzmann constant
M	molecular weight
m	particle mass
n	number density
P	pressure
r	separation of two interacting particles
T	temperature
t	time
t_D	deflection time
u	r^{-1}
u_0^*	smallest root of equation (21.A.2)
v	particle velocity
X,Y,Z	defined in equations (21.19) or(21.26) to (21.28)
x	mole fraction
x,y,z	position co-ordinates
α	fractional ionization
β	arc sin (u_0^{*-1})
γ	2 arc tan $(1/\sqrt{g^*})$
Δ	defined by equation (21.39)
ϵ	critical value of energy of interaction of two particles
η	viscosity
η_{MIX}	viscosity of two-component mixture
θ	is defined in equation (21.23)
Λ	ratio of critical impact parameters (equation 21.7)
λ	mean free path

μ reduced mass $\frac{m_1 m_2}{m_1 + m_2}$ of two-particle system

ν force power constant

ρ min. separation of centres of two atoms

ρ' min. separation of centres of atom and ion

σ critical value of separation of two particles

ϕ potential energy of two interacting particles

χ angle of deflection of each of two colliding particles in a centre-of-mass frame of reference

ψ = arc sin u^*/u_0^*

$\Omega^{(p,s)}$ collision integral defined in equation (21.14)

Subscripts

a atoms

e electrons

i ions

x,y,z direction co-ordinates

min minimum value

1,2 components of a binary mixture, particularly helium and cesium, respectively

- vector

Superscripts

* reduced (dimensionless) quantity (see equation (21.16))

- mean value

CHAPTER 22

COLLISION CROSS SECTIONS

by

I.R. McNab

22.1 INTRODUCTION

Many experiments presently being performed on methods of generating power directly with thermionic diodes or magnetoplasmadynamic devices use cesium, pure or diluted, as the working fluid. To evaluate the electrical conductivity of the gas or plasma the contribution made by collisions of electrons with neutral cesium atoms must be known. An increase in the number of such collisions per unit time reduces the mobility of the electrons and hence the electrical conductivity. The relationship is

$$\sigma_o = \frac{n_e e^2}{m_e \nu_M} \qquad \text{.....(22.1)}$$

where

$$\nu_M = \frac{e}{m\mu} \quad , \qquad \text{.....(22.2)}$$

σ_o is the scalar conductivity, n_e, e and m_e are the number concentration, charge and mass of the electrons, ν_M is the collision frequency for momentum transfer between electrons and cesium atoms and μ is the electronic mobility.

Equation (22.1) is valid only where electrons and cesium atoms are present; if other particles exist in appreciable numbers the collision frequency is modified.

For many gases ν_M may be replaced by ν_o, the elastic scattering collision frequency, since the values agree to within 10 per cent; however, recent theoretical calculations (discussed below) indicate that this is not valid for cesium.

The elastic scattering collision frequency (ν_o) between electrons and neutral atoms is given by

$$\nu_o = N Q_o v_e \qquad \text{.....(22.3)}$$

where N is the number concentration of neutral atoms, v is the electron speed

$\theta=0 \qquad \phi=0$

where $d\sigma/d\Omega$ is the differential cross section for scattering the electron into the solid angle $d\Omega = \sin\theta \; d\theta \; d\phi$.

The momentum transfer collision frequency is given by a similar expression:

$$\nu_M = N Q_M v \qquad .....(22.5)$$

where Q_M is the momentum transfer cross section:

$$Q_M = \int_{\theta=0}^{2\pi} \int_{\phi=0}^{2\pi} \frac{d\sigma}{d\Omega} (1 - \cos\theta) \sin\theta \; d\theta \; d\phi \qquad .....(22.6)$$

and the mean fractional energy loss per collision is

$$\delta = \frac{2 m_e Q_M}{M Q_o} \qquad .....(22.7)$$

M being the atomic mass.

The cross sections and collision frequencies averaged over a Maxwellian distribution may be found from the following equations:

average elastic scattering cross section

$$\bar{Q}_o = \int_o^\infty f_o (v) \; Q_o (v) \; dv \qquad .....(22.8)$$

average momentum transfer cross section

$$\bar{Q}_M = \int_o^\infty f_o (v) \; Q_M (v) \; dv \qquad .....(22.9)$$

average momentum transfer collision frequency per atom

$$\frac{\bar{\nu}_M}{N} = \int_o^\infty f_o (v) \; Q_M (v) \; v \, dv \qquad .....(22.10)$$

and the average total collision frequency is defined in a similar fashion.

In the above equations

$$f_o(v) = 4\pi v^2 \left(\frac{m}{2\pi kT}\right)^{3/2} \exp\left(-\frac{mv^2}{2kT}\right) \qquad .....(22.11)$$

is the Maxwellian distribution of velocities for the electrons; it is the distribution most often assumed in plasmas, although not always valid.

22.2 EXPERIMENTAL INVESTIGATIONS

Until recently experimental data on the cross sections of cesium (and other elements) at electron energies below one electron volt have been sparse. Brodes measurements[1] cover a large energy range, from electron energies greater than 100eV to about 0.8 eV; the low energy values obtained are shown in Fig. 22.1. The results obtained by Boeckner and Mohler[2] have recently been corrected by Phelps in the light of later experiments by Mohler[3]. Phelps found that the collision frequency per atom was constant over the range ~0.2 to 0.4 eV (Fig. 22.2); a collision cross section derived from these results using the relation

$$\bar{\nu} = \frac{4}{3} N Q v \qquad .....(22.12)$$

is shown in Fig. 22.1. Recent experiments at low electron energies in cesium appear to have confused, rather than clarified the situation.

Using a conductivity cell with concentric and parallel-plate electrode geometry, Mullaney[4] has derived collision cross sections which are lower than those of Brode or Mohler (Fig. 22.1). The cross sections are averaged over some electron distribution; as with most experiments of this type the electron energy distribution is not known accurately.

Roehling[5] has used a similar apparatus with a parallel-plate electrode geometry to measure cross sections up to about 2000°K. The results agree closely with Mullaney's, being lower than those of Brode and Mohler; a Maxwellian velocity distribution for the electrons is claimed.

Morgulis and Korchevoi[6], using an arc discharge between tungsten cathodes in cesium vapour measured an electron-cesium atom cross section of $\sim 50 \times 10^{-16}$ cm^2 at an electron temperature of about 5000°K. This value is similar to those found by Mullaney and Roehling, but at a much higher temperature (Fig. 22.1).

Chen and Raether[7] conducted a series of experiments on helium-cesium mixtures and pure cesium plasmas using microwave techniques. In the temperature range 450° to 550°K they find that the average momentum transfer cross section is

best represented by

$$\bar{Q}_m = \frac{1.61\times10^{-20}}{T_e} - \frac{9.63\times10^{-12}}{T_e^{\frac{1}{2}}} + 2.03\times10^{-13} \text{ cm}^2 .$$

These collision cross sections are shown in Fig. 22.1 where it can be seen that they are much higher than other values previously found.

From electrical conductivity measurements in various gas mixtures Harris[8] finds an average momentum transfer collision cross section for cesium of about 300×10^{-16} cm^2 and a collision frequency ($\nu_M/_N$) of 8×10^{-7} cm^3/sec at a temperature of 1750°K.

Using the method of phase shifts and including the effects of polarization, Robinson[9] has evaluated theoretically the average elastic scattering cross section, momentum transfer cross section and the momentum transfer collision frequency for cesium; the results are shown in Figs.22.1 and 22.2. In view of the wide scatter of experimental data Robinson's calculations will be useful in estimating the electrical properties of cesium plasmas in the energy range below 1 eV. As Robinson points out, the calculations are of a preliminary nature and more accurate theory may be required to obtain complete agreement with experiment.

Measurements in a static cesium plasma by Ralph[10] gave values for the cesium cross section of 2390×10^{-16} cm^2 and 1570×10^{-16} cm^2 at a temperature of 1050°K. These are much higher than other results reported by Ralph[11] at 1500°K, which yielded 200×10^{-16} cm^2.

22.3 CONCLUSIONS

Although several measurements of collision cross sections and collision frequencies have recently been made for cesium, experimental data is still widely divergent. If all the experimental data is correct the cross section of cesium atoms at low energies exhibits a hitherto unexpected energy-dependence. The theoretical calculations of Robinson[9] lie within the range of the experimental values. For most of the calculations in other Chapters of this report a constant cesium atom cross section of 300×10^{-16} cm^2 has been used: reference to the experimental values shows that this is a reasonable approximation.

REFERENCES

1 BRODE, R.B. Rev. Mod. Phys. Vol. 5, p.257. 1933

2 BOECKNER, C., and MOHLER, F.L. Bur. Stand. J. Research. Vol. 10, p.357. 1933

3 MOHLER, F.L. Bur. Stand. J. Research. Vol. 9, p.403, 1932. Vol. 10, p.771, 1933. Vol. 16, p.227, 1936. Vol. 17, p.45, p.849, 1938

4 MULLANEY, G.J. A determination of the collision cross section of slow electrons with cesium atoms. GERL report 61 RL 2864C. October 1961

5 ROEHLING, D. University of California report. August, 1962

6 MORGULIS, N.D., and KORCHEVOI, Y.P. Mobility and scattering cross section of electrons in weakly ionized cesium plasma. Soviet Physics Technical Physics, Vol. 7, No. 7, p.655. 1963

7 CHEN, C.L., and RAETHER, M. Collision cross sections of slow electrons and ions with cesium atoms. Phys. Rev. Vol. 128, p.2679. 1962

8 HARRIS, L.P. Electrical conductivity of cesium seeded atmospheric pressure plasmas near thermal equilibrium. J. Appl Phys. Vol 34, p.2958. 1963

9 ROBINSON, L.B. Theoretical elastic collision frequency between electrons and neutral atoms in a cesium plasma. Phys. Rev. Vol. 127, p.2076. 1962

10 RALPH, J.C. Electrical conductivity measurements on cesium vapour and cesium plus inert gas mixtures. IEE Conference report series No. 4. 1963

11 RALPH, J.C. Zh. tekh. Fiz. Vol. 32, p.766. 1962

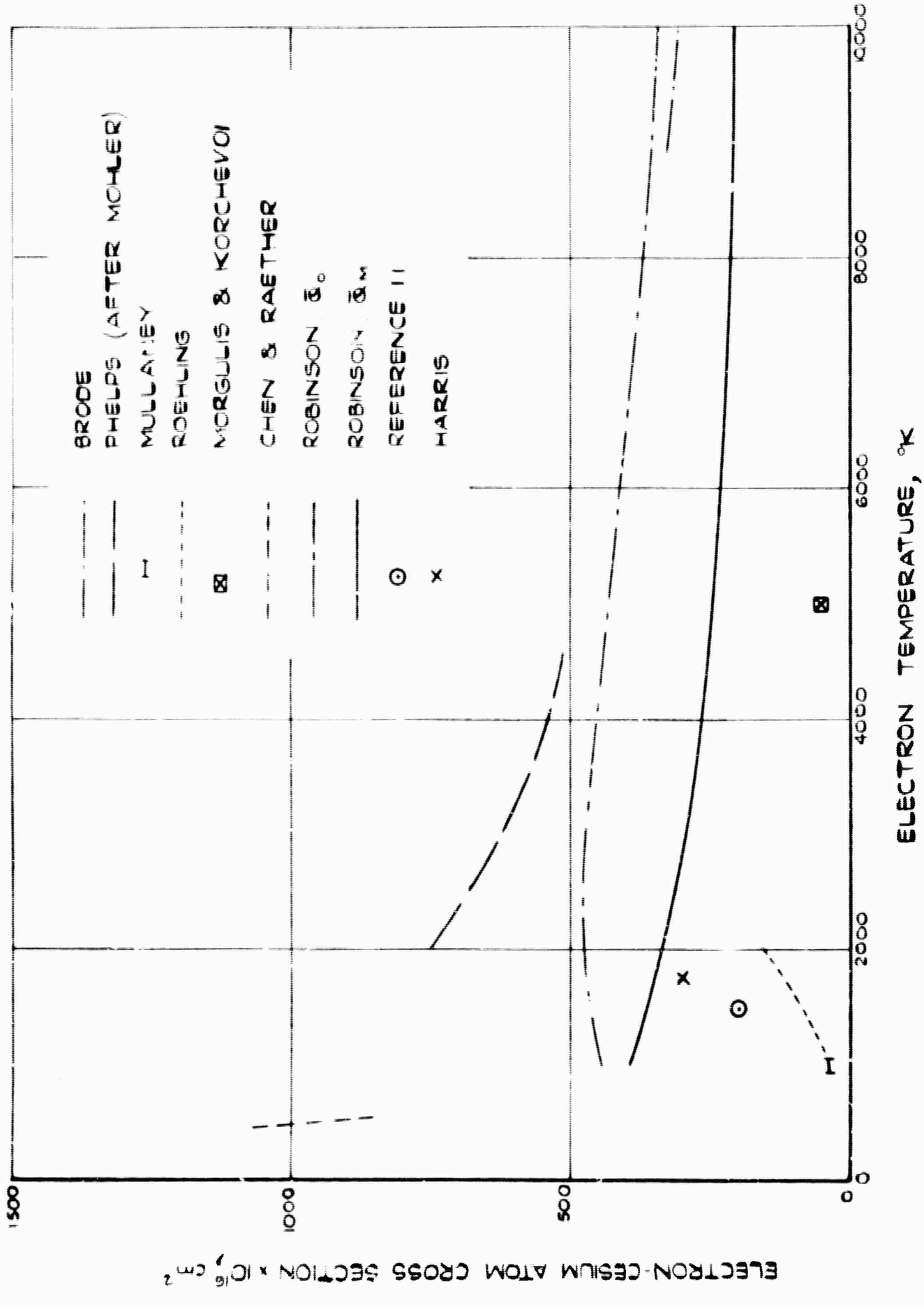

MEASURED AND CALCULATED ELECTRON-CESIUM ATOM COLLISION CROSS SECTIONS

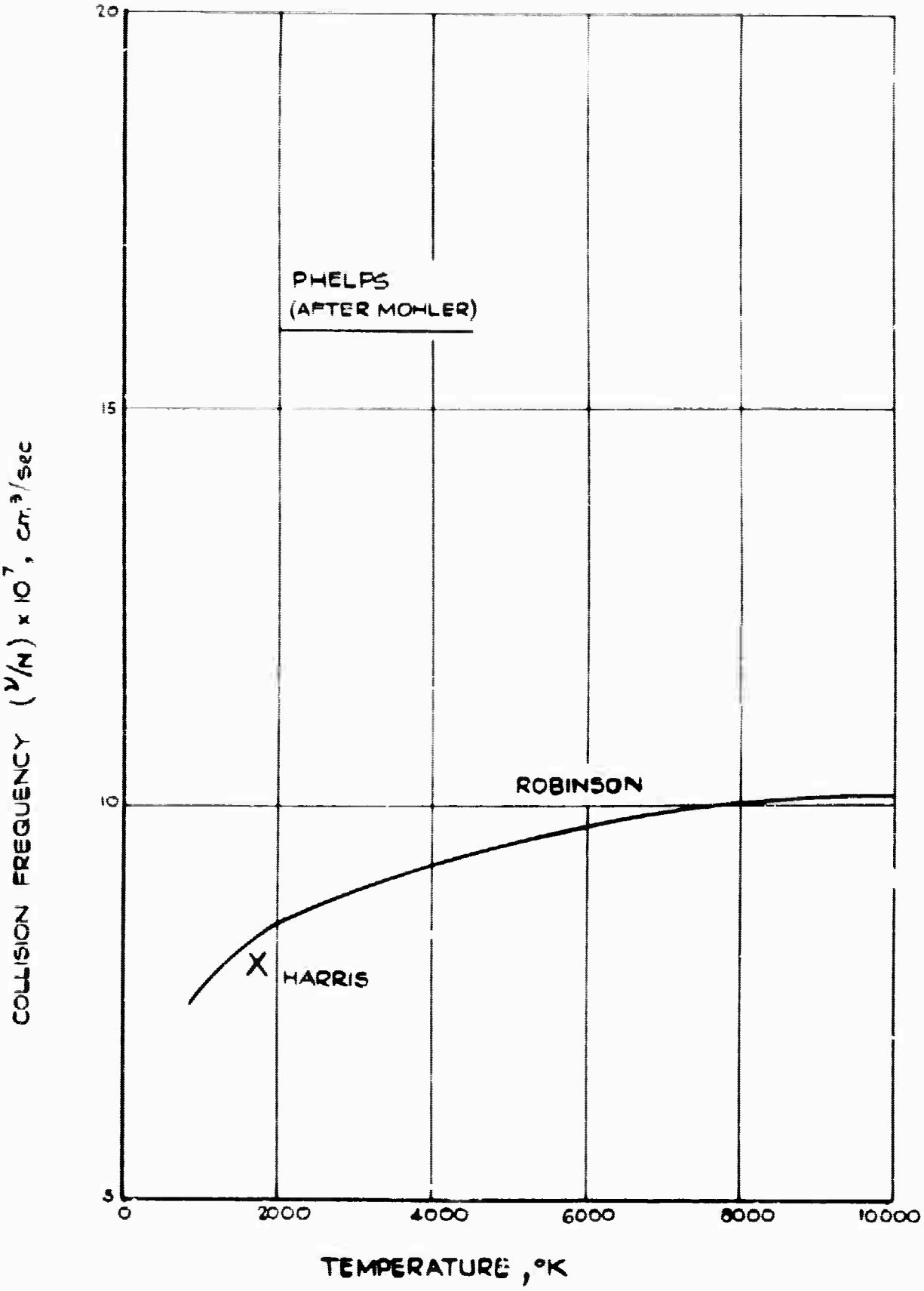

MEASURED AND CALCULATED COLLISION FREQUENCIES FOR CESIUM

BLANK PAGE

SEED FRACTION OPTIMIZATION

by

I.R. McNab

23.1 INTRODUCTION

In analyses of MPD generators in which the electrical conductivity of the parent gas is increased by the addition of a seed element the scalar conductivity is usually quoted as

$$\sigma_o = \frac{n_e e^2}{m_e \nu_{eT}} \qquad \ldots\ldots (23.1)$$

where, if electron-ion interactions can be neglected

$$\nu_{eT} = \nu_{e-P} + \nu_{e-a}$$

$$= v_e \left(q_{e-P} n_P + q_{e-a} n_a\right) \qquad \ldots\ldots (23.2)$$

If the seed fraction (χ) is small ($\chi = n_a/n_P$) maximizing conductivity with respect to χ shows that the optimum seed fraction is

$$\chi_{opt} = q_{e-P}/q_{e-a} \qquad \ldots\ldots (23.3)$$

χ_{opt} is usually about 0.01 for alkali metal seeded inert or combustion gases. In view of the rather sparse, and often suspect, data on collision cross sections at the low electron energies relevant to MPD generation, χ_{opt} is often assumed constant.

Considerable attention is presently being focussed on the production of extrathermal ionization in closed cycle MPD generators by various means, but particularly on magnetically-induced ionization by which interaction of the electrons with the electric field in the generator causes the electron temperature to be considerably increased over the gas temperature. When this occurs ionic scattering of electrons becomes an important factor in the determination of the electronic collision frequency and hence electrical conductivity. Since the electron-ion collision frequency is (quite strongly) dependent on the electron temperature the optimum seed fraction is no longer the unique quantity defined by equation (23.3) but is a function of the working conditions of the generator

even when q_{eP} and q_{ea} are constant. The selection of the optimum seed fraction for this case and the consequences of the temperature dependence are examined here.

23.2 SIMPLE THEORY

It will be assumed that the Saha equation[1] can be used to obtain the fractional ionization of the gas at the electron temperature so that

$$\frac{X^2}{1-X^2}\, p_{T_S} = f(T_e) \qquad \ldots\ldots (23.4)$$

where $$f(T_e) = (kT_e)^{5/2} \left(\frac{2\pi m_e}{h}\right)^{3/2} \frac{g_e g_i}{g_a} \cdot \exp\left(-\frac{eV_i}{kT_e}\right) \qquad \ldots\ldots (23.5)$$

In the simple theory developed in this section it will be assumed that the fractional ionization is small (that is $X \ll 1$ or $n_e \ll n_a$). Under these conditions, Saha's equation becomes

$$X^2\, p_{T_S} = f(T_e) \qquad \ldots\ldots (23.6)$$

Making the additional assumption that, while T_e is greater than T, $n_e T_e \ll n_a T$, then

$$p_{T_S} = n_a kT \qquad \ldots\ldots (23.7)$$

$$p_T = p_{T_S} + p_I = (n_a + n_P)\, kT\ ; \qquad \ldots\ldots (23.8)$$

and, by definition $$\chi = \frac{n_a}{n_a + n_P} \qquad \ldots\ldots (23.9)$$

so that $$p_{T_S} = \chi p_T \qquad \ldots\ldots (23.10)$$

and Saha's equation becomes

$$X^2 = \frac{f(T_e)}{\chi p_T} \qquad \ldots\ldots (23.11)$$

The electron concentration may be found from

$$n_e = \frac{X\chi p_T}{kT} \qquad \ldots\ldots (23.12)$$

Combining equations (23.5),(23.8),(23.11) and (23.12) yields

$$n_e = \chi^{1/2} (n_a + n_P)^{1/2} \frac{T_e^{5/4}}{T^{1/2}} \left(\frac{2\pi m_e k}{h^2}\right)^{3/4} \left(\frac{g_e g_i}{g_a}\right)^{1/2} \exp\left(-\frac{eV_i}{2kT_e}\right) \ldots. (23.13)$$

where $(n_a + n_P)$ can be inserted as data appropriate to chosen gas temperatures and total pressures. The seeding atom concentration and parent atom concentration

are obtained from

$$n_a = \chi(n_a + n_P) \qquad \ldots\ldots (23.14)$$

$$n_P = (1-\chi)\ (n_a + n_P) \qquad \ldots\ldots (23.15)$$

For a seeded gas in which ionic scattering of electrons is important the total collision frequency is

$$\nu_{eT} = v_e\ (q_{e-P} n_P + q_{e-a} n_a + q_{e-i}\ n_i\ ) \qquad \ldots\ldots (23.16)$$

where, from Spitzer[2]

$$q_{e-i} = \frac{A}{T_e^{\,2}}\ \ln\left(\frac{B' T_e^{\,3/2}}{n_e^{\,1/2}}\right) \qquad \ldots\ldots (23.17)$$

where $A = \dfrac{e^4}{256\pi(\epsilon_o k)^2}$; $B' = \dfrac{12\pi\ (\epsilon_o k)^{3/2}}{e^3}$

and, for a Maxwellian distribution,

$$v_e = \left(\frac{8kT_e}{\pi m_e}\right)^{1/2} \qquad \ldots\ldots (23.18)$$

Combining equations (23.1), (23.13), (23.14), (23.15) and (23.16) an expression for conductivity in terms of seeding fraction is obtained

$$\sigma_o = \frac{E\,\chi^{1/2}}{F(1-\chi) + G\chi + H\chi^{1/2}\,[I - \frac{1}{4}\ln\chi]} \qquad \ldots\ldots (23.19)$$

where

$$C = \left(\frac{g_a g_i}{g_a}\right)^{1/2} \left(\frac{2\pi m_e k}{h^2}\right)^{3/4}$$

$$D = eV_i/2k$$

$$E = \frac{e^2}{m} \left(\frac{n_a+n_P}{T}\right)^{1/2} T_e^{\,5/4}\ C\ \exp\left(-\frac{D}{T_e}\right)$$

$$F = v_e q_{e-P}\ (n_a+n_P)$$

$$G = v_e q_{e-a} (n_a+n_P)$$

$$H = \frac{v_e A}{T_e^{\,5/4}} \left(\frac{n_a+n_P}{T}\right)^{1/2} C \exp\left(-\frac{D}{T_e}\right)$$

$$I = \ln\left[\frac{B' T_e^{\,7/8}\ T^{1/4}}{(n_a+n_P)^{1/4} C^{1/2}}\right] + \frac{D}{2T_e}$$

Differentiating conductivity in equation (23.19) with respect to seeding fraction and setting the result equal to zero yields a quadratic for optimum seeding fraction for which the solution is

$$X_{opt} = \frac{F}{G-F} + \frac{H^2}{8(G-F)^2} + \frac{H^2}{8(G-F)^2}\left[1 + \frac{16F(G-F)}{H^2}\right]^{1/2} \quad \ldots\ldots (23.20)$$

For the case when ionic collisions can be neglected ($H \approx 0$, occurring at low fractional ionization) equation (23.20) yields

$$X_{opt} = \frac{F}{G-F} = \frac{q_{eP}}{q_{eP}+q_{ea}} \quad \ldots\ldots (23.21)$$

Usually $q_{ea} >> q_{eP}$ so that this reduces to equation (23.3). (The difference between equations (23.3) and (23.21) is due to the different definitions of seeding fraction used in the two cases.)

When ionic collisions are important, equation (23.20) shows that the optimum seeding fraction is increased over the value given in equation (23.21): the greater the effect of ionic collisions, the greater the optimum seeding fraction, up to a maximum of unity.

However, equation (23.20) is not very useful in examining the effects of extrathermal ionization on seeding fraction since such effects generally cause high fractional ionizations, so that the approximations used in deriving equation (23.20) become invalid and a more accurate approach is required.

23.3 ACCURATE TREATMENT

If the fractional ionization is high it is necessary to use the exact Saha equation (equation 23.4) in which the total seed pressure is expressed in terms of known constants of the system (total gas pressure and temperature).

Now

$$p_{T_S} = n_e kT_e + n_i kT + n_a kT$$

$$= n_e kT_e + n_S kT \quad \ldots\ldots (23.22)$$

since $n_e = n_i$

and $n_S = n_e + n_a$

Using $X = n_e/n_S$ equation (23.22) becomes

$$p_{T_S} = kn_S (XT_e + T)$$

or, using a more accurate definition of seeding fraction than that of section 23.1, that is

$$\chi = \frac{n_S}{n_T}$$

where $n_T = n_P + n_S = n_P + n_a + n_e$,

$$p_{T_S} = k\chi n_T (XT_e + T) \qquad \ldots\ldots (23.23)$$

At constant pressure n_T is a variable so that an expression is required relating n_T and p_T. Using the previous conditions

$$p_T = n_e kT_e + n_i kT + n_a kT + n_P kT$$

$$= n_e kT_e + n_T kT.$$

Now

$$n_e = Xn_S$$

$$= X\chi n_T \qquad \ldots\ldots (23.24)$$

so that $p_T = kn_T (X\chi T_e + T)$ $\qquad \ldots\ldots (23.25)$

Eliminating n_T from equations (23.23) and (23.25) yields

$$p_{T_S} = \frac{\chi(XT_e + T)p_T}{X\chi T_e + T} \qquad \ldots\ldots (23.26)$$

so that the Saha equation (23.4) becomes

$$\frac{X^2\chi(XT_e + T)p_T}{(1-X^2)(X\chi T_e+T)} = f(T_e) \qquad \ldots\ldots (23.27)$$

Thus for given χ, T_e, T and p_T this cubic equation must be solved for X. When X is found n_e may be obtained from equations (23.24) and (23.25):

$$n_e = \frac{X\chi p_T}{k(X\chi T_e+T)} \qquad \ldots\ldots (23.28)$$

and the remaining required quantities follow.

Thus $n_T = n_e/X\chi$ $\qquad \ldots\ldots (23.29)$

$$n_P = n_T(1-\chi) \qquad \ldots\ldots (23.30)$$

$$n_a = n_T\chi(1-X) \qquad \ldots\ldots (23.31)$$

The scalar conductivity of the gas is again obtained from equation (23.1) and the total electronic collision frequency from equation (23.16). Writing

$$v_e q_{eP} = F_1 T_e^{1/2}$$

$$v_e q_{e-a} = G_1 T_e^{1/2}$$

and $$Av_e = H_1 T_e^{1/2}$$

gives

$$\sigma_o = \frac{n_e (e^2/m_e)}{T_e^{1/2} F_1 (1-\chi) n_T + T_e^{1/2} G_1 \chi (1-\chi) n_T + \frac{H_1 n_e}{T_e^{3/2}} \ln\left(\frac{B' T_e^{3/2}}{n_e^{1/2}}\right)} \quad .. (23.32)$$

where A and B' have been defined previously. Substitution in this equation of the values of n_e, n_T and other parameters previously calculated will give the conductivity.

In Section 23.2 it was shown that in the simple evaluation of electrical conductivity an explicit relation for the optimum seeding fraction can be obtained. In the general case a simple explicit expression for X_{opt} cannot be obtained although equations governing the value of X_{opt} may be set up as follows.

Rewriting equation (23.32) in the form

$$\sigma_o = \frac{X(e^2/m_e)}{T_e^{1/2} F_1 (1-\chi)/\chi + T_e^{1/2} G_1 (1-X) + \frac{H_1 X}{T_e^{3/2}} \ln\left(\frac{B T_e^{3/2}}{n_e^{1/2}}\right)} ,$$

and differentiating yields

$$d\sigma_o = \frac{e^2/m_e \left\{ F_1 T_e^{1/2} \left[X d\chi/\chi^2 + (1-\chi) dX/\chi \right] + G_1 T_e^{1/2} dX + H_1 X^2 dn_e / 2 T_e^{3/2} n_e \right\}}{(\nu_{eT})^2} \quad ..... (23.33)$$

Using $a = T_e/T$ and $b = f(T_e)/p_T$ equation (23.27) becomes

$$aX^3\chi (1+b) + X^2(\chi+b) - abX\chi - b = 0 \quad ..... (23.34)$$

which, when differentiated, yields

$$\left\{ 3aX^2(1+b\chi) + 2X(1+b) - ab\chi \right\} dX = \left\{ a(1+b)X^3 + X^2 - abX \right\} d\chi \quad ..... (23.35)$$

Differentiation of equation (23.28) gives

$$dn_e = \frac{(X d\chi + \chi dX) T p_T}{k(X\chi T_e + T)^2} \quad ..... (23.36)$$

Elimination of dX, dn_e, X and n_e from equations (23.28) and (23.33) to (23.36)

will give an equation for $d\sigma/dX$ in terms of X and various constants. The condition $d\sigma/dX = 0$ will then give an equation having X_{opt} as one of its roots. Since it is possible to solve explicitly the general cubic equation, it is also possible to perform the elimination explicitly and obtain an equation $\phi(X_{opt}) = 0$, but the extent of manipulation required usually renders this impracticable.

23.4 COMPUTATION AND RESULTS

The Saha equation (23.34) was solved for fractional ionization by Newton's method using $(b/1+b)^{1/2}$ as a first approximation to X. This converged satisfactorily to the correct root for the range of values of X and T_e considered. The particle number concentrations can then be obtained from equations (23.28) to (23.31) and the electrical conductivity from equation (23.32). In view of the probable length of calculation, numerical solution of equations (23.33) to (23.36) to obtain the optimum conductivity was not attempted.

The resulting values of conductivity for helium-cesium mixtures are shown in Fig. 23.1 as a function of seeding fraction and electron temperature. The conductivity is shown as the ratio of the conductivity at an arbitary seeding fraction to that of the pure cesium. Cross sections of 6.1×10^{-20} m^2 and 320×10^{-20} m^2 were used for electron-helium and electron-cesium collisions respectively (McNab[3] and Chapter 22 of this report). The calculations were performed for constant gas temperature (1000°K) and pressure (1 ata) with varying electron temperatures (1000° to 5000°K). Fig. 23.2 shows the magnitude of the optimum and pure alkali metal conductivities as a function of electron temperature. Using Fig. 23.1 and 23.2 the actual magnitude of the scalar conductivity may easily be found for any seeding fraction.

The specific power of a segmented-electrode generator, neglecting ion slip, is simply proportional to $\sigma_o B^2$, thus, since σ_o is independant of magnetic field (at local static temperature and pressure conditions), the specific power curves for a segmented-electrode generator as a function of seeding fraction are exactly the same shape but are displaced by an amount depending on B.

For the transverse conductivity $(\sigma_o/1+\beta_e^2)$ this is not true since β_e is a function of the magnetic field strength; Fig. 23.3 and 23.4 show $\sigma_o/1+\beta_e^2$ as a function of seeding fraction for several values of B and electron temperatures of 2000° and 5000°K, the static gas temperature and pressure being the same as before.

The power density of a solid-electrode generator is proportional to $\sigma_o B^2/1+\beta_e^2$; this is shown in Fig. 23.5 and 23.6 for the same conditions as in

Fig. 23.3 and 23.4.

The specific power of a Hall generator is proportional to $\sigma_o B^2 \beta_e^2 / 1+\beta_e^2$ and this is shown in Fig. 23.7 and 23.8, again for the same conditions.

In addition to the dependence of specific power (P) on conductivity and magnetic field there is also a gas velocity (U) dependence:

$$P \propto U^2$$

$$\propto M^2 \gamma_M R_M \quad \text{..... (23.37)}$$

where γ_M and R_M are the ratio of specific heats and gas constant for the mixture respectively. Assuming that both helium and cesium are ideal monatomic gases with $\gamma = 5/3$, the specific power for constant expansion is proportional to the gas mixture composition only through the R_M term. The mixture gas constant is proportional to the fraction by weight (α) of each constituent, so that, in general

$$R_M = \sum_j \alpha_j R_j$$

and, for helium-cesium mixtures

$$R_M = \alpha_{CS} R_{CS} + \alpha_{He} R_{He}$$

or, if α is the fraction by weight of cesium,

$$R_M = \alpha R_{CS} + (1-\alpha) R_{He} \quad \text{..... (23.38)}$$

Using the quantities of Section 23.4 it can be shown that the relation between α and X is

$$\alpha = \frac{X m_S}{X(m_S - m_P) + m_P} \quad \text{..... (23.39)}$$

Combining equations (23.38) and (23.39), R_M may be evaluated as a function of seeding fraction; the result is shown in Fig. 23.9. Fig. 23.10 shows the product $\sigma_o R_M$, upon which the power density of a segmented electrode generator depends, while Fig. 23.11 to 23.16 show the transverse conductivity and specific power dependence for solid-electrode and Hall generators, including the effects of R_M.

23.5 DISCUSSION AND CONCLUSIONS

Fig. 23.1 shows the ratio of mixture conductivity to pure seed metal conductivity (σ/σ_1) as a function of seeding fraction (X) for several electron temperatures in cesium-helium mixtures; the optimum seed fraction increases with electron temperature fairly rapidly above about 4000°K. At an electron temperature of 5000°K the optimum seeding fraction is very high (~0.8), so that, for the conditions examined here, the maximum conductivity is obtained with pure

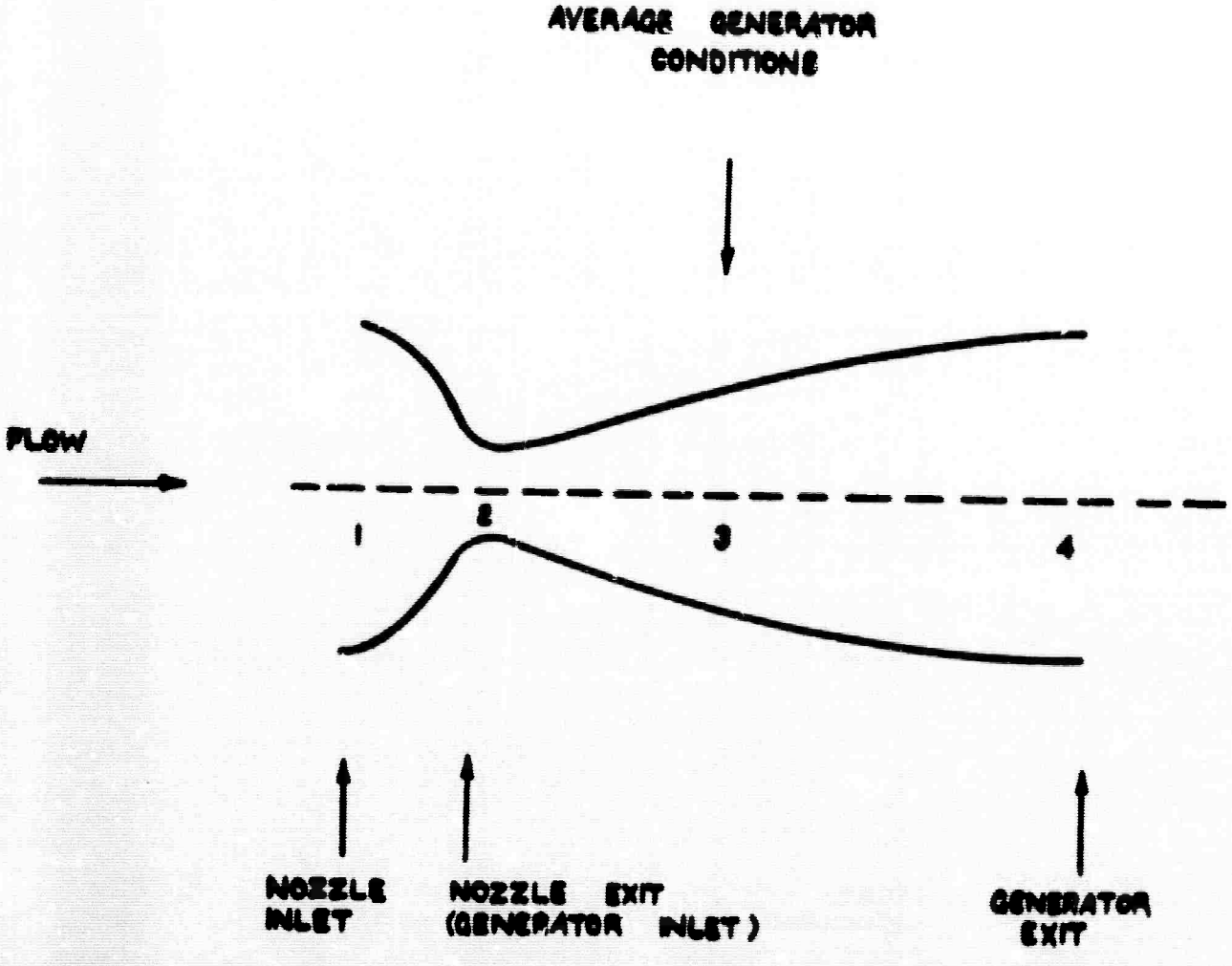

MPD GENERATOR AND NOZZLE STATIONS

FIG 27-1

cesium. As the electron temperature increases the variation of σ/σ_1 with X becomes less rapid and off-optimum operation has less effect, and factors other than electrical conductivity (e.g. engineering problems or the cost of cesium) could determine the seed fraction.

Fig. 23.2 shows the optimum for helium-cesium and pure cesium conductivities as a function of electron temperature the steep initial rise is apparent.

Fig. 23.3 and 23.4 show the transverse conductivity ($\sigma_o/1+\beta_e^2$) as functions of seeding fraction for various magnetic field strengths (B). As B increases the transverse conductivity decreases and, for $T_e = 2000^oK$ the optimum X tends to unity (pure alkali metal).

Fig. 23.5 and 23.6 show the product of the transverse conductivity and B^2 for the same values of magnetic field as previously. Again, as B increases, the optimum seeding fraction tends to unity for $T_e = 2000^oK$, and for $T_e = 5000^oK$ the optimum seeding fraction is always unity.

Fig. 23.7 and 23.8 show the term $\sigma_o\beta_e^2B^2/1+\beta_e^2$ as functions of B and X. As B increases, this term (which is proportional to the specific power of a Hall generator) increases and the optimum tends to unity. The optimum seeding fraction is very much lower than in the previous cases.

As stated in Section 23.4, in addition to the dependence of specific power for an MPD generator on conductivity and magnetic field, there is also a dependence on seeding fraction through the velocity term. This can be reduced to a dependence on the mixture gas constant, R_M, which is given as a function of seeding fraction in Fig. 23.9.

For a segmented-electrode generator, neglecting ion slip and using equation (23.37),

$$\hat{P} = \sigma_o R_M B^2 \qquad \ldots\ldots (23.40)$$

where $$\hat{P} = P/\gamma_M M^2 TK(1-K) \qquad \ldots\ldots (23.41)$$

The product $\sigma_o R_M$ is shown in Fig. 23.10 as a function of seeding fraction and electron temperature. The optimum seeding fraction is now relatively insensitive to the electron temperature (compare with Fig. 23.1) and is close to one atomic percent. Since σ_o is independent of B (at local static temperature and pressure conditions) the normalized specific power curves (P versus X) for different magnetic field strengths have the same shape but are displaced by amounts depending on B^2.

The manner in which the transverse conductivity (shown in Fig. 23.3 and 23.4)

is modified by the variation of gas constant is shown in Fig. 23.11 and 23.12, where $\sigma_o R_M/1+\beta_e^2$ is given as a function of X and B. Again the maximum value is obtained with smallest magnetic fields, but, although as B increases the optimum seeding fraction tends to unity, it is less than that of Fig. 23.3 and 23.4.

For a solid-electrode generator the specific power, neglecting ion slip, is

$$P = \sigma_o R_M B^2/1+\beta_e^2 \qquad \ldots\ldots (23.42)$$

This is shown in Fig. 23.13 and 23.14 as a function of seeding fraction and magnetic field for $T_e = 2000^o$ and 5000^oK. In both cases P and the optimum seeding fraction increase as B increases, the optimum being in the approximate range $0.1 < X < 0.01$.

For a Hall generator, again neglecting ion slip, the specific power is

$$\hat{P} = \frac{\sigma_o \beta_e^2 R_M B^2}{1+\beta_e^2} \qquad \ldots\ldots (23.43)$$

This is shown in Fig. 23.15 and 23.16 for the same conditions as in the previous figures. The optimum seeding fraction is much smaller in these two cases than for the segmented- or solid-electrode generators, being $<0.01^a/o$.

For the calculations reported here $\gamma_M = 5/3$ and $T = 1000^oK$; taking $M = 0.5$ and $K = 0.5$ gives $\gamma_M M^2 TK(1-K) \propto 10^2$, so that the actual specific power may readily be obtained from $\hat{P}$.

In any practical MPD generator local gas parameters will vary with position in the channel; the gas parameters used here ($T = 1000^oK$ and $p = 1$ ata) may represent typical values for a large-scale nuclear MPD generator. The techniques used here may easily be adapted to give the best seeding fraction for maximum electrical conductivity or specific power for any other gas mixture. No mechanism whereby electron temperature elevation is achieved has been postulated; different methods of extrathermal ionization yield different dependence of electron temperature on gas parameters.

The conclusions found here relating to the dependence of scalar conductivity on seeding fraction are similar to those quoted by Zimin and Popov[4] except that they relate to elevated electron temperatures and low gas temperatures, thus being directly applicable to closed-cycle nuclear-MPD generators.

REFERENCES

1 SAHA, M.N. and SAHA, H.K. 'A treatise on modern physics' Vol. 1, The Indian Press Ltd. Allahabad and Calcutta 1934.

2 SPITZER, L. jr. 'Physics of fully ionized gases' Interscience tracts on physics and astronomy. No. 3, 1956

3 McNAB, I.R. 'The electrical properties of a cesium-helium plasma' C.A. Parsons Report NRC 61-12, March 1961

4 ZIMIN, E.P. and POPOV, V.A. 'Determining the optimum composition of gaseous mixtures in the presence of seeding' I.E.E. Conference Report Series No. 4, 1963,

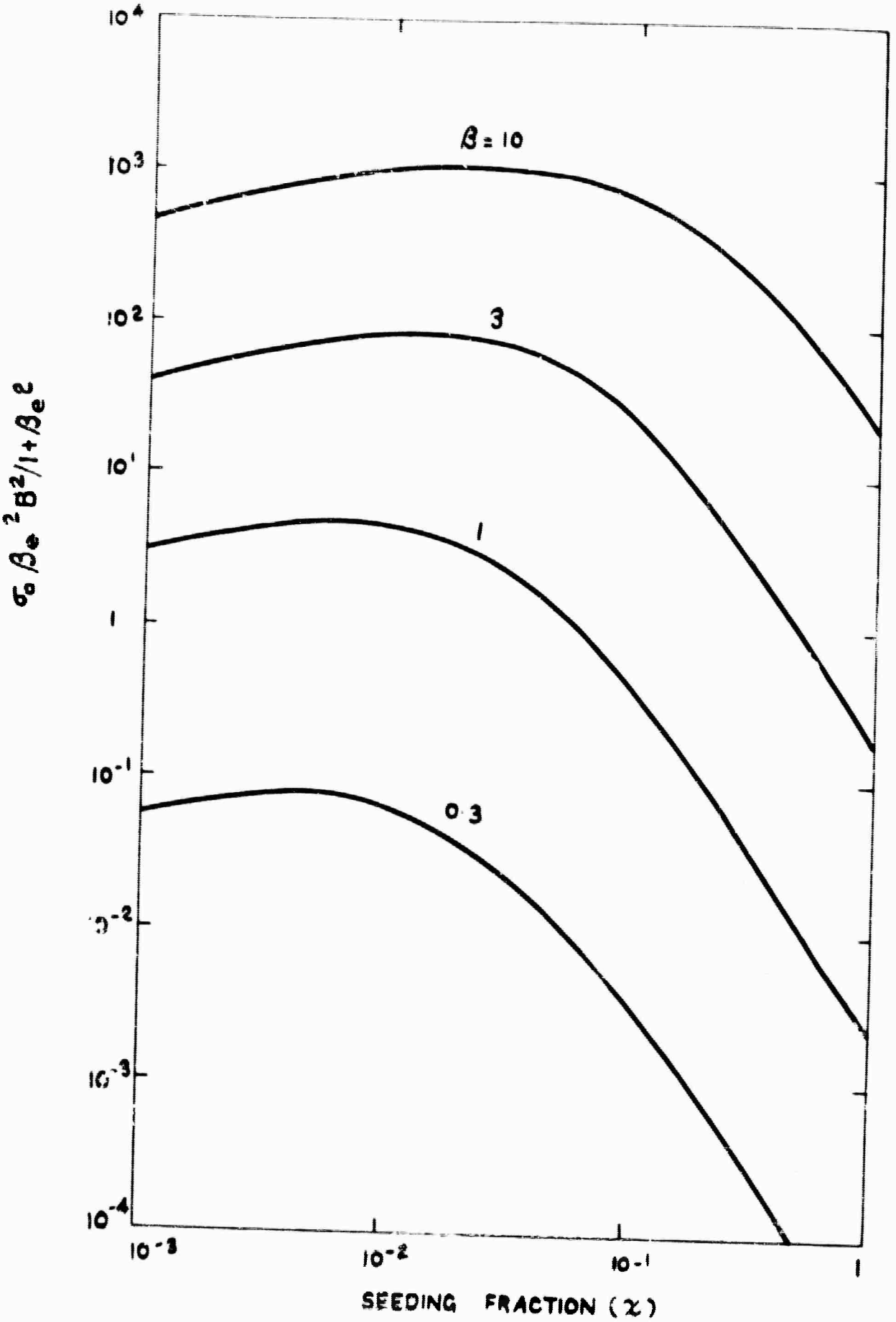

VARIATION OF $\sigma_0 \beta_e^2 B^2/1+\beta_e^2$ WITH SEEDING FRACTION FOR $T_e = 2000\ ^\circ K$

FIG23·7

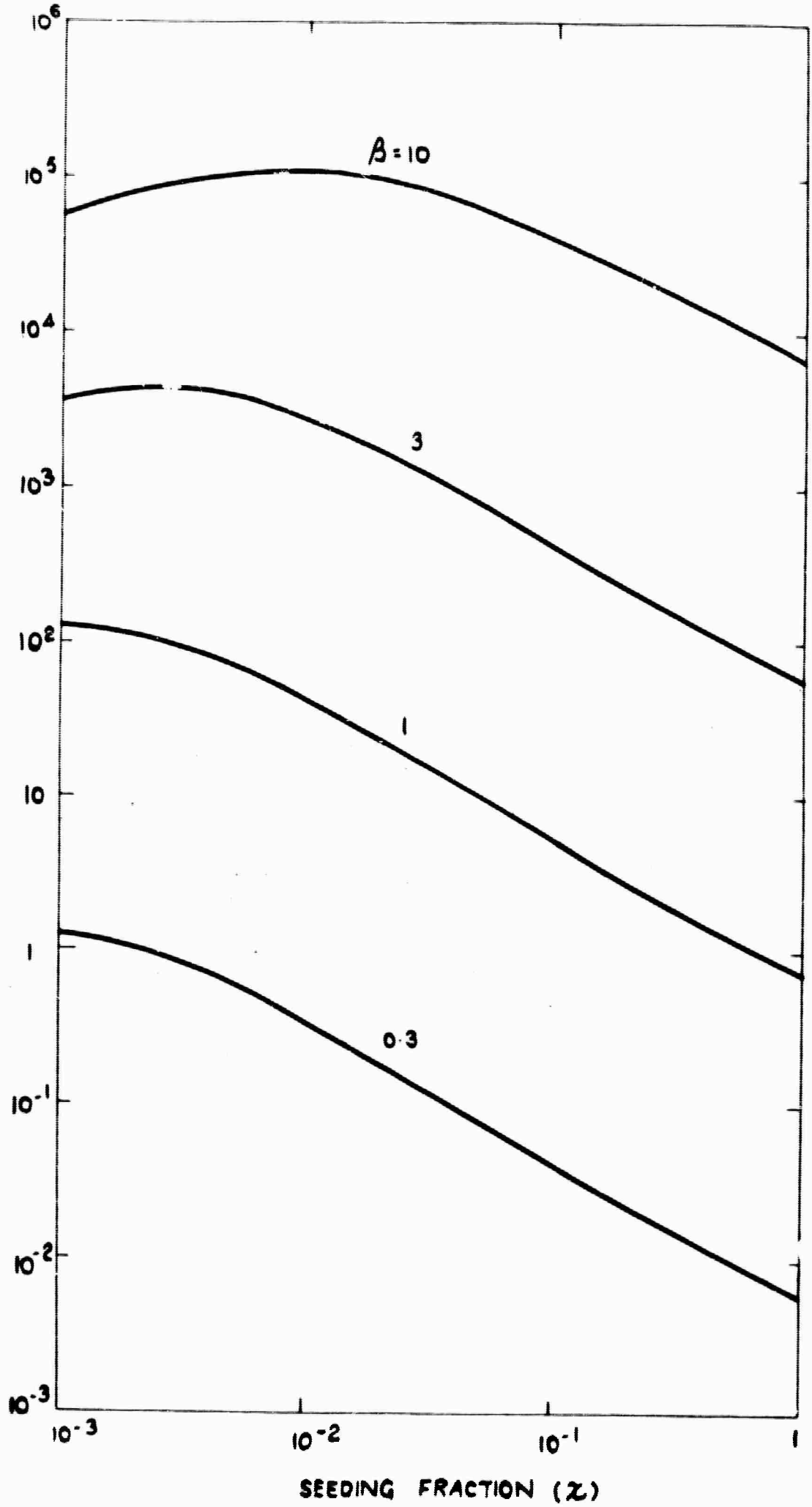

ARIATION OF $\sigma_0 \beta_e^2 B^2/1+\beta_e^2$ WITH SEEDING FRACTION
OR T_e 5000 °K

FIG23·8

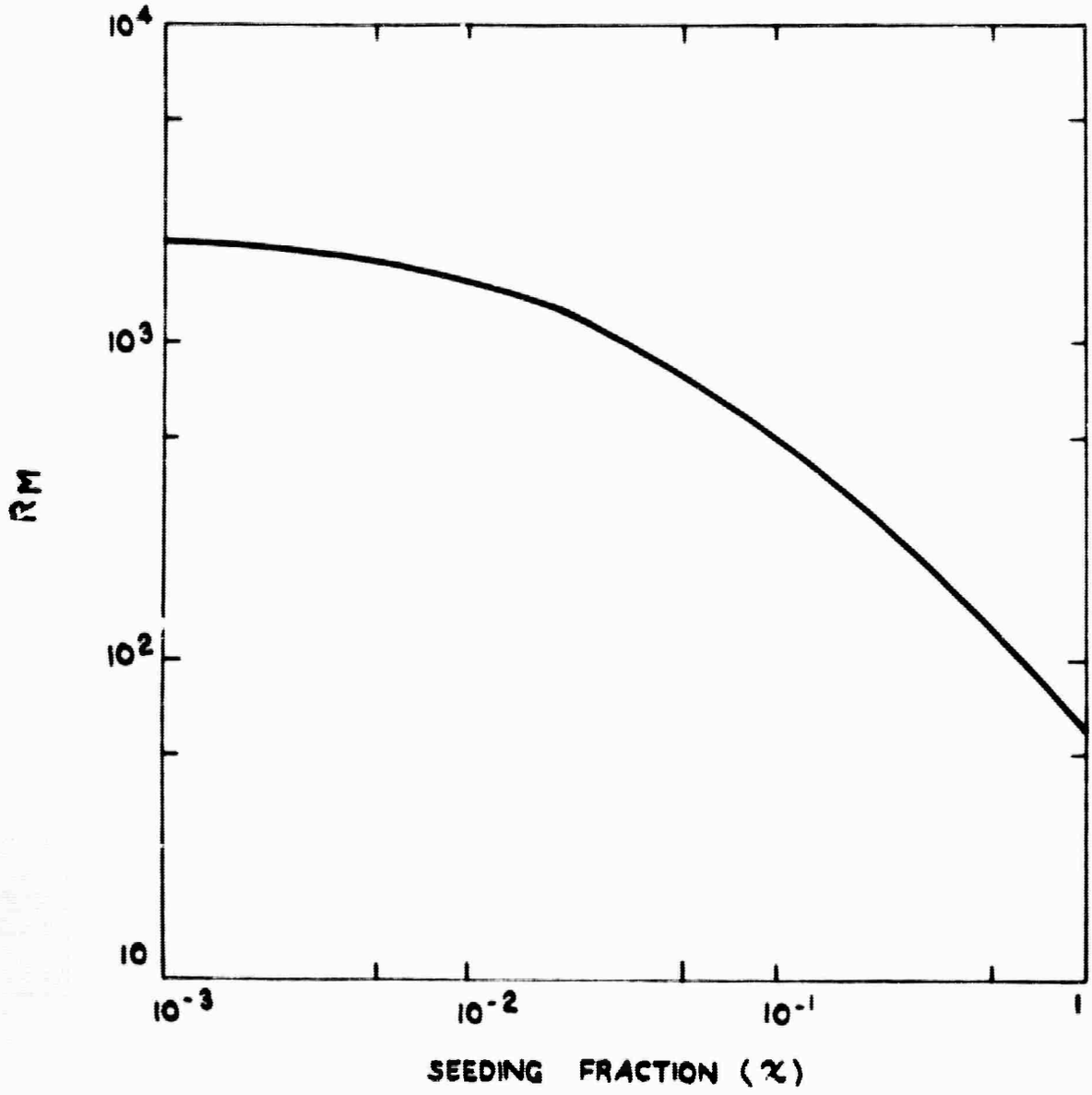

VARIATION OF GAS CONSTANT WITH SEEDING FRACTION FOR CESIUM – HELIUM MIXTURE

FIG23·9

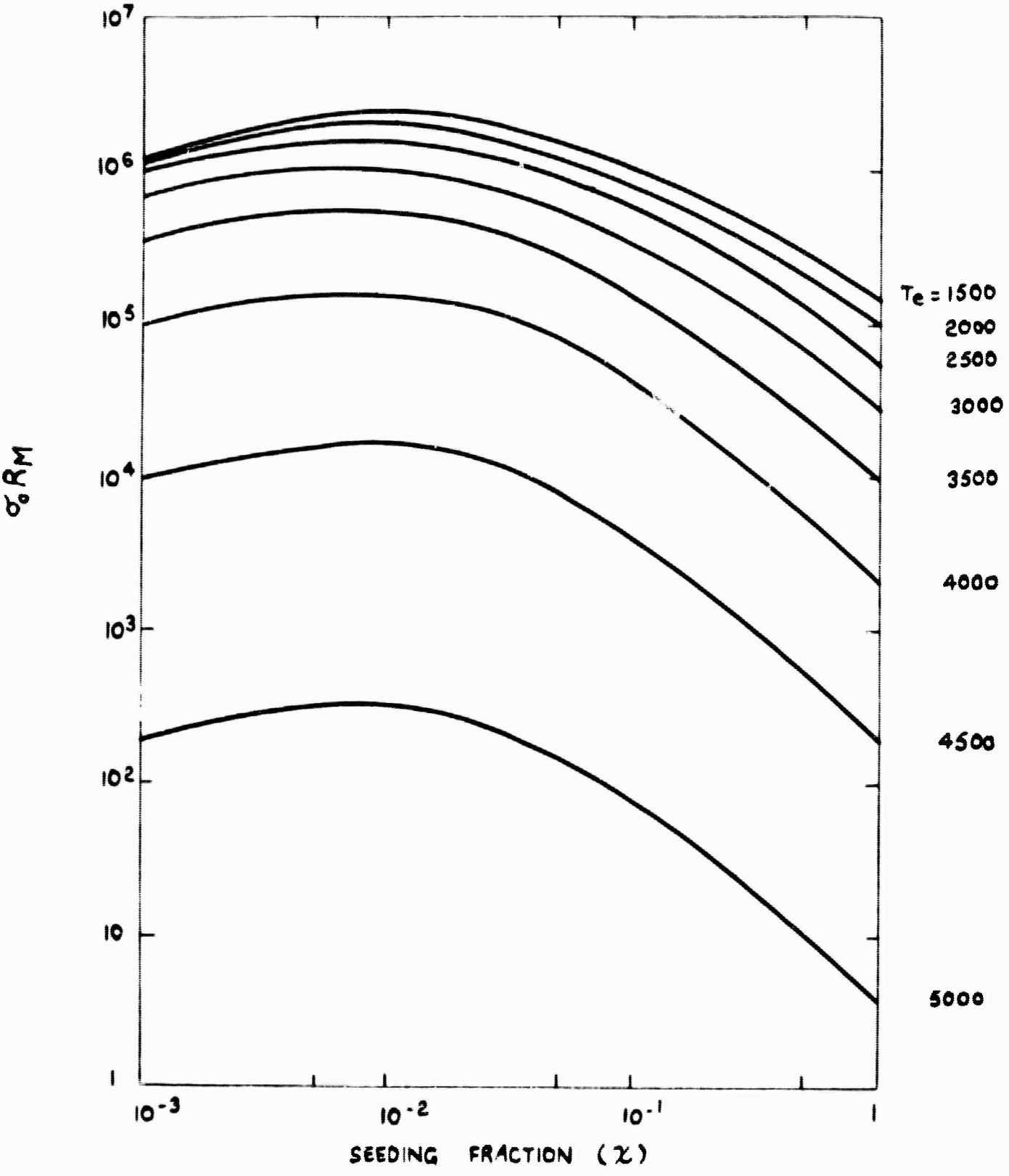

VARIATION OF $\sigma_0 R_M$ WITH SEEDING FRACTION AND ELECTRON TEMPERATURE

FIG23·10

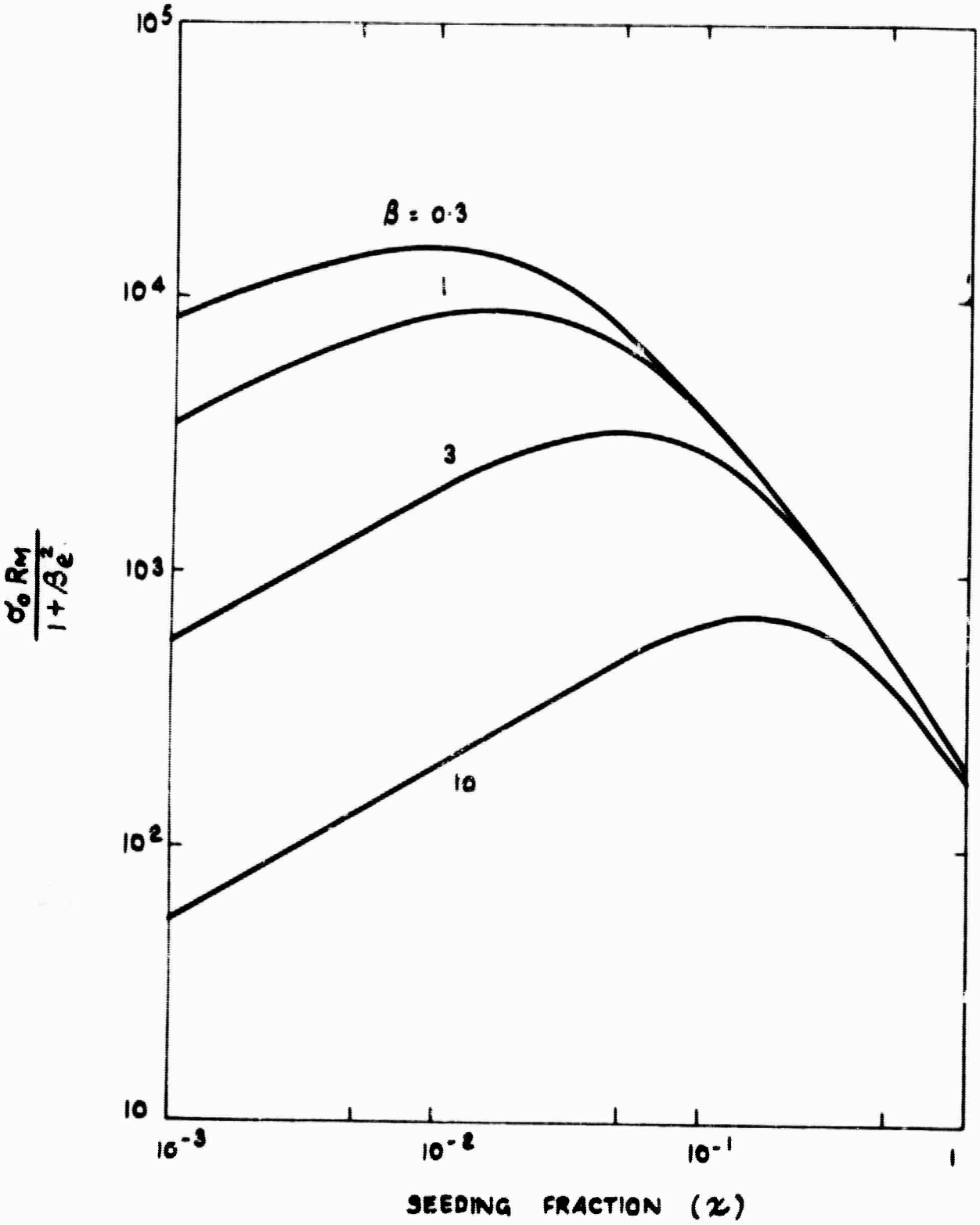

VARIATION OF $\sigma_0 R_M / 1 + \beta_e^2$ WITH SEEDING FRACTION FOR $T_0 = 2000\ ^\circ K$

FIG23·11

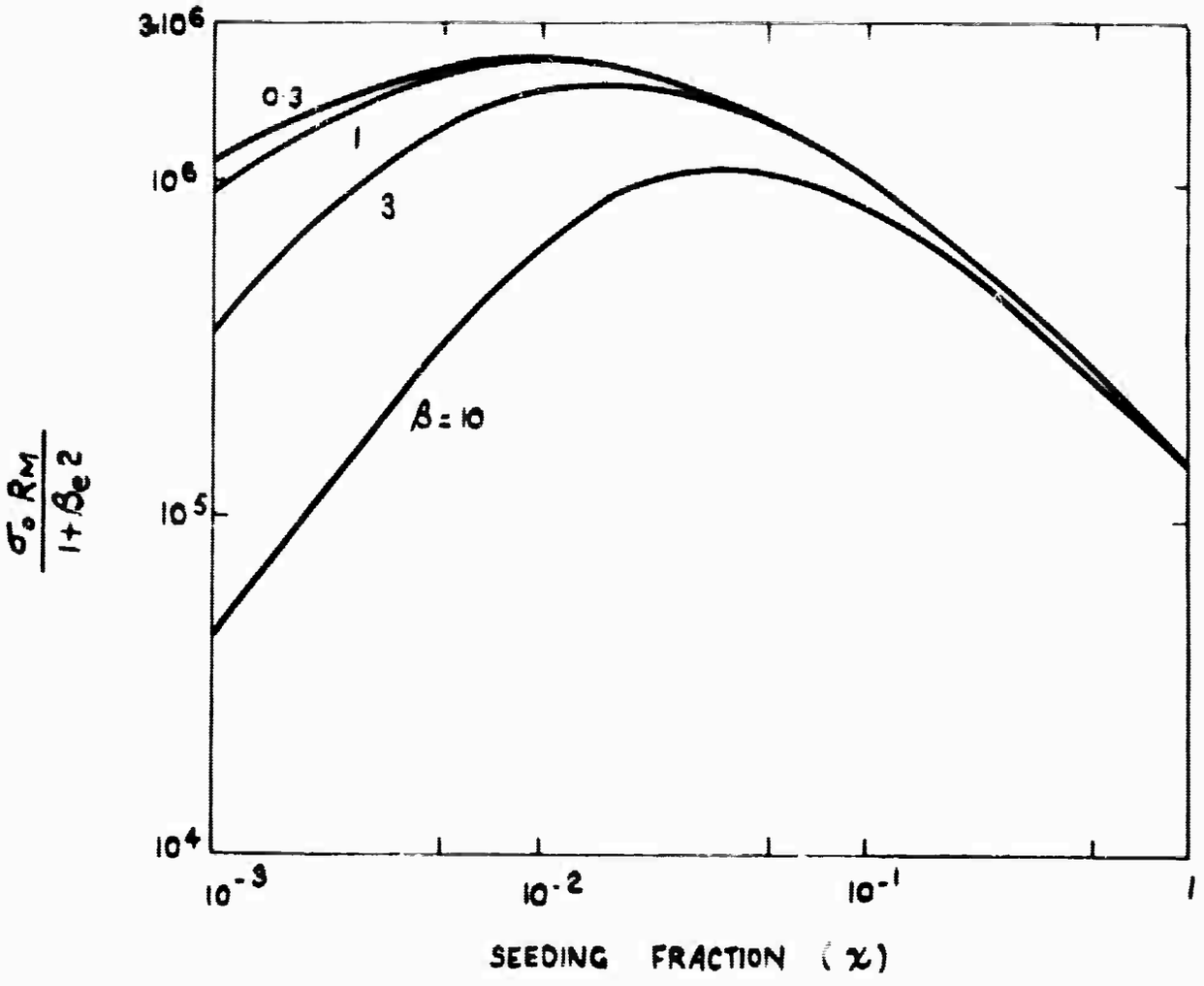

VARIATION OF $\sigma_0 R_M / 1+\beta_e^2$ WITH SEEDING FRACTION FOR T_e 5000 °K

FIG 23·12

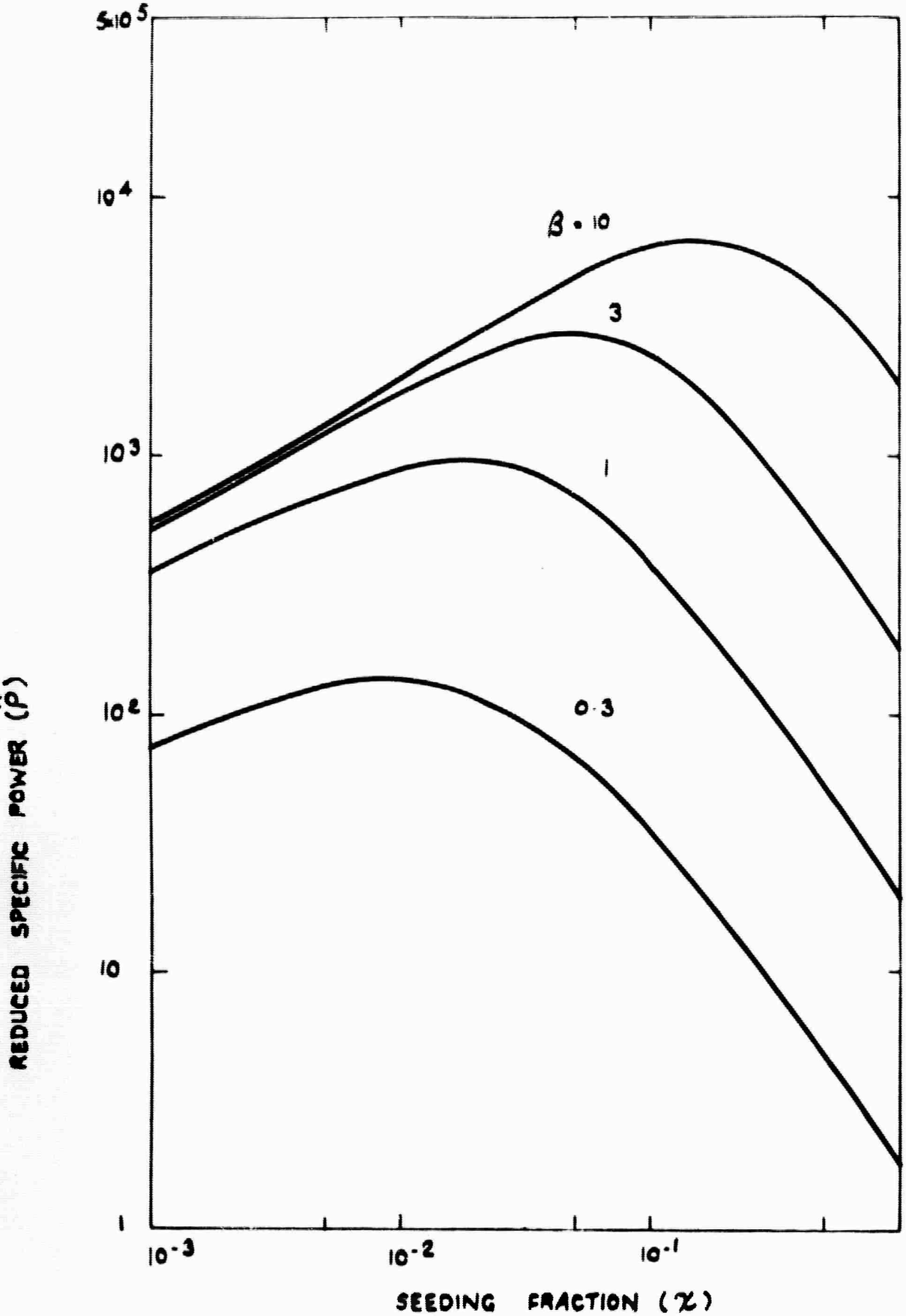

VARIATION OF REDUCED SPECIFIC POWER WITH SEEDING

FIG23·13

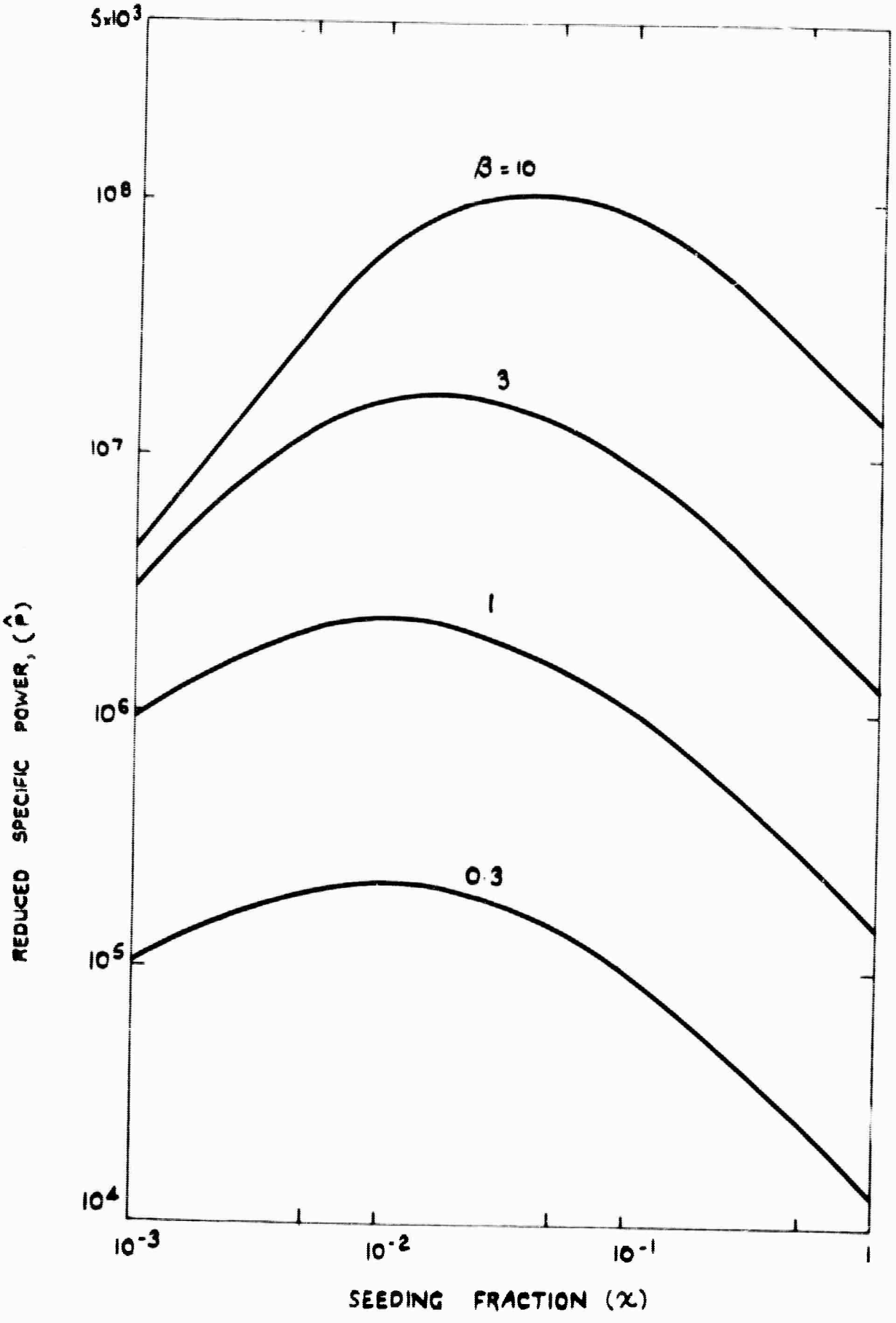

VARIATION OF REDUCED SPECIFIC POWER WITH SEEDING FRACTION FOR A SOLID ELECTRODE GENERATOR WITH T_e = 5000 °K

FIG 23·14

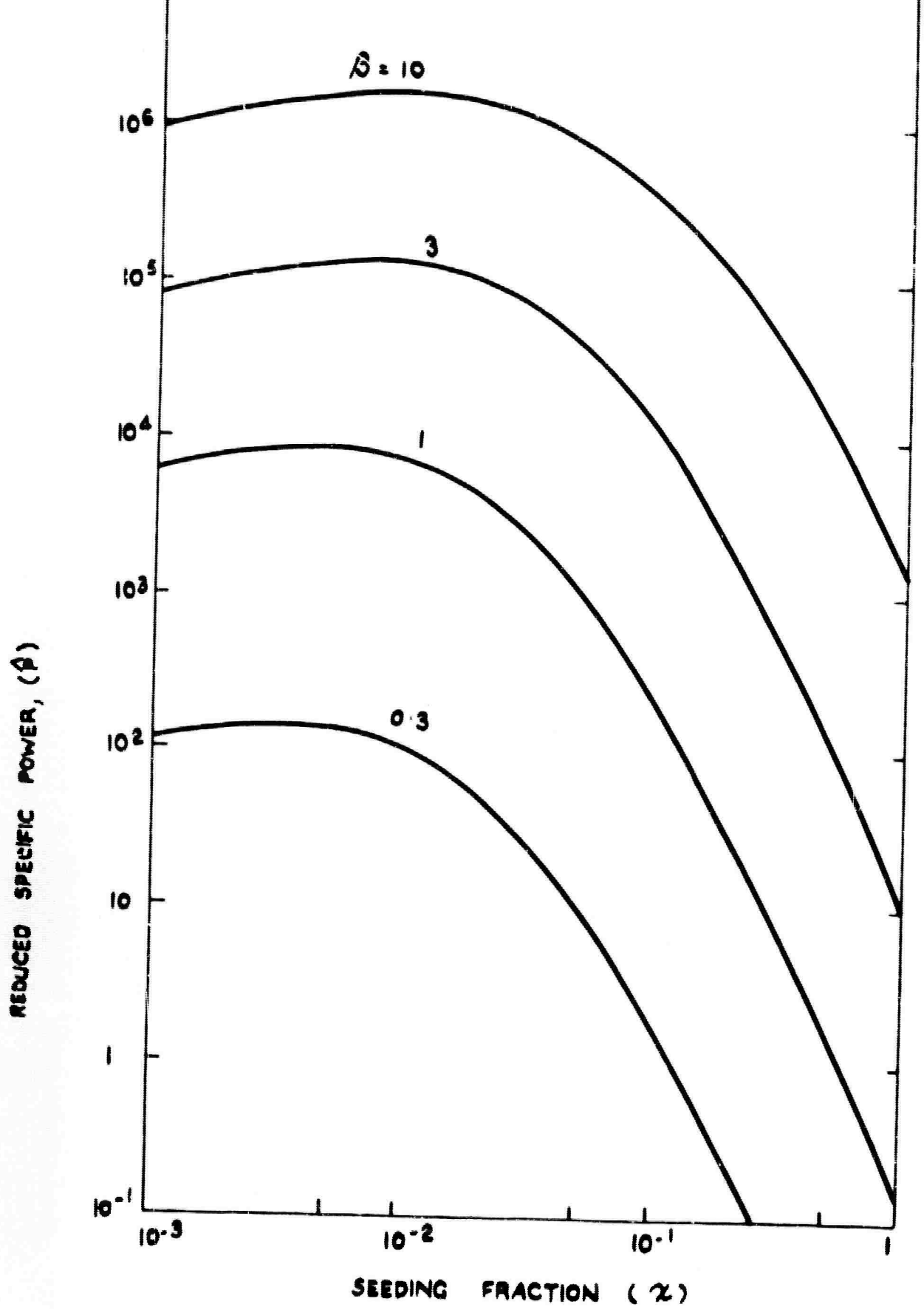

VARIATION OF REDUCED SPECIFIC POWER WITH SEEDING FRACTION IN A HALL GENERATOR WITH $T_e = 2000\ ^\circ K$

FIG23·15

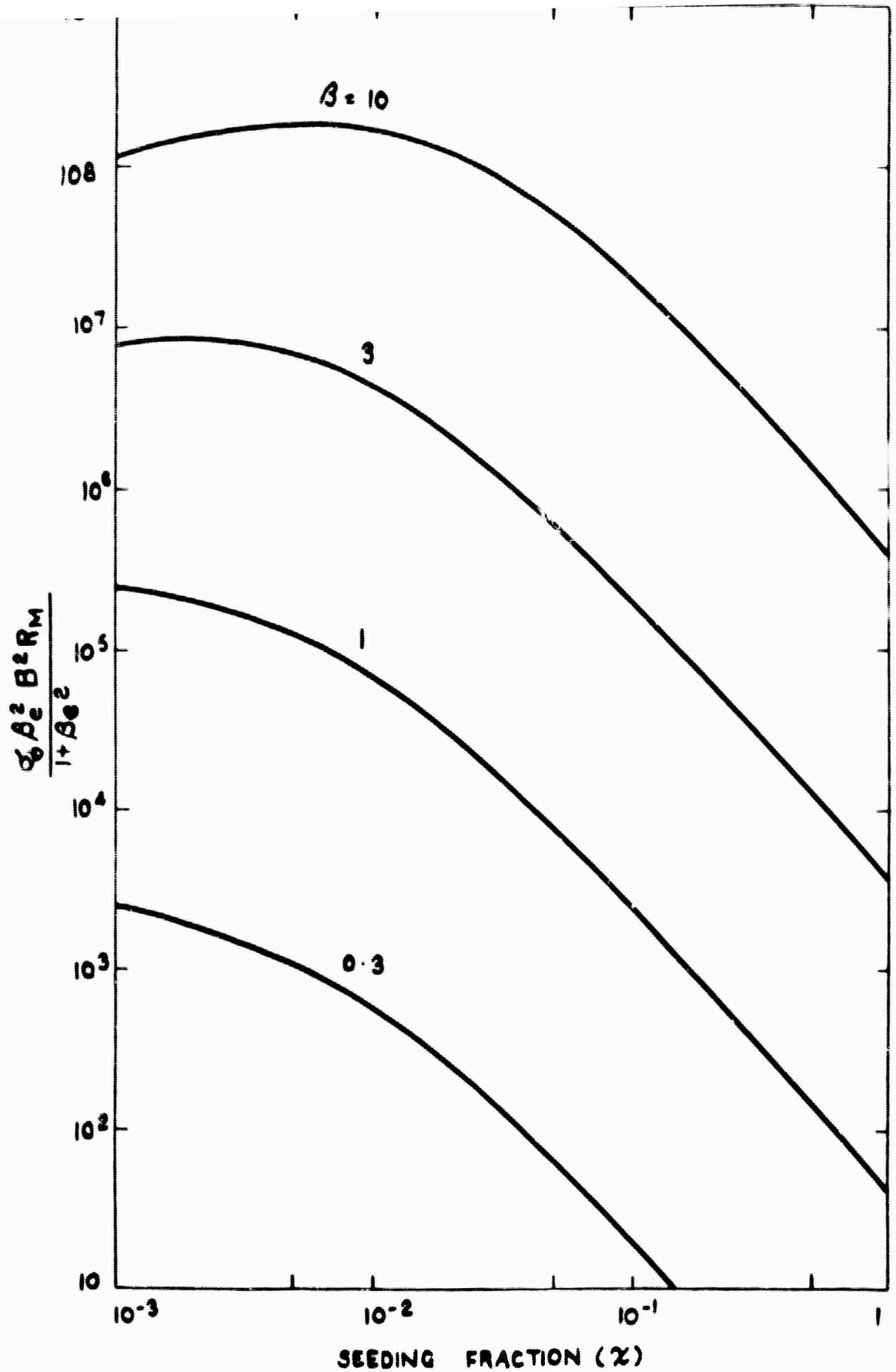

VARIATION OF REDUCED SPECIFIC POWER WITH SEEDING FRACTION IN A HALL GENERATOR WITH $T_e = 5000\ ^\circ K$

FIG 23·16

B	magnetic field strength
e	electronic charge
$f(T_e)$	defined in equation (23.5)
g	statistical weight
h	Planck's constant
k	Boltzmann's constant
m	particle mass
M	Mach number
n	particle concentration
p	static pressure
P	power density
$\hat{P}$	defined in equation (23.41)
q	collision cross section
R	gas constant
T	static gas temperature
T_e	electron temperature
U	flow velocity
v	random particle velocity
V_i	ionization potential
X	fractional ionization
α	fractional weight
β_e	Hall coefficient
γ	specific heat ratio
ϵ_o	free space permittivity
σ	electrical conductivity
ν	electron collision frequency
χ	seeding fraction

SUBSCRIPTS

a	atom
e	electron
i	ion
j	jth species
M	mixture
o	scalar
opt	optimum
P	parent gas
S	seed gas
T	total
1	means $\chi = 1$

NOZZLE FLOW

by

I.R. McNab

24.1 INTRODUCTION

Neglecting Hall effects and ion slip, the specific power (power output per unit volume, P) of a segmented electrode MPD generator is

$$P = \sigma V^2 B^2 K(1-K) \qquad \ldots\ (24.1)$$

All MPD generators built or under construction obtain the directed (flow) motion from the initial thermal energy of the gas by expansion through a convergent or convergent-divergent nozzle. In this process the static temperature and pressure fall and the velocity is increased.

When thermal equilibrium exists in the gas the scalar electrical conductivity depends on temperature as

$$\sigma = F(p,T) \exp(-D/T) \qquad \ldots\ (24.2)$$

where $F(p,T)$ is a function of static gas temperature (T) and pressure (p) and D is constant for a given gas (mixture). The temperature dependence of conductivity in the range of interest for MPD generation is determined primarily by the exponential term.

Thus, for constant magnetic field strength and loading factor, σV^2 may be maximized, giving maximum specific power. This calculation has been performed by several workers (for example, Sutton[1]) and the results indicate that the optimum Mach number for maximum σV^2 lies below unity ($0.6 \lesssim M \lesssim 0.8$) for both closed cycle (seeded inert gas) and open cycle (seeded combustion products) devices.

The basic limitations on the power obtainable from a closed cycle nuclear heated MPD generator is the working temperature of the reactor, this limits the maximum total enthalpy of the working fluid and hence the maximum value of σV^2. The working temperatures of present generation inert gas cooled reactors are not high enough to permit economic MPD power to be generated from a device working at thermal equilibrium conditions. Future developments of nuclear

reactors to yield higher working temperatures, while resulting in higher MPD generator outputs, will introduce more severe materials problems, capable only of long term and/or expensive solution. This paradox may be resolved if the electrical conductivity of the working fluid can be increased without appreciable increase of the gas temperature; high specific powers could then be obtained without severe materials problems.

Several methods of obtaining this extra thermal ionization in closed cycle MPD generators have been suggested, for example: high voltage electron beams[2], high current arcs[2], fission product β rays[2], r.f.[3], magnetically induced ionization[4] and photoionization[5]. While some of these methods will undoubtedly prove valuable, none has yet been conclusively demonstrated in an MPD generator of substantial power output.

24.2 NON-EQUILIBRIUM FLOW

A further method of producing extra thermal ionization, which has received little attention since its original suggestion (independently) by Lindley[6] and Eschenroeder and Daiber[7], is to utilize an extremely rapid expansion of the working fluid through a large area ratio nozzle to produce a high rate of fall of gas temperature. When the temperature falls rapidly in a gas many internal adjustments must be made by molecular collisions. For example, the energy of molecular vibrations must be reduced, chemical reactions must take place at a different rate, a new balance must be found between atoms and molecules, and ions and electrons must recombine to form neutral particles. All these adjustments require a large number of collisions between particles before a new equilibrium is established. If the temperature changes more rapidly than equilibrium is established, non-equilibrium flow results.

Many investigations, both theoretical[8-15] and experimental[16-19], on non-equilibrium flows have been published recently; most are concerned primarily with molecular gases or gas mixtures where vibrational and dissociative non-equilibrium are the dominant factors. This interest arises because the usual domains in which such flows are encountered relate to real or simulated (shock tube and wind tunnel) high altitude hypersonic and missile re-entry conditions in air, and similar conditions in combustion gases (for example, ignition in hypersonic ramjets). In general, the theoretical solutions of such problems are complicated. Because the changes of energy during the relaxation processes usually form a significant fraction of the total enthalpy of the gas, the quasi-one-dimensional flow equations must be

solved simultaneously with the rate equations which determine the population densities of the (many) species present. In many cases the required rate coefficients are not fully known.

The flow of a monatomic recombining gas is rather more simple since valid simplifying assumptions can be made concerning the number of species present, consequently fewer rate equations are required to characterize the flow. For example, the recombination mechanism may be assumed to be controlled by only one excited atomic state. One significant difference between a recombining atomic gas and a relaxing molecular gas is that the electron temperature may be considerably higher than the temperature of the heavy particles in the atomic gas. This leads to reduced recombination, amongst other effects.

In order to examine the consequences of non-equilibrium nozzle flow on the design and power output of MPD generators the following investigation has been carried out: while later investigations may show that this non-equilibrium effect is insignificant in large scale devices, it will undoubtedly be important in analyzing the performance of small devices, such as that at IRD.

24.3 THEORY

The most common concept of a closed-cycle nuclear fuelled MPD generator envisages the working fluid to be an inert gas seeded with small amounts of an alkali metal; flow through the expansion nozzle of this type of generator will be considered here.

The assumption of small fractional seeding, which is generally valid, enables considerable simplification to be made in the analysis since the energy involved in the ionization and recombination processes in the seed element form only a small fraction of the total enthalpy of the working fluid and thus may be neglected.

Consequently, neglecting boundary layers and shock phenomena, the quasi-one-dimensional flow equations for the parent gas only can be assumed to approximate adequately the flow along the nozzle axis. An additional simplification resulting from the assumption of small fractional seeding is that the thermodynamic properties of the mixture approximate closely those of the parent gas, and are taken as such in this analysis.

The flow will be assumed 'isentropic', so that it can be described by the following equations

continuity $$\frac{d\rho}{\rho} + \frac{dV}{V} + \frac{dA}{A} = 0 \qquad \ldots. (24.3)$$

enthalpy $$dT + \frac{VdV}{Cp} = 0 \qquad \ldots. (24.4)$$

state $$\frac{dp}{p} - \frac{d\rho}{\rho} - \frac{dT}{T} = 0 \qquad \ldots. (24.5)$$

Mach number $$^2\frac{dM}{M} - \frac{2dV}{V} + \frac{dT}{T} = 0 \qquad \ldots. (24.6)$$

and, for a process with an isentropic efficiency $\eta = {}^{dT}/_{dT'}$

$$\frac{dT}{T} - \eta\frac{\gamma-1}{\gamma}\frac{dp}{p} = 0 \qquad \ldots. (24.7)$$

where dT is the actual temperature change, dT' is the isentropic temperature change and η accounts for friction effects in the nozzle expansion.

For a given nozzle profile:

$$A = b\ f(x) \qquad \ldots. (24.8)$$

Combination of equations (24.3-8) gives

$$\frac{d\ M}{dx} = \frac{\eta M\left(1 + \frac{\gamma-1}{2} M^2\right)\ df(x)}{\left[\gamma M^2 - \eta(\gamma-1)\ M^2 - \eta\right] f(x)\ dx} \qquad \ldots. (24.9)$$

$$\frac{dT}{dx} = \frac{\eta M^2\ T\ (\gamma-1)\ \ d\ f(x)}{\left[\gamma M^2 - \eta\ (\gamma-1)\ M^2 - \eta\right] f(x)\ dx} \qquad \ldots. (24.10)$$

Solution of these equations in conjunction with the explicit relations

$$V = M\ (\gamma RT)^{\frac{1}{2}} \qquad \ldots. (24.11)$$

and

$$\rho = \frac{m}{bf(x)V} \qquad \ldots. (24.12)$$

enables the flow through the nozzle to be described if the nozzle profile and starting conditions are known.

To complete the description of non-equilibrium flow two further equations are required, describing the rate of production and loss of electrons and the electron energy balance respectively.

The most general form of the electron energy equation will include the energy interchange between electrons and heavier species (atoms and ions) by elastic and inelastic collisions, the energy gain during recombination, the energy lost during ionization, radiation and thermal conduction in the electron gas. While equations have been formulated which contain all these terms[20], they are subject to considerable doubt regarding their accuracy and require large

computers for their solution. Approximate solutions have been found inaccurate in certain regions (predicting negative temperatures[21]). In the present analysis the electron temperature is assumed equal to the gas temperature throughout the expansion. This assumption should cause the electrical conductivity at the nozzle exit (that is, inlet to the MPD generator) to be lower than the true value since higher electron temperatures would reduce the rate of recombination and give a high electron density and conductivity. (This will be partially offset by the increased electron collision frequency.)

The equation governing the rate of production and loss of electrons is obtained from the recombination and ionization rates. The recombination mechanisms considered here are three body electron-electron-ion, three body electron-atom-ion and radiative:

$$A + e^- \underset{\alpha_1}{\overset{\beta_1}{\rightleftharpoons}} A^+ + 2e^-$$

$$A + B \underset{\alpha_2}{\overset{\beta_2}{\rightleftharpoons}} A^+ + e^- + B$$

$$A \underset{\alpha_3}{\overset{\beta_3}{\rightleftharpoons}} A^+ + e^-$$

the rate coefficients being α_1, α_2, and α_3 respectively.

The corresponding ionization coefficients (β_1,β_2 and β_3) are obtained from the recombination coefficients using the condition that the rates must be equal at equilibrium, thus

$$\beta_1 = \alpha_1 \left(\frac{n_e^2}{n_A}\right)_s \quad \text{etc.}$$

The net rate of production of electrons per unit volume

$$S = \beta_1 n_A n_e + \beta_2 n_A n_B + \beta_3 n_A - \alpha_1 n_e^3 - \alpha_2 n_e^2 n_B - \alpha_3 n_e^2$$

then becomes

$$S = n_e^2 (\alpha_1 n_e + \alpha_2 n_B + \alpha_3) \left[\left(\frac{n_e^2}{n_A}\right)_s \frac{n_{A_2}}{n_e} - 1 \right] \quad \ldots\ (24.13)$$

The net rate of production of electrons per unit volume in a volume V^1 containing N_e ($\equiv n_e V^1$) electrons is

$$S = \frac{1}{V^1} \frac{dN_e}{dt} = \frac{1}{V^1} \frac{d(n_e V^1)}{dt}$$

For a moving system and when the fractional ionization and seeding fraction are small, this becomes

$$S = \rho \frac{d\left(n_e/\rho\right)}{dt} = \frac{\chi_\rho V}{m_p} \frac{dX}{dx} \quad \ldots\ (29.14)$$

Using this expression for S, equation (24.13) becomes

$$\frac{dX}{dx} = \frac{m_p n_e^2}{\rho V X} \left(\alpha_1 n_e + \alpha_2 n_B + \alpha_3\right)\left[\left(\frac{n_e^2}{n_A}\right)_s \frac{n_A}{n_e^2} - 1\right] \quad \ldots\ (24.15)$$

Simultaneous solution of equations (24.9), (24.10) and (24.15), in conjunction with equations (24.11), (24.12) and the relation

$$n_e = X \rho V/m_\rho \quad \ldots\ (24.16)$$

enables the flow through the nozzle and variation of electron density to be described when the nozzle area is specified as a function of distance and the starting conditions are known (See Appendix 24.A).

The scalar electrical conductivity may then be obtained from

$$\sigma = \frac{n_e e^2}{m_e \nu_e} \quad \ldots\ (24.17)$$

where

$$\nu_e = v_e \Sigma_j q_{ej} n_j \quad \ldots\ (24.18)$$

and the cross sections employed are

$$q_{e\text{-}He} = 6.1.10^{-20}\ m^2$$

$$q_{e\text{-}Cs} = 310.10^{-20}\ m^2$$

$$q_{e\text{-}Cs^+} = \frac{1.84.10^{-6}\ n_e \ln_e}{T^{3/2}} \left[\frac{1.24.10^7 T^{3/2}}{n_e^{\frac{1}{2}}}\right]$$

from references 22, 23 and 24 respectively.

This value of conductivity may then be compared with the equilibrium value of conductivity obtained when n_e is determined from the Saha equation:

$$\left(\frac{n_e^2}{n_A}\right)_s = CT^{3/2} \exp\left(-D/T\right) \quad \ldots\ (24.19)$$

where

$$C = \frac{2\pi m_e k}{h^2}^{3/2} \frac{g_e g_i}{g_a} \quad , \quad D = eV_i/k$$

are constant for a given gas (mixture).

24.4 CALCULATIONS

The theory outlined above has been used to construct a computer programme to determine the electrical conductivity through a nozzle. The calculations have been performed for the operating conditions of the MPD generator under construction at IRD. The working fluid is helium seeded with one atomic percent of cesium; the appropriate data are given in Table 24.1.

The IRD MPD generator is designed to operate supersonically and consequently has a convergent-divergent nozzle of which two sides are parallel and two are axially symmetric. In equation (24.8), b is twice the width of the nozzle and f(x) is the height from the centre line. The nozzle profile (Fig24.1) is composed of three regions, being cosinusoidal at inlet and exit and circular near the throat:

$$x < a_1 \quad , \quad f(x) = b_1 \cos(b_2 x) + b_3 \qquad \ldots\ (24.20)$$

$$a_1 < x < a_2 \quad , \quad f(x) = b_4 - \tfrac{1}{2}\left[b_5 - 4(x^2 - b_6 x + b_7) \right]^{\frac{1}{2}} \qquad \ldots\ (24.21)$$

$$x > a_2 \quad , \quad f(x) = b_8 \cos\left[b_9 \left(2 - \frac{x}{b_{10}}\right) \right] + b_{11} \qquad \ldots\ (24.22)$$

Difficulties have been encountered in the solution of the equations because of this profile: where the curves join, discontinuities in the second derivative exist and these cause unsmooth variation in the theoretical flow, for example in the derivative of the Mach number, temperature, etc. In practice, such variations will probably be smoothed out by boundary layers.

Additional difficulties are encountered in the solution of the differential equations for dM/dx and dT/dx since these become indeterminate near M=1 (for η=1). These have been overcome by the use of equation (24.A6) near the throat. Mach number is substituted into this, giving the nozzle area, use of equations (24.8) and (24.21) then enables nozzle distance to be obtained. Thus all the thermodynamic and flow parameters are known at each point along the throat. Initial versions of the programme extrapolated electron density across this throat region, however it was later found more accurate to extrapolate fractional ionization (so that dX/dx remains constant). The region over which this extrapolation is performed is a small fraction of the nozzle length and appreciable error is unlikely to be incurred.

The isentropic efficiency in the present calculations is assumed to be unity to the throat and 0.9 afterwards.

24.5 RESULTS AND DISCUSSION

Figures 24.2 to 24.8 show typical results obtained for two sets of data (T_o = 1500° and 2000°K, p_o = 1 atm) in a helium-cesium mixture. (Other data for these results being given in Table 24.1.)

Figure 24.2 shows the variation of Mach number through the supersonic nozzle; as equation (24.A6) indicates, the Mach number depends only on the profile of the nozzle provided the ideal conditions are obeyed. As with most of the results given here, rapid variation of the Mach number in the region of the nozzle throat (x = 1.905 cm) is evident.

Figure 24.3 shows the variation of static gas temperature through the nozzle for the two sets of data presented here. For both these cases the static gas pressure at the nozzle exit is 0.05 atm, consequently, if equilibrium conditions (as given by Saha's equation[25] at the gas temperature) were obeyed, the electron concentration at the nozzle exit would be very low. That is, the conditions at the generator inlet would be far from the optimum (found by maximizing σV^2) mentioned in Section 24.1. The non-equilibrium electron concentrations (found from equation (24.15) and (24.16)) is shown in Figure 24.4, and while the concentrations drop on expansion, in both cases the nozzle exit value is not more than an order of magnitude less than the inlet value.

Figures 24.5 and 24.6 compare the equilibrium (as given by Saha) and non-equilibrium (as found using the values shown in Fig. 24.4) electrical conductivities as a function of the distance through the nozzle for T_o = 1500° and 2000°K respectively. (Note the ordinate scale in both cases.) The non-equilibrium conductivity for T_o = 1500°K exhibits a slight but definite rise through the nozzle. This occurs because, even though the electron density decreases, the opposing effect caused by the decrease in temperature has a greater effect. In Fig. 24.6 the two effects approximately cancel and the non-equilibrium electrical conductivity is sensibly constant. In both cases the equilibrium conductivity drops rapidly (near and after the throat region) to very low values.

The effects of the non-equilibrium conductivity on the power output of an MPD generator are shown in Figs. 24.7 and 24.8 where the quantities σV^2 are shown as a function of Mach number in the nozzle. For a segmented electrode generator, neglecting Hall and ion slip effects

$$\sigma V^2 = \frac{P}{B^2 K(1-K)}$$

hence if B = 2 webers/m^2 and K = 0.5, the quantity σV^2 is numerically equal to the specific power (in MWe/m^3).

For comparison the specific powers obtainable using equilibrium conditions are shown in both Figures. These equilibrium power densities exhibit the previously mentioned maximum at a Mach number of about 0.5. The non-equilibrium power densities, however, increase monotonically with Mach number to values greater than 10^6 and 10^8 MWe/m^3 for T_o = 1500° and 2000°K respectively. The ratio of non-equilibrium to equilibrium specific power at the nozzle exit in the two cases are about 10^{10} and 10^8. A more practical comparison of equilibrium and non-equilibrium specific power at nozzle exit, with the equilibrium specific power at the optimum Mach number: these ratios are about 45 and 20 for T_o = 1500° and 2000°K respectively, that is, they are worthwhile increases. Comparison of Figs. 24.7 and 24.8 shows that the non-equilibrium power density at nozzle exit for T_o = 1500°K is approximately the same as the equilibrium power density at the optimum Mach number for T_o = 2000°K. That is, operation of a nozzle to give semi-frozen flow (as far as electrical conductivity is concerned) permits the same power density to be achieved at a stagnation temperature about 500°K lower than for the equilibrium case (for these particular conditions).

The recombination coefficients used in the evaluation of equation (24.15) are[26]:

three body electron-electron-ion

$$\alpha_1 = 1.1.10^{-20}\ T^{-9/2}$$

three body electron-atom-ion (Thomson coefficient)

$$\alpha_2 = 6.10^{-34}\ T^{-5/2}$$

and the radiative recombination coefficient

$$\alpha_3 = 3.10^{-16}\ T^{-3/4}$$

Of these, for the conditions examined in the present calculations α_1 has the greatest effect, thus the energy loss by radiation implied by the inclusion of the radiative process is not significant.

In the immediate future further calculations will be performed using the present computer programme, with slight modifications (for example using the plasma mixture gas constant). It is hoped that a more refined calculation including the electron energy balance will eventually be undertaken, although, as mentioned in Section 24.3, the calculations will be more complicated than present ones.

REFERENCES

1 SUTTON, G.W. The theory of magnetoplasmadynamic power generators. G.E. Space Sciences Laboratory Report R62 SD990, December 1962

2 STERNGLASS, E.J., TSU, T.C., GRIFFITH, G.L. and WRIGHT, J.H. MHD power generation by non-thermal ionization and its application to nuclear energy conversion. Third Symposium on the Engineering Aspects of MHD. Rochester, March 28 1962

3 GOURDINE, M.C. Non-equilibrium r.f. plasmas for MPD energy conversion. Magnetoplasmadynamic electrical power generation conference. Newcastle, 6 September 1962. I.E.E. Conference Report Series No.4, 1963

4 KERREBROCK, J.L. Conduction in gases with elevated electron temperature. Second Symposium on the Engineering Aspects of MHD. Philadelphia, 9 March 1961. Columbia U.P. New York and London 1962

5 MAITLAND, A. A criterion for assessing methods of producing non-equilibrium ionization. Magnetoplasmadynamic electrical power generation conference, Newcastle, 9 September 1962. I.E.E. Conference Report Series No.4, 1963

6 LINDLEY, B.C. Magnetoplasmadynamic power generation experiment. C.A. Parsons & Co. Ltd, NRC Report 60-92 September 1960

7 ESCHENROEDER, A.Q. and DAIBER, J.W. Ionization non-equilibrium expanding flows. Paper presented at ARS Meeting, 5-8 December 1960. Washington

8 LIGHTHILL, M.J. Dynamics of a dissociating gas. J. Fluid Mech. Vol 2, p. 1, 1957

9 FREEMAN, N.C. J. Fluid Mech. Vol 4, p. 4, 1958

10 ESCHENROEDER, A.Q. BOYER, D.W. and HALL, J.G. Non-equilibrium expansions of air with coupled chemical reactions. Phys. Fluids, Vol 5, p. 615, 1962

11 TREANOR, C.E. and MARRONE, P.V. Effect of dissociation on the rate of vibrational relaxation. Phys. of Fluids, Vol 5, p. 1022, 1962

12 STOLLERY, J.L and SMITH, J.E. A note on the variation of vibrational temperature along a nozzle. J. Fluid Mech. Vol 13, p. 225, 1962

13 BLYTHE, P.A. Non-equilibrium flow through a nozzle. J. Fluid Mech. Vol 17, p. 126, 1963

14 APPLETON, J.P. Structure of a Prandtl-Meyer expansion in an ideal dissociating gas. Phys. Fluids. Vol 6, p. 1057, 1963

15 ESCHENROEDER, A.Q. Entropy changes in non-equilibrium flows. Physics of Fluids, Vol 6, p. 1408, 1963

16 PETSCHEK, H. and BYRON, S. Approach to equilibrium ionization behind strong shock waves in Argon. Ann. of Phys. Vol 1, p. 270, 1957

17 WILSON, J. An experiment to measure the recombination rate of oxygen. J. Fluid Mech. Vol 15, p. 497, 1963

18 CLAYDEN, W.A. and COLEMAN, P.L. Distribution of electron density and temperature in an arc heated low density wind tunnel. RARDE Report 57/63, October 1963

19 CURTIS, J.T., BURKE, A.F. and HAYMAN, R.A. An analytical and experimental study of the ionized flow field about a hemisphere cylinder and its effect on the radiation patterns of a slot antenna. Cornell Aeronautical Lab. Inc. Report AFCRL 63-339, August 1963

20 WILSON, J.A. University of Southampton, Ph.D. Thesis, 1962

21 BRAY, K.N.C. and WILSON, J.A. Electron-ion recombination in Argon. Magnetoplasmadynamic electrical power generation conference. Newcastle, 6 September 1962. I.E.E. Conference Report Series No.4, 1963

22 HINNOV, E. and HIRSCHBERG, J.G. Electron-ion recombination in dense plasmas. Phys. Rev. Vol 125, p. 795, 1962

23 This report, Chapter 22

24 SPITZER, L. JR. Physics of fully ionized gases. Interscience Tracts on Physics and Astronomy. No.3, 1956

25 SAHA, M.N. and SAHA, H.K. A treatise on modern physics. Vol 1. The Indian Press Ltd. Allahabad and Calcutta 1934

26 McNAB, I.R. and ROBINSON, C.A. Electron-ion recombination in MPD generators. Proc. MPD Power Generation Conference, Newcastle, September 1962. I.E.E. Conference Report Series No.4 1963

27 SHAPIRO, A.H. The dynamics and thermodynamics of compressible fluid flow. Ronald Press Co., New York 1953

APPENDIX 24.A

STARTING CONDITIONS

The procedure used here to obtain the starting values for the nozzle is as follows:

From the equations of state $p = \rho RT$, ... (24.A1)

continuity $m = \rho AV$, ... (24.A2)

enthalpy $T_o = T + \frac{V^2}{2Cp}$, ... (24.A3)

and Mach number $M^2 = \frac{V^2}{\gamma RT}$ .... (24.A4)

the criterion for M=1 to be achieved at the throat of a convergent-divergent supersonic nozzle working isentropically is

$$\frac{m\, T_o^{1/2}}{p_o} = \frac{A^*}{Cp^{\frac{1}{2}}} \left(\frac{2}{\gamma + 1}\right)^{\gamma/\gamma - 1} \left[\frac{\gamma + 1}{\gamma - 1}\right]^{1/2} \frac{\gamma}{\sqrt{2}} \qquad \text{.... (24.A5)}$$

Thus for a given nozzle throat area and given gas, selection of the inlet stagnation temperature and pressure detmines the mass flow.

From the relation given by Shapiro[27] for the isentropic flow of a perfect gas

$$\frac{A}{A^*} = \frac{1}{M}\left[\frac{2}{\gamma + 1}\left(1 + \frac{\gamma - 1}{2} M^2\right)\right]^{\frac{\gamma + 1}{2(\gamma - 1)}} \qquad \text{.... (24.A6)}$$

The inlet Mach number may be obtained from the nozzle inlet area.

Knowing the inlet Mach number the static temperature and pressure may easily be determined from the above equations, and the remainder of the entrance conditions follow.

TABLE 24.1

DATA USED IN CALCULATIONS (MKS UNITS)

$a_1 = 1.635592232.10^{-2}$
$a_2 = 1.98069310.10^{-2}$
$b_1 = 9.46798320.10^{-3}$
$b_2 = 1.3962884.10^{2}$
$b_3 = 9.5820168.10^{-3}$
$b_4 = 6.0833.10^{-3}$
$b_5 = 1.48026156.10^{-4}$
$b_6 = 3.81.10^{-2}$
$b_7 = 3.85392939.10^{-4}$
$b_8 = 3.99766848.10^{-3}$
$b_9 = 1.28817056$
$b_{10} = 2.54.10^{-2}$
$b_{11} = 2.35233152.10^{-3}$

$b = 0.0762$
$C = 2.415.10^{21}$
$D = 4.518.10^{4}$
$C_p = 5.2285.10^{3}$
$R = 2.075.10^{3}$
$\gamma = 1.658$
$X = 10^{-2}$
$\eta = 0.9$ for $\alpha > 0.0195$

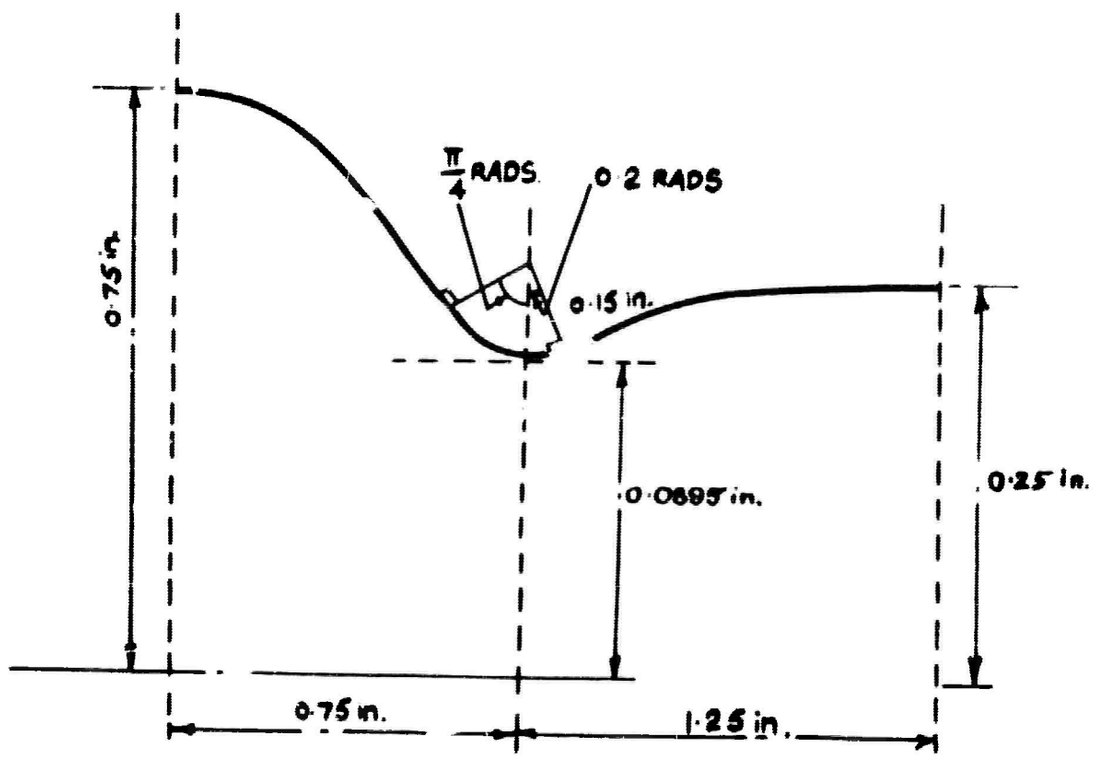

NOZZLE PROFILE FOR IRD GENERATOR
(ASSEMBLY I)
NOT TO SCALE

FIG 24.1

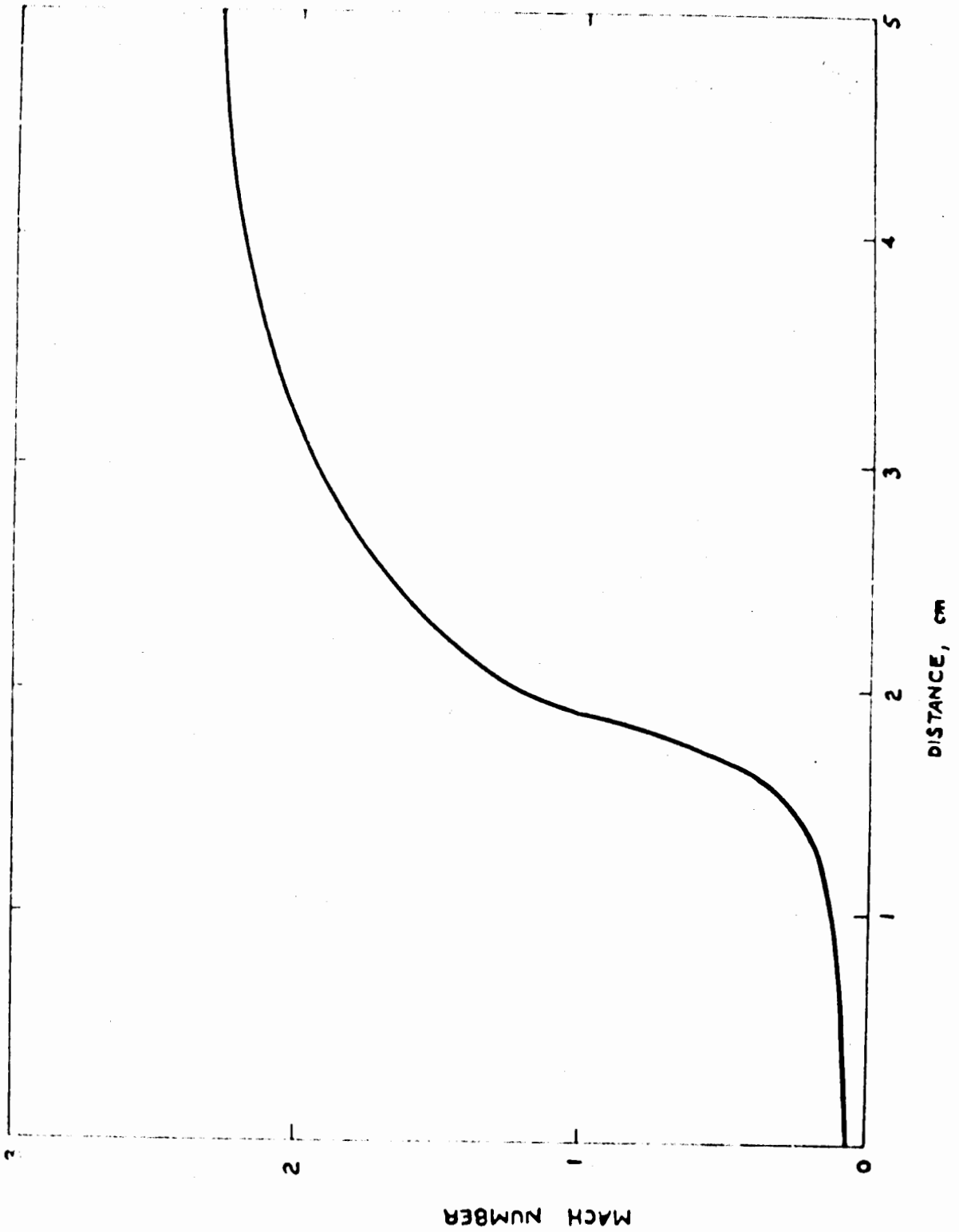

In.

VARIATION OF MACH NUMBER THROUGH SUPERSONIC NOZZLE

24.1

FIG24·2

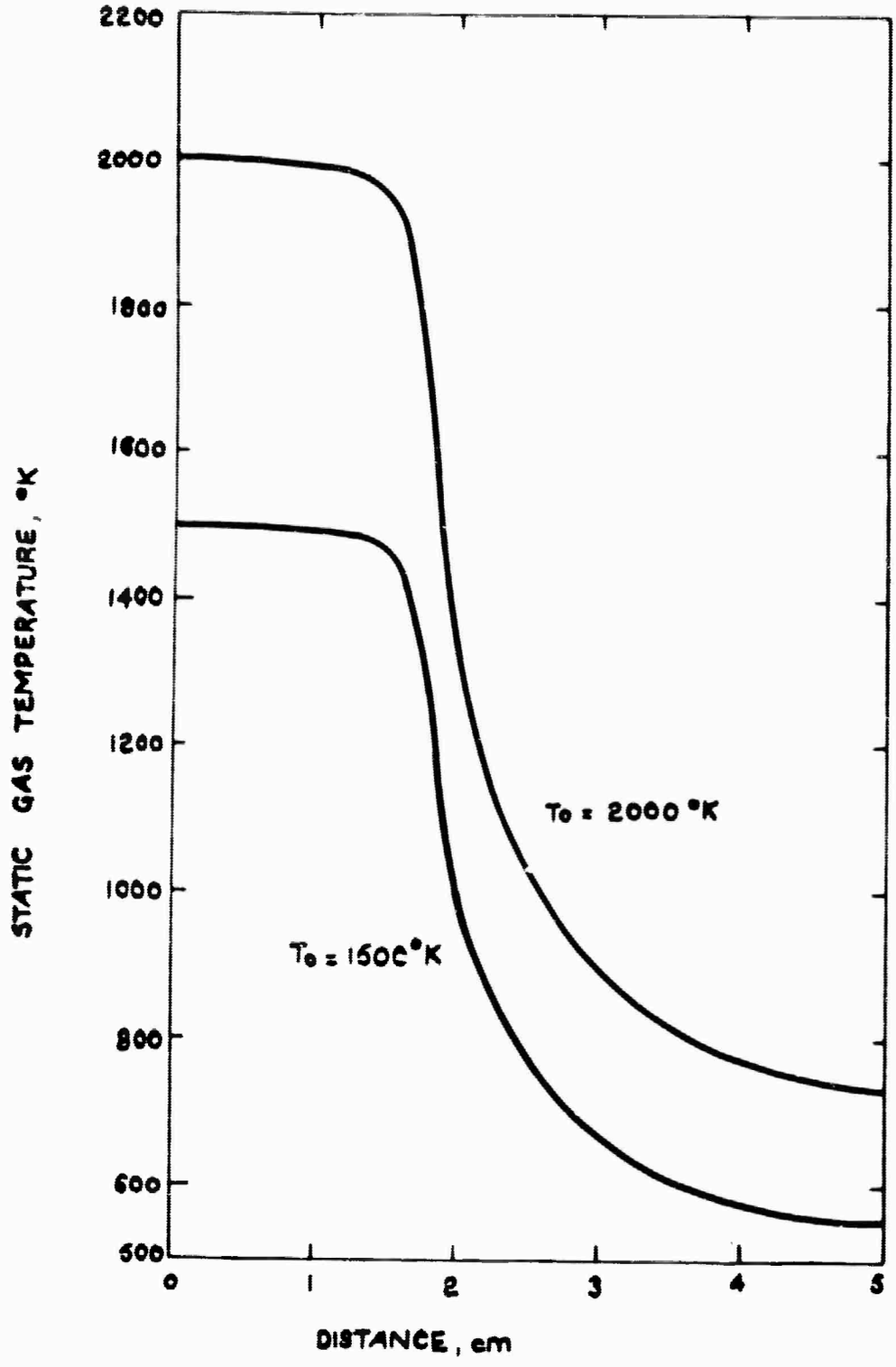

VARIATION OF STATIC GAS TEMPERATURE IN SUPERSONIC NOZZLE

FIG24·3

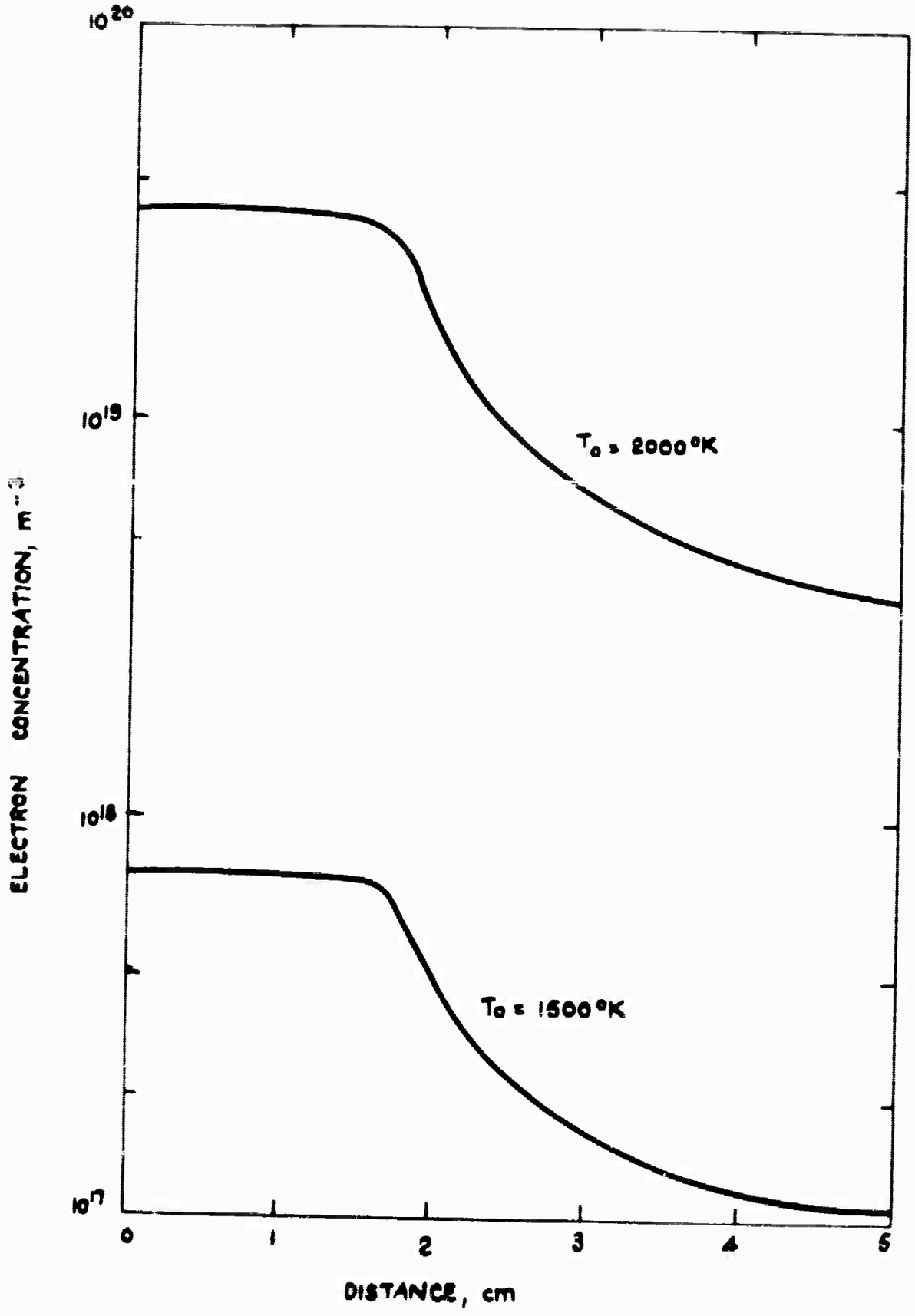

VARIATION OF NON-EQUILIBRIUM CONCENTRATION IN SUPERSONIC NOZZLE

FIG24·4

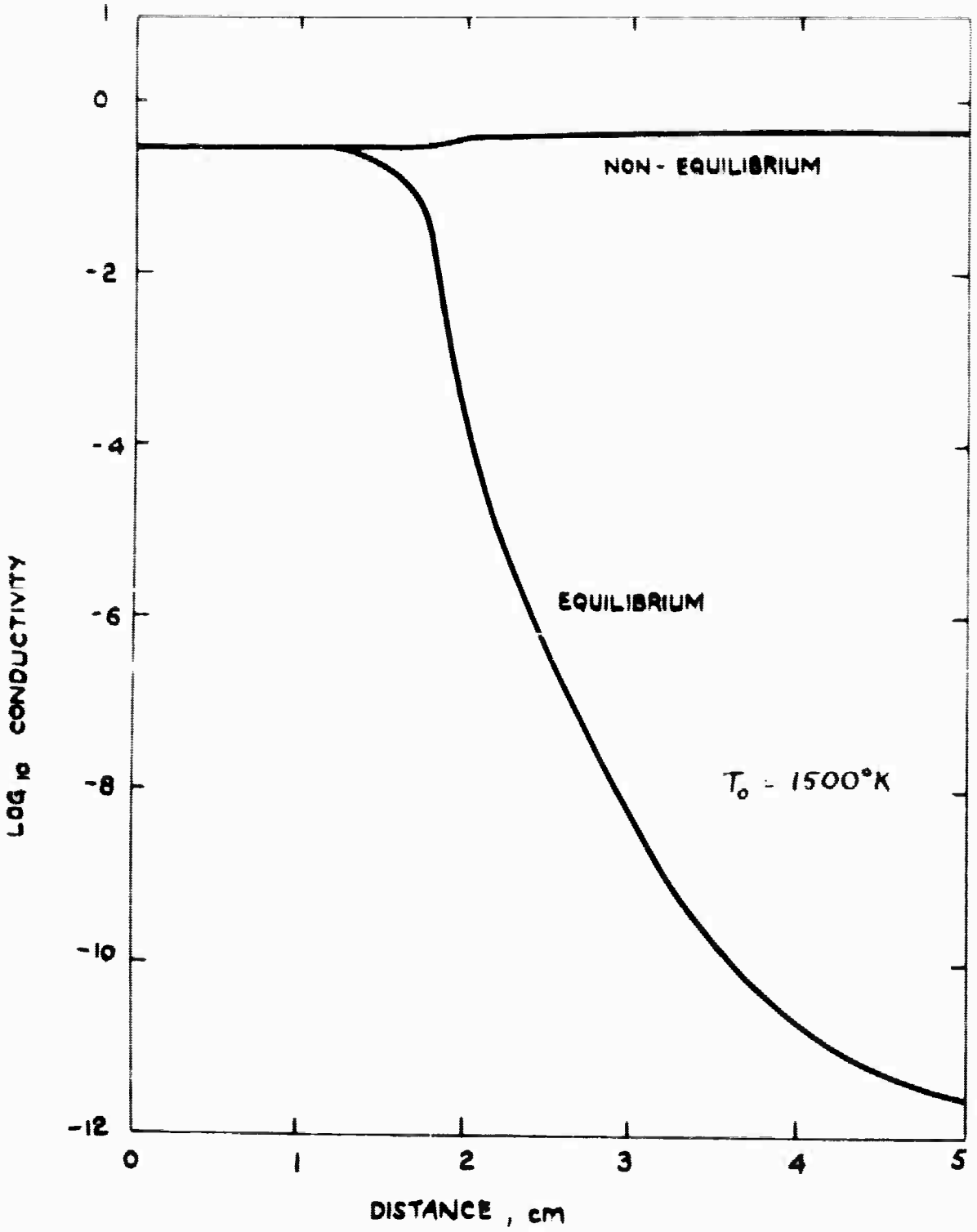

VARIATION OF ELECTRICAL CONDUCTIVITY WITH DISTANCE THROUGH NOZZLE FOR EQUILIBRIUM AND NON-EQUILIBRIUM FLOWS

FIG24·5

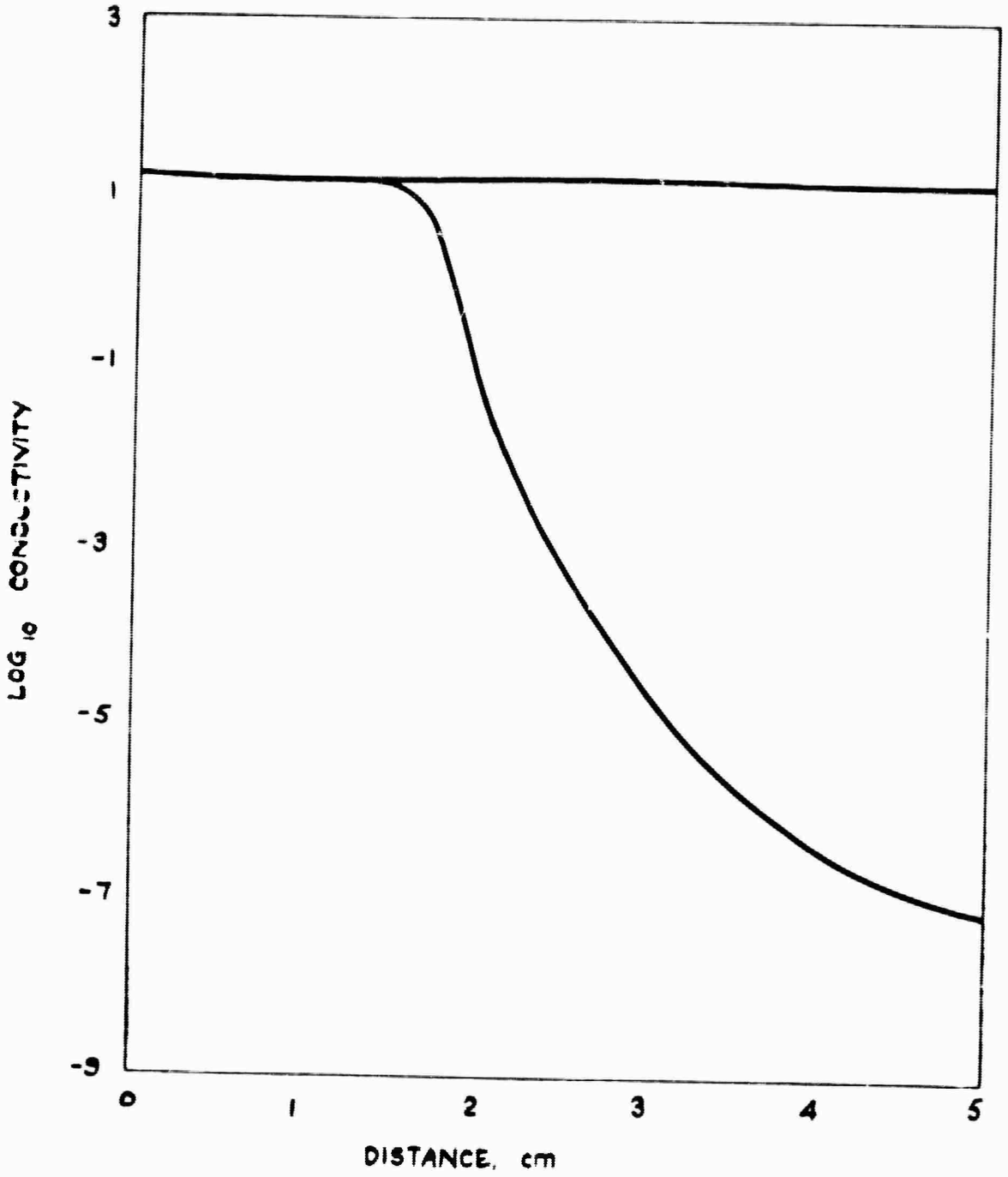

VARIATION OF ELECTRICAL CONDUCTIVITY WITH DISTANCE THROUGH NOZZLE FOR EQUILIBRIUM AND NON-EQUILIBRIUM FLOWS (T_o = 2000°K)

FIG 24.6

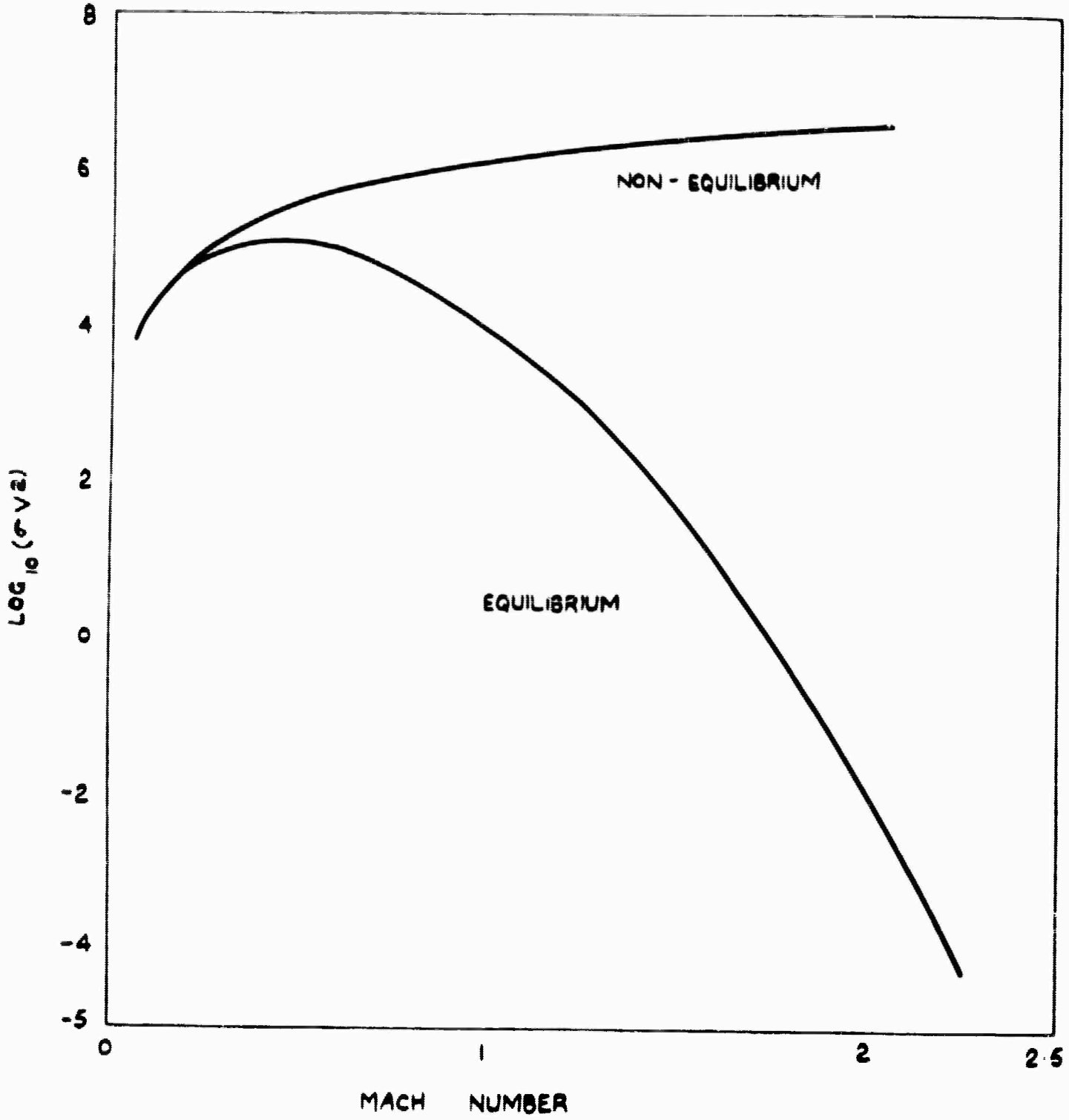

VARIATION OF σV^2 WITH MACH NUMBER FOR EQUILIBRIUM AND NON-EQUILIBRIUM FLOWS ($T_0 = 1500°K$)

FIG 24.7

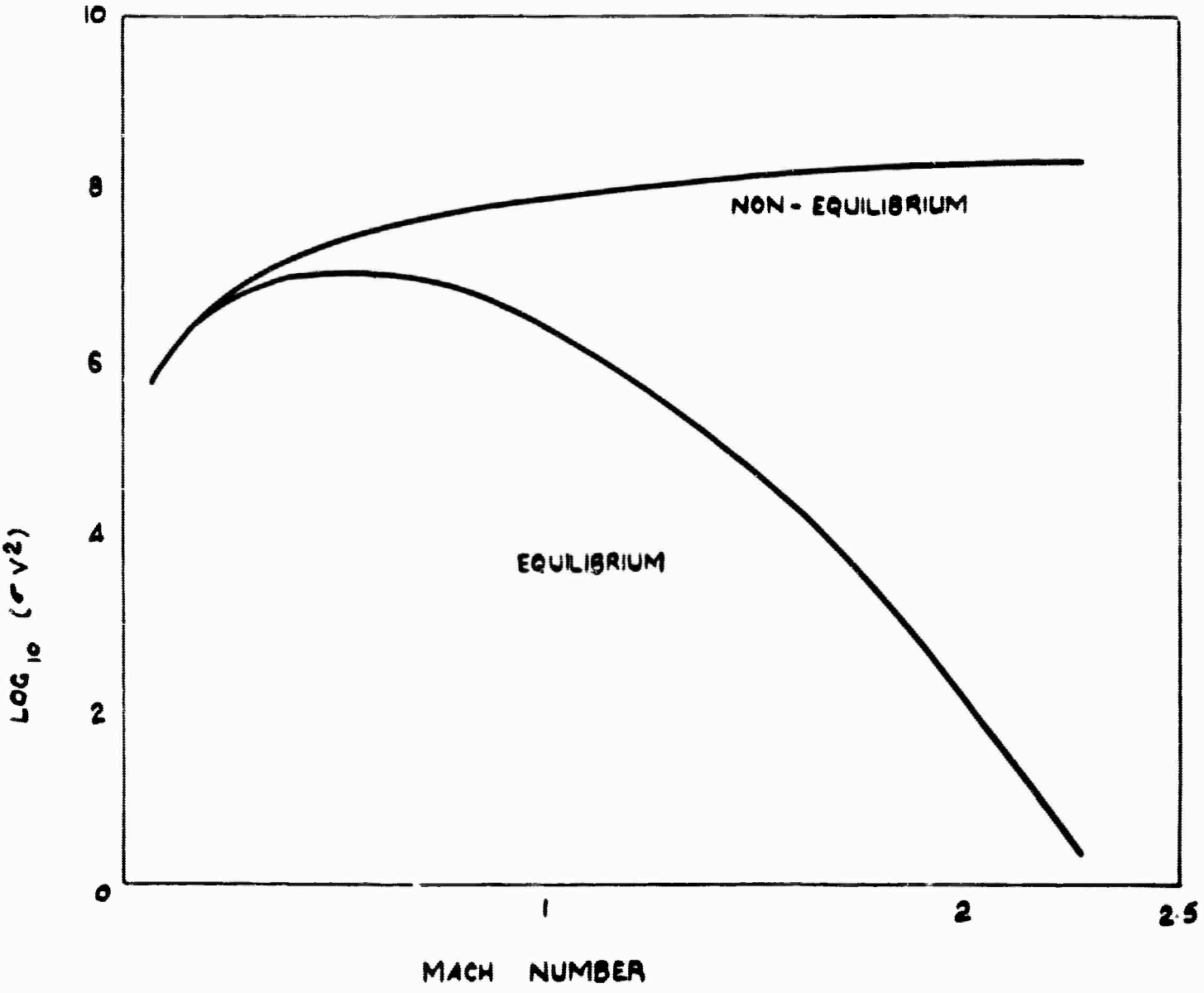

VARIATION OF σV^2 WITH MACH NUMBER FOR EQUILIBRIUM AND NON-EQUILIBRIUM FLOW ($T_0 = 2000°K$)

FIG 24.8

NOMENCLATURE

A		nozzle cross sectional area
A^*		sonic throat area
$a_{1,2}$		see equations (24.20), (24.21) and (24.22)
B		magnetic field strength
b		twice nozzle breadth
b_{1-11}		see equations (24.20), (24.21) and (24.22)
C		constant in Saha equation (24.19)
C_p		specific heat at constant pressure
D		eVi/k
e		electronic charge
F	=	$F(p,T)$, see equation 24.2
f	=	$f(x)$ - half nozzle height
$g_{e,i,a}$		atomic statistical weight
h		Planck's constant
K		loading factor
k		Boltzmann's constant
M		Mach number
m		particle mass
n		particle concentration
P		specific power
p		static pressure
q		collision cross section
R		gas constant
S		net rate of production of electrons
T		static gas temperature
T_o		stagnation temperature
V		flow velocity
V_i		ionization potential
v		random particle velocity
X		fractional ionization
α		recombination coefficient
β		ionization coefficient
γ		specific heats ratio
σ		electrical conductivity
ρ		gas density

η	isentropic efficiency
X	seeding fraction
ν	collision frequency

Subscripts

A	seed gas (cesium)
B	parent gas (helium)
S	denotes Saha equilibrium

BLANK PAGE

FLOW PROCESSES IN MPD GENERATORS

by

I.R. McNab

25.1 INTRODUCTION

An investigation of some of the processes occurring in a magnetoplasmadynamic (MPD) channel to assess their effect on flow parameters has been attempted, quantitative estimates being obtained for the IRD experiment. The first test section of the IRD generator (described fully elsewhere[1]) differs from other MPD devices in several respects: the working fluid is very pure ($\lesssim$ 30 ppm total gaseous impurity) inert gas (helium) seeded with up to three atomic percent of an alkali metal (cesium); the accelerating nozzle is designed for a high (20:1) pressure ratio, giving very high velocity flow (Mach number $\sim$ 2.5) at the nozzle exit; and the generator channel is of constant area with segmented electrodes.

Although the problems under investigation here refer to flow in the channel, consideration must be given to nozzle processes since these determine the inlet conditions to the channel. Thermodynamic equilibrium is assumed at inlet to the nozzle; that is, the components of the gas mixture (inert gas atoms, seed atoms, ions and electrons) are uniformly dispersed, have the same temperature, and the fractional ionization of the alkali metal is determined by the Saha relation[2]. It is also assumed that there is no fringing of the magnetic field into the nozzle.

In the absence of a magnetic field, electrons and alkali metal ions and atoms have negligible effect on the bulk flow processes since the seeding fraction is small (generally less than 1%). The solution of the flow equations for the expansion nozzle yields expressions for, inter alia, the temperature and pressure at the exit from the nozzle. From these two parameters, for a given seeding material, the electron density may be determined, assuming thermal equilibrium ionization as given by the Saha equation. However, owing to the extremely rapid expansion of the plasma in the nozzle, at least two non-equilibrium effects may occur. The first of these is an above-equilibrium electron temperature at the exit from the nozzle. This effect has been

previously examined[3] and found to be negligible for the conditions of the IRD generator. Secondly, owing to the rapid expansion of the plasma, recombination may not take place rapidly enough to assure the thermal equilibrium electron concentration. Under these conditions the flow is said to be 'semi-frozen' and the electron concentration at the exit of the nozzle is considerably higher than that given by application of the Saha equation. (The electron temperature, however, is the same as the gas temperature). The thermodynamic parameters found from solution of the flow equation for the nozzle, see Chapter 24, together with the electron concentration for the semi-frozen flow case, are used as the inlet conditions to the channel for the present evaluation.

In the constant cross-sectional area generator channel the flow equations are modified by the $J \times B$ forces arising from interaction with the magnetic field. These modifications consist of a term in the momentum equation for the magnetic decelerating force, and a term in the energy equation for the electrical power extracted. Both these terms contain the electrical conductivity and, hence, the electron concentration. Because of this, in contrast to the nozzle, (which has no applied magnetic field), the electron concentration may have considerable effect on the flow parameters.

The electron concentration may be governed by one of several mechanisms; two only are considered here. The first is thermal ionization at the gas temperature and pressure; in the second, postulated by Kerrebrock[4], Hurwitz et al[5], Neu[6], Brocher[7] and Wright and Swift-Hook[8], the electrons have a higher temperature than the remainder of the gas by virtue of the induced electric field. Replacing the gas temperature in Saha's equation by this electron temperature yields an electron density greater than the equilibrium value. BenDaniel and Tamor[9] have shown, by consideration of the rate equations for ionization, excitation, recombination and de-excitation of cesium, that the use of the electron temperature in Saha's equation is valid for MPD generator conditions.

In Section 25.2 (largely based on McNab and Cooper[10]) the flow equations are solved assuming ionization equilibrium at an elevated electron temperature which is obtained by the methods outlined in Hurwitz et al[5]. Section 25.3 details more recent calculations using equations giving the rate of change of electron temperature and electron concentration.

25.2 IONIZATION EQUILIBRIUM AT THE ELECTRON TEMPERATURE

25.2.1 Solution of the flow equations

In the solution of the flow equations the following assumptions have been made:

(i) the flow is steady-state and one-dimensional (i.e. boundary layers are small compared with the duct width; reverse currents which are thought to occur in the boundary layer are neglected);

(ii) the properties of the bounding surfaces are not considered except for the estimation of friction and heat loss at the walls, both of which are assumed uniform along the channel;

(iii) the power output of the generator is determined by processes in the gas only (for example, possible current saturation due to thermionic emission characteristics of the electrode material is ignored);

(iv) end loop losses are neglected;

(v) the energy released or absorbed in the association or dissociation of the seed material, together with that released if recombination occurs, is neglected;

(vi) impurities, which generally reduce the electron density and hence power output, are absent.

The validity of these assumptions is discussed in Section 25.2.5.

25.2.1.1 Non-zero magnetic field

For the system shown in Fig. 25.1 the following equations apply (the symbols being explained in the Nomenclature):

Energy

Change in total energy = $mC_p dT_o$

This is composed of:

(a) heat losses to walls = $-\frac{4h\,(T_{aw}-T_w)\,A\,dx}{D}$

(b) net electrical power extracted = $-\underline{E}.\underline{J}\,A\,dx = -\sigma B^2 V^2 K(1-K)A\,dx$

hence

$$\frac{mC_p dT_o}{A} = -\sigma B^2 V^2 K(1-K)\,dx - \frac{4h(T_{aw}-T_w)\,dx}{D} \qquad \ldots\ldots (25.1)$$

Momentum

Rate of change of momentum = mdV

This is due to:

(a) force due to pressure change = Adp

(b) force due to friction $= \frac{2f\rho V^2 A dx}{D}$

(c) force due to MPD interaction $= -\underline{J} \times \underline{B}\, A dx = -\sigma B^2 V(1-K) A dx$

hence

$$\frac{m dV}{A} = -dp - \frac{2f\rho V^2 dx}{D} - \sigma B^2 V(1-K)dx \qquad \ldots\ldots (25.2)$$

Continuity

$$\frac{m}{A} = \rho V \qquad \ldots\ldots (25.3)$$

State

$$p = \rho RT \qquad \ldots\ldots (25.4)$$

Enthalpy

$$T_o = T + \frac{V^2}{2C_p} \qquad \ldots\ldots (25.5)$$

From equation 25.1 to 25.5 an expression may be obtained giving the stagnation temperature as a function of the gas velocity and overall parameters of the system only (see Appendix 25.A, equation 25.A.7).

The velocity may be obtained as a function of distance in the following manner. Using equations (25.1) and (25.A.2) to eliminate dT_o, the following expression is obtained:

$$\frac{dx}{dV} = \frac{K_4 T_o - K_7 V^2}{V(K_5 V^2 - K_6)} \qquad \ldots\ldots (25.6)$$

On integration, assuming T_o constant, this yields:

$$x + \text{constant} = \ln \left\{ (V^2 - K_8)^{K_{12}} \cdot V^{K_{13}} \right\} \qquad \ldots\ldots (25.7)$$

where $K_{12} = \frac{K_1 T_o}{2K_3} - \frac{K_7}{2K_5}$

and $K_{13} = \frac{K_1 T_o}{2K_3}$

The constant in this equation is evaluated from the initial conditions. The assumption of constant T_o is valid if the integration is performed over small velocity intervals since T_o varies slowly compared with the other flow parameters.

Having obtained T_o as a function of velocity and distance, all the remaining thermodynamic quantities may be obtained from equations (25.3), (25.4) and (25.5),

together with the definition of the Mach number:

$$M^2 = \frac{V^2}{\gamma RT} \qquad \ldots\ldots (25.8)$$

25.2.1 ? Zero magnetic field

When B=0, the functions $f_1'(V)$ and $g_1'(V)$ in equation (25.A.4) become

$$f_1'(V) = \frac{K_3K_4}{K_1V(K_5'V^2-K_6)}$$

$$g_1'(V) = \frac{K_3K_7V}{K_1(K_5'V^2-K_6)}$$

where $K_5' = 2fm/Ad$, the other symbols having been previously defined. Equation (25.A.4) may then be integrated in the same manner as before, using an integrating factor. In this case the integration may be performed directly, without a binomial expansion, to give:

$$T_o = \frac{K_3K_7V}{K_1K_5'(V^2-K_8')^{1/2}} \left\{ \ln\left[V + (V^2-K_8')^{1/2} \right] + \text{constant} \right\} \qquad \ldots\ldots (25.9)$$

where $K_8' = \frac{2Ah(T_{aw}-T_w)(\gamma-1)}{\gamma fmC_p}$

From equations (25.9) and (25.7), T_o and the remaining thermodynamic quantities may be obtained as a function of distance for the case when B=0.

25.2.2 Electrical conductivity

The scalar electrical conductivity of a plasma is

$$\sigma = n_e e\mu_e + n_i e\mu_i \qquad \ldots\ldots (25.10)$$

according to simple theory. In most cases the contribution from the ions may be neglected because of their large mass and consequent low mobility compared with that of the electrons. Thus equation (25.10) becomes

$$\sigma = n_e e\mu_e = \frac{n_e e^2}{m_e \nu_{TOT}} = 2.814 \times 10^{-8} \frac{n_e}{\nu_{TOT}} \text{ mho/m} \qquad \ldots\ldots (25.11)$$

where n_e is the electron concentration (per m^3) and ν_{TOT} is the total electron collision frequency for momentum transfer. For a gas mixture containing j atomic species

$$\nu_{TOT} = \Sigma_j \nu_{ej} \qquad \ldots\ldots (25.12)$$

hence for a helium-cesium plasma under the conditions of interest for MPD generators (i.e. no Cs_2 or H_e^+):

$$\nu_{TOT} = \nu_{e-Cs^+} + \nu_{e-Cs} + \nu_{e-He} \qquad \ldots\ldots (25.13)$$

(Note that there is no ν_{e-e} term in this expression, because electron-electron collisions have negligible effect on the total electron momentum.)

The collision frequency is given in terms of atomic cross section by

$$\nu_{ej} = v_e Q_{ej} n_j = \left\{\frac{8kT_e}{\pi m_e}\right\}^{1/2} Q_{ej} n_j = 6.211 \times 10^3 T_e^{\frac{1}{2}} Q_{ej} n_j \text{ sec}^{-1} \qquad \ldots\ldots (25.14)$$

(in mks units) for a Maxwellian velocity distribution.

From a previous assessment of experimentally-obtained low energy cross-sections[11] a constant value of 6.1×10^{-20} m^2 has been used for Q_{e-He} to give

$$\nu_{e-He} = 3.79 \times 10^{-16} T_e^{\frac{1}{2}} n_{He} \qquad \ldots\ldots (25.15)$$

Little data is available for the electron-cesium atom collision cross-section at low energies. Brode[12] gives $Q_{e-Cs} = 3.1 \times 10^{-18}$ m^2 at 0.40 eV, and this figure has been used, assumed constant, to give

$$\nu_{e-Cs} = 1.93 \times 10^{-14} T_e^{\frac{1}{2}} n_{Cs} \qquad \ldots\ldots (25.16)$$

The equivalent cross-section for electron-ion collisions is given by Spitzer[13]:

$$Q_{ei} = \frac{e^4}{256\pi(\epsilon_0 kT_e)^2} \ln \Lambda = \frac{2.96 \times 10^{-10}}{T_e^2} \ln \Lambda \text{ m}^2 \qquad \ldots\ldots (25.17)$$

where
$$\Lambda = 1.24 \times 10^7 \frac{T_e^{3/2}}{n_e^{1/2}} \qquad \ldots\ldots (25.18)$$

thus
$$\nu_{e-Cs^+} = \frac{1.84 \times 10^{-6}}{T_e^{3/2}} n_e \ln\left\{\frac{1.24 \times 10^7}{n_e^{1/2}} T_e^{3/2}\right\} \qquad \ldots\ldots (25.19)$$

Equations (25.11), (25.13), (25.15), (25.16) and (25.19) may be used to obtain the conductivity of the gas when the electron concentration is known; n_e is evaluated for two different cases below.

25.2.2.1 Equilibrium at the gas temperature

The electron concentration is:

$$n_e = \frac{pX}{kT} = 7.24 \times 10^{22} \frac{pX}{T} \text{ m}^{-3} \qquad \ldots\ldots (25.20)$$

p being the partial pressure of the cesium vapour in newton.m^{-2}. The fractional ionization (X) for cesium obtained from Saha's equation[2] at the gas temperature, is given by:

$$\mathrm{Log}_{10}\left\{\frac{X^2}{1-X^2}\,p\right\} = -\frac{1.956\times10^4}{T} + \frac{5}{2}\log_{10}T - 1.477 \qquad \ldots\ldots (25.21)$$

25.2.2.2 Equilibrium at the electron temperature

According to Hurwitz et al[5], the electron field induced by the magnetic field in an MPD generator channel will cause an elevated electron temperature. For a segmented electrode generator the relative temperatures when equilibrium is obtained are:

$$\frac{T_e}{T} = 1 - \frac{\gamma(1-K)^2 M^2\beta^2}{3\delta} \qquad \ldots\ldots (25.22)$$

where $$\beta = \omega_e\tau = 1.76\times10^{11}\, B/\nu_{TOT} \qquad \ldots\ldots (25.23)$$

In equation (25.22), δ is a factor accounting for possible inelastic collisions, deviations from the Maxwellian distribution function, and non-constant collision frequency. For a monatomic gas $\delta \approx 1$ and an elevated electron temperature is fairly readily achieved. (In combustion gases δ may be 10^2 or 10^3, owing to inelastic collisions, and small electron temperature elevation is likely.)

The electron temperature is obtained from Saha's equation when the gas temperature is replaced by the electron temperature. According to BenDaniel and Tamor[9], this is valid for MPD generators. Equation (25.22) is actually a simplified version of Sutton's equation.

25.2.3 Computations

Equation (25.A.7) is obtained by integration, assuming σ to be constant over the velocity interval $(V)_j^{j+1}$, a mean value, $\bar{\sigma}$, being used. The temperature and pressure obtained as a result of this integration are used in the calculation of a new value of the conductivity ${}^{j+1}\sigma_n$ at the end of the velocity interval. The process is then repeated using a new value of conductivity ($\sigma = \frac{{}^{j}\sigma + {}^{j+1}\sigma_n}{2}$) in equation (25.A.7). After several iterations, when ${}^{j+1}\sigma_n = {}^{j+1}\sigma_{n+1}$ the values of ${}^{j+1}T$, ${}^{j+1}p$, etc. constitute the solution at the end of the velocity interval.

The electrical conductivity is a function of the electron concentration and the electron temperature. In the case considered in section 25.2.2.1 $(T_e = T)$, n_e could be found directly using equations (25.20) and (25.21). However, for the case of elevated electron temperature (section 25.2.2.2) an iterative solution for n_e and T_e was necessary, taking place within that described above for σ. This consisted of solving simultaneously the equation obtained by combining equations (25.20) and (25.21) (T replaced by T_e), which is of the form:

$$n_e = \phi\ (T_e) \qquad \text{(a)}$$

and an equation of the form

$$T_e = \psi\ (n_e), \qquad \text{(b)}$$

resulting from the combination of equations (25.13), (25.22) and (25.23).

Since (b) is of the form represented in Fig. 25.2, difficulty was experienced in obtaining the solution when it lay on the almost vertical part of the curve. The procedure finally used, although cumbersome, did not give rise to the difficulties experienced in attempting other methods (in some cases the solution oscillated between two, or even three, values).

Equations (a) and (b) were combined to give an implicit function of T_e only:

$$\eta\ (T_e) = 0 \qquad \ldots\ldots\ (25.24)$$

and increasing values of T_e were substituted in $\eta(T_e)$ until it became zero. Thus $^{j+1}T_e$ and $^{j+1}n_e$ were obtained, so that σ could be calculated. A flow diagram for the procedure is shown in Fig. 25.3.

The input values and constants used in this calculation are given in Tables 25.1 and 25.2.

25.2.4 Results

Investigations were made for three conditions: zero magnetic field; equilibrium at the gas temperature; and elevated electron temperature. The first case, being that of no power extraction, consists of the solution of the equations of supersonic flow in a constant area duct, including friction and heat transfer. With power extraction for both equilibrium and elevated electron temperature, the effect of varying the magnetic field, B, and the load factor, K, was investigated.

The results for equilibrium at the gas temperature show very little dependence on these parameters, mainly because of the very low electrical conductivity, so that the friction and heat transfer terms in the flow equations dominate those describing the MPD interactions. Thus, since the effect of power extraction is negligible, the solution is almost identical with that for zero magnetic field, the only effect being that the length for supersonic flow decreases slightly with increasing magnetic field, because of the contribution of the magnetic drag term in the momentum equation.

In contrast, the results for elevated electron temperature show considerable dependence on the magnetic field (see Table 25.3): the electrical conductivity is

high ($\geq 10^2$ mho/m) so that electrical power extraction and magnetic drag control the flow. The latter is particularly important, the length for supersonic flow being significantly altered for varying magnetic field, (Fig. 25.9). Fig. 25.10 shows the variation of Mach number with distance for various values of the load factor, K. A reduction in K causes a significant decrease in the length for supersonic flow, in accordance with the expression for magnetic drag.

Figs. 25.4 - 25.10 illustrate variation of the flow parameters with distance and magnetic field. Except in the case of Fig. 25.10 the load factor has a constant value of 0.8. On these graphs the curve for B = 0 represents the cases both of zero magnetic field and equilibrium at the gas temperature, since, as stated above, the results agree to within a few percent.

Figs. 25.11 - 25.13 demonstrate the variation with distance of the electrical parameters for equilibrium at the gas temperature. In Fig. 25.13 a value of 1.0 was used for B; however, since in this case the conductivity and velocity are virtually independent of magnetic field, the variation of power output with distance may be obtained directly for any value of B by scaling according to

$$P = \sigma V^2 B^2 K (1-K) d$$

The results for elevated electron temperature are shown in Figs. 25.14 - 25.18 as a function of distance and magnetic field. Since the length for supersonic flow varies so widely in this case, the graphs are plotted against a reduced distance which is the ratio of the distance from inlet to channel (x) to the length of supersonic flow (x_s) (i.e. distance at which M = 1).

25.2.5 Discussion

25.2.5.1 Supersonic-subsonic transition

The system, expansion nozzle - MPD channel - diffuser, for the IRD generator is shown in Fig. 25.19(a) and the originally predicted performance[14] (namely, acceleration from subsonic to supersonic in the expansion nozzle, supersonic flow in the channel with M = 1 at the exit and subsequent sobsonic diffusion of the flow) of curve 1 in Fig. 25.19(b). The present calculations indicate that when B = 0 or when the gas temperature and electron temperature are equal and the effect of power extraction on the flow is small, M = 1 will occur at about 14 cm from the beginning of the channel (see Table 25.3). Allowing for the probable inaccuracy in the estimation of the friction and heat transfer coefficients, the present 15 cm channel is satisfactory for these conditions.

The case where $T_e > T$ however, gives considerably different results.

Fig. 25.4 indicates that M = 1 will occur well before the end of the channel; a typical result of this type is shown by curve 2 of Fig. 25.19(b), M = 1 being predicted at the point A. This is physically impossible in a constant area channel with boundary layers of constant thickness. It is probable under these conditions that the boundary layer will become progressively thicker as the Mach number decreases to unity and thinner when the bulk of the flow becomes subsonic. The flow in this region may be very complex, with many shocks being formed, and may be unstable. Choking in the channel could cause the mass flow to be reduced so that supersonic flow in the nozzle would no longer be achieved; an unstable system giving alternate choking in the nozzle and channel could possibly occur.

If this situation is to be avoided, Fig. 25.9 (which shows the distance for which M = 1 as a function of magnetic field) may be interpreted as indicating the maximum permissible channel length as a function of magnetic field, neglecting the effects of boundary layers.

25.2.5.2 Flow regime

The type of flow - laminar to turbulent - occurring over a flat plate or in a tube is determined mainly by the Reynolds number, which is a measure of the ratio of the inertial force to the viscous force. For a tube this is

$$Re = \rho \frac{V_m D}{\mu_1} = \frac{V_m D}{\nu_1}$$

where Vm is the mean velocity across the tube, D is the hydraulic mean diameter, μ_1 is the dynamic viscosity and $\nu_1 = \mu_1/\rho$ the kinematic viscosity. The flow is usually laminar for Re < 2300 and turbulent for larger values. However, this condition is not strictly obeyed: for example, when extreme care has been taken in the design and construction of experimental systems laminar flow has been observed at far higher Reynolds numbers. A transition region, in which unsteady turbulent flow occurs, usually exists up to Re $\simeq 10^4$, above which, for many cases, fully developed turbulent flow may be assumed. Fully developed turbulent flow and fully developed laminar flow are amenable to a mathematical treatment but there is no adequate model for the transition region.

Using the continuity equation (25.3) with the mean velocity V_m

$$Re = \frac{mD}{A\mu_1} \qquad \ldots\ldots (25.25)$$

and, taking μ_1 to be that for pure helium and D to be the hydraulic mean diameter of the channel,

$$D = \frac{4A}{P_i} \qquad \ldots\ldots (25.26)$$

The Reynolds number is shown in Fig. 25.20 as a function of temperature. Fully developed turbulent flow may not be set up, since the Reynolds number is considerably less than 10^4.

To estimate the velocity profile and thickness of the laminar boundary sublayer in the channel, fully developed turbulent flow will be assumed and the relations given by Eckert[15] used. The velocity profile may be divided into three regions depending on the distance away from the tube wall. Using a dimensionless velocity $V^\dagger$ and a dimensionless distance from the tube wall $y^\dagger$ these regions are:

$$\left.\begin{array}{lll} \text{laminar sublayer} & y^\dagger < 5 & V^\dagger = y^\dagger \\ \text{buffer zone} & 5 < y^\dagger < 30 & V^\dagger = 5 \ln y^\dagger - 3.05 \\ \text{turbulent core} & y^\dagger > 30 & V^\dagger = 2.5 \ln y^\dagger - 5.5 \end{array}\right\} \quad ..(25.27)$$

In equations (25.27)

$$y^\dagger = \frac{y}{\nu_1}\sqrt{\frac{\tau_w}{\rho}}$$

and

$$V^\dagger = V\sqrt{\frac{\rho}{\tau_w}}$$

where τ_w is the wall shearing stress given by

$$\sqrt{\frac{\tau_w}{\rho}} = \frac{0.2\ V_m}{Re^{\frac{1}{8}}}, \qquad \ldots\ldots (25.28)$$

so that

$$y^\dagger = 0.1\ Re^{\frac{7}{8}}\ \frac{2y}{D}$$

$$V^\dagger = 6.2\ Re^{\frac{1}{8}}\ \frac{V}{V_s} \qquad \ldots\ldots (25.29)$$

where $D/2$ is the hydraulic mean radius and y the distance from the wall, and V_s is the axial velocity, given by $V_s = \frac{V_m}{0.82}$. This velocity distribution, V/V_s, is shown in Fig. 25.21 as a function of $2y/D$ for a Reynolds number of 5000.

In discussing turbulent flow and velocity profiles it has been assumed that the cross-section of the channel is circular, taking a mean diameter from equation (25.26). Most MPD channels, for magnet economy and other reasons, have a rectangular cross-section and the boundary layer thickness will not be uniform over the channel perimeter. Curves of constant velocity for a pipe of rectangular cross-section (as measured by Nikuradse, in Schlichting[16]) are shown in Fig. 25.22 as an example of this effect.

An additional complication concerns the entrance conditions to the channel. If a fluid enters a channel from a large container, the velocity distribution in the inlet region varies with distance along the channel. Near the inlet region the velocity distribution is almost uniform, changing through viscous effects until a fully-developed velocity profile is established and remains constant further downstream. It is this constant velocity profile which has been discussed above and which is shown in Fig. 25.21. According to Nikuradse the fully-developed turbulent velocity profile for a pipe of circular cross-section exists after an inlet length of 25 to 40 diameters from entrance. The value for a rectangular channel is not known, even less the velocity profile for a supersonic flow emerging from a convergent-divergent nozzle. Thus the above assumption of a fully developed velocity profile may well be incorrect, but is limited by present knowledge in fluid mechanics.

The above discussion concerning the velocity profile in a channel refers to conditions in the absence of a magnetic field. For flow in a magnetic field, insufficient data is available at present to permit definite predictions of turbulent or laminar flow for a given configuration. A magnetic field acting on an electrically-conducting fluid tends to suppress turbulence through the internally induced electric fields in small regions of turbulence, the overall effect being to flatten the velocity profile. Thus in the channel of the IRD device the flow may be in the turbulent transition region when the magnetic field is zero but laminar for non-zero magnetic fields above a certain value.

Lock[17] found that a transverse magnetic field has a stabilizing effect on the laminar flow of a conducting fluid between parallel plates. The experiments of Lehnert[18], however, showed a destabilizing effect due to the magnetic field. This illustrates that at present the interaction of a magnetic field with a moving electrically-conducting fluid is not completely understood.

Wu[19] has considered Hartmann flow (laminar and incompressible with viscous and magnetic forces) to investigate the effects of reverse currents in the boundary layers on the power output of an MPD generator. The reverse currents arise because the velocity in the boundary layer may be less than the ratio of the electric to magnetic field ($-E/B$) so that the plasma is accelerated in this region rather than being slowed down. Thus part of the power generated in the main stream is lost in the boundary layer. Wu shows that, for the same pressure gradient:

$$\frac{\langle P \rangle_{\text{viscous}}}{P_{\text{inviscid}}} = \langle F \rangle^2 \left[\frac{1 - K}{1 - K \langle F \rangle} \right] \qquad \ldots\ldots (25.30)$$

where $F = F(y)$ is a factor determining the velocity distribution across the channel. For Hartmann flow

$$\langle F \rangle \approx 1 - \frac{1}{R_h} \qquad \ldots\ldots (25.31)$$

for large values of R_h, the Hartmann number. For the IKD generator, taking typical values in the channel, $R_h \approx 80$ and $K = 0.5$, the power ratio is $\sim 96\%$. Blackman and Jones[20] estimate that the power ratio may be as low as 25% for small shock tube channels.

25.2.5.3 Channel wall losses

The friction factor at the wall of the alumina channel has been estimated assuming helium only to be present. Cesium affects the viscosity appreciably owing to the large mass, as has been shown theoretically[21]. No experimental data are at present available and no quantitative estimate of the effect of seeding has been attempted. The tendency will be for the friction factor to increase with increasing cesium seeding.

Heat loss through the walls has been estimated for alumina, assuming only convection and conduction in the gas. There may, in addition, be appreciable radiation from a hot cesium plasma, which should be taken into account in the energy balance; no experimental data are available upon which quantitative estimates may be based.

Another assumption implicit in neglecting wall properties is the neglect of the power lost by current leakage through the alumina. Consideration of the highest measured electrical conductivity for alumina[22] ($\sigma \approx 10^{-4}$ mho/cm at 1600°K) shows that the loss of power is small ($\sim$ watts) compared with other losses (see below for end leakage and eddy current losses).

25.2.5.4 Electrode processes

Pain and Smy's[23] power generation experiments with a combustion-driven argon shock tube showed that large power outputs could be obtained through an MPD interaction without any apparent evidence of emission from the electrodes. These results are contrary to those of Maycock et al[24], who have observed considerable deterioration of electrodes in an open-cycle combustion device. There appears to be no conclusive evidence on the electrode emission mechanism in MPD generators.

25.2.5.5 End loop and leakage losses

At the entrance to and exit from the magnetic field region there is a reverse flow of electric current, known as eddy current or end loop loss.

This has been considered in some detail by Sutton[25] and Dzung[26] amongst others. Sutton found that the losses increase as the loading factor increases or as the aspect ratio of the channel decreases. The losses can best be offset by extending the magnetic field region. Dzung considered the Hall effect in his evaluation and found that the losses increase rapidly with β for a continuous electrode system, but are not so severe for a segmented configuration. Numerical values showing the loss in power output may be found in these papers.

In addition to these losses, the power output of a generator may be considerably reduced by leakage currents from the generator region to an earthed portion of the system. Way et al[27] have estimated this effect for constant conductivity throughout the considered length. Their theory has been extended here for non-constant conductivity. Under these conditions the total power output of a segmented electrode generator when end leakage occurs is

$$P = \sigma V^2 B^2 \pi (1 - K) (1 - C) LA \qquad \ldots\ldots (25.32)$$

where σ and V are the average conductivity and velocity in the generating region and C is the end leakage factor given by (see Appendix 25.8):

$$C = \frac{\beta^2}{1+\beta^2} \left\{ 1 - \frac{1}{\frac{(1+\beta^2)}{2s} \frac{\sigma_s}{\sigma} + 1} \right\} \qquad \ldots\ldots (25.33)$$

For a given β in the generator region this expression shows that end leakage decreases when $L/2s$ decreases and when σ_s/σ decreases. For the present IRD system $L/2s$ is large (~ 10) and σ_s/σ in the downstream part of the generator will be close to unity, owing to the small amount of recombination occurring over the distance s(~ 1 cm.); thus the end losses may be expected to be high. Fig. 25.23 shows C as a function of $L/2s$ for several values of β and when $\sigma_s/\sigma=1$, while Fig. 25.24 shows C as a function of σ_s/σ for several values of β.

To reduce end leakage there must be a considerable length of free insulator at each side of the active generator region and the conductivity should be small outside the active region. If the magnetic field is correctly designed there should be little leakage upstream when $L/2s$ is small. Downstream of the generator region the same applies, with the addition that recombination will also act to decrease the electron density, which however is high in the generator region (see Fig. 25.25(c)). If the downstream leakage is appreciable and the length of insulator is limited by external pressure requirements it may be necessary to introduce some electron attaching element or radical downstream of the generator region to reduce the conductivity.

25.2.5.6 Cesium dissociation

The effect of the dissociation of cesium by the reaction

$$Cs \rightleftharpoons Cs^+ + e^- \qquad \ldots\ldots (25.34)$$

on the specific heat of an equilibrium mixture of cesium is shown in Fig. 25.26 (from Clifton[29]). The ranges of temperature and pressure in the channel for the conditions of interest here are 900° - 1800°K and 40-120 mm of Hg (total pressure), that is, cesium pressure 0.4 - 1.2 mm of Hg. For these conditions the effect of dissociation is small (Fig. 25.26) and the specific heat of cesium is close to the value $^{5R}u/2 = 4.96$ cal/°K mole for any monatomic gas, including helium.

Fig. 25.27 (also from Clifton[29]) shows the percentage of Cs_2 in cesium vapour as a function of temperature for various total cesium pressures. The lowest cesium temperature and pressure anticipated in the channel will be 900°K and 0.4 mm Hg (at the channel entrance). For these conditions less than 0.01 atomic percent Cs_2 will be present (Fig. 25.27); thus there will be no noticeable contribution to the specific heat of cesium from the reaction

$$2Cs \rightleftharpoons Cs_2 \qquad \ldots\ldots (25.35)$$

Figs. 25.26 and 25.27 have been derived assuming thermodynamic equilibrium. For a non-equilibrium system, as for example when electron heating occurs, dissociation of cesium by the above reactions (equations 25.34 and 25.35) may have a pronounced effect on the specific heat of the gas mixture.

25.3 IONIZATION NON-EQUILIBRIUM

25.3.1 Introduction

In the previous section the results obtained when the MPD equations for constant area flow, taking into account wall friction and heat transfer, were solved for the cases of ionization at the gas temperature and at the electron temperature. The computer programme used was, however, not sufficiently fast or versatile to permit all the required investigations to be undertaken. Preliminary results obtained with a faster (machine orders) programme, in which several important modifications and generalisations of the previous equations have been made, will now be discussed. One of the most important modifications is the use of an equation governing magnetically-induced ionization non-equilibrium.

25.3.2 Equations

The energy equation for a compressible fluid in the absence of magnetic

interactions is[30]

$$mC_p dT_o = \frac{-4h\,(T_{aw}-T_w)\,Adx}{D} \qquad \ldots\ldots (25.36)$$

The adiabatic wall temperature (T_{aw}) for subsonic flow is defined by

$$T_{aw} = rT_o + (1-r)\,T; \qquad \ldots\ldots (25.37)$$

this definition may not be valid for supersonic flow.

The heat transfer coefficient (h) in equation (25.36) is obtained from the friction factor (f) using Reynolds analogy:

$$h = \rho V C_p f/2, \qquad \ldots\ldots (25.38)$$

which is accurate to a few percent for fully developed turbulent flow. Using the friction factor (see below)

$$f = 0.079/Re_D^{1/4} \qquad \ldots\ldots (25.39)$$

gives

$$h = 0.0395\rho V C_p/Re_D^{1/4} \qquad \ldots\ldots (25.40)$$

An alternative way of expressing the heat transfer coefficient is by means of the Stanton number:

$$h = \rho V C_p St$$

Using this expression, together with the relation

$$St = Nu/PrRe,$$

the empirical relation obtained by Durham et al[31] for helium (neglecting entrance effects) is

$$Nu = 0.034Re^{0.8}\,Pr^{0.4}$$

and a Prandtl number of 0.75 gives

$$h = 0.0405\rho V C_p/Re^{0.2},$$

which is in fair agreement with equation (25.40). Equation (25.40) is used in the present calculations.

The momentum equation for a compressible fluid in the absence of magnetic interactions is

$$mdV + Adp = -\frac{2f\rho V^2 Adx}{D} \qquad \ldots\ldots (25.41)$$

where the friction coefficient (f) is defined as the ratio wall shearing stress to the dynamic head of the stream:

$$f = 2\tau_w/\rho V^2 \qquad \ldots\ldots (25.42)$$

(Note: the friction coefficient is sometimes defined as four times greater than

this). According to Eckert and Drake[32] for fully developed turbulent flow the friction coefficient is given by Blasius's law

$$f = a'/Re_D^{1/4} \qquad \ldots\ldots (25.43)$$

where a' is a coefficient equal to 0.079 and the Reynolds number is calculated with the mean velocity in the channel and the hydraulic diameter (D).

Combination of equations (25.3), (25.36) and (25.40) with the addition of the electrical energy extraction term yields the MPD constant-area energy equation

$$\frac{dT_o}{dx} = - \frac{2a' (T_{aw}-T_w)}{Re_D^{1/4} D} + (\underline{E}.\underline{j}) \frac{A}{\dot{m}C_p} \qquad \ldots\ldots (25.44)$$

Combination of equations (25.3), (25.41), (25.43) and (25.A.1), together with the magnetic braking force term, yields the MPD constant area momentum equation

$$\frac{dV}{dx}\left[\frac{\gamma+1}{2\gamma} - \frac{RT_o}{V^2}\right] = - \frac{R}{V}\frac{dT_o}{dx} - \frac{2a'V}{Re_D^{1/4} D} + (\hat{\underline{i}}\,\underline{j} \times \underline{B})\frac{A}{\dot{m}} \quad \ldots (25.45)$$

For a coordinate system with a plasma flowing in the positive x direction and a magnetic field in the positive z direction

$$\underline{E}.\underline{j} = - \frac{\sigma V^2 B^2 \left\{\beta_e^2 K_H(1-K_H) + K(1-K)(1+\beta_e\beta_i)^2\right\}}{(1+\beta_e\beta_i)\left[(1+\beta_e\beta_i)^2 + \beta_e^2\right]} \qquad \ldots\ldots (25.46)$$

and

$$\hat{\underline{i}}\,(\underline{j} \times \underline{B}) = - \frac{\sigma V B^2 \left[(1+\beta_e\beta_i)^2(1-K) + \beta_e^2 K_H\right]}{\left[(1+\beta_e\beta_i)^2 + \beta_e^2\right](1+\beta_e\beta_i)} \qquad \ldots\ldots (25.47)$$

where for a solid-electrode generator $K_H = 0$, for a segmented-electrode generator $K_H = 1-K$, and for a Hall generator $K = 0$: in the present calculations a segmented-electrode system has been evaluated.

One of the more important differences between these investigations and those reported in Section 25.2 is the use of an equation giving the rate of change of electron temperature due to electron heating, collisional energy exchange and ionization or deionization processes[33]:

$$\frac{5}{2} n_e k V \frac{dT_e}{dx} = \underline{j}_e.\underline{E}^* - 3m_e n_e k (T_e - T)\delta \sum_j \frac{\nu_{ej}}{m_j} - eV_i \left(\frac{dn_e}{dt}\right)_i \qquad \ldots\ldots (25.48)$$

In equation (25.48),

$$\underline{j}_e.\underline{E}^* = \frac{\sigma V^2 B^2}{(1+\beta_e^2)}\left[\frac{\beta_e^2 K_H^2}{(1+\beta_e\beta_i)^2} + (1-K)^2\right] \qquad \ldots\ldots (25.49)$$

and, using a three-body electron-electron-ion recombination coefficient α and assuming that ionization is determined from this by the condition that the two rates must be equal at equilibrium,

$$\left(\frac{dn_e}{dt}\right)_1 = \alpha n_e^3 \left[\frac{n_a}{n_e^2}\left(\frac{n_e^2}{n_a}\right)_s - 1\right] \qquad \ldots\ldots (25.50)$$

The total rate of change of electron concentration is obtained from the rate of change due to ionization and recombination plus the rate of change due to overall changes in the gas density; thus

$$V\frac{dn_e}{dx} = \alpha n_e^3 \left[\frac{n_a}{n_e^2}\left(\frac{n_e^2}{n_a}\right)_s - 1\right] + \frac{XXV\, d\rho}{m_p + Xm_a\, dx} \qquad \ldots\ldots (25.51)$$

From the enthalpy equation (25.5)

$$\frac{dT}{dx} = \frac{dT_o}{dx} - \frac{V}{C_p}\frac{dV}{dx} \qquad \ldots\ldots (25.52)$$

and from the continuity equation (for a constant-area generator)

$$\frac{d\rho}{dx} = -\frac{\rho}{V}\frac{dV}{dx} \qquad \ldots\ldots (25.53)$$

The six simultaneous differential equations (25.44), (25.45), (25.48), (25.51) (25.52) and (25.53) are integrated using the auxiliary equations (25.46), (25.47) (25,49) and (25.50).

The Saha fractional ionization is found from

$$\frac{X_s^2}{1-X_s^2} = \frac{(kT_e)^{5/2}}{X(1+X)p_T} L' \exp(-\Delta/T_e) \qquad \ldots\ldots (25.54)$$

where

$$L' = \left(\frac{2\pi m_e}{h^2}\right)^{3/2} \frac{g_e g_i}{g_a}$$

and

$$\Delta = eV_I/k \qquad \ldots\ldots (25.54a)$$

The equilibrium electron and atom concentrations are given by

$$(n_e)_s = \frac{X_s X (1+X) p_T}{(1+X_s)\, kT} \qquad \ldots\ldots (25.55)$$

and

$$(n_a)_s = \frac{(1-X_s)(n_e)_s}{X_s} \qquad \ldots\ldots (25.56)$$

The non-equilibrium atom concentrations are obtained from

$$n_a = \frac{\chi p_T}{kT} - (1+\chi)n_e \qquad \ldots\ldots (25.57)$$

and

$$n_p = \frac{p_T}{kT} - 2n_e - n_a, \qquad \ldots\ldots (25.58)$$

where

$$p_T = \frac{mRT}{AV}, \qquad \ldots\ldots (25.59)$$

$$\chi = \frac{n_e+n_a}{n_p} \qquad \ldots\ldots (25.60)$$

and

$$X = \frac{n_e}{n_e+n_a} \qquad \ldots\ldots (25.61)$$

The scalar electrical conductivity is found from the usual expression (see Section 25.2.2) and the Hall and ion effects are found using

$$\beta_e = \frac{eB}{m_e \nu_e} \qquad \ldots\ldots (25.62)$$

and

$$\beta_i = \frac{eB}{m_i \nu_{iT}}, \qquad \ldots\ldots (25.63)$$

where

$$\nu_{iT} = \left(\frac{8kT}{\pi m_i}\right)^{1/2} (Q_{ip} n_p + Q_{ia} n_a) \qquad \ldots\ldots (25.64)$$

The remaining quantities required for the solution of the six differential equations are given in Section 25.2.

25.3.3 Numerical solution of equations

The set of equations given in Section 25.3.2 may be solved by a numerical step method to give the variation of flow and field parameters along the channel length. Initially the values of the main variables (T_o,V,T,T_e,n_e and ρ) are known at the channel inlet. From equation (25.59), knowing the mass flow, the channel cross-sectional area and the gas constant the total pressure (p_T) may be found. Knowing p_T and the seeding fraction (defined in (25.60)) the cesium atom concentration (n_a) can be obtained from equation (25.57) and, using (25.58), the helium atom concentration. Knowing the electron, cesium atom and helium atom concentrations the total electronic and ionic collision frequencies can be found using equations (25.14) and (25.64); all collision cross sections are assumed constant in these preliminary calculations with the exception of that for electron ion collisions (equation (25.17)). Using equations (25.62), (25.63) and (25.11), β_e, β_i and σ can now be evaluated. Knowing the seeding fraction and the electron and cesium atom concentrations the non-equilibrium fractional ionization (X) is

found from equation (25.61). Then, using the equilibrium fractional ionization from equation (25.54), the equilibrium electron and cesium atom concentrations are found from equations (25.55) and (25.56).

This rather inelegant procedure (outlined above) is required if the assumption of low fractional ionization is not valid (as is often true for the case of extrathermal ionization) and when non-equilibrium extrathermal ionization is investigated, that is when equation (25.48) is used rather than the simple expression derived from it (equation (25.22)).

It is now possible to integrate the six simultaneous differential equations (25.44), (25.45), (25.48), (25.51), (25.52) and (25.53). This is carried out using the fourth-order Runge-Kutta process which requires evaluation of each of the derivatives at the point under consideration; these are obtained as follows.

From equation (25.46) $\underline{E}.\underline{j}$ is calculated using the values of β_e, β_i and σ found previously, then using

$$\mu_1 = 5.1\times10^{-7}\, T^{2/3} \qquad \ldots\ldots (25.65)$$

the Reynolds number

$$Re = \frac{mD}{A\mu_1} \qquad \ldots\ldots (25.66)$$

may be obtained. Using a recovery factor of 0.85 in equation (25.37), T_{aw} is obtained and, since T_w is supplied as data, dT_g/dx (equation (25.44)) is obtained. Using dT_g/dx and evaluating equation (25.47) dV/dx is found from equation (25.45). Obtaining $\underline{j}.\underline{E}^*$ from equation (25.49) and the values of $(n_a)_s$, $(n_e)_s$ and ν_{eT} calculated above, dT_e/dx is found from equation (25.48). Knowing dT_g/dx and dV/dx, equation (25.52) gives dT/dx; equation (25.53) gives $d\rho/dx$ and thus dn_e/dx can be evaluated using equation (25.51).

The integration process gives values of T_g, V, T, T_e, ρ and n_e at $x = h$ where h is the step length. The above procedure is then repeated along the channel until the exit distance is reached or until the Mach number becomes unity, whereupon the calculation stops.

25.3.4 Discussion and results

Several important differences between the investigations reported in Sections 25.2 and 25.3 have already been mentioned. In addition to these differences the gas constant, specific heat at constant pressure and ratio of specific heats used in the calculations of section 25.3 are those for a helium-cesium mixture rather than for pure helium as in Section 25.2. Thus, although

the channel entrance data are self-consistant and closely approximate the nozzle exit conditions in most respects, there is not complete agreement since the present nozzle calculations employ data for pure helium. The manner by which the gas constant for a cesium-helium mixture is calculated is given in Chapter 23 of this report; for a 1% cesium-helium mixture the gas constant is about 75 per cent of that for pure helium.

The essential difference between the present calculations and the earlier ones (Section 25.2) is that non-equilibrium values of electron temperature and concentration may be evaluated. Thus the effects on the flow and electrical parameters of entrance to and exit from the generator region may be examined in some detail. For example, if non-equilibrium flow occurs in the nozzle, the effects on generated power in the channel may be examined; the decay of electrical conductivity on exit from the magnetic field region and its effect on end leakage can also be investigated. The continuation of non-equilibrium flow from the nozzle into the channel in the absence of magnetic field can also be examined. In the present programme the magnetic field is a step function, being zero outside the generator region. Later calculations may enable the magnetic field strength to be varied as a function of channel distance. (In the present programme only the wall temperature (T_w) can be expressed as a function of channel distance; when sufficient experimental data on wall temperature are available this will be used.)

Under typical operating conditions in the channel the heat transfer coefficient, h (equation (25.40), derived from Reynolds analogy), used in Section 25.3 is about three times greater than that of Section 25.2; this will not make a great difference to the flow conditions when power extraction occurs.

The only calculations carried out to date have been with a segmented-electrode system; however, the programme can readily be used for either a solid-electrode or Hall generator configuration, but no account is taken of finite segmentation. In later versions of the IRD MPD channel, electrodes are placed only in the central region of the channel, and long blank sections are left at either end to reduce end leakage. The flow in these three separate regions of the channel can be examined by varying the loading factor appropriately, that is, K=1 (and therefore K_H=0) in the channel region where no electrodes exist.

In equation (25.48), δ is a factor accounting for inelastic collisions and a non-Maxwellian distribution, given by

$$\delta = \frac{\Sigma_j x_j m_j \Sigma_j x_n Q_{ej} \delta_j m_j^{-1}}{\Sigma_j x_j Q_{ej}} \qquad \ldots\ldots (25.67)$$

where

$$x_j = \frac{n_{e,j}}{n_e + \Sigma_j n_j} \qquad \ldots\ldots (25.68)$$

In the present calculations $\delta = 1$ is assumed, but this can readily be changed to take into account such effects as inelastic collisions due to molecular impurities.

In equation (25.50) the three body electron-electron-ion recombination coefficient used is that given by Hinnov and Hirschberg[34]:

$$\alpha = 1.1 \times 10^{-20} T_e^{-9/2} ; \qquad \ldots\ldots (25.69)$$

this has been shown to be the most appropriate under MPD generator conditions[35], being close to the recent value obtained by Bates et al[36].

The data used for the calculations reported here is tabulated in Table 25.4 it is similar in several respects to that given in Tables 25.2 and 25.3 for the calculations of Section 25.2. Figs. 25.28 to 25.35 inclusive show the results obtained using this data for a magnetic field strength of 0.5T. (Note the semi-logarithmic scales of Figs. 25.32, 25.33 and 25.34.) These curves may be compared with the corresponding ones for the calculations of Section 25.2. While the general form of most the the curves correspond, there are several points worthy of note, as outlined below.

Fig. 25.32 shows the electron temperature as a function of distance down the channel. The rapid rise of electron temperature (within the first centimetre from channel inlet) is clearly visible. This finite rise time for the electron temperature is governed, through equation (25.48), by the rate at which energy is supplied to the electrons by the electric field, the rate at which it is lost by elastic collisions and by ionizing collisions. When these processes equilibriate the electron temperature is close to the value given in Fig. 25.14 which was obtained using the equilibrium form of equation (25.48) (that is, equation (25.22)) for the same magnetic field (the minor differences are due to the use of slightly different constants).

However, although the electron temperature rises rapidly, the electron concentration, which is obtained from equation (25.51), follows this variation much more slowly, as may be seen from Fig. 25.33 (compare with Fig. 25.16). Taking an average flow velocity of 3000 m/sec in the channel the rise time for electron concentration is ~30 μsec, compared with 3 μsec for the electron temperature. This rate of rise of electron concentration is determined from the reverse process of three body electron-electron-ion recombination as given by Hinnov and Hirschberg. While this procedure may be in some error far from equilibrium, an unpublished survey of several quoted electron-atom ionization rates

shows that they are considerably further from agreement than the recombination rates.

The slow rate of rise of electron concentration will probably not be significant in a large-scale MPD generator, but the influence on the IRD channel may be very important.

Fig. 25.34 shows the scalar electrical conductivity of the helium-cesium plasma determined from equation (25.11). As expected, the conductivity follows the general form of the electron concentration curve, being initially low, and rising slowly to a value of ~130mho/m (compare Fig. 25.17). The small drop in conductivity in the first centimetre channel distance is a real effect and occurs because the electron temperature here has increased more rapidly than the electron concentration.

The specific power (power output per unit channel volume) is shown in Fig. 25.35 as a function of distance down the channel. As with the electrical conductivity there is a small drop in power in the first centimetre of channel, for the same reason. The specific power then increases rapidly, being determined primarily by the rate of increase of electrical conductivity. A maximum value (~ 32 MWe/m^3) is reached, beyond which the specific power decreases. The reason for this is that the electrical conductivity has become sensibly constant but the flow velocity is decreasing at an increasingly rapid rate. The area under the curve multiplied by the channel cross sectional area (4.8 cm^2) yields an ideal power output of about 0.8kWe, (neglecting effects of finite segmentation) for a magnetic field (B) of 0.5 T the power output increases approximately as B^2.

Comparison with the previously determined corresponding figures for B=0.5 shows that a Mach number of unity for the present calculations occurs at x=14cm from inlet, compared with about 10 cm for calculations of Section 25.2 (see Fig. 25.9 for example). This arises mainly because of the lower average magnetic interaction in the latest calculations, mainly due to lower levels of electrical conductivity.

While only a few simple calculations using the latest programme have been reported here several other investigations can and will be made. Although the programme is by no means ideal, omitting, for example, the effects of finite electrode segmentation, MPD boundary layer formation, electrode sheath formation and flow inhomogeneities, it is considerably more general and versatile than programmes hitherto used for MPD investigations.

REFERENCES

1 LINDLEY, B.C. An MPD power generation experiment using helium-cesium. Proceedings of the Third Symposium on Engineering Aspects of MHD. University of Rochester, U.S.A. March 1962

2 SAHA, M.N. and SAHA, H.K. A treatise on modern physics. Vol. 1. The Indian Press Ltd. Allahabad and Calcutta, 1934.

3 McNAB, I.R. and LINDLEY, B.C. Electron temperature in the rapid expansion of a plasma flow. Advances in MHD. Pergammon 1963

4 KERREBROCK, J.L. Conduction in gases with elevated electron temperature. Proceedings of the Second Symposium on Engineering Aspects of MHD. University of Pennsylvania. March 1961. Columbia University Press.

5 HURWITZ, H., SUTTON, G.W. and TAMOR, S. Electron heating in MHD power generators. ARS Journal vol. 32, No. 8, p.1237, 1962

6 NEU, H. Electron heating in Hall-fields of MPD generators (Magnetoplasma-dynamic Electrical Power Generation, I.E.E. Conference Series No. 4, 1963.

7 BROCHER, E.F. On the elevation of electron temperature in MHD generators and its effect on the gas conductivity. Ibid.

8 WRIGHT, J.K. and SWIFTHOOK, D.T. Magnetohydrodynamic Generation with Elevated Electron Temperature. Proc. Phys. Soc. vol.80, p.465, 1962.

9 BENDANIEL, D.J. and TAMOR, S. Non-equilibrium ionization in MHD Generators G.E.R.L. Report No.62-RL-(2922E) January 1962.

10 McNAB, I.R. and COOPER, N.A. Flow processes in MPD generators. IRD report 63-82, October 1963.

11 McNAB, I.R. The electrical properties of a cesium-helium plasma. C.A. Parsons, NRC 61-12. March 1961.

12 BRODE, R.B. Rev. Mod. Phys. vol. 5, p.257, 1933

13 SPITZER, L. JR. Physics of fully ionized gases. Interscience Tracts on Physics and Astronomy No. 3. 1956

14 LINDLEY, B.C. Magnetohydrodynamic Power Generation Experiment. C.A. Parsons NRC 60-92. Sept. 1960

15 ECKERT, E.R.G. An introduction to the transfer of heat and mass. McGraw-Hill, New York

16 SCHLICHTING, H. Boundary layer theory. p.415. Pergammon Press, London 1955

BLANK PAGE

17 LOCK, R.C. The stability of an electrically conducting fluid between parallel plates under a transverse magnetic field. Proc. Roy. Soc. vol. A233, p.105, 1955.

18 LEHNERT, B. An instability of laminar flow of mercury caused by an external magnetic field. Proc. Roy. Soc. vol.A233, p 299, 1955

19 WU, J.C. Effects of viscosity in MPD generators. Magnetoplasmadynamic Electrical Power Generation (I.E.E. Conference Series No.4, 1963)

20 BLACKMAN, V.H. and JONES, M.S. MHD Power Generation studies in Rectangular Channels. Proc. 2nd Symposium on Engineering Aspects of MHD. University of Pennsylvania. March 1961. Columbia University Press.

21 McNAB, I.R. The viscosity of helium-cesium mixtures. IRD 63-59. July 1963

22 COHEN, J. Electrical conductivity of alumina. Amer. Ceram. Soc. Bull. vol.38 No.9, p.441, 1959

23 PAIN, H.J. and SMY, P.R. Experiments on power generation from a moving plasma. J. Fluid Mech. vol.10, part 1, pp.51-64. 1961

24 MAYCOCK, J., NOE, J.A. and SWIFTHOOK, D.T. Permanent Electrodes for Magnetohydrodynamic Power Generation. Letter to Nature, vol.193, p.467 1962

25 SUTTON, G.W. Electrical and pressure losses in an MHD channel due to end current loops. G.E. Space Sciences Laboratory Rept. R59SD431. July 1959

26 DZUNG, L.S. Hall effect and end loop losses of MHD generators. Magnetoplasmadynamic Electrical Power Generation. (I.E.E. Conference Series No. 4, 1963)

27 WAY, S. et al. Long life closed loop MHD research and development unit. Interim Scientific Report No. 1. June 11th 1962. Westinghouse Research Labs. Report. Pittsburgh, Pennsylvania, U.S.A.

28 HARRIS, L.P. and COBINE, J.D. The significance of the Hall effect for three MHD generator configurations. ASME paper number 60-WA-329. November 1960

29 CLIFTON, D.G. Ideal gas treatment of the equilibrium composition, enthalpy function, and heat capacity of cesium vapour and cesium plasma. Los Alamos Scientific Laboratory Report L.A. 2419. August 1960

30 SHAPIRO, A.H. The dynamics and thermo-dynamics of compressible fluid flow. The Ronald Press Company New York 1953

31 DURHAM, F.P., NEAL, R.C. and NEWMAN, H.J. 'High temperature heat transfer to a gas flowing in heat generating tubes with high heat flux' Reactor Heat Transfer Conference 1956. USAEC TID-7529 (Part 1) Book 2.

32 ECKERT, E.R.G. and DRAKE, R.M. Heat and mass transfer. McGraw-Hall Book Co. Inc. New York, Toronto and London 1955

33 SUTTON, G.W. The theory of magnetohydrodynamic power generators. G.E. Space Sciences Lab Report R62SD990 December 1962

34 HINNOV, E. and HIRSCHBERG, J.G. Electron-ion recombination in dense plasmas. Phys. Rev. vol.125, p.795, 1962.

35 McNAB, I.R. and ROBINSON, C.A. Electron-ion recombination in MPD generators. Magnetoplasmadynamic Electrical Power Generation Conference, Newcastle Sept. 1962 (I.E.E. Conference report series no. 4, 1963)

36 BATES, D.R., KINGSTON, A.E. and McWHIRTER, R.W.P. Recombination between electrons and atomic ions. Proc. Roy. Soc. A, vol.267, p.297-312, 1962.

APPENDIX 25.A

DERIVATION OF STAGNATION TEMPERATURE

From equations (25.3) and (25.4)

$$dp = \frac{mR\ dT}{A\ V} - \frac{mRTdV}{AV^2}$$

while from equation (25.5)

$$dT = dT_o - \frac{VdV}{C_p}$$

Combining these equations gives an expression for dp in terms of T_o and V only:

$$dp = \frac{mRdT_o}{AV} - \frac{m(\gamma-1)dV}{A\gamma} - \frac{mRT_odV}{AV^2} + \frac{m(\gamma-1)dV}{2A\gamma} \qquad \ldots\ldots (25.A.1)$$

Using equations (25.2) and (25.3) to eliminate ρ:

$$\frac{mdV}{A} + dp + \frac{2mfVdx}{AD} + \sigma B^2(1-K)Vdx = 0$$

and using equation (25.A.1) to eliminate dp gives an expression in which the only variables are x, V and T:

$$\left[\frac{m(\gamma+1)}{2A\gamma} - \frac{mRT_o}{AV^2}\right]dV + \frac{mRdT_o}{AV} + \left[\frac{2mf}{AD} + \sigma B^2(1-K)\right]Vdx = 0 \qquad \ldots\ldots (25.A.2)$$

When this is combined with the energy equation (25.1) to eliminate dx a linear differential equation of first order for T_o in terms of V is obtained:

$$\frac{K_1 dT_o}{dV} + \frac{(K_2V^2+K_3)K_4T_o}{V(K_5V^2-K_6)} = \frac{K_7V(K_2V^2+K_3)}{(K_5V^2-K_6)} \qquad \ldots\ldots (25.A.3)$$

in which

$$K_1 = mC_p/A$$

$$K_2 = \sigma B^2K(1-K)$$

$$K_3 = 4h(T_{aw}-T_w)/D$$

$$K_4 = mR/A$$

$$K_5 = \frac{2fm}{AD} - \sigma B^2(1-K)\left[\frac{\gamma-1}{\gamma}K - 1\right]$$

$$K_6 = 4h(T_{aw}-T_w)\ (\gamma-1)/\gamma C_pD$$

$$K_7 = m(\gamma+1)/2A\gamma.$$

Equation (25.A.3) may be written in the usual form:

$$\frac{dT_o}{dV} + T_o f_1(V) = g_1(V) \qquad \ldots\ldots (25.A.4)$$

where $f_1(V)$ and $g_1(V)$ are functions of V given by:

$$f_1(V) = \frac{K_4(K_2V^2+K_3)}{K_1V(K_5V^2-K_6)}$$

$$g_1(V) = \frac{K_7V(K_2V^2+K_3)}{K_1(K_5V^2-K_6)}$$

The solution to this equation is obtained by multiplying through equation (25.A.4) by the integrating factor, $\exp\left\{\int f_1(V)dV\right\}$, and then integrating the resultant equation. This operation yields an expression for stagnation temperature in terms of velocity:

$$T_o = \frac{K_7V}{K_1K_5(V^2-K_8)^{K_9}} \int (K_2V^2+K_3)V^{2K_{10}} \left(1-\frac{K_8}{V^2}\right)^{K_{10}} dV \qquad \ldots\ldots (25.A.5)$$

where $K_8 = K_6/K_5$

$$= \frac{4h(T_{aw}-T_w)(\gamma-1)}{\gamma C_p D\left\{\frac{2fm}{AD} - \sigma B^2(1-K)\left[\frac{\gamma-1}{\gamma}K - 1\right]\right\}}$$

$$K_9 = \frac{K_4}{2K_1}\left[\frac{K_2}{K_5} + \frac{K_3}{K_6}\right]$$

$$= \frac{\gamma-1}{2\gamma}\left\{\frac{\sigma B^2K(1-K)}{\left[\frac{2fm}{AD} - \sigma B^2(1-K)\left(\frac{\gamma-1}{\gamma}K - 1\right)\right]} + \frac{\gamma}{\gamma-1}\right\}$$

and $K_{10} = K_9 - 1$

Provided $V^2 > K_8$, $(1 - K_8/V^2)^{K_{10}}$ may be expanded binomially and the integral in equation (25.A.5) then becomes:

$$K_2 \int (V^{2K_{10}+2} - a_1V^{2K_{10}} + a_2V^{2K_{10}-2} \quad \ldots)\, dV$$

$$+ K_3 \int (V^{2K_{10}} - a_1V^{2K_{10}-4} + a_2V^{2K_{10}-4} \quad \ldots)\, dV \qquad \ldots\ldots (25.A.6)$$

where $a_1 = K_PK_{10}$

$$a_2 = \frac{K_{10}(K_{10}-1)K_8^{\,2}}{2!}$$

$$a_3 = \frac{K_{10}(K_{10}-1)(K_{10}-2)K_8^{\,3}}{3!}$$

When the magnetic field is non-zero there are no singularities so that the integral may be evaluated to give

$$T_o = \frac{K_{11}V^{2+3K_{10}}}{(V^2-K_8)^{K_9}} \left\{ \frac{K_2V^2}{2K_{10}+3} + \frac{b_1}{2K_{10}+1} + \frac{b_2}{(2K_{10}-1)V^2} + \frac{b_3}{(2K_{10}-3)V^4} + \ldots \right.$$

$$\left. \ldots + \frac{\text{const}}{V^{1+2K_{10}}} \right\} \qquad \ldots\ldots (25.A.7)$$

where $b_1 = -K_2a_1 + K_3$

$b_2 = K_2a_2 - K_3a_1$

$b_3 = -K_2a_3 + K_3a_2$

$b_4 = K_2a_4 - K_3a_3$

etc.

and $K_{11} = K_7/K_1K_5$.

From this equation T_o is obtained as a function of velocity.

APPENDIX 25.B

END LEAKAGE LOSSES

The power output of an MPD generator is

$$P = \underline{E} \cdot \underline{J}\, LA \qquad \ldots\ldots (25.B.1)$$

$$= E_z J_z LA \qquad \ldots\ldots (25.B.2)$$

for the co-ordinate system of Fig.25.25(a)

For a segmented electrode system with no end leakage

$$E_z = - KVB \qquad \ldots\ldots (25.B.3)$$

$$J_z = \sigma\, VB(1-K) \qquad \ldots\ldots (25.B.4)$$

thus
$$P = \sigma V^2B^2K(1-K)LA \qquad \ldots\ldots (25.B.5)$$

Way et al[27] suggest that end leakage losses may be accounted for by use of an end leakage factor which is contained in the current term:

$$J_z = (1-C)(1-K)\sigma VB \qquad \ldots\ldots (25.B.6)$$

so that
$$P = \sigma V^2B^2K(1-K)(1-C)LA \qquad \ldots\ldots (25.B.7)$$

According to their calculations

$$C = \frac{\beta^2}{1+\beta^2}\left\{1 - \frac{1}{\frac{(1+\beta^2)L}{2s} + 1}\right\}; \qquad \ldots\ldots (25.B.8)$$

L is the active length of generator and s the distance between the outer electrodes and the adjacent earthed portion of the (symmetric) system (Fig.25.25(a))

Way's end leakage factor has been estimated assuming a constant conductivity from x=0 to x=L + 2s. However, with electron heating, the electrical conductivity is much higher in the magnetic field region than it is outside it; thus this assumption is no longer true. For this case an alternative expression may be obtained for C, as shown below. The magnetic field is assumed constant in the region L and zero outside these limits, corresponding to the ideal practical case.

For the co-ordinate system of Fig. 25.25(a)

$$J_x = \frac{-\sigma}{1+\beta^2}\,(E^*_x + \beta\, E^*_z) \qquad \ldots\ldots (25.B.9)$$

$$J_y = \sigma E^*_y \qquad \ldots\ldots (25.B.10)$$

$$J_z = \frac{\sigma}{1+\beta^2} \left(E_z^* - \beta E_x^*\right) \quad \text{..... (25.B.11)}$$

where $\underline{E}^* = \underline{E} + \underline{V} \times \underline{B}$ (see Harris and Cobine[28]) ..... (25.B.12)

Now
$$\left.\begin{aligned} V_x &= V \; ; \; V_y = V_z = 0 \\ B_y &= B \; ; \; B_x = B_z = 0 \end{aligned}\right\} \quad \text{..... (25.B.13)}$$

so that $E_x^* = E_x$ ..... (25.B.14)

$$E_y^* = E_y \quad \text{..... (25.B.15)}$$

$$E_z^* = E_z + VB \quad \text{..... (25.B.16)}$$

and
$$J_x = \frac{\sigma}{1+\beta^2} \left(E_x + \beta E_z + \beta VB\right) \quad \text{..... (25.B.17)}$$

$$J_y = \sigma E_y \quad \text{..... (25.B.18)}$$

$$J_z = \frac{\sigma}{1+\beta^2} \left(E_z + VB + \beta E_x\right) \quad \text{..... (25.B.19)}$$

For a segmented electrode generator with no end losses $J_x = 0$, and $J_y = 0$; thus

$$E_x = -\beta(E_z + VB) \quad \text{..... (25.B.20)}$$

When end leakage does occur a similar form for E_x may be assumed:

$$E_x = -\beta a(E_z + VB) \quad \text{..... (25.B.21)}$$

where 'a' is a constant to be evaluated, then

$$J_x = \frac{\sigma\beta}{1+\beta^2} (1-a)(E_z + VB) \quad \text{..... (25.B.22)}$$

and
$$J_z = \sigma \frac{(1+\beta^2 a)}{1+\beta^2} (E_z + VB) \quad \text{..... (25.B.23)}$$

E_x and E_z refer to the fields within the generator region L. For a segmented electrode generator E_x is negative (see equation (25.B.20)) thus the potential along the axis of the generator is as shown in Fig.25.25(b). The total voltage developed axially along the generator is $-LE_x$, thus the field in the end region is

$$E_s = -\frac{LE_x}{2s} \quad \text{..... (25.B.24)}$$

and the current density is

$$J_x = \sigma_s E_s \quad \text{..... (25.B.25)}$$

where σ_s is the conductivity in the end region, which differs from that in the active region σ.

Using equations (25.B.21), (25.B.22), (25.B.24) and (25.B.25) gives

$$a = \frac{1}{1 + \frac{\sigma_s L(1+\beta^2)}{\sigma \quad 2s}} \qquad \ldots\ldots (25.B.26)$$

From equations (25.B.3), (25.B.6) and (25.B.23)

$$C = \frac{\beta^2(1-a)}{1+\beta^2} \qquad \ldots\ldots (25.B.27)$$

thus

$$C = \frac{\beta^2}{1+\beta^2}\left\{1 - \frac{1}{\frac{(1+\beta^2)L\sigma_s}{2s\sigma} + 1}\right\} \qquad \ldots\ldots (25.B.28)$$

Inspection of this equation shows that it reduces to Way's[27] expression (equation (25.B.8)) when $\sigma_s = \sigma$. The equation may be re-written as

$$C = \frac{\beta^2 \frac{L}{s}\frac{\sigma_s}{\sigma}}{(1+\beta^2)\frac{L}{s}\frac{\sigma_s}{\sigma} + 2} \qquad \ldots\ldots (25.B.29)$$

1 the

25.B.26)

25.B.27)

25.B.28)

quation

5.B.29)

TABLE 25.1

INPUT VALUES TO CHANNEL (SEMI-FROZEN FLOW IN NOZZLE)

$N_e = 3 \times 10^{18}\ m^{-3}$

$N_{Cs} = 4 \times 10^{21}\ m^{-3}$

$N_{He} = 4 \times 10^{23}\ m^{-3}$

$\nu_{e\text{-}Cs^+} = 1.2 \times 10^{9}\ sec^{-1}$

$\nu_{e\text{-}He} = 4.8 \times 10^{9}\ sec^{-1}$

$\nu_{e\text{-}Cs} = 2.4 \times 10^{9}\ sec^{-1}$

$\nu_{TOT} = 8.3 \times 10^{9}\ sec^{-1}$

$\sigma = 10$ mho.m^{-1}

$p = 5 \times 10^{3}$ newton $.m^{-2}$ (= 0.05 ata)

$T = 874^{\circ}K$

$V = 4100$ m. sec^{-1}

$T_o = 2500^{\circ}K$

TABLE 25.2

CONSTANTS OF CHANNEL

$h = 10^{2}$ watt. m^{-2}. $^{\circ}K^{-1}$

$T_{aw}-T_w = 1000^{\circ}K$

$\gamma = 1.658$

$m = 5.6 \times 10^{-3}$ kg. sec^{-1}

$f = 10^{-2}$

$A = 4.8 \times 10^{-4}\ m^2$

$C_p = 5.192 \times 10^{3}\ m^2.sec^{-2}.\ ^{\circ}K^{-1}$

$R_u = 8.310 \times 10^{3}$ joule.kgm^{-1}. $^{\circ}K^{-1}$

$W = 4.003$

$K = 0.8$ unless otherwise stated.

TABLE 25.3

DISTANCE FROM INLET AT WHICH M= 1 (for conditions of Tables 25.1 and 25.2)

B	x_s	
0	14.25×10^{-2} m	
0.5	10.90	elevated T_e
1.0	4.043	elevated T_e
1.5	1.627	elevated T_e
0.5	14.18	equilibrium $T_e = T$
1.0	14.06	equilibrium $T_e = T$

TABLE 25.4

DATA FOR CALCULATIONS OF SECTION 25.3

HELIUM-CESIUM MIXTURES

CHANNEL CONSTANTS

χ = 0.01

R_{MIX} = 1569 joule/kgm.^{o}K

γ_{MIX} = 1.6657

B = 0.5 webers/m^2

K = 0.8

a' = 0.079

C_{pMIX} = 3926 joule/kgm.^{o}K

m = 0.00645 kgm/sec

D = 0.01890 m

A = 0.00048 m^2

T_w = 1250^{o}K

STARTING DATA

ρ_1 = 0.0376 kgm/m^3

T_1 = 875^{o}K

n_{e_1} = 3.10^{18}/m^3

T_{e1} = 875^{o}K

V_1 = 3570 m/sec

T_{o1} = 2500^{o}K

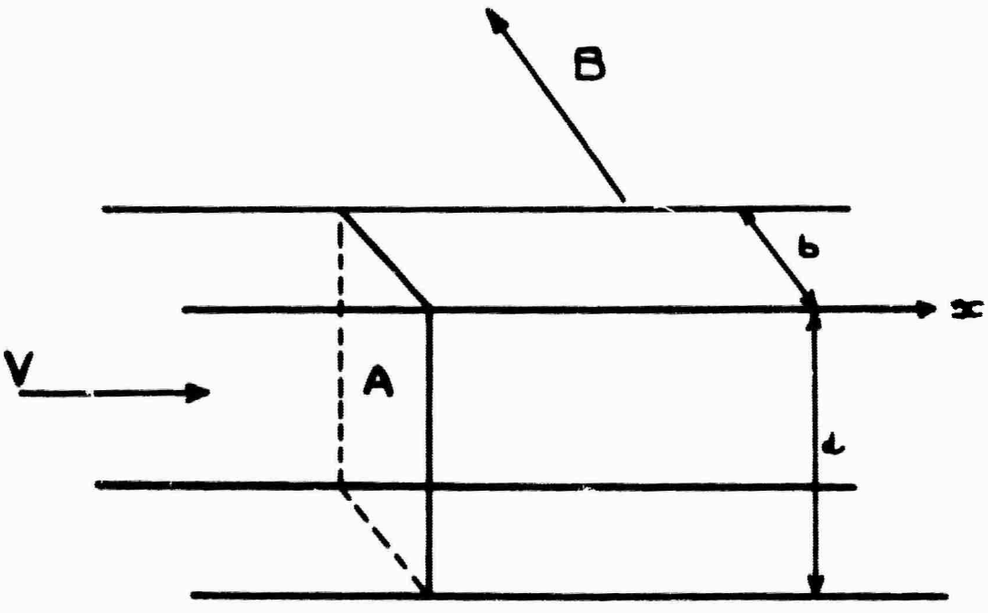

CONSTANT AREA GENERATOR CHANNEL

FIG 25.1

ELECTRON TEMPERATURE (Te), °K

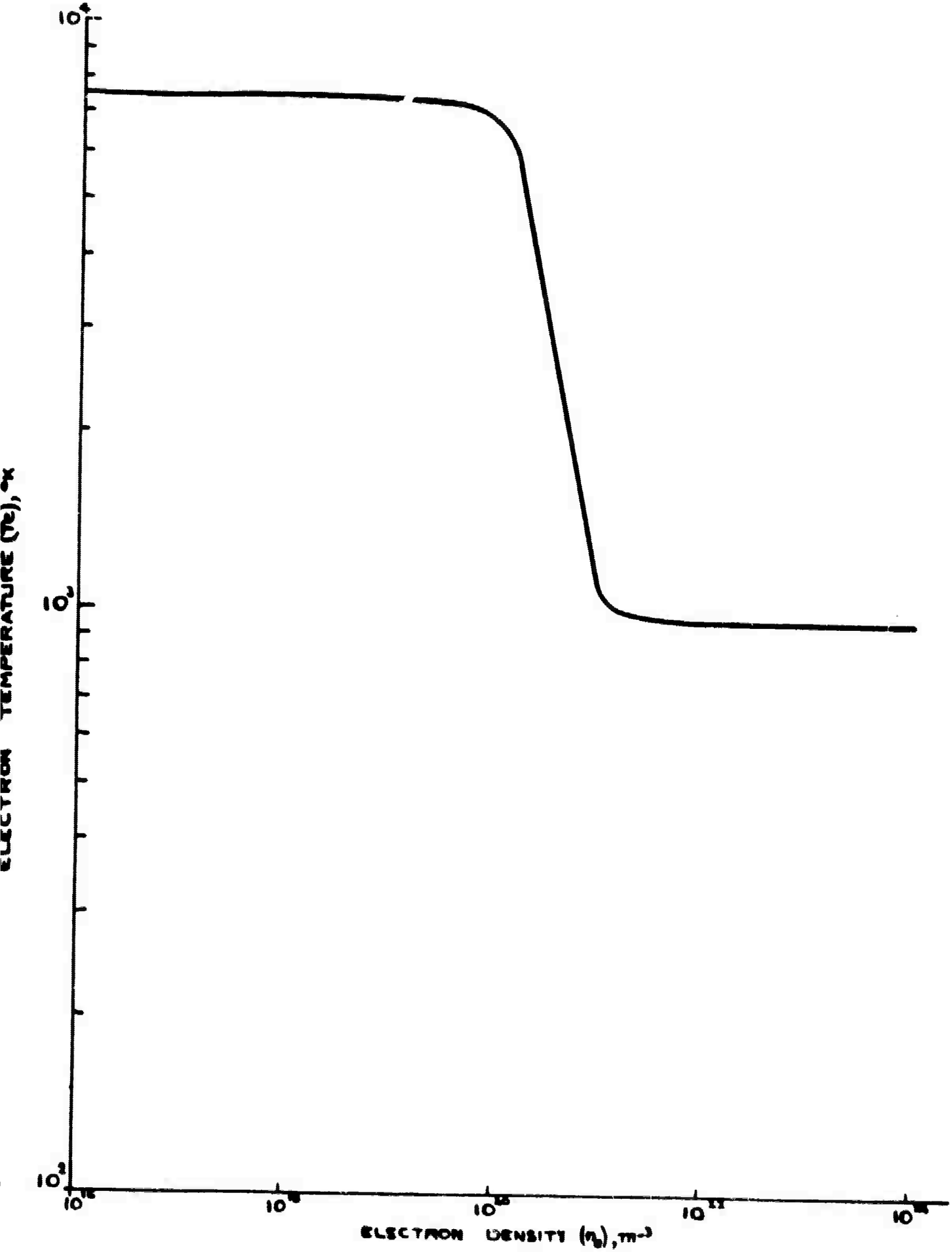

T_e, n_e RELATION FOR ELEVATED ELECTRON TEMPERATURE (EON. 2522)

FIG 25.2

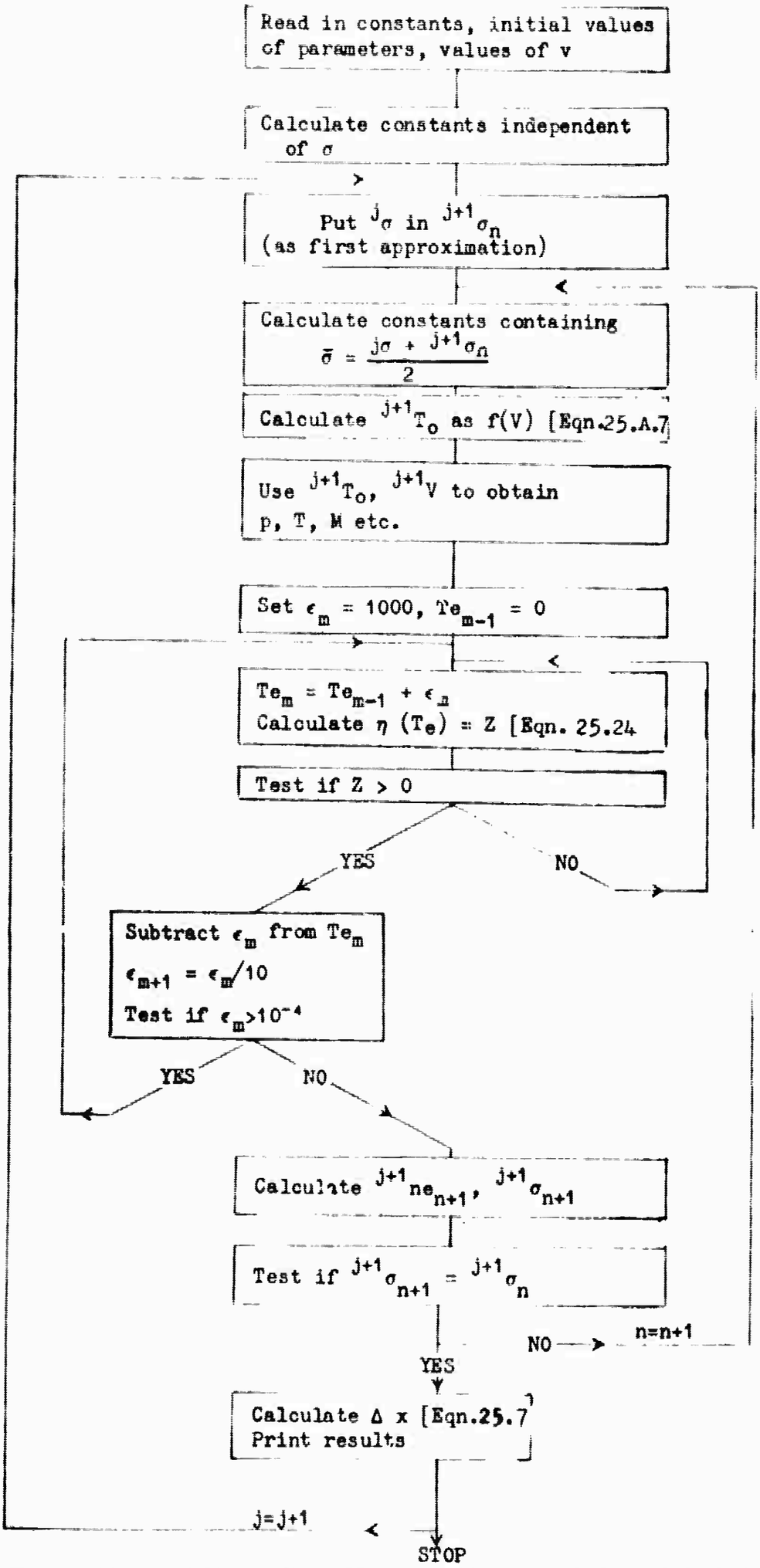

FLOW DIAGRAM OF COMPUTER PROGRAMME ELEVATED ELECTRON TEMPERATURE

FIG 25·3

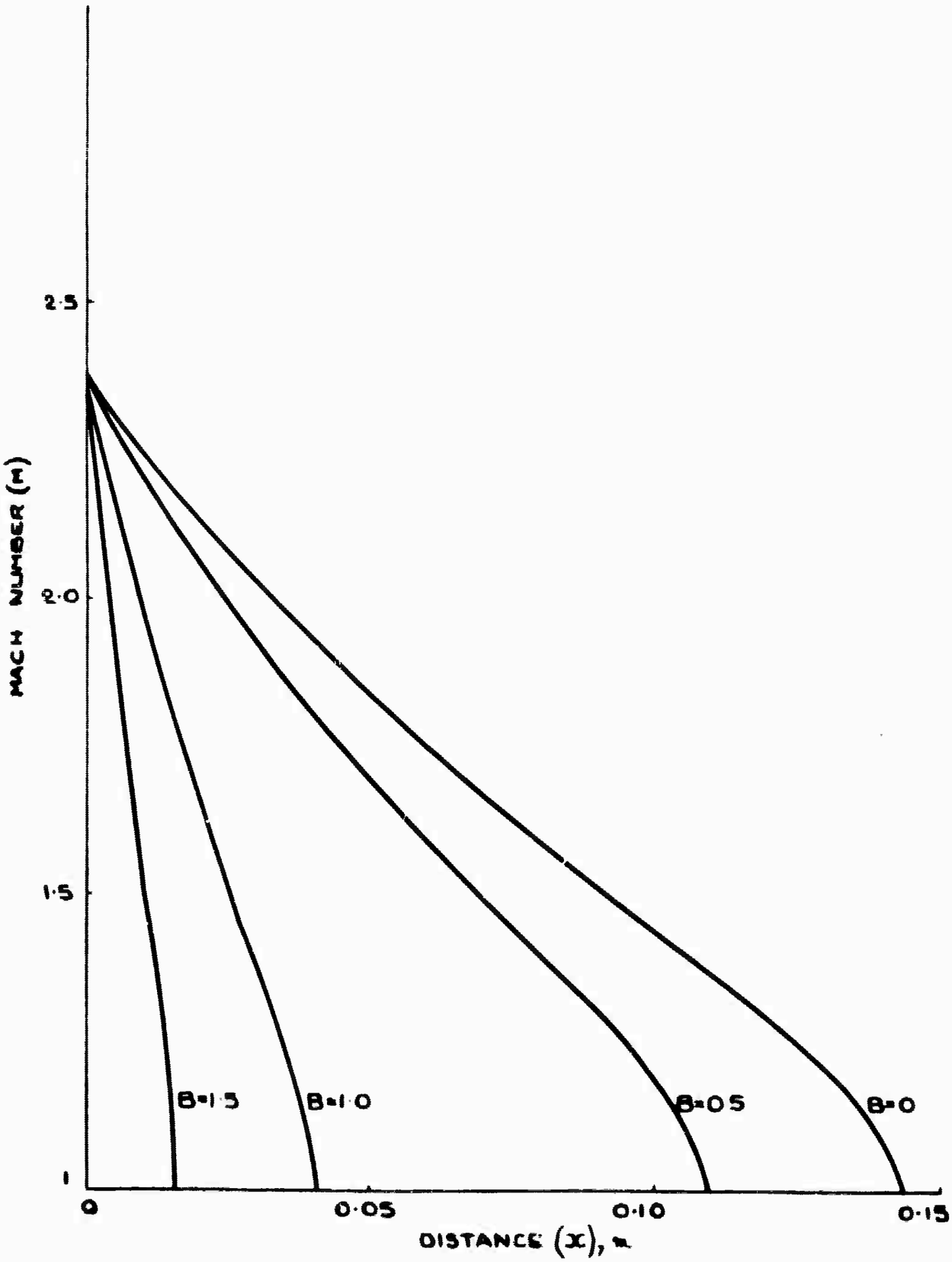

MACH NUMBER AS A FUNCTION OF DISTANCE

FIG 25·4

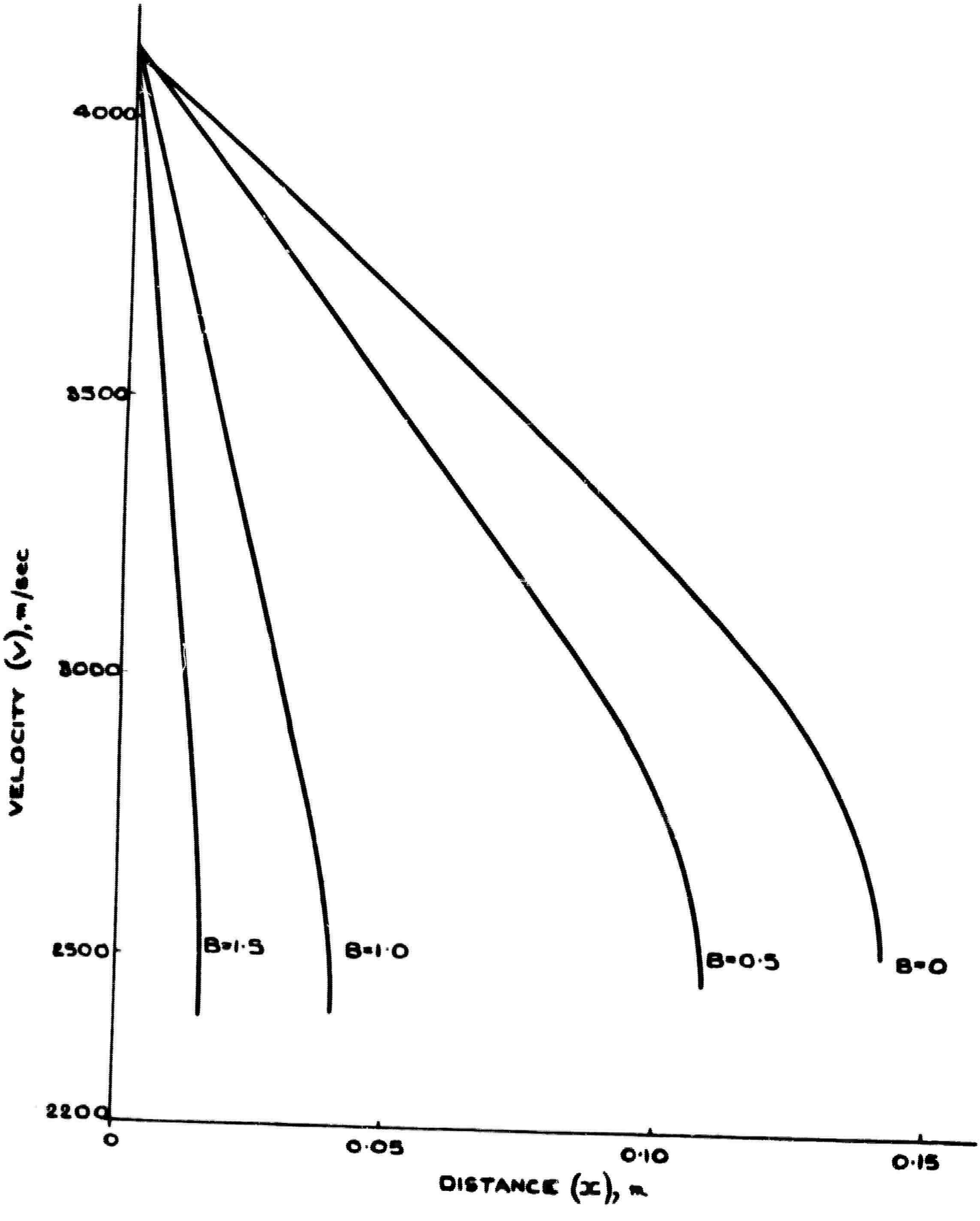

VELOCITY AS A FUNCTION OF DISTANCE

FIG 25·5

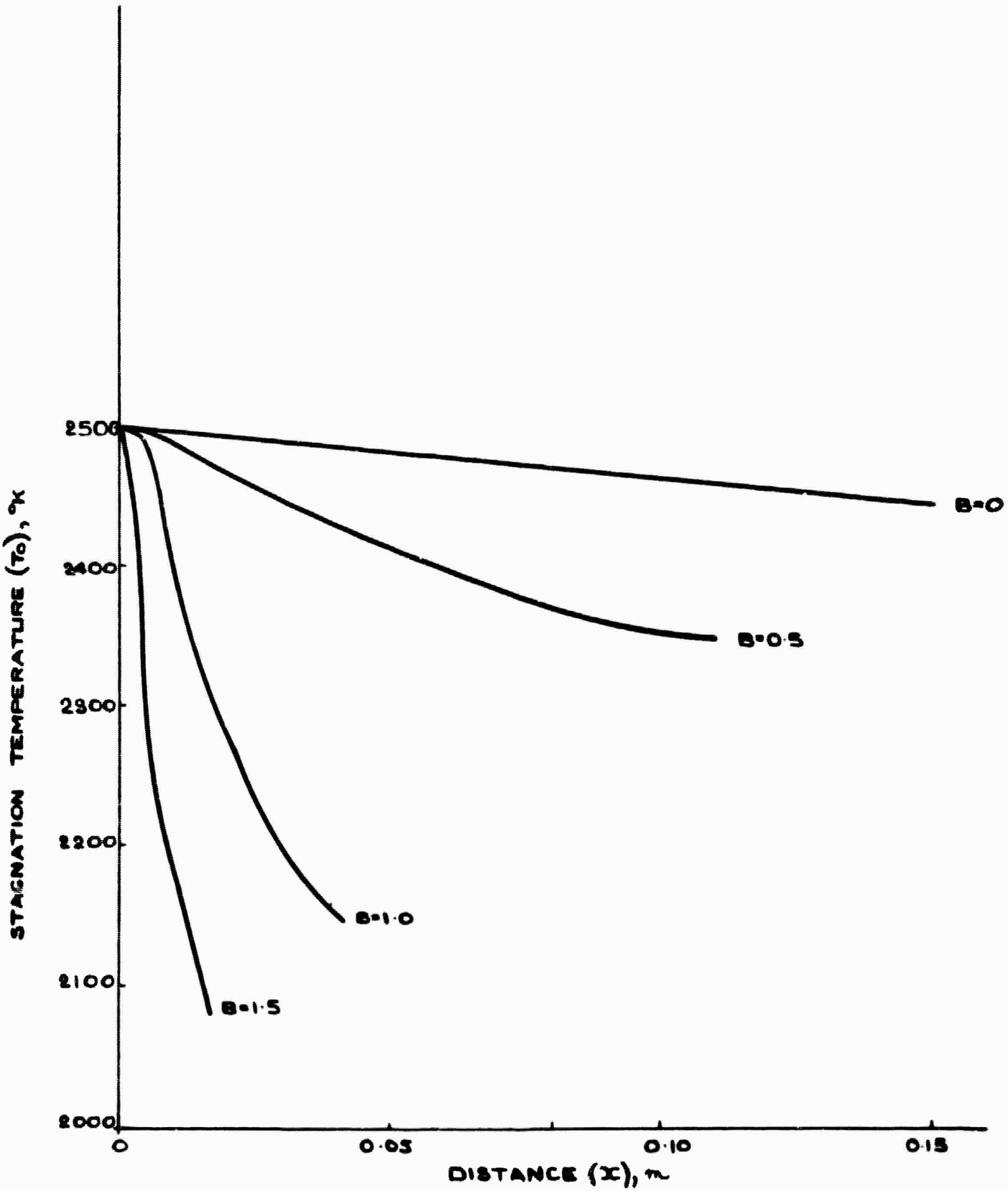

STAGNATION TEMPERATURE AS A FUNCTION OF DISTANCE

FIG 25·6

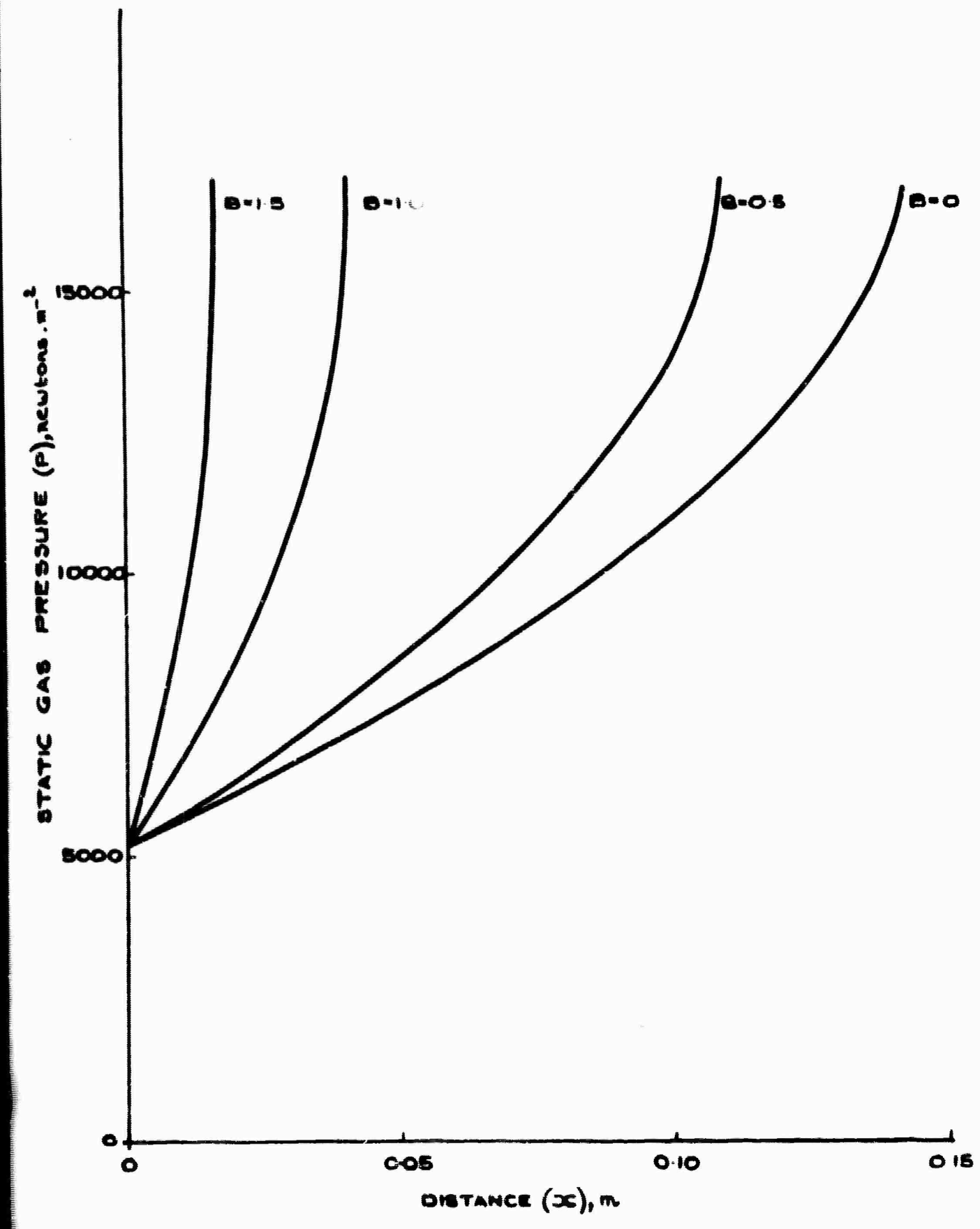

GAS PRESSURE AS A FUNCTION OF DISTANCE

FIG 25·7

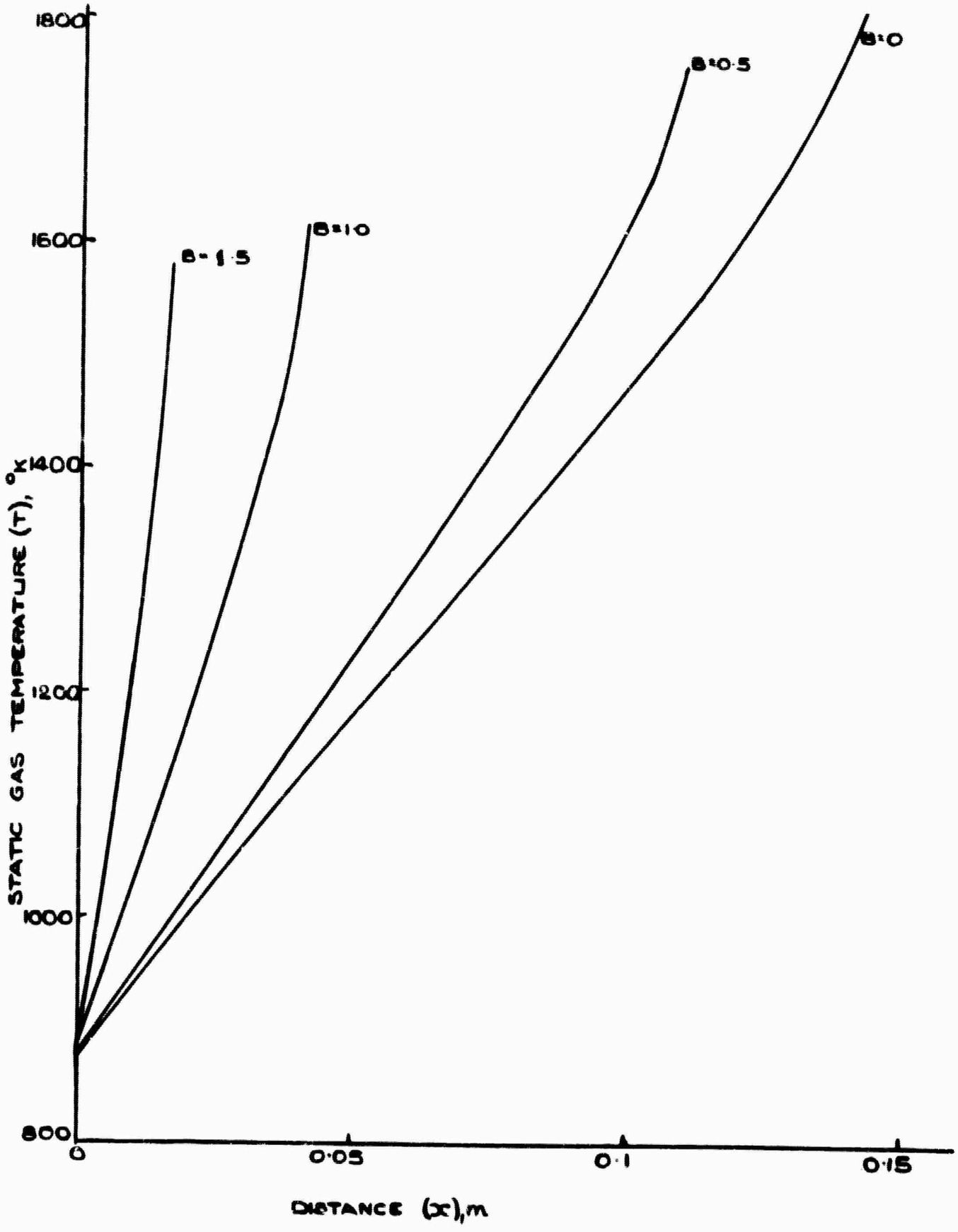

GAS TEMPERATURE AS A FUNCTION OF DISTANCE

FIG 25·8

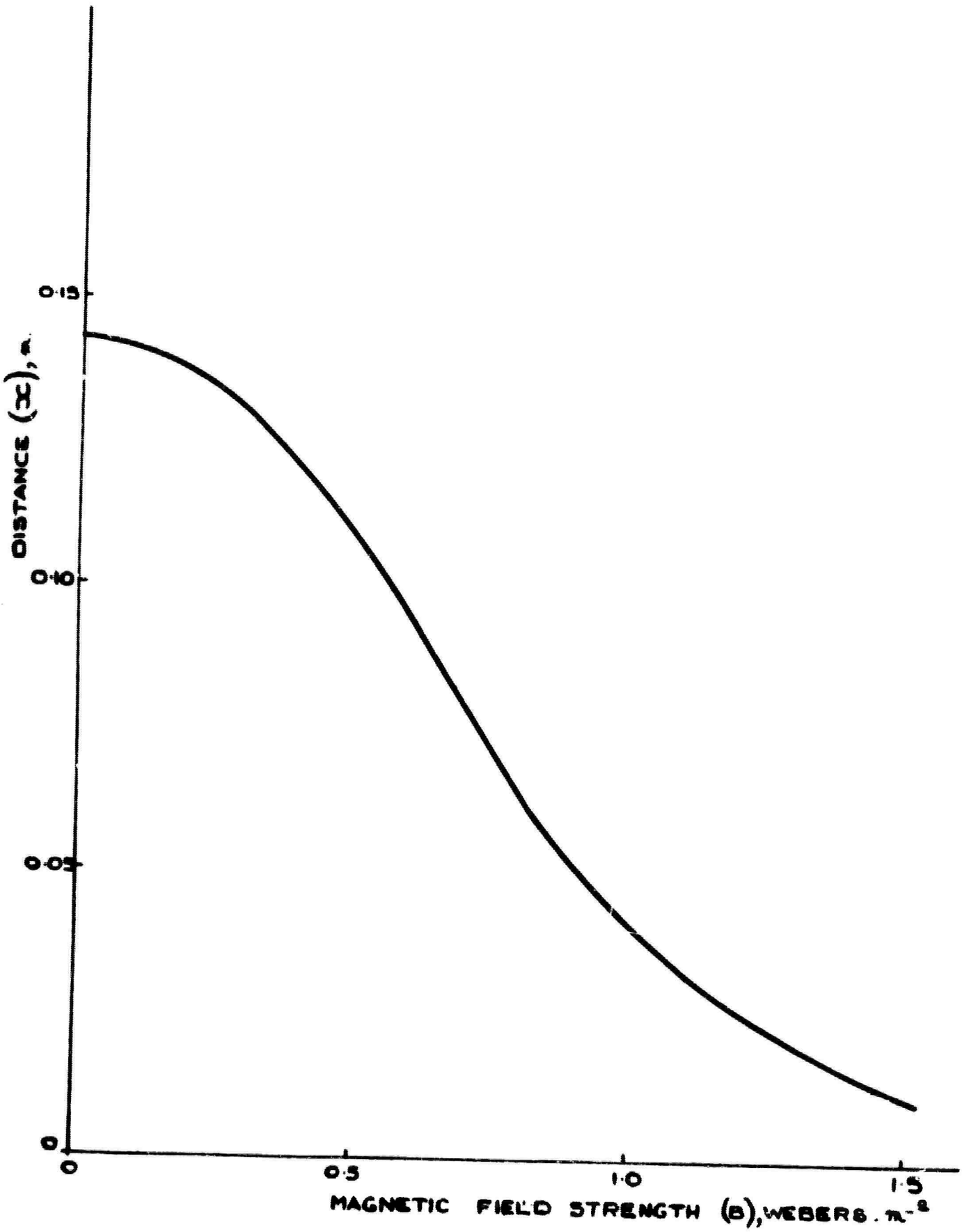

LENGTH FOR SUPERSONIC FLOW AS A FUNCTION OF MAGNETIC FIEL

FIG 25·9

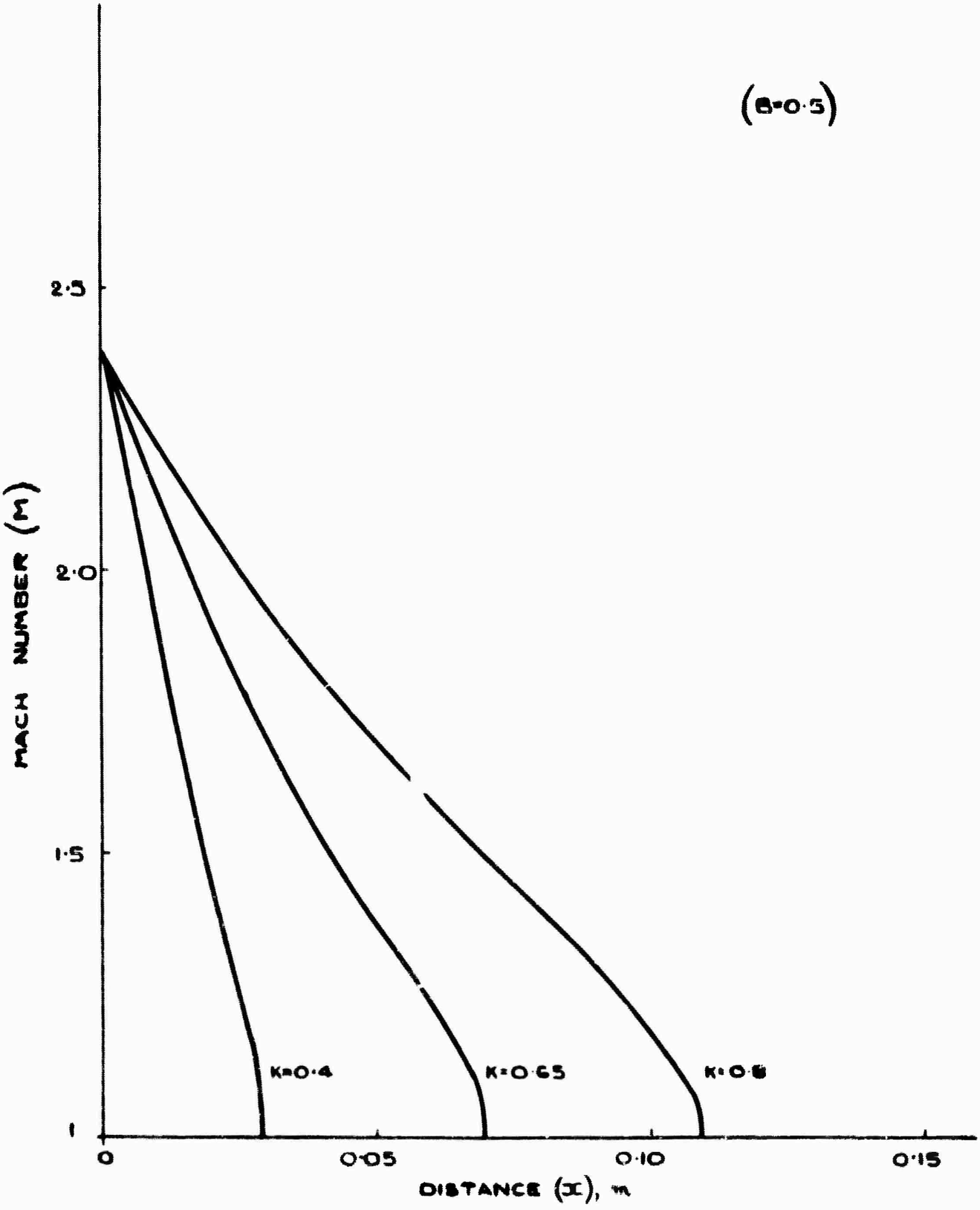

MACH NUMBER AS A FUNCTION OF DISTANCE AND LOAD FACTOR

FIELD

9

FIG 25·10

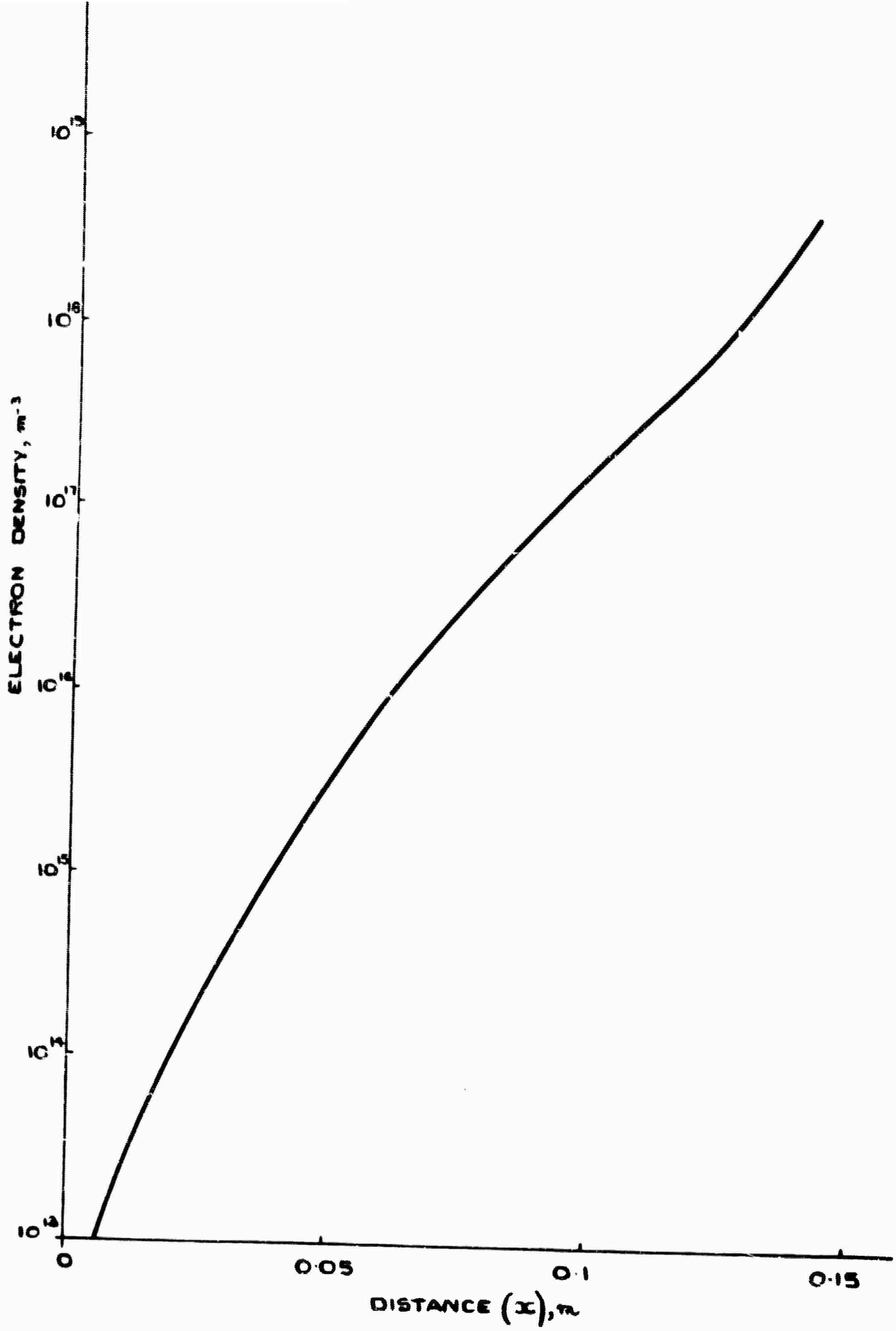

ELECTRON DENSITY AS A FUNCTION OF DISTANCE ($T_e = T$)

FIG 25·11

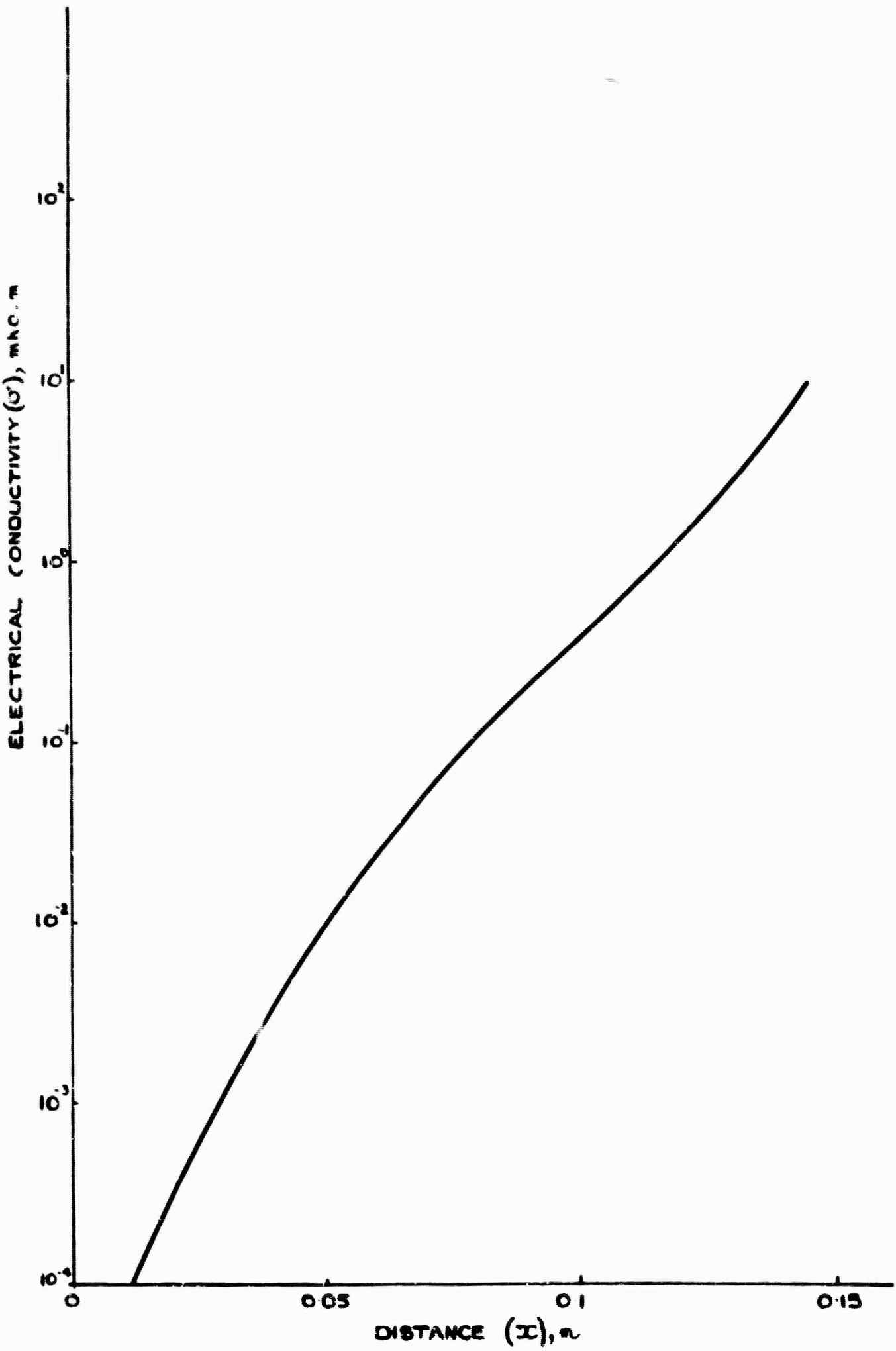

ELECTRICAL CONDUCTIVITY AS A FUNCTION OF DISTANCE (Te=T)

FIG 25·12

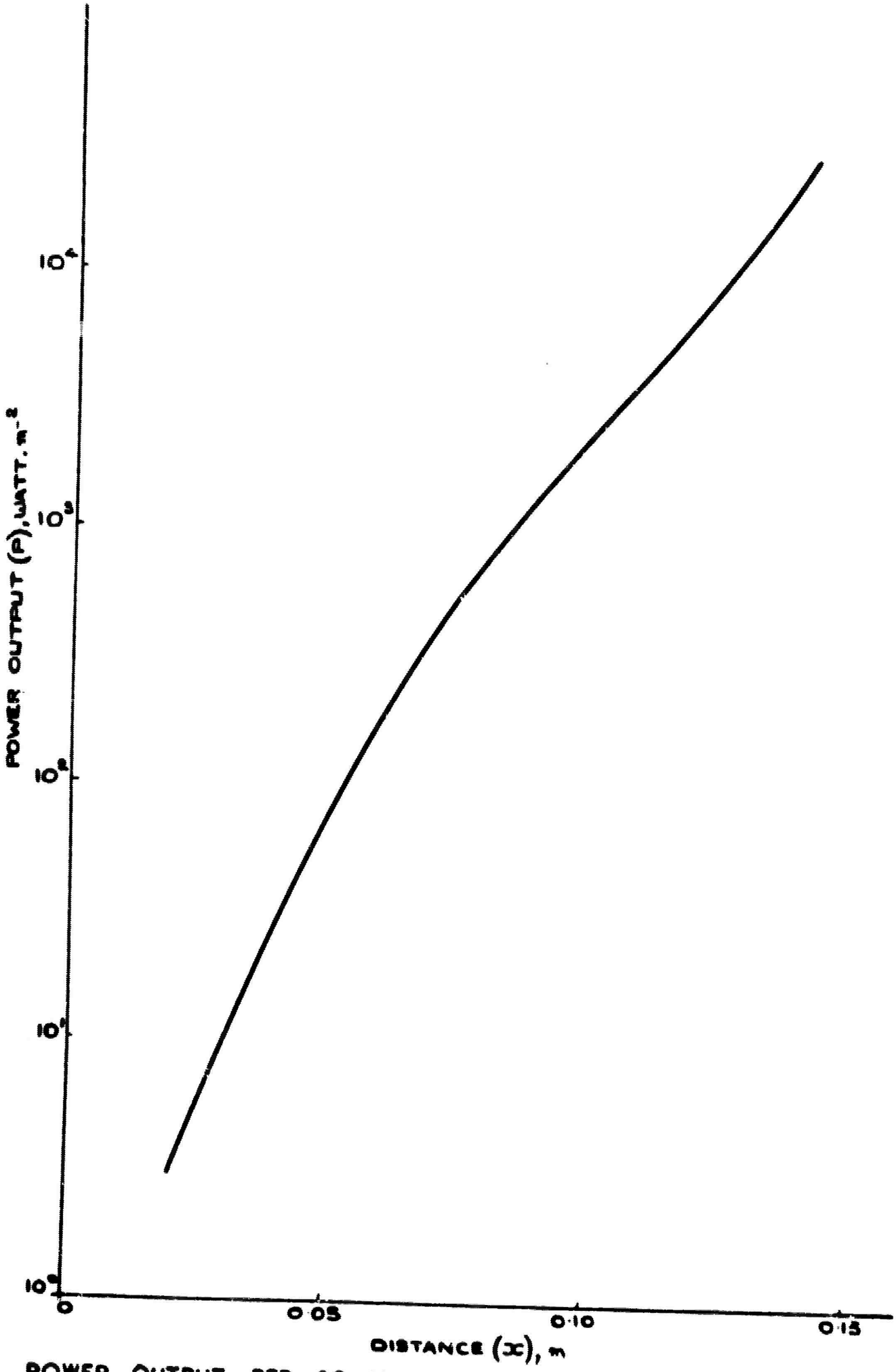

POWER OUTPUT PER SQUARE METRE OF ELECTRODE SURFACE AS A FUNCTION OF DISTANCE $T_0 = T$, B=10

FIG 25·13

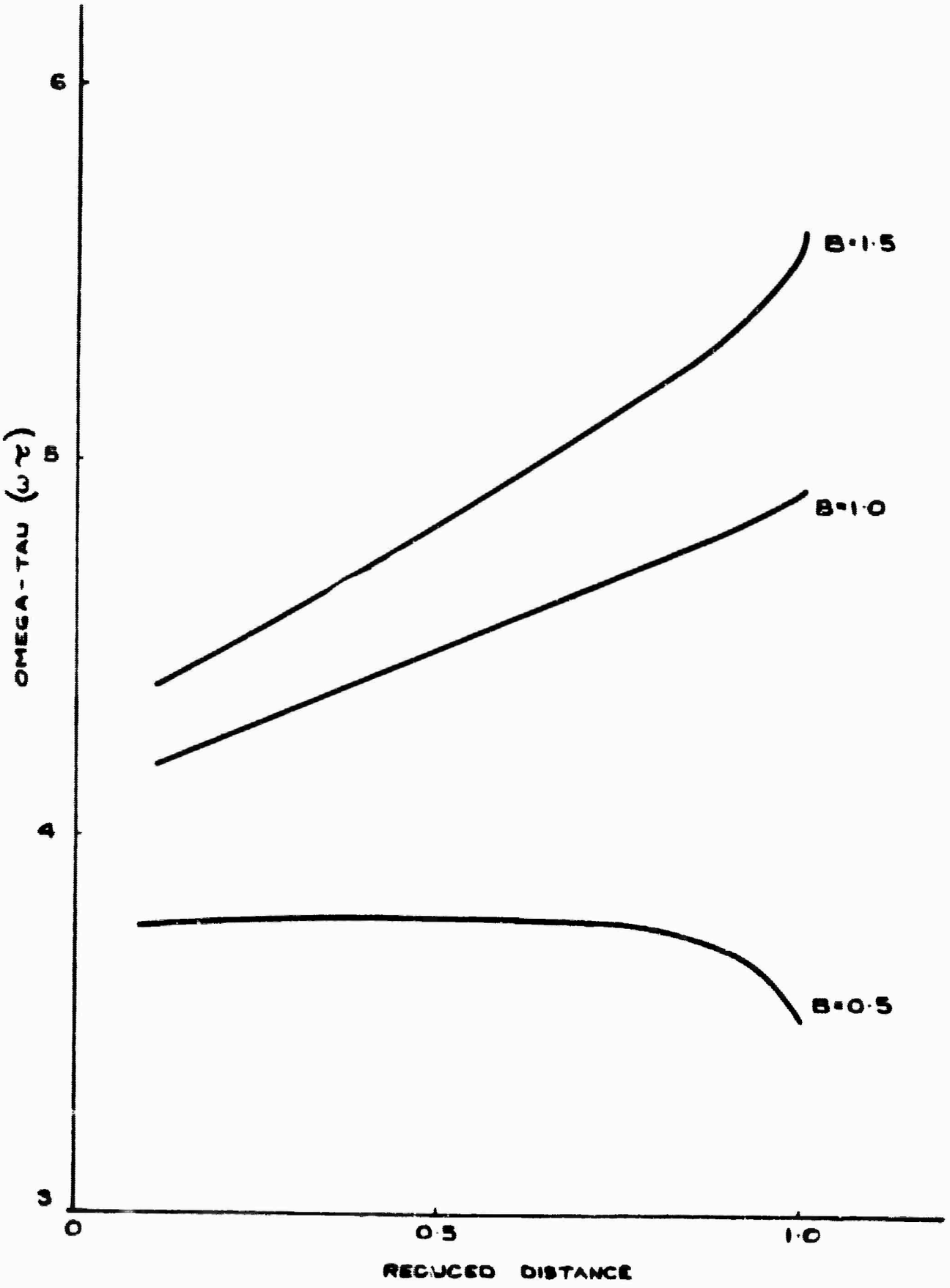

OMEGA–TAU AS A FUNCTION OF REDUCED DISTANCE

FIG 25·14

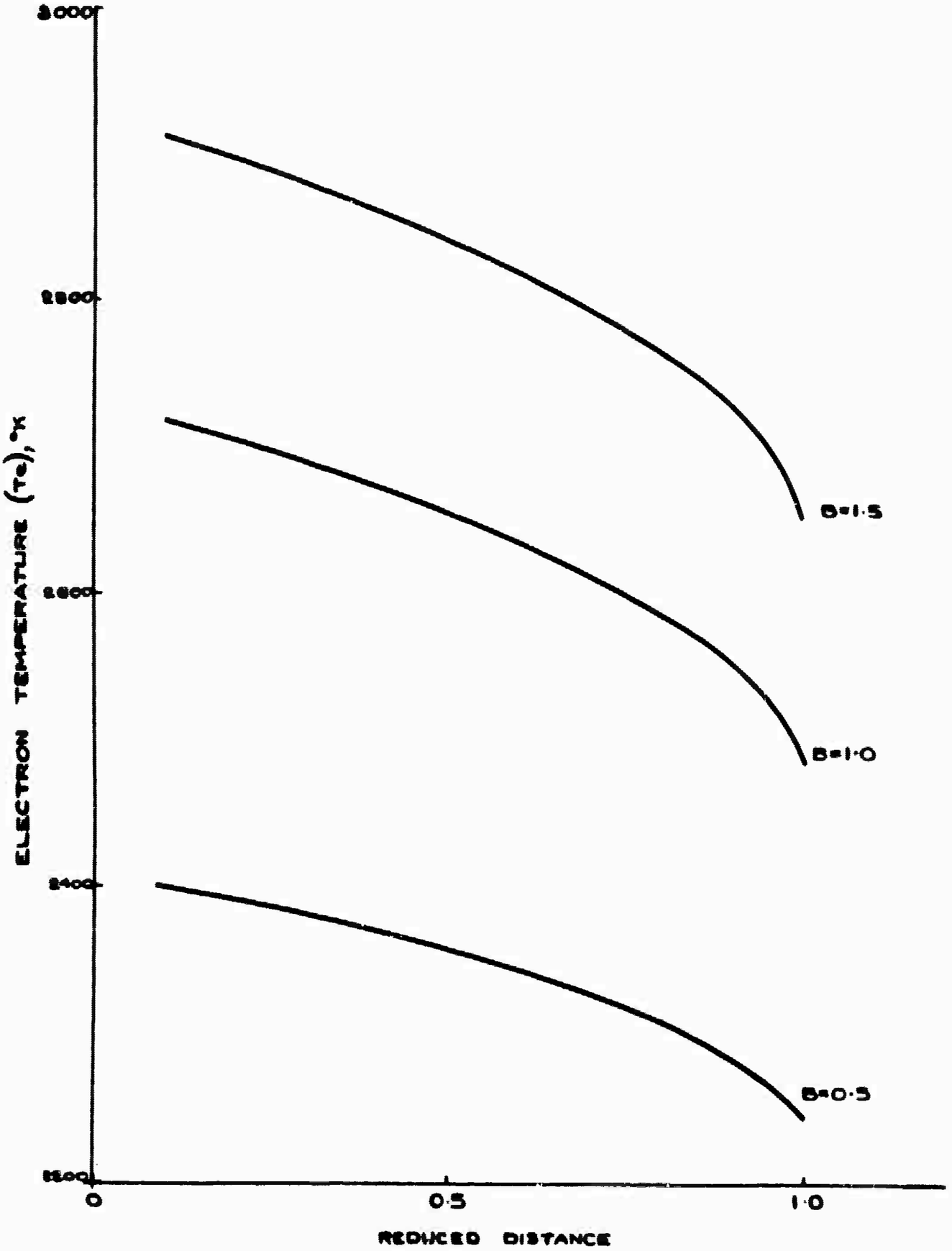

ELECTRON TEMPERATURE AS A FUNCTION OF REDUCED DISTANCE

FIG 25·15

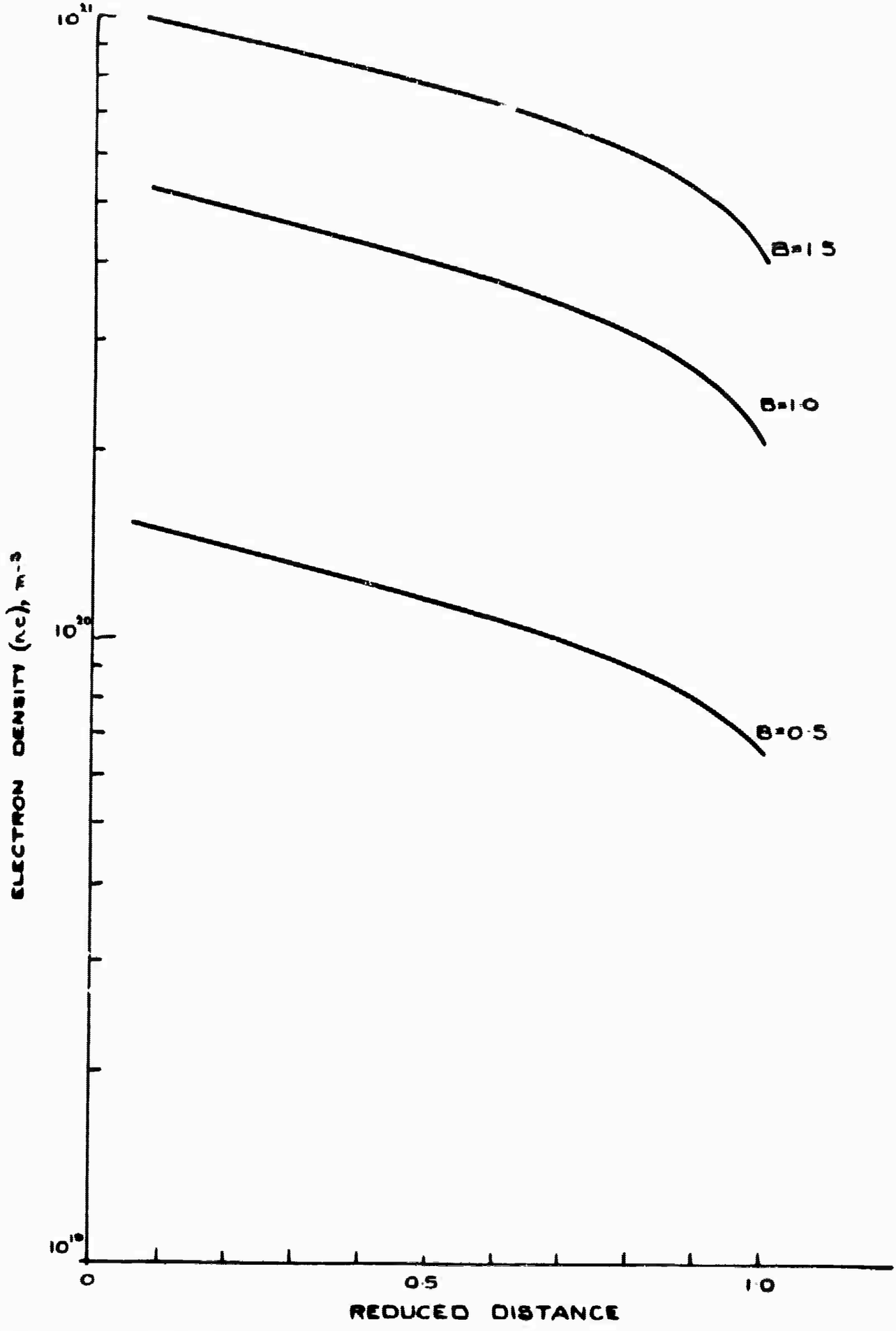

ELECTRON DENSITY AS A FUNCTION OF REDUCED DISTANCE

FIG 25·16

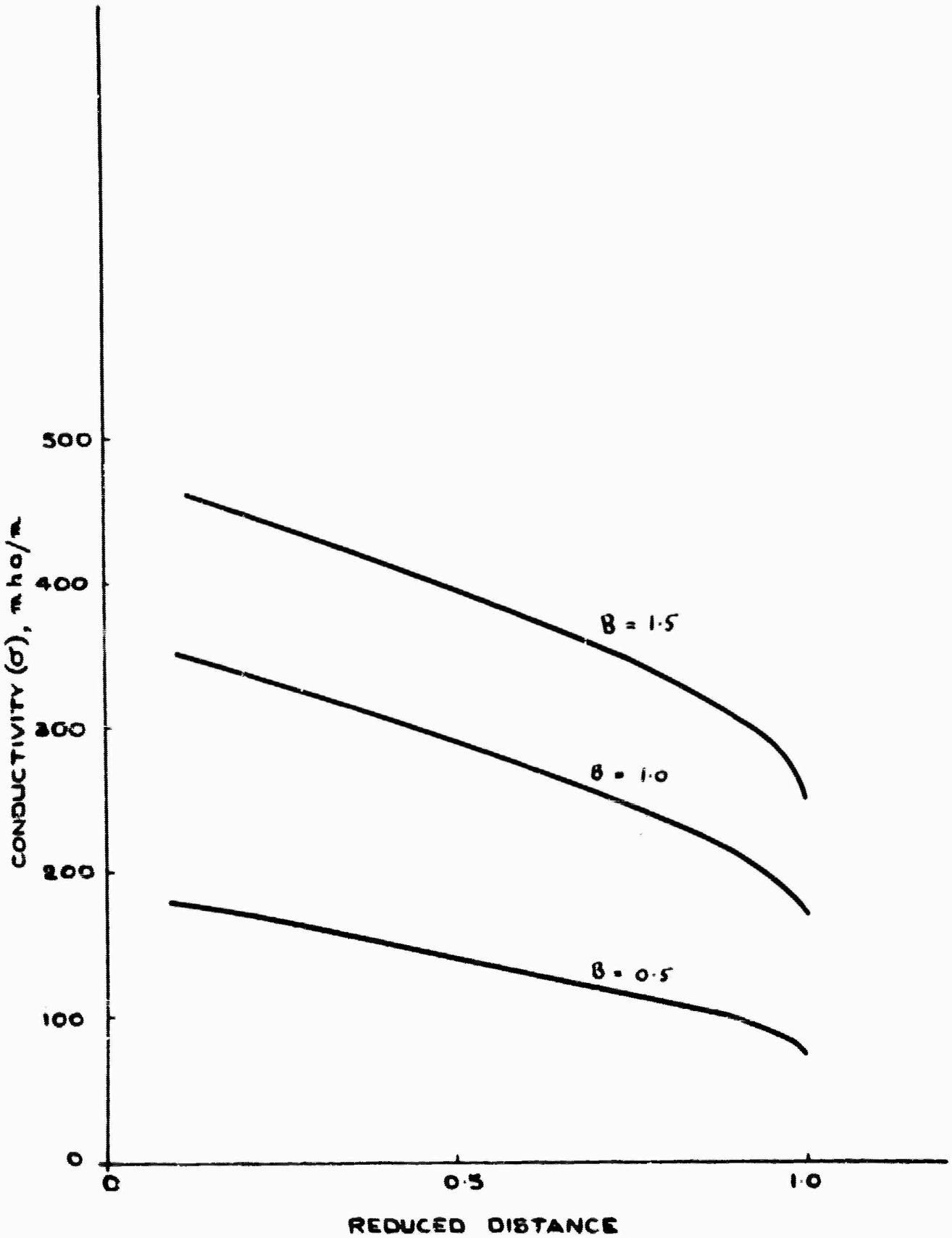

ELECTRICAL CONDUCTIVITY AS FUNCTION OF REDUCED DISTANCE

FIG 25·17

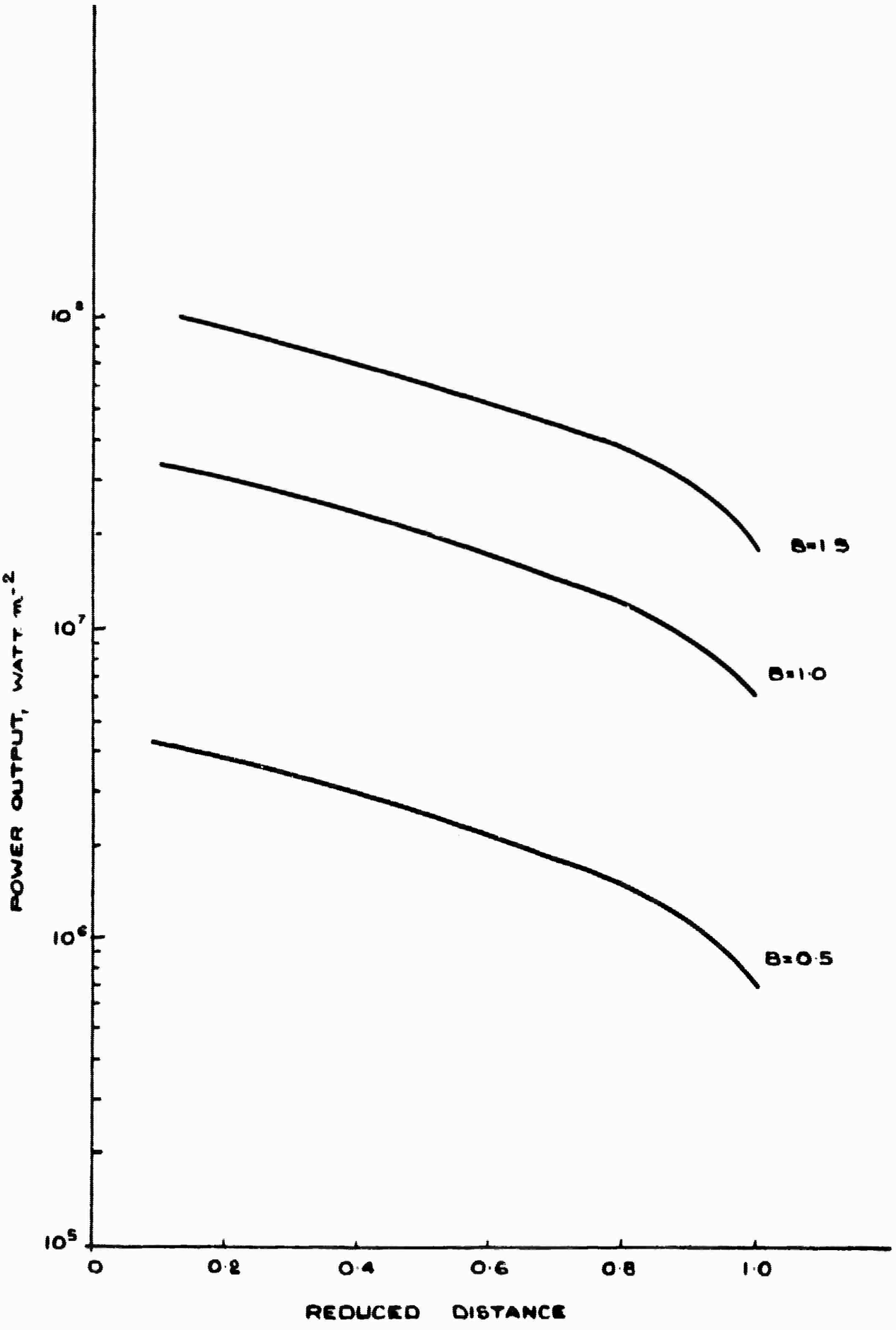

POWER OUTPUT PER SQUARE METRE OF ELECTRODE SURFACE AS A FUNCTION OF REDUCED DISTANCE

FIG 25·18

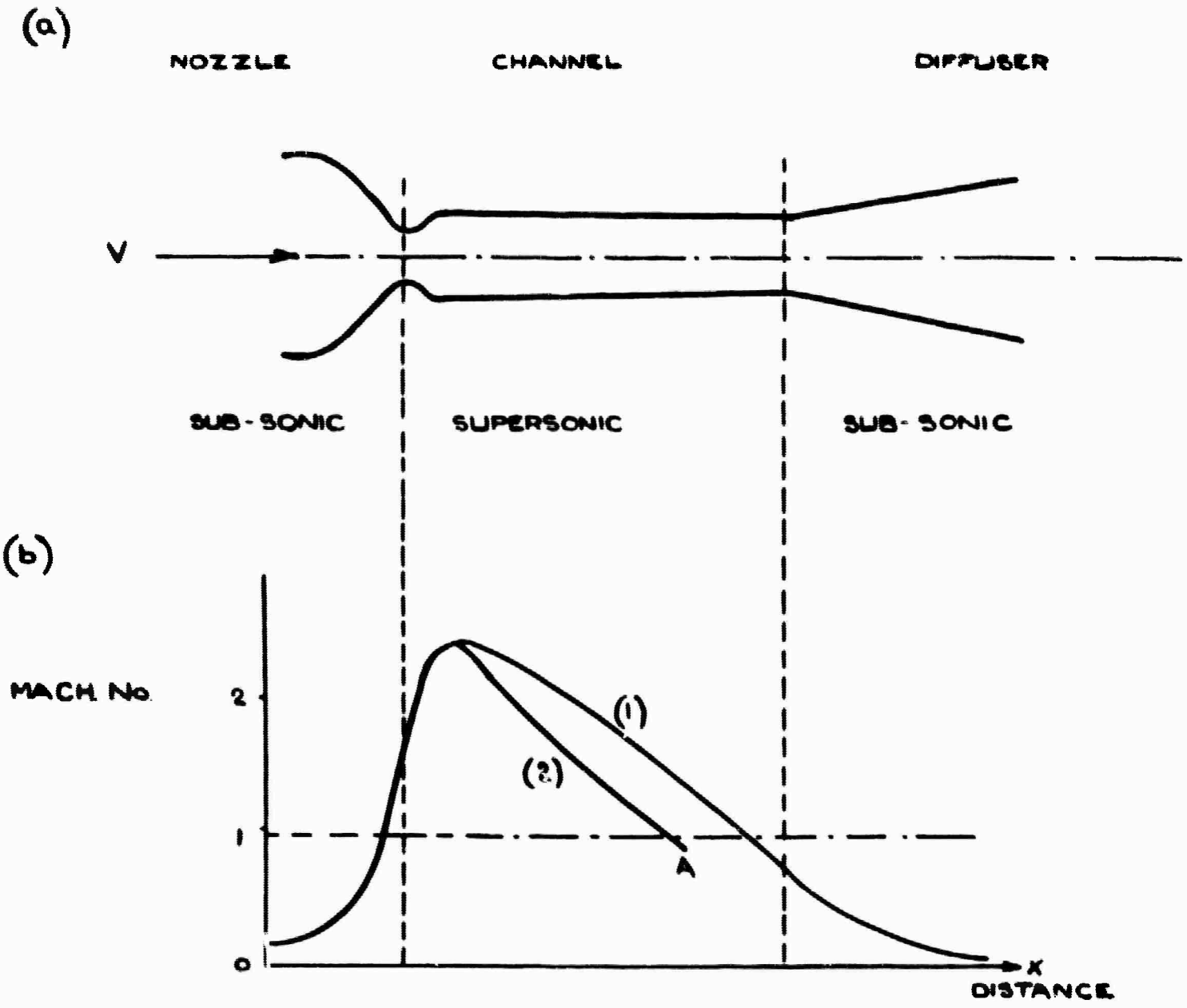

PERFORMANCE CHARACTERISTICS OF IRD MPD GENERATOR CHANNEL I

FIG 25·19

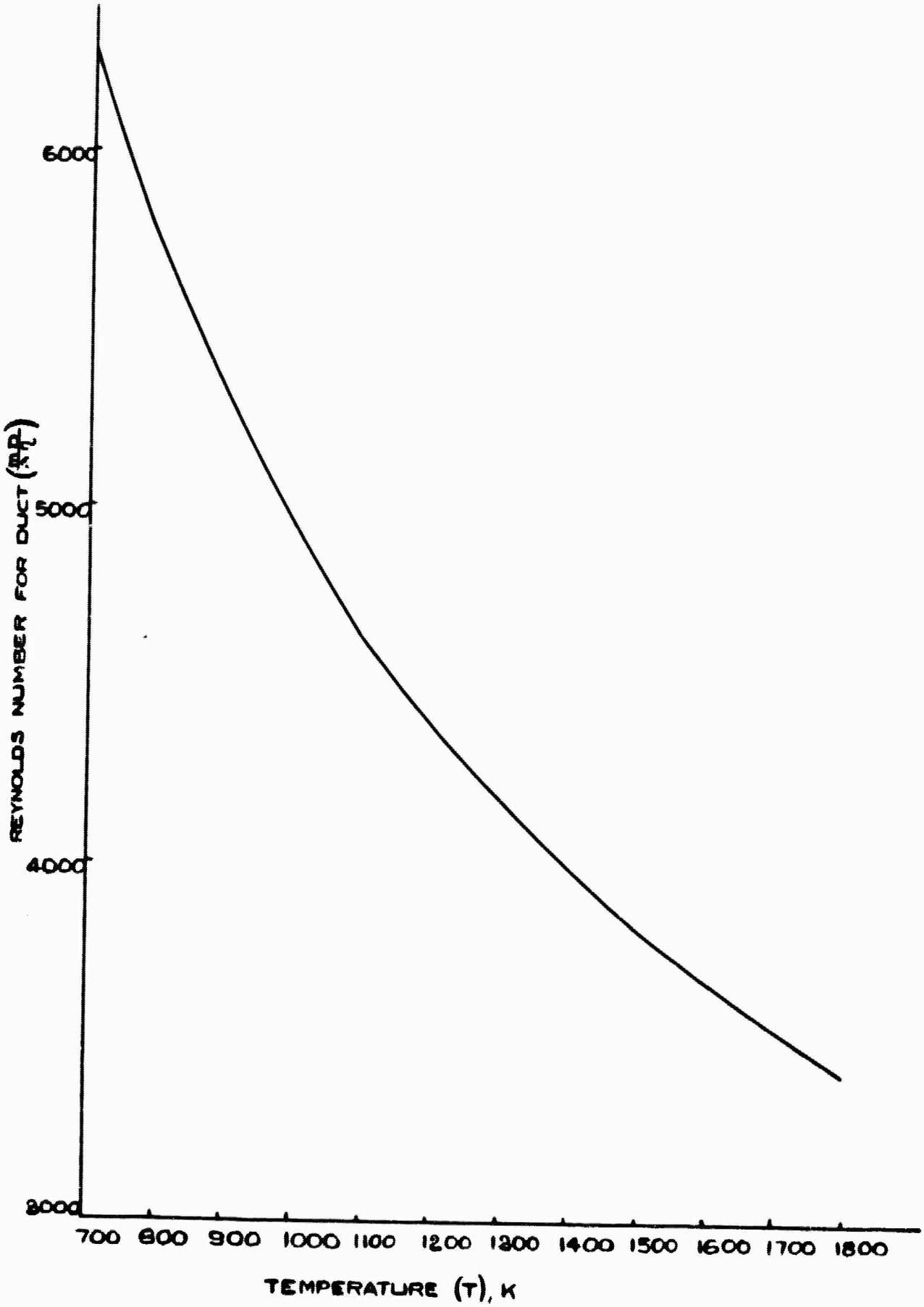

VARIATION OF REYNOLDS NUMBER WITH TEMPERATURE

FIG 25·20

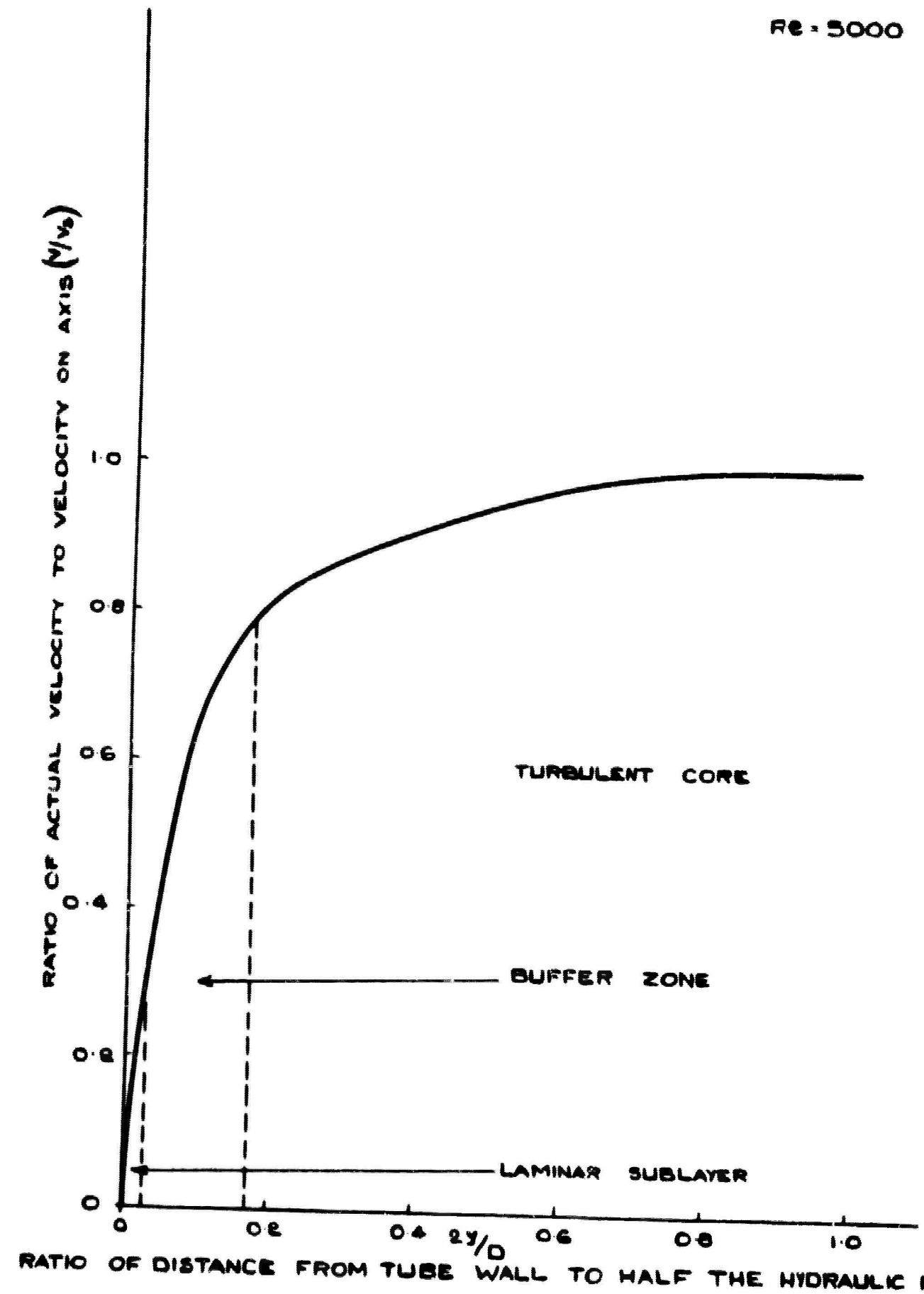

VELOCITY DISTRIBUTION

FIG 25·2

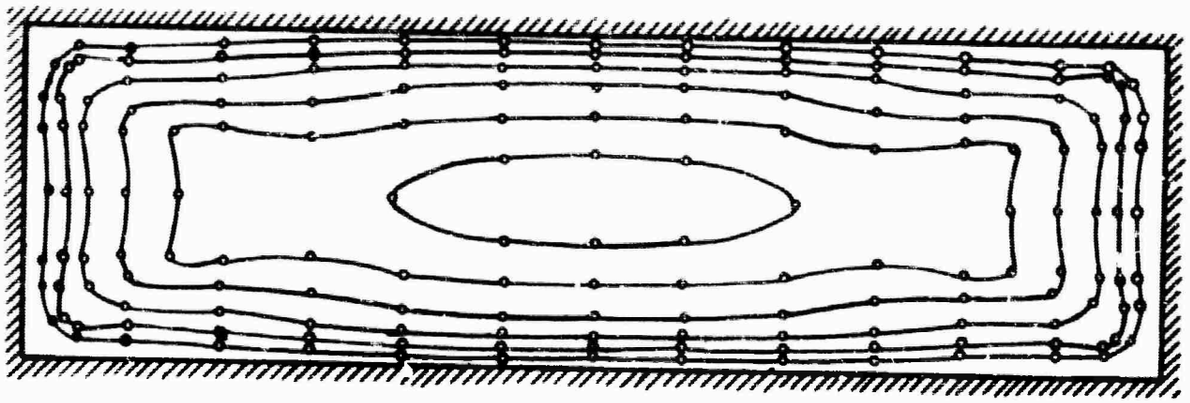

AMETER

CURVES OF CONSTANT VELOCITY FOR PIPE OF RECTANGULAR CROSS-SECTIO

FIG 25·22

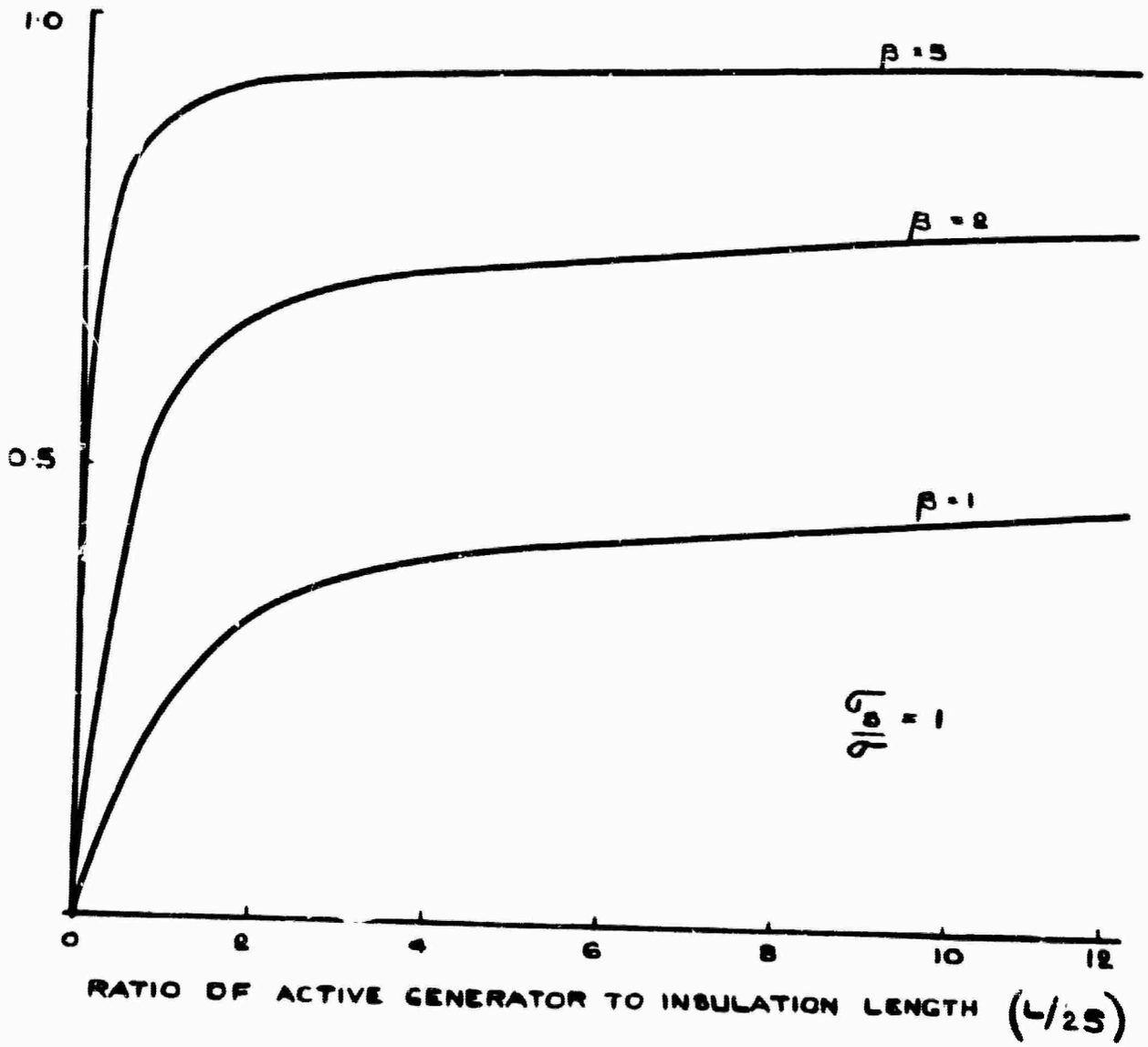

END LEAKAGE FACTOR

FIG 25·23

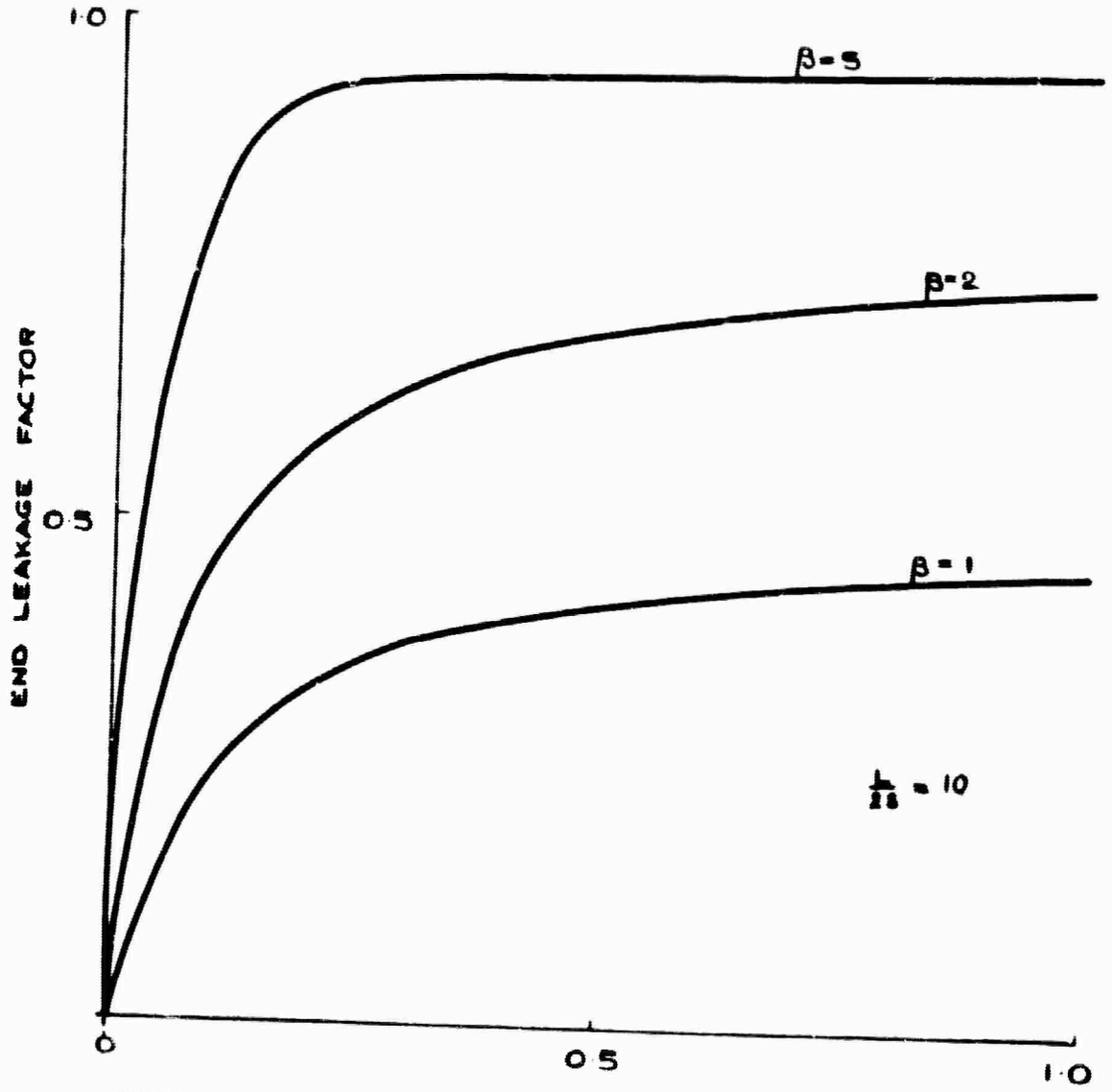

END LEAKAGE FACTOR

FIG 25·24

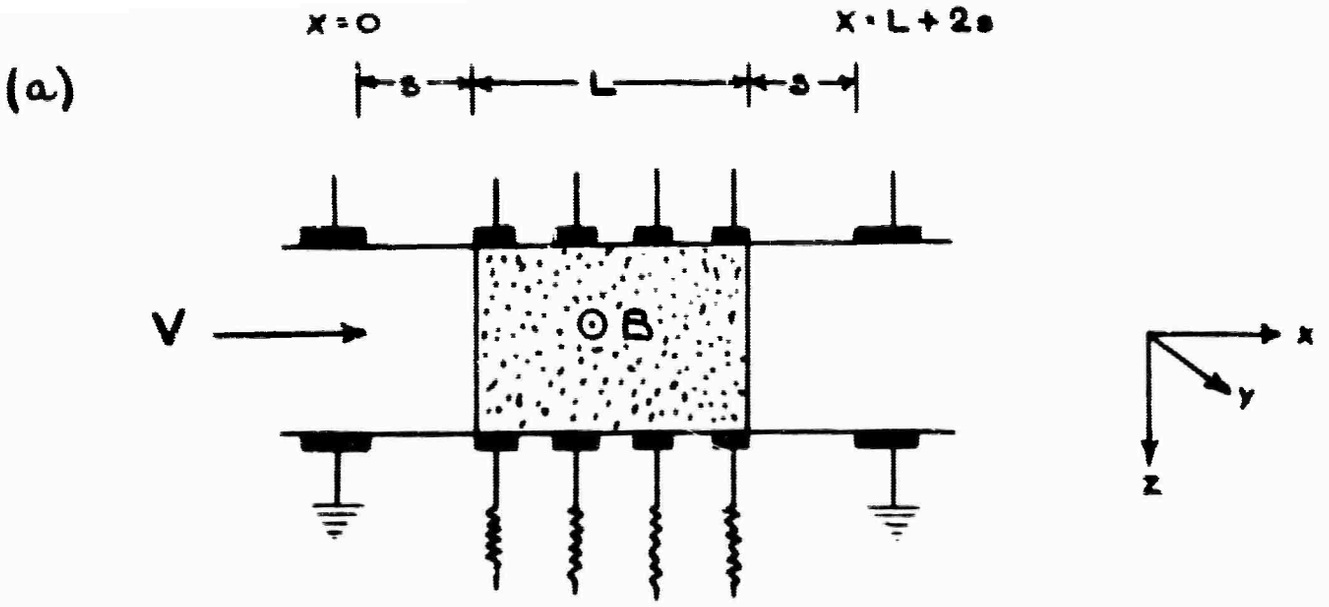

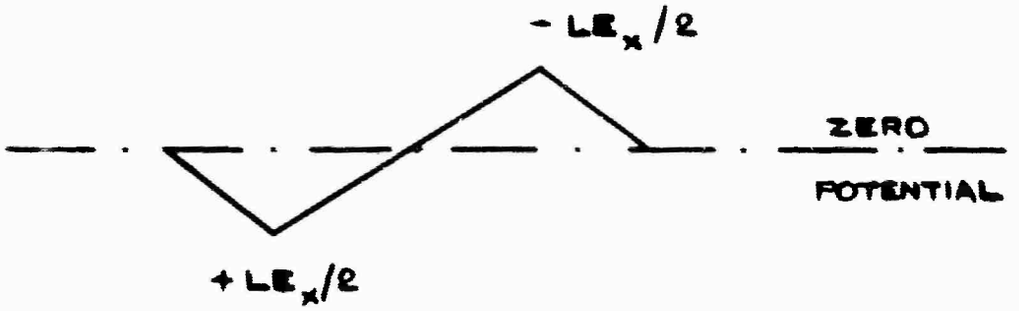

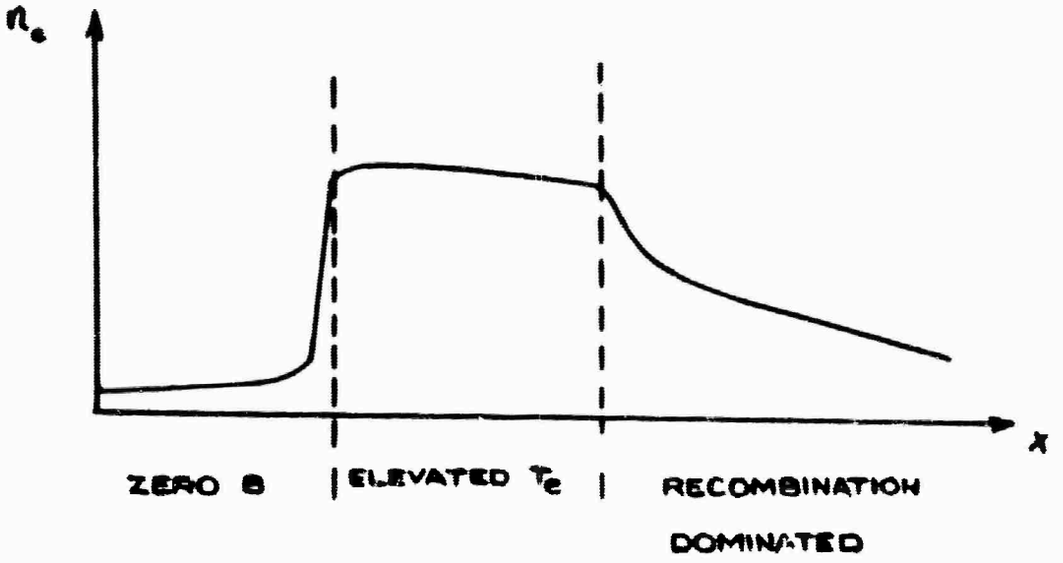

GENERATOR SECTION, POTENTIAL AND ELECTRON DENSITY FOR END LEAKAGE CALCULATIONS

FIG. 25-25

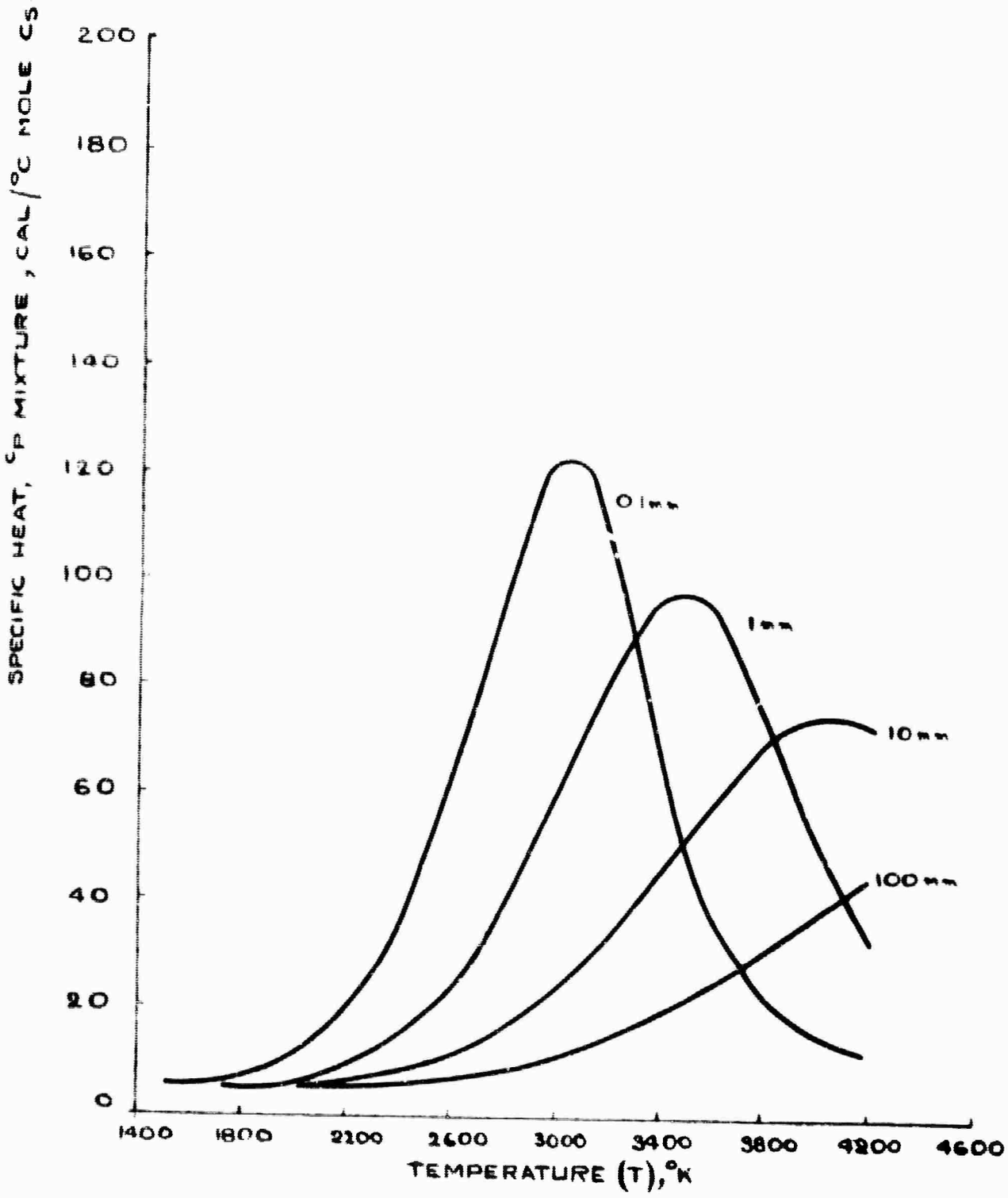

SPECIFIC HEAT AS A FUNCTION OF TEMPERATURE FOR AN EQUILIBRIUM MIXTURE OF CESIUM

FIG. 25-26

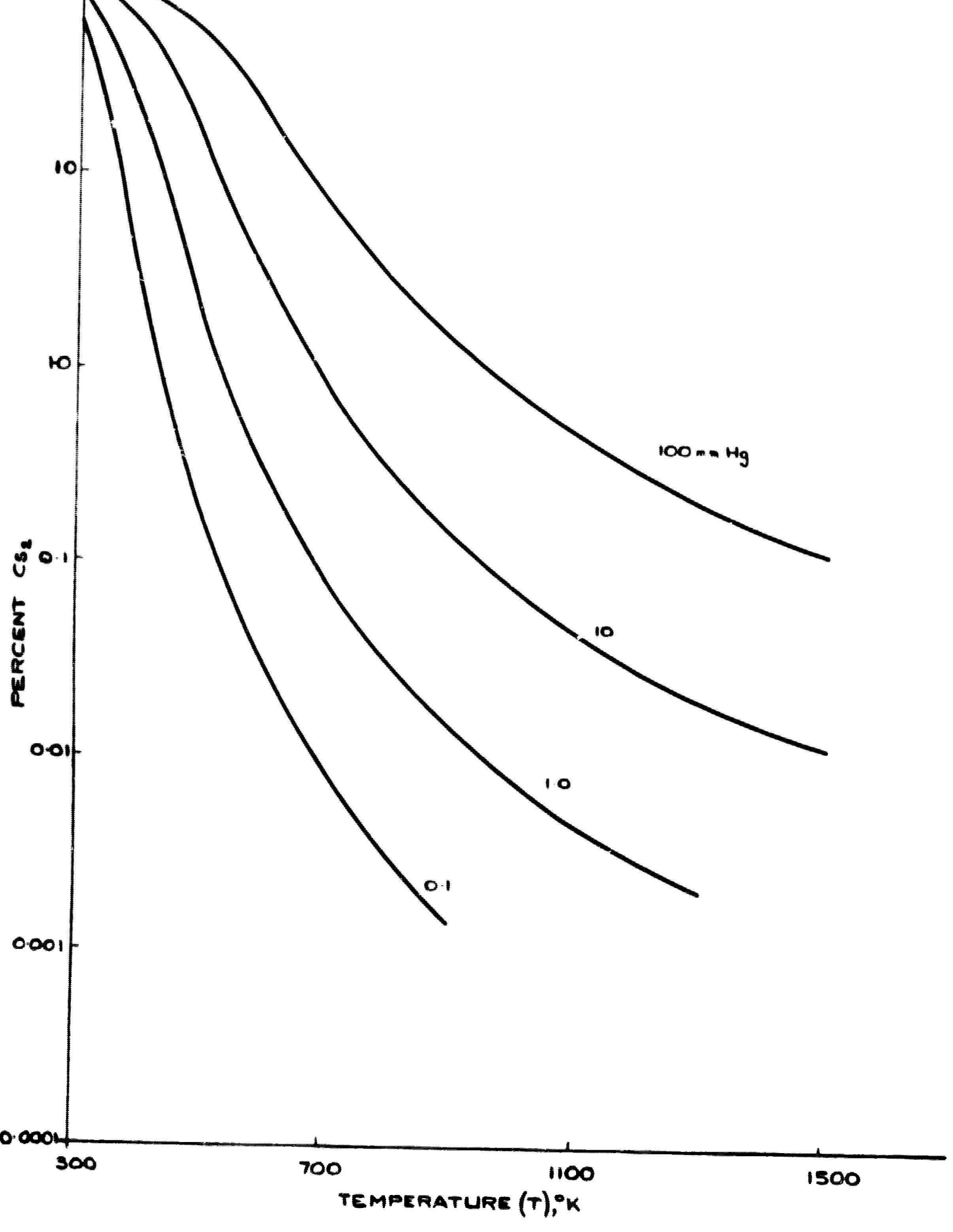

PERCENTAGE Cs_2 IN CESIUM VAPOUR AS A FUNCTION OF TEMPERATURE

FIG.25·27

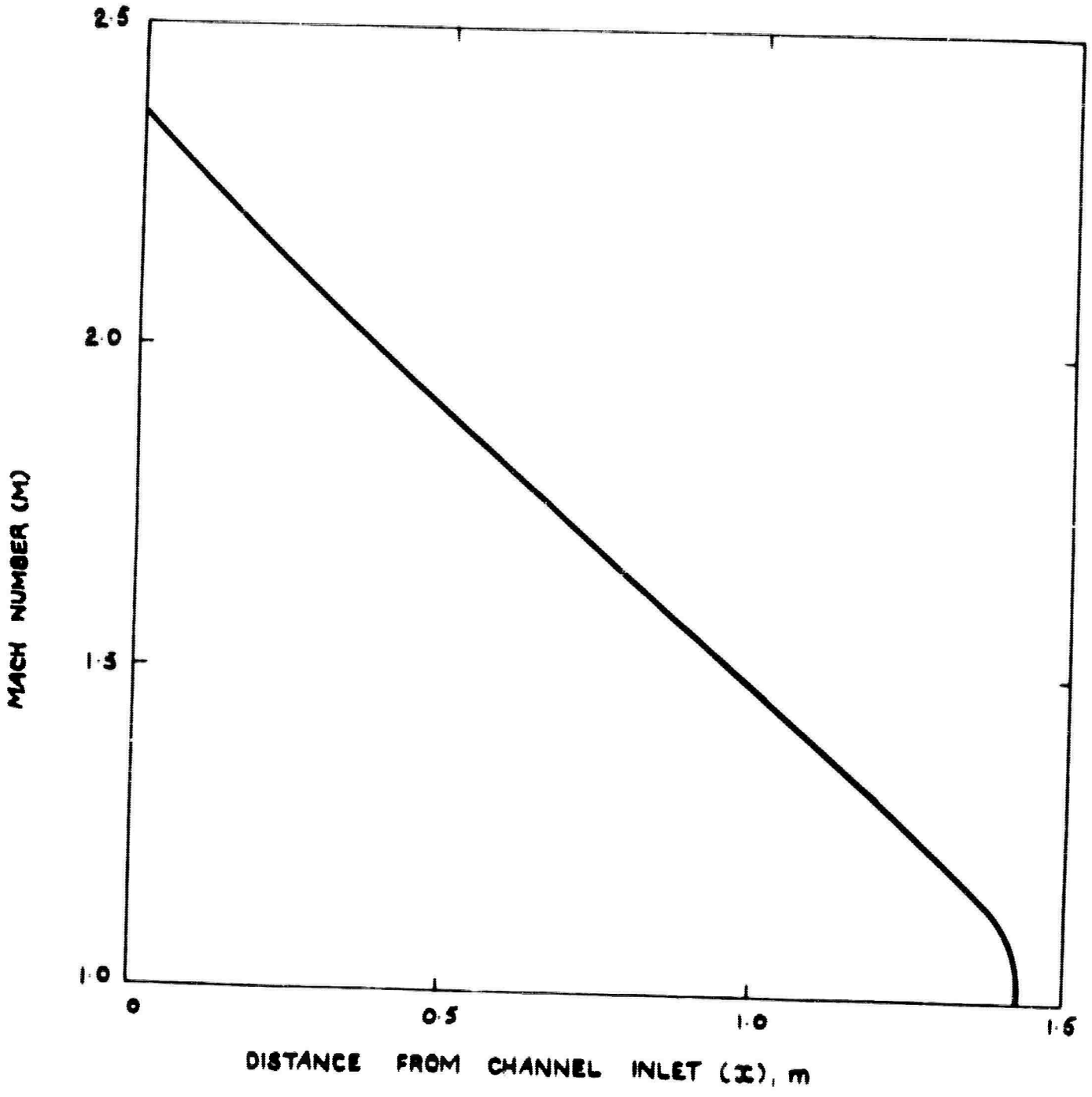

MACH NUMBER AS A FUNCTION OF DISTANCE FROM CHANNEL INLET

FIG25·28

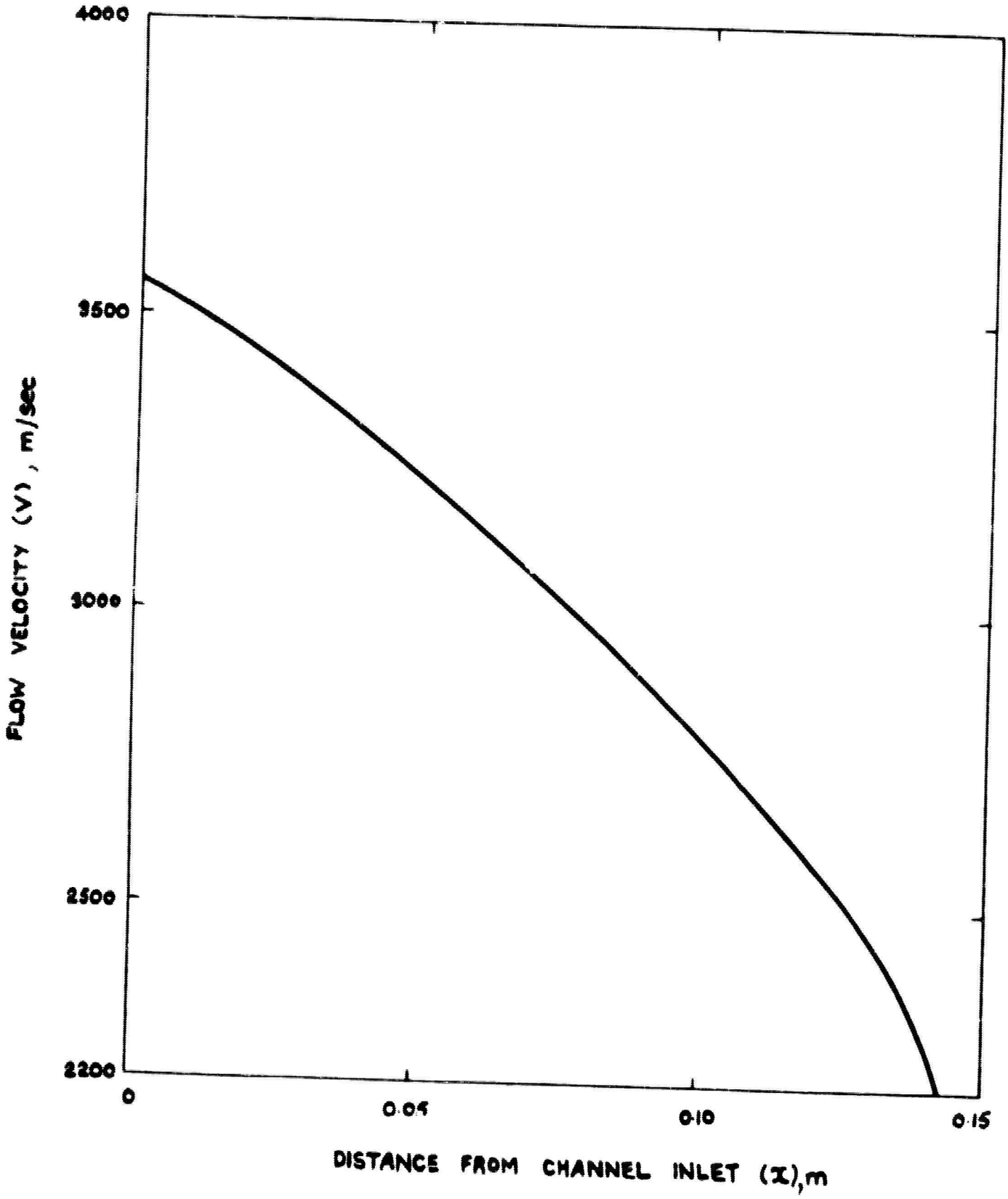

PLASMA FLOW VELOCITY AS A FUNCTION OF DISTANCE FROM CHANNEL INLET

FIG25·29

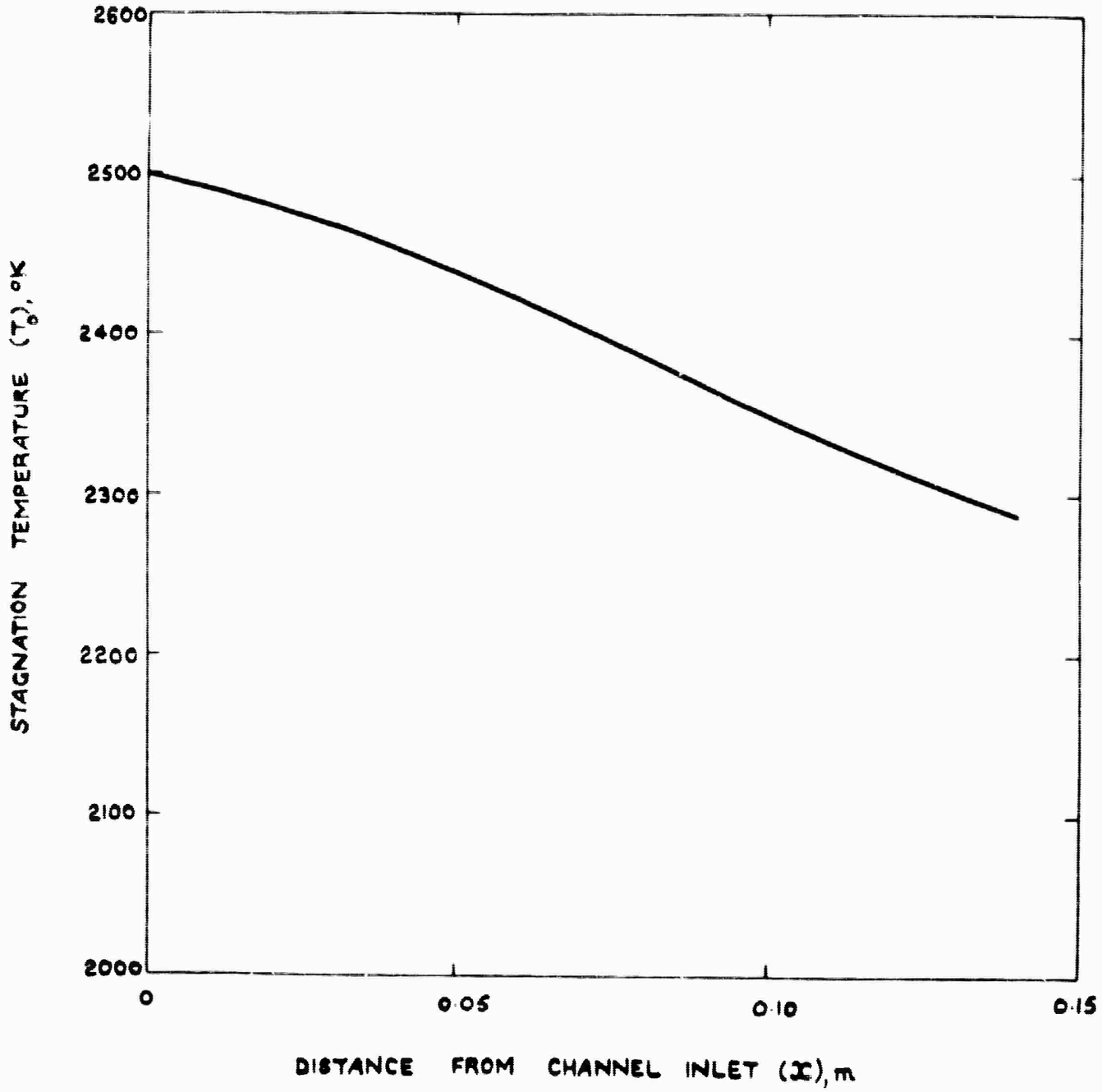

STAGNATION TEMPERATURE AS A FUNCTION OF DISTANCE FROM CHANNEL INLET

FIG25·30

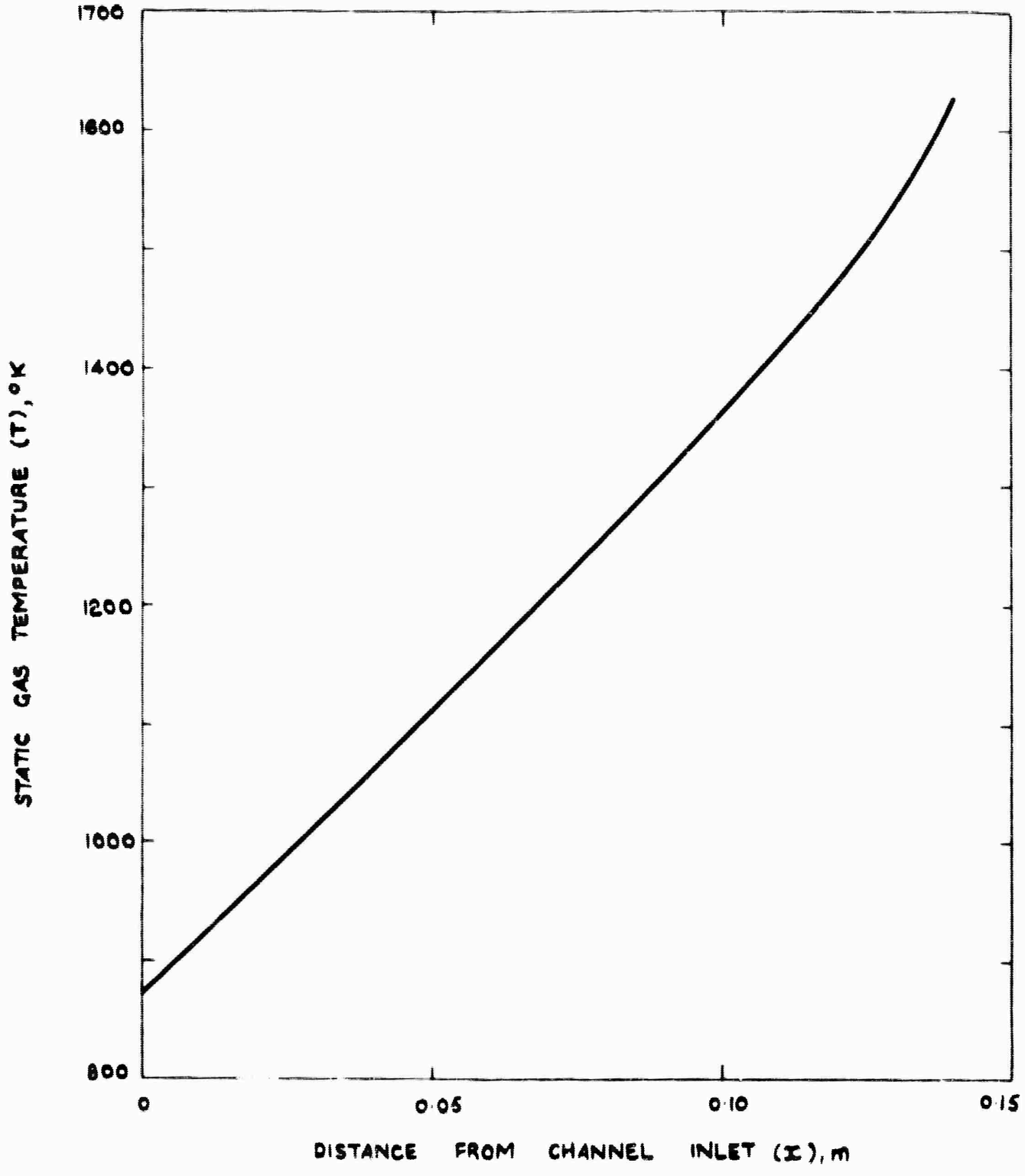

STATIC GAS TEMPERATURE AS A FUNCTION OF DISTANCE FROM CHANNEL INLET

FIG25·3

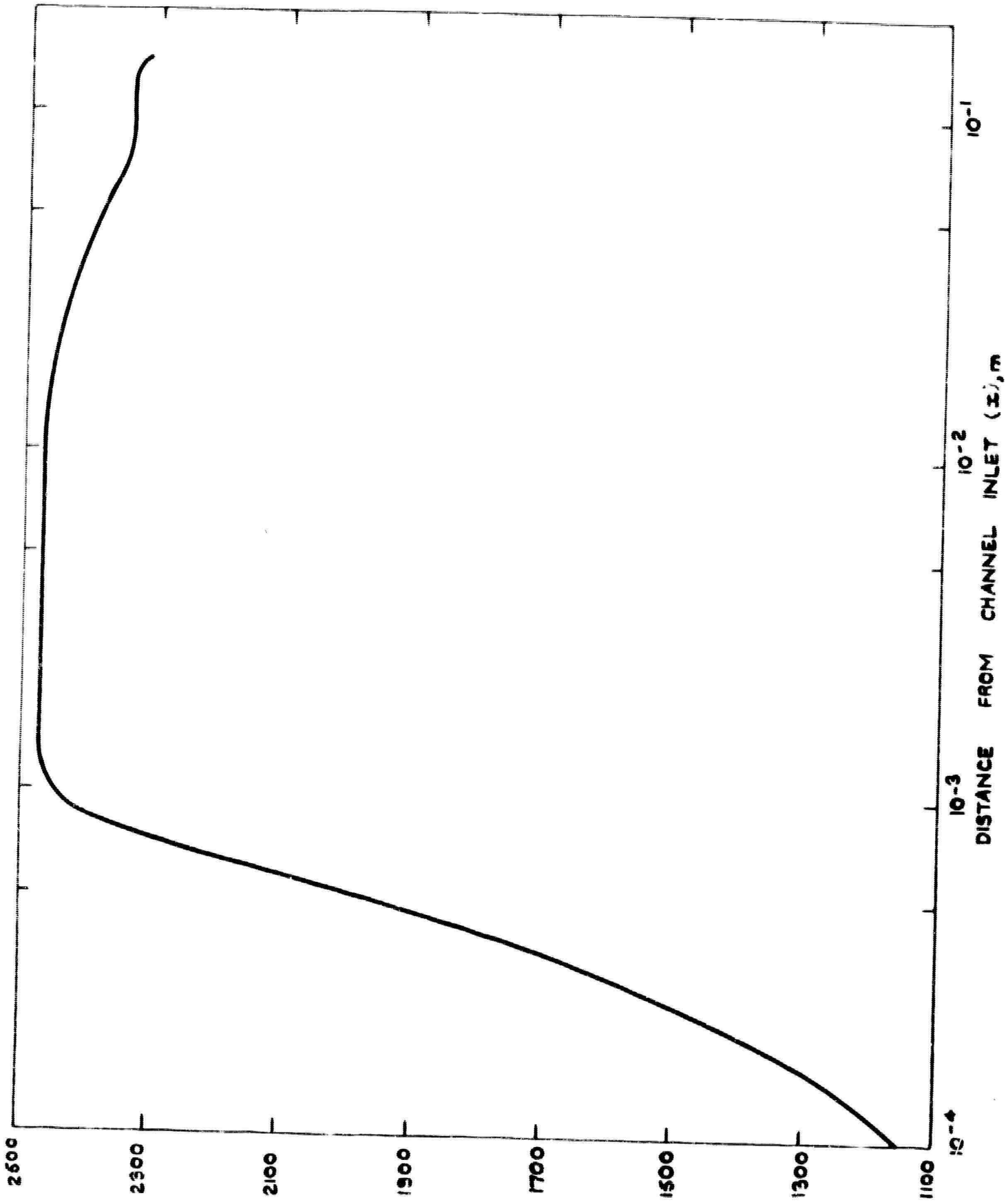

ELECTRON TEMPERATURE AS A FUNCTION OF DISTANCE FROM CHANNEL INLET

FIG 25·32

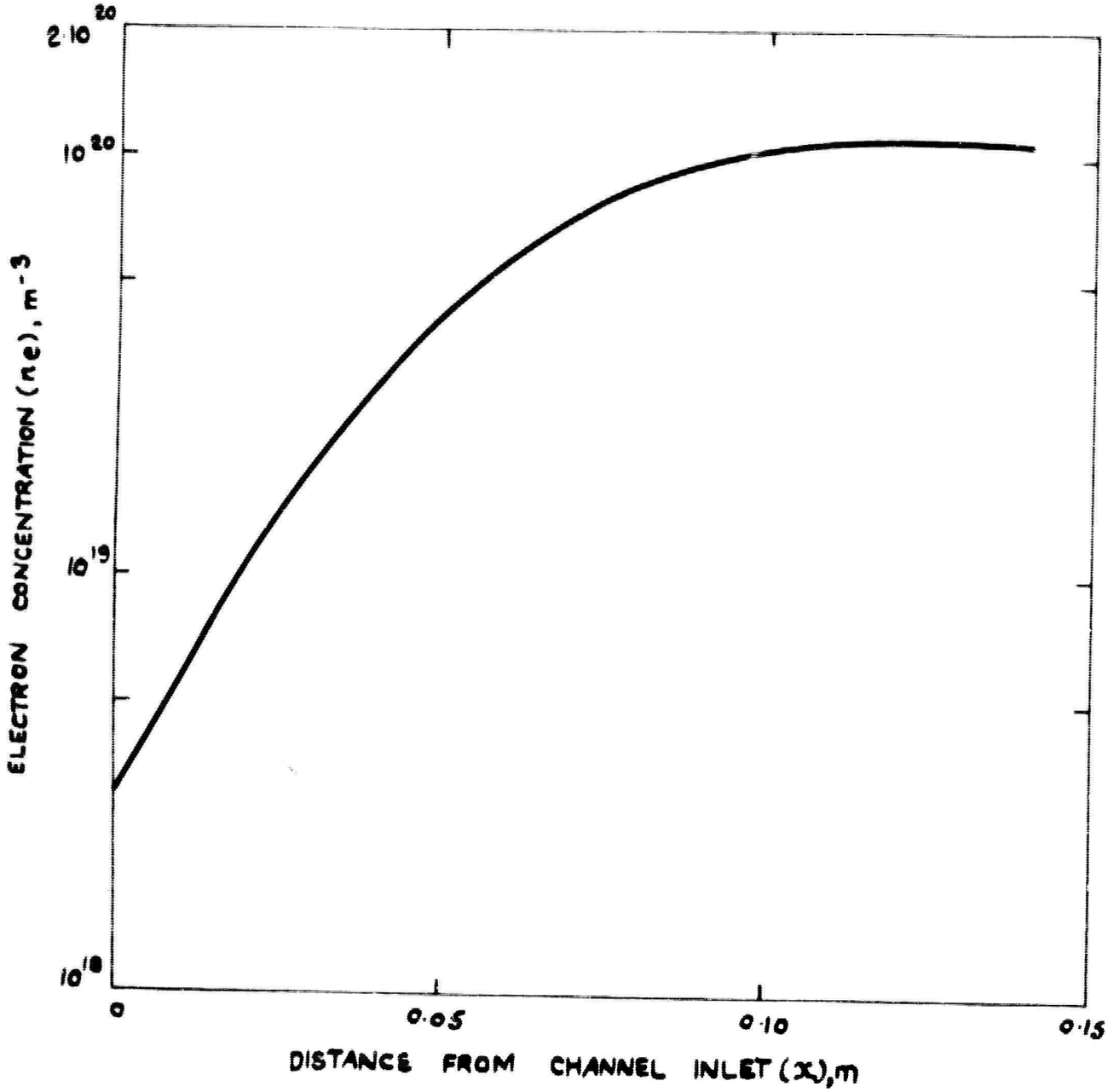

ELECTRON CONCENTRATION AS A FUNCTION OF DISTANCE FROM CHANNEL INLET

FIG25·3

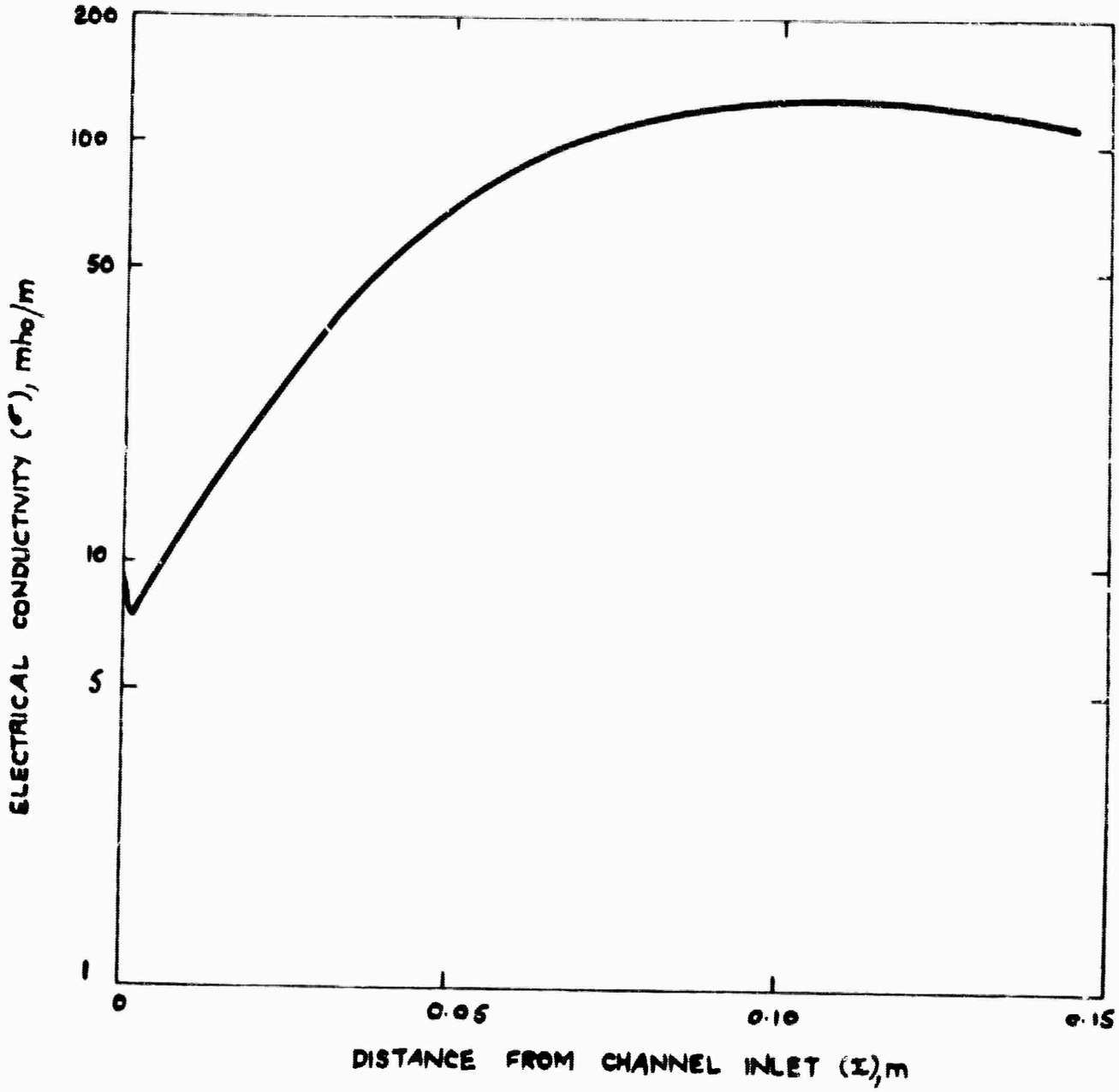

ELECTRICAL CONDUCTIVITY AS A FUNCTION OF DISTANCE FROM CHANNEL INLET

FIG25:34

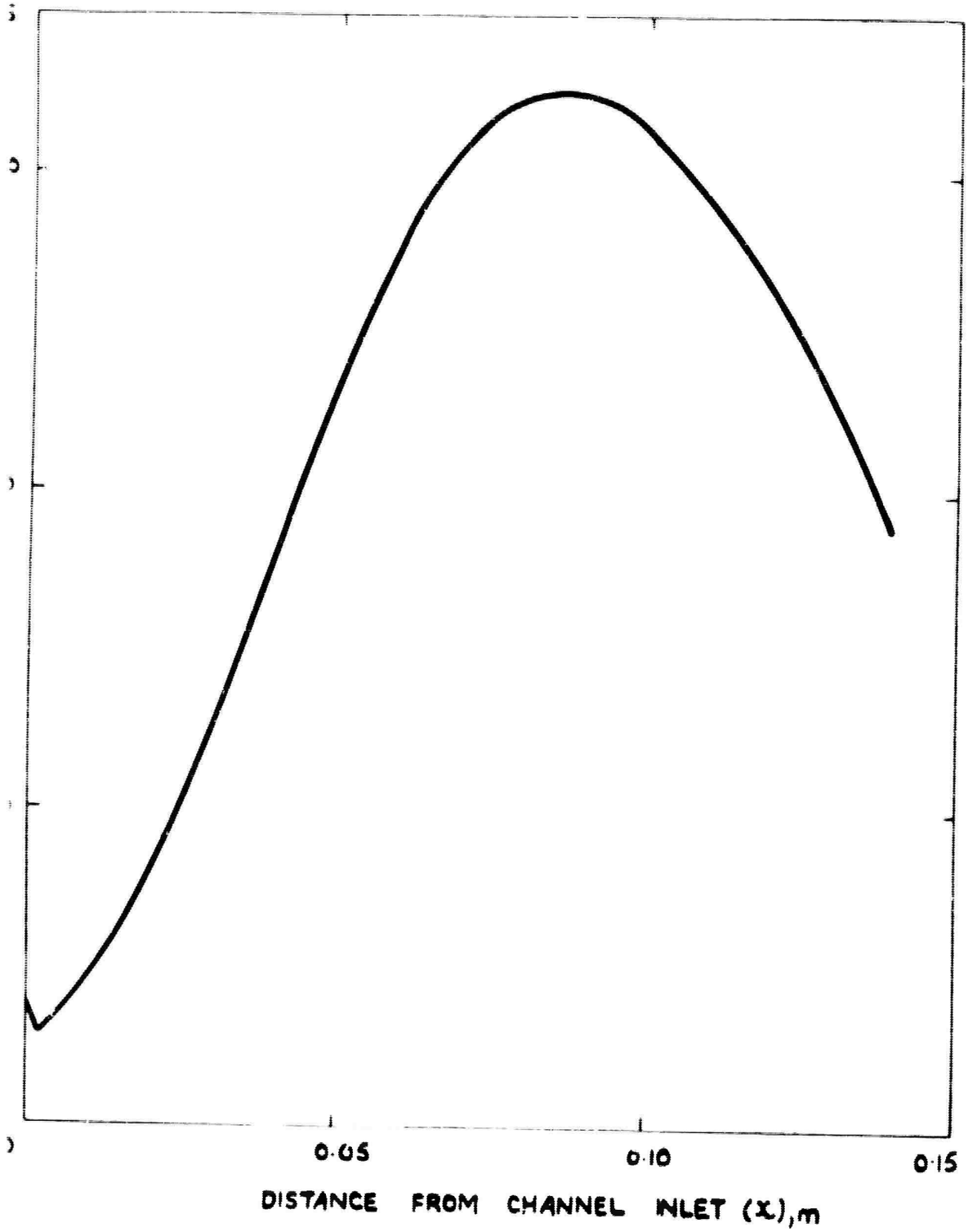

ECIFIC POWER AS A FUNCTION OF DISTANCE FROM
IANNEL INLET

FIG 25·35

A
a
a_1, a_2
a'
B
b_1, b_2 etc
C
Cp
D
d
E
E_s
e
F
f
f_1
g_1
h
$\hat{i}$
J or j
K
K_H
K_1.....
K_8, K_9, K_{10}
K_{11}, K_{12}, K
k
L
L'
M
m
m_e
Nu
n
P
Pr
p
p_1

cross sectional area

function defined in App. 25.B. equ. 25.B.21

functions defined on App.25.A

friction coefficient constant

magnetic field strength

functions defined on App. 25.A

end leakage factor

specific heat at constant pressure

hydraulic mean diameter

distance between lectrodes

electric field strength

electric field strength in end region (see App.25.B)

electronic charge

velocity distribution factor (see equ. 25.30)

friction coefficient

function defined on p.25.27

function defined on p.25.27

heat transfer coefficient

unit vector in +x direction

electric current density

loading factor

axial loading factor

functions defined on App. 25.B

functions defined on App. 25.B

functions defined on App. 25.B

Boltzmann's constant

active length of generator

see equ. 25.54a

Mach number

mass flow

electronic mass

Nusselt number

particle number density

power output

Prandtl number

pressure

perimeter (=2(b+d) for rectangular channel)

Q	collision cross section
R	gas constant
Re	Reynolds number
R_h	Hartmann number
R_u	Universal gas constant
r	recovery factor
St	Stanton number
s	length of insulator
T	static gas temperature
T_{aw}	adiabatic wall temperature
T_e	electron temperature
T_o	stagnation temperature
T_w	wall temperature
V	flow velocity
V_i	ionization potential
V_m	mean flow velocity in channel
V_s	flow velocity along axis
v	random particle velocity
W	molecular weight
X	fractional ionization
x	distance along channel from inlet
x_s	length with M>1
y	distance from channel wall
α	recombination coefficient
β	Hall coefficient
γ	ratio of specific heats
Δ	see equ. 25.54a
δ	factor ~1 (see Sections 25.2.22 and 25.3.4)
ϵ_o	permittivity of free space
χ	seeding fraction
η	function defined in equ. 25.24
Λ	function defined in equ(25.18)
μ	particle mobility
μ_1	dynamic viscosity
ν	collision frequency
ν_1	kinematic viscosity
ρ	density

σ	electrical conductivity
σ_s	conductivity in end region (see App.B)
τ	mean collision time
τ_w	wall shearing stress
ϕ	function defined in Sect. 25.2.3
ψ	function defined in Sect. 25.2.3
ω	cyclotron frequency

SUBSCRIPTS

x,y,z	direction of axes in Cartesian coordinates
e,i,a	electrons, ions and atoms
j	jth species
TOT	total
Cs^+,Cs,He	Cesium ion (singly charged), cesium atom, helium atom
n	order of iteration (in computations)
S	Saha equilibrium conditions
P	parent gas atom } section 25.3
a	seed gas atom } section 25.3
T	total } section 25.3
M	mixture } section 25.3

SUPERSCRIPTS

*	moving coordinate system
j	velocity interval (in computations)
†	dimensionless quantity

BLANK PAGE

THE CONSTANT MACH NUMBER MPD GENERATOR

by

T.S. Wilkinson

26.1 INTRODUCTION

Direct-current MPD generators are generally of two types according to the working fluid: the open-cycle combustion generator and the closed-cycle generator, probably with a nuclear heat source. High gas velocities are advantageous in each. However, the losses associated with transonic flow will probably be prohibitive; gas velocities consistent with high subsonic Mach numbers should lead to greatest overall economy.

The open-cycle generator is suitable for use as a topping unit for an otherwise conventional steam cycle but it seems likely that a certain amount of oxygen enrichment will prove to be necessary. Consequently, the specific heat (Cp) of the gas will be high and the effective ratio of specific heats (γ) will not be much greater than unity.[1] For a given pressure ratio across the generator the temperature drop will thus be relatively small and constant velocity flow will not differ greatly from flow at constant Mach number.

The closed-cycle generator will almost certainly use an inert gas having a high ratio of specific heats. In this case constant Mach number flow will almost certainly be more economical than flow at constant velocity. It is proposed to establish a general treatment of the case of constant Mach number flow of a monatomic gas, so that the various types of generator for example, as described by Lindley[2]) become special cases.

26.2 THEORY

The one-dimensional flow equations are

$$\text{energy:}\quad \rho U C_p \frac{dT}{dx} + \rho U^2 \frac{dU}{dx} = \frac{-E_x I_x}{J} - \frac{E_y I_y}{J} - \frac{4h(T-T_o)}{D} \qquad \text{.....(26.1)}$$

$$\text{momentum:}\quad \rho U \frac{dU}{dx} + \frac{dp}{dx} = -I_y B - \frac{4f}{D} \rho \frac{U^2}{2} \qquad \text{.....(26.2)}$$

$$\text{state:}\quad p = \rho RT \qquad \text{.....(26.3)}$$

continuity: $w = \rho U_n$ .....(26.4)

Mach number: $M^2 = \frac{U^2}{\gamma RT}$ .....(26.5)

Differentiating equation (26.5) gives $\frac{1}{U}\frac{dU}{dx} = \frac{1}{2T}\frac{dT}{dx}$ .....(26.6)

and substitution of (26.3), (26.5), and (26.6) into (26.1) and (26.2) gives

$$\left(1+\frac{\gamma-1}{2}M^2\right)\frac{1}{T}\frac{dT}{dx} = -\frac{(E_x I_x + E_y I_y)}{\rho U T C_p J} - 4St\left(1-\frac{T_o}{T}\right) \qquad .....(26.7)$$

$$\frac{1}{P}\frac{dp}{dx} = -\frac{I_y B}{P} - \frac{\gamma M^2}{2}\left(\frac{4f}{d}+\frac{1}{T}\frac{dT}{dx}\right) \qquad .....(26.8)$$

Ohm's law can be written in the form,

$$I_x = \frac{\sigma}{1+\beta^2}\left[-E_x + \beta(UB - E_y)\right] \qquad .....(26.9)$$

$$I_y = \frac{\sigma}{1+\beta^2}\left[\beta E_x + (UB - E_y)\right] \qquad .....(26.10)$$

The maximum value which E_y can take is UB, therefore it will be assumed that, in general $E_y = K_y UB$ where $0 \leq K_y \leq 1$. Similarly max E_x = UB hence E_x can be defined as $K_x \beta UB$.

Thus $$I_y = \frac{\sigma UB}{1+\beta^2}\left[\beta^2 K_x + 1 - K_y\right], \qquad .....(26.11)$$

and $$I_x = \frac{\sigma\beta UB}{1+\beta^2}\left[-K_x + 1 - K_y\right], \qquad .....(26.12)$$

and $$K_x = (1-K_y) - \frac{(1+\beta^2) I_x}{\sigma\beta UB} \quad . \qquad .....(26.13)$$

Thus $$E_x I_x + E_y I_y = \frac{\sigma\beta^2 U^2 B^2}{1+\beta^2} K_x(1-K_x-K_y) + \frac{\sigma U^2 B^2}{1+\beta^2} K_y (1-K_y+\beta^2 K_x). \qquad .....(26.14)$$

Substituting equation (26.14) into (26.7)

$$\left(1+\frac{\gamma-1}{2}M^2\right)\frac{d\hat{T}}{d\hat{x}} = -\frac{\gamma-1}{\gamma}\sigma_1\frac{U_1 B^2}{P_1}\sqrt{A_1}\frac{\beta^2}{1+\beta^2}\hat{\sigma}\hat{T}^{\frac{3}{2}}\left[K_x(1-K_x-K_y)+\frac{K_y}{\beta^2}(1-K_y+\beta^2 K_x)\right] -$$

$$- 4\frac{St}{D}(\hat{T}-\hat{T}_o) \qquad .....(26.15)$$

where $\hat{T} = \frac{T}{T_1}$, $\hat{\sigma} = \frac{\sigma}{\sigma_1}$, $\hat{D} = \frac{D}{\sqrt{A_1}}$ etc.

Substituting equation (26.11) into (26.8).

$$\frac{d\hat{p}}{d\hat{x}} = -\sigma_1 \frac{U_1 B^2}{P_1} \sqrt{A_1} \frac{\hat{\sigma}\hat{T}^{\frac{1}{2}}}{1+\beta^2} (1 - K_y + \beta^2 K_x) - \frac{\gamma M^2}{2} \left(\frac{4f}{\hat{D}} + \frac{1}{\hat{T}} \cdot \frac{d\hat{T}}{d\hat{x}}\right) \hat{P} \quad \ldots\ldots(26.16)$$

A number of possible cases may now be discussed.

(1) Segmented electrodes

In this case K_y will be specified, I_x will be zero and thus $K_x = 1 - K_y$.

(2) Continuous electrodes

In this case K_y will be specified and K_x will be zero.

(3) Hall generator

In this case K_{x1} will be specified and K_x will be computed from equation (26.13). K_y will be zero.

(4) Series-connected generator

It is assumed that this case is one of series connection with K_y a specified constant and $K_x = 1 - K_y$ as in the case (1) above. However the channel width must now be chosen so that the total current in a sheer at any x is constant.

(5) Angled current generator

This particular case has not been dealt with previously. K_y will again be specified but K_x will be given by

$\epsilon (1 - K_y)$ where $0 < \epsilon < (1 - K_y)$.

(6) Angled potential generator

This case is interesting from the engineering point of view as inclined tubular duct walls having a fixed angle with respect to the x direction can be used. K_{x1} will be specified and K_x will be computed from equation (26.13). K_y will thus be $\frac{K_x \alpha}{\beta}$, where α is constant.

According to Sutton et al[3] electron temperature T_e will in general be ff. ent to gas temperature T, the ratio of these two being largely determined by

the rate of energy dissipation in the gas, namely:

$$\frac{T_e}{T} = 1 - \frac{\gamma M^2}{3}\beta^2\left[\frac{E_x I_x + (E_y - UB) I_y}{\sigma U^2 B^2}\right]$$

i.e. from equation (26.14)

$$\frac{T_e}{T} = 1 + \frac{\gamma M^2}{3}\beta^2\left[(1-K_y)\left(1-\frac{K_y+\beta^2}{1+\beta^2}K_x\right) + \frac{\beta^2 K_x}{1+\beta^2}(K_y + K_x - 1)\right]$$

$$= 1 + \frac{\gamma M^2\beta^2}{3(1+\beta^2)}\left[(1-K_y)^2 + \beta^2 K_x^2\right] \qquad .....(26.17)$$

In the general case $K_{x1} = \epsilon(1 - K_{y1})$ and thus K_x is computed from (26.13) for all other x. Furthermore the tangent of the tube angle (α) will always be given by $\frac{\beta K_y}{K_x}$. Only in case (6) above will this angle be constant as β will undoubtedly vary with x.

Generally K_x may be written $\epsilon(1 - K_y)$ so that by equation (26.13)

$$\epsilon = 1 - \frac{(1+\beta^2) I_x}{(1-K_y)\sigma\beta UB} \qquad .....(26.18)$$

In this notation equations (26.15), (26.16) and (26.17) reduce to:

$$(1 + \frac{\gamma-1}{2}M^2)\frac{d\hat{T}}{d\hat{x}} = -(\frac{\gamma-1}{\gamma})\sigma_1\frac{U_1B^2}{P_1}\sqrt{A_1}\frac{\hat{\sigma}\hat{T}^{\frac{3}{2}}}{(1+\beta^2)\hat{P}}$$

$$\left[K_y(1-K_y)(1+\beta^2\epsilon) + \beta^2\epsilon(1-K_y)^2(1-\epsilon)\right] - \frac{4St}{D}(\hat{T}-\hat{T}_o)$$

$$.....(26.19)$$

$$\text{and } \frac{d\hat{p}}{d\hat{x}} = -\sigma_1\frac{U_1B^2}{P_1}\sqrt{A_1}\frac{\hat{\sigma}\hat{T}^{\frac{3}{2}}}{(1+\beta^2)}(1-K_y)(1+\beta^2\epsilon) - \frac{\gamma M^2}{2}(\frac{4f}{\hat{D}} + \frac{1}{\hat{T}}\frac{d\hat{T}}{d\hat{x}})\hat{p} \qquad .....(26.20)$$

$$\text{and } \frac{\hat{T}_e}{\hat{T}} = 1 + \frac{\gamma M^2}{3}(\frac{\beta^2}{1+\beta^2})(1-K_y)^2(1+\epsilon^2\beta^2) \qquad .....(26.21)$$

The above equations are now sufficiently general to treat cases (1) to (5) simply by choosing K_y and ϵ_1. However, case (6) presents some difficulty in that K_y is a function of K_x and is thus a function of x. In this case equation

ELECTRON TEMPERATURE AS A FUNCTION OF DISTANCE FROM CHANNEL INLET

FIG 25·32

(26.13) is still true and K_x is given by:

$$K_x = \frac{\beta}{\alpha+\beta}\left(1 - \frac{(1+\beta^2)I_x}{\sigma\beta U_B}\right) \qquad \ldots\ldots(26.22)$$

In every case

$$I_x = \frac{I_{x1}}{A} = \frac{I_{x1}\hat{p}}{\hat{T}^{\frac{1}{2}}} \qquad \ldots\ldots(26.22)$$

where $$I_{x1} = \frac{\sigma_1\beta_1 U_1 B (1-\epsilon_1)(1 - K_{y1})}{1+\beta_1^2} .$$

As a result, equation (26.18) becomes:

$$\epsilon = 1 - \frac{(1+\beta^2)(1-\epsilon_1)\hat{p}}{(1+\beta_1^2)\hat{\sigma}\hat{\beta}\hat{T}} \qquad \ldots\ldots(26.23)$$

whilst K_x in case (6) (equation (26.22)) becomes:

$$K_x = \frac{\beta}{\alpha+\beta}\left(1 - \hat{p}\frac{(1+\beta^2)(1-\epsilon_1)(1-K_{y1})}{(1+\beta_1^2)\hat{\sigma}\hat{\beta}\hat{T}}\right) . \qquad \ldots\ldots(26.24)$$

In the above equations $\hat{\beta} = \frac{\beta}{\beta_1}$.

Certain difficulties remain. The hydraulic mean diameter D, which is used in dimensionless form in equations (26.19) and (26.20) as $\hat{D} = D/\sqrt{A_1}$, is a complex function of pressure and temperature as shown below.

Suppose the channel is rectangular with dimensions b x d,

then $D = \frac{2bd}{(b+d)}$

If b = d (square duct), $D = \sqrt{A}$; but when b = 4d, $D = 0.8\sqrt{A}$; thus a suitable approximation for D in equations (26.19) and (26.20) seems to be

$$\hat{D} = a_o\sqrt{\frac{A}{A_1}} = a_o\frac{\hat{T}^{\frac{1}{4}}}{\hat{p}^{\frac{1}{2}}} \qquad \ldots\ldots(26.25)$$

where $0 < a_o < 1$.

Before solutions of the flow equations may be sought the relationship between the plasma properties σ and β and the state parameters p, T, and Te, must be established. In fact there is still considerable doubt about the correct relations but it is possible that they are of the following form:

$$\beta = \left[a_1 \frac{\hat{T}_e^{\frac{1}{2}} \hat{p}}{\hat{T}} + a_2 \frac{\hat{p}^{\frac{1}{2}}}{\hat{T}^{\frac{1}{2}}} \frac{\exp(\kappa - /\hat{T}_e)}{\hat{T}_e^{\frac{3}{4}}} \ln \Lambda \right]^{-1} \qquad \ldots\ldots(2$$

where $\Lambda = a_3 \frac{\hat{T}_e^{9/8} \hat{T}}{\hat{p}^{\frac{1}{4}}} \exp(\kappa/2\hat{T}_e)$

i.e. $\beta = \left[a_1 \frac{\hat{T}_e^{\frac{1}{2}} \hat{p}}{\hat{T}} + a_2 \frac{\hat{p}^{\frac{1}{2}}}{\hat{T}^{\frac{1}{2}}} \frac{\exp(-\kappa/\hat{T}_e)}{\hat{T}_e^{\frac{3}{4}}} \left(\frac{\kappa}{2\hat{T}_e} + \ln a_3 \frac{\hat{T}_e^{9/8} T^{\frac{1}{4}}}{\hat{p}^{\frac{1}{4}}} \right) \right]^{-1} \qquad \ldots\ldots(2$

and $\hat{\sigma} = a_4 \frac{\hat{\beta} \hat{p}^{\frac{1}{2}}}{\hat{T}^{\frac{1}{2}}} \hat{T}_e^{\frac{3}{4}} \exp(-\kappa/\hat{T}_e) \qquad \ldots\ldots(2$

Every one of the above quantities is dimensionless. The coefficients a_i, which are also dimensionless, are:

$$a_1 = (a_6 + a_7 X) \frac{p_1 m}{k T_1^{\frac{1}{2}} eB}$$

$$a_2 = a_8 \frac{X^{\frac{1}{2}} p_1^{\frac{1}{2}}}{k^{\frac{1}{2}} T_1^{5/4}} \frac{m}{eB}$$

$$a_3 = a_9 T_1^{9/8} \left(\frac{k\Gamma_1}{p_1 X} \right)^{\frac{1}{4}} = a_9 T_1^{\frac{11}{8}} \left(\frac{k}{p_1 X} \right)^{\frac{1}{4}}$$

and $a_4 = \frac{1}{\hat{T}_{e1}^{\frac{3}{4}}} \exp(-\kappa/\hat{T}_{e1})$

where $\kappa = \frac{q e}{2kT_1}$

a_6 to a_9 inclusive are coefficients which depend on the gas and seed. Referring now to equations (26.19) and (26.20), an expression for polytropic efficiency will be developed. In an adiabatic expansion:

$$\frac{T}{T_1} = \left(\frac{p}{p_1} \right)^{\eta \frac{\gamma - 1}{\gamma}} ; \quad 0 \leq \eta \leq 1$$

i.e. $\hat{T} = \hat{p}^{\eta \frac{\gamma - 1}{\gamma}}$

Thus, neglecting heat transfer,

$$\eta = \frac{\gamma}{\gamma-1}\frac{\hat{p}}{\hat{T}}\frac{d\hat{T}}{d\hat{p}}$$

Dividing the first term of (26.19) by the appropriate term of (26.20) (i.e. neglecting the friction pressure drop term $4f'/\hat{D}$) and assuming that $\frac{\gamma M^2}{2}\frac{1}{\hat{T}}\frac{d\hat{T}}{d\hat{x}}$ only forms a small part of $\frac{d\hat{p}}{d\hat{x}}$

$$\eta = K_y + \frac{\beta^2\epsilon(1-K_y)(1-\epsilon)}{1+\beta^2\epsilon} \qquad .....(26.29)$$

Thus if $1 > \epsilon$, then $\eta > K_y$. However, comparison of efficiencies should always be made on the basis of similar power densities as it is always possible to obtain higher efficiencies by reducing the rate of power extraction in a segmented electrode generator; and there will be a reduction in power density if $\epsilon < 1$. Alternatively, comparison of power densities may be made under conditions of similar efficiency. As an example, take $K_y = 0.8$, $\beta = 2$, $\epsilon = 0.5$.

$$\eta = 0.8 + \frac{4 \times 0.5 \times 0.2 \times 0.5}{1 + 4 \times 0.5}$$

$$= 0.866$$

Referring to equation (26.19), power density is proportional to

$$\eta\,(1+\beta^2\epsilon)\,(1-K_y)$$

Therefore at the same efficiency η, power density simply depends upon

$$(1+\beta^2\epsilon)\,(1-K_y)$$

substituting $K_y \simeq 0.8$, $\beta = 2$, $\epsilon = 0.5$, this is equal to

$$(1 + 4 \times 0.5)\,(1 - 0.8) = 0.6,$$

whereas, if $K_y = 0.866$, $\beta = 2$, $\epsilon = 1$, it is equal to

$$(1 + 4)\,(1 - 0.866) = 0.66$$

The following questions may therefore be asked. Are there any circumstances in which

$$(1+\beta^2\epsilon)\,(1-K_y) > (1+\beta^2)\,(1-\eta)\,,$$

where $$\eta = K_y + \frac{\beta^2\epsilon(1-K_y)(1-\epsilon)}{1+\beta^2\epsilon}\,.$$

Making the above substitution, the following inequality is obtained:

$$\epsilon\ (1 + \beta^2) > 1 + \beta^2\epsilon$$

It would seem that $\epsilon > 1$ is a possible answer but the cancellations made above are legitimate if $1 - \epsilon$ is negative, therefore the answer is in the negative.

Another possibility remains: it is that although the power density would seem to be reduced on the above argument, equation (26.21) shows that $\epsilon > 1$ would mean greatly increased electron temperature. Following a similar procedure to that adopted above, the possibility that

$$(1-K_y)^2 (1+ \epsilon^2\beta^2) > (1-\eta)^2 (1+\beta^2) \quad \text{will be investigated.}$$

Substitution for η from the expression above leads to

$$0 > (1 - \epsilon)^2$$

which is clearly impossible.

Thus it is clear that if efficiency is to be sacrificed in order to increase power densities (by virtue of increased electron temperature) there is no better way to achieve this end than by use of the segmented electrode generator, whether this be series connected or not.

26.3 HALL-MODE OPERATION

In the case of the Hall generator, or other systems which approximate to it, certain interesting effects (which may settle the issue of enhanced electron temperature one way or the other) may be observed. The following is a qualitative explanation of such effects:

For a Hall generation equations (26.21) and (5.23) become

$$\frac{\hat{T}_e}{\hat{T}} = 1 + \frac{\gamma M^2}{3} \frac{\beta^2}{1+\beta^2} (1 + \epsilon^2\beta^2) \qquad \text{.....(26.30)}$$

and

$$\epsilon = 1 - \left(\frac{1+\beta^2}{1+\beta_1^2}\right) \frac{(1 - \epsilon_1)\hat{p}}{\hat{\sigma}\beta\hat{T}} \qquad \text{.....(26.31)}$$

and if the variation of β with $\hat{T}e$ is assumed to be slow compared with $\hat{\sigma}$ which varies approximately as $\hat{T}e^{10}$ then the form of the above equations between Te and ϵ is as follows:

$$\epsilon = 1 - \frac{c}{T_e^{10}} \qquad \text{.....(26.32)}$$

and $$\beta^2 \epsilon^2 = b(\hat{T}_e - 1) - 1 \qquad \ldots\ldots(26.33)$$

Possible solutions are represented by intersections of the above curves of ϵ versus $\hat{T}e$ which are drawn below with Hall current (proportional to $(1 - \epsilon_1)$) as parameter.

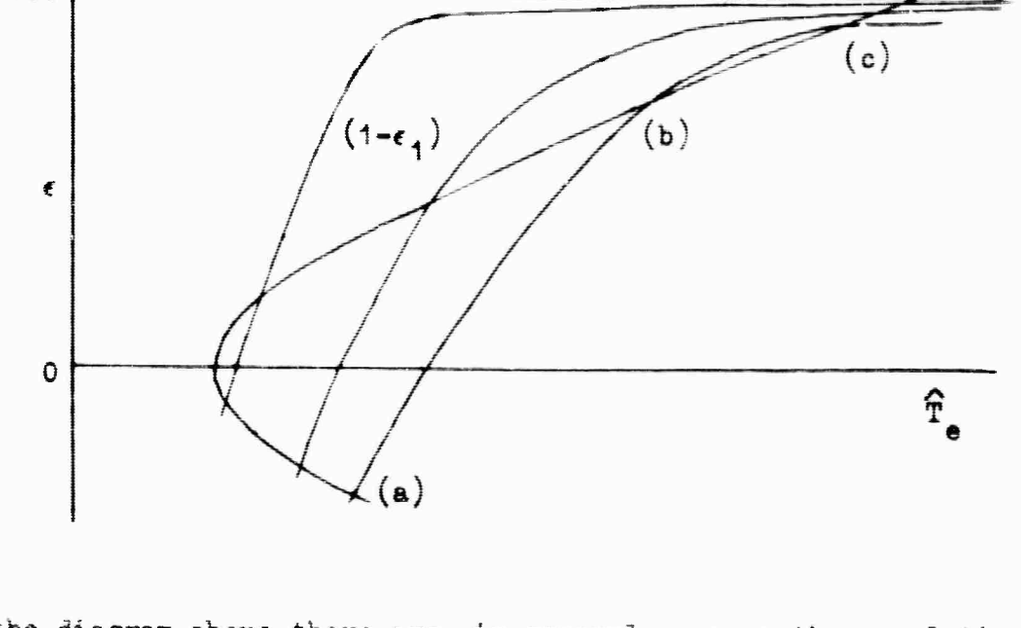

From the diagram above there are, in general, one or three solutions of the equations ((a), (b), (c)), however it is found that solutions at low T_e or ϵ are always unstable and only the highest are stable. However, for best efficiency a Hall generator should always have $\epsilon < 0.5$ so the result of this instability is high power density (high T_e) but very poor efficiency.

26.4 DISCUSSION

The equations developed in this report are in a convenient form for forward integration on a digital computer. In fact they have already been programmed and a number of preliminary calculations have been carried out. It is intended that the scope of the programme will be extended further to include magnet and compressor power. When this has been done it will be possible to calculate (by trial and error) the optimum values, from the thermal efficiency standpoint, of all the independent parameters of the system.

For example, if optimum seed fraction is calculated by maximising σU^2 or by some similar device, the result will inevitably be a function of pressure, temperature, flux density etc. However if simultaneous optimisation of all the independent parameters is carried out as proposed, the optimum seed fraction will then be the best for the optimum pressure and temperature range, and therefore for the unit of highest overall efficiency.

The preliminary calculations carried out on the computer have drawn attention in the case of Hall type generators to a phenomenon akin to voltage breakdown which has not yet been fully investigated: it is a consequence of electron temperature elevation due to the presence of the magnetic field and its effect is to reduce the efficiency of the expansion considerably. This could preclude the use of Hall generators altogether.

REFERENCES

1 CRAMPTON, F.J.P., and WILKINSON, T.S. An open cycle MPD generator optimization study. IEE Conference Report Series No. 4 1963

2 Research programme on magnetoplasmadynamic power generation. Technical summary report for December 1961 to 30 November 1962. IRD 63-1

3 HARWITZ, H., SUTTON, G.W., and TAMOR, S. Electron heating in magnetohydrodynamic power generation. ARS Journal, Vol. 32, No. 8, p.1237-1243. August 1962

CHAPTER 27

OPTIMIZATION OF LARGE-SCALE NUCLEAR MPD SYSTEMS*

by

B.C. Lindley and I.R. McNab

27.1 INTRODUCTION

Research related to the eventual use of magnetoplasmadynamic (MPD) generators, for large-scale electrical power production and for other purposes, is currently in progress. The coal-, oil- or gas-fired open cycle system utilizes the alkali metal seeded combustion products as the working fluid while the closed cycle system, with a nuclear reactor as the heat source, uses an alkali metal seeded inert gas.

Here cesium (with the lowest ionization potential of any material), although expensive, is adopted for closed cycle systems; because of the difficulty of complete seed recovery in the open cycle system, a cheap potassium compound is employed. For thermal ionization, the electrical conductivities of cesium-seeded inert gases are comparable with those of potassium-seeded combustion products at temperatures about 500°C higher, so that the closed cycle system has an immediate advantage over the fired system. In inert gas plasmas there also exists the possibility of achieving high electrical conductivities through magnetically-induced extra thermal ionization[1] at quite moderate gas temperatures (1200°-1800°C). If operation at such low temperatures can be proven, the direct gas-cooled nuclear reactor closed cycle scheme appears attractive.

In a nuclear cycle selection of the operating pressure level presents difficulties: the reactor should operate at as high a pressure (typically 10-20atm) as is technically and economically feasible (to improve heat transfer for a permissible pressure loss and pumping power) whereas the MPD generator benefits in plasma electrical conductivity by operation at low pressures (1 atm or less).

27.2 GENERATOR PERFORMANCE

27.2.1 General

In optimizing the specific power in an MPD generator the usual procedure

* International symposium on magnetchydrodynamic electrical power generation Paris, 6 - 10 July 1964.

is to maximize σV^2 assuming thermal ionization conditions; subsonic Mach numbers (about 0.5 for helium-cesium) result.

With magnetically-induced ionization the ratio of electron to gas temperature (T_e/T) increases with increasing Mach number and Hall number of the flow. The most important ionization process in an MPD generator is through electron collisions; consequently, if $T_e/T > 1$ can be achieved, the restriction on flow velocity (imposed by thermal ionization at the low static temperatures associated with high Mach numbers) no longer applies, and there is the possibility of operating supersonically with high specific power. In this case the expansion pressure ratio in the accelerating nozzle will be high, so that the reactor operates at a much higher pressure level than the MPD duct.

27.2.2 Theory

Assuming that the flow velocity is small at entrance to the nozzle ($M_1 << 1$) the static temperature and pressure are closely approximated by the stagnation conditions. After an isentropic expansion in the nozzle, the static temperature and pressure, and velocity are as follows (and see Fig. 27.1):

$$T_2 = T_o \left[1 + \frac{\gamma-1}{2} M_2^{\ 2} \right]^{-1} \qquad \ldots\ldots (27.1)$$

$$p_2 = p_o (T_2/T_o)^{\gamma/\gamma-1} \qquad \ldots\ldots (27.2)$$

$$V_2 = M_2 (\gamma R T_2)^{1/2} \qquad \ldots\ldots (27.3)$$

In the generator duct,

$$\frac{T_4}{T_2} = \left(\frac{p_4}{p_2} \right)^{\eta \frac{\gamma-1}{\gamma}} \qquad \ldots\ldots (27.4)$$

Selecting a typical value of T_2/T_4, p_4 may be evaluated, and the average generator conditions may be approximated by using

$$p_3 = \frac{p_4 + p_2}{2}$$

and hence, from equation (27.4), the corresponding T_3.

Then $$M_3 = M_2 \, (T_2/T_3)^{1/2} \qquad \ldots\ldots (27.5)$$

and $$n_{p_3} = p_3/kT_3 \qquad \ldots\ldots (27.6)$$

Magnetically-induced extra-thermal ionization may be investigated using the equation derived by Hurwitz et al[2] for a segmented-electrode generator (all

the quantities given below apply to region 3 of the generator):

$$\frac{T_e}{T} = 1 + \frac{\gamma(1-K)^2 M^2 \beta_e^2}{3\delta(1+\beta_e\beta_i)^2} \qquad \ldots\ldots (27.7)$$

An iterative method is required for the solution of this equation since, in general and in the cases considered here, β_e is a function of T_e, excluding analytic solution of equation (27.7).

Then

$$\beta_e = \frac{eB}{m_e \nu_e} \qquad \ldots\ldots (27.8)$$

where

$$\nu_e = n_p \left(\frac{8kT_e}{\pi m_e}\right)^{1/2} (q_{e-p} + \chi q_{e-n}) \qquad \ldots\ldots (27.9)$$

and

$$\beta_i = \mu_i B \qquad \ldots\ldots (27.10)$$

Having obtained T_e, the corresponding electron concentration is obtained from Saha's equation[3]:

$$n_e = T_e^{5/4} \left(\frac{\chi n_p}{T}\right)^{1/2} \left(\frac{2\pi m_e k}{h^2}\right)^{3/4} \left(\frac{g_e g_i}{g_a}\right)^{1/2} \exp\left(-\frac{eV_i}{2kT_e}\right) \qquad \ldots\ldots (27.11)$$

in which it is assumed that the fractional ionization $(n_e/n_a) = n_e/\chi_{np}$ is determined by Saha's equation at the electron temperature and also that the fractional ionization is such that $(n_e/n_i)^2 \ll 1$.

For thermal equilibrium ionization, equation (27.11) is used to give the electron concentration, the electron temperature being replaced by the gas temperature.

The scalar electrical conductivity is

$$\sigma = \frac{n_e e^2}{m_e \nu_e} \qquad \ldots\ldots (27.12)$$

and the specific power for a segmented-electrode generator is

$$P_3 = \frac{\sigma_3 V_2^2 B^2 K(1-K)}{(1+\beta_e\beta_i)_3} \qquad \ldots\ldots (27.13)$$

27.3 SPECIFIC POWER

27.3.1 Operating conditions and data

The effects of reactor operating pressure on the specific power (electrical power output per unit volume of generator duct) in a segmented-electrode constant-

velocity subsonic MPD generator have been examined using the simple quasi-one dimensional theoretical model described in Section 27.2. Helium-cesium and argon-cesium mixtures are investigated for thermal equilibrium and magnetically-induced non-thermal ionisation. Wall friction and heat transfer losses are neglected. In a first series of calculations, a generator inlet Mach number of 0.6 is assumed; in a second series the Mach number is increased to supersonic values.

Data for the calculations are given in Table 27.1. The electron-helium atom collision cross section is obtained from a previous survey of experimental measurements[4]. The electron-argon atom cross section is obtained from an approximate curve fit to Brodes results[5]. Although several measurements of the electron-cesium atom cross section have recently been made, there still exists considerable discrepancy and an average is adopted (see chapter 22). The ionic mobilities are from the measurements of Chanin and Biondi[6] (Ce^+ - He and Cs^+ - A) and the recent measurements of Chanin and Steen[7] (Cs^+ - Cs); the total mobility is obtained from

$$\frac{1}{\mu_1} = \frac{1}{\mu_1} + \frac{1}{\mu_2} \qquad \ldots\ldots (27.14)$$

27.3.2 Results

Using equations (27.1) to (27.14) and the data given in Table 27.1, a Pegasus Autocode programme has been constructed to perform the calculations.

Specific powers for a generator inlet Mach number of 0.6 are shown in Figs.27.2 and 27.3, and as a function of Mach number in Figs.27.4 and 27.5.

The ratio ϕ (enhancement in specific power) is shown in Fig. 27.6 for the parameters of Figs. 27.2 and 27.3.

27.4 DISCUSSION

27.4.1 Constant Mach number

In Fig. 27.2, both for thermal equilibrium and elevated elctron temperature conditions, maximum specific powers are obtained at particular values of reactor pressure, depending on the applied magnetic field. The maxima occur because of two opposing effects: as p_o decreases, and other parameters remain constant, the electrical conductivity increases; and as p_o decreases ion slip becomes increasingly important in the specific power equation (27.13), giving a reduction in power.

The maxima for equilibrium and non-equilibrium conditions occur at different pressures because of the different form of dependence of the electrical conductivity

and ion slip terms in each case. Over the central pressure range the specific power for non-equilibrium conductivity is very much higher than for thermal equilibrium, but at very high and very low reactor operating pressures non-equilibrium effects are relatively unimportant. The curves for different magnetic fields cross at certain pressures because of the dominance of ion slip so that an optimum magnetic field exists in this low pressure regime. At typical reactor operating pressures ($\gtrsim$ 10 atm) the specific power increases monotonically with magnetic field over the range considered. The loci of points are shown for which ϕ = 10 and 100% at high operating pressures; as the magnetic field is increased the reactor may be operated at higher pressures.

For argon-cesium a lower range of pressure and a seeding fraction of 0.01 are considered. In the argon-cesium mixture the electron-argon atom cross section varies appreciably with electron energy (κ = 0.02 represents an optimum value for helium-cesium in which the electron-helium atom cross section is nearly independent of electron energy); χ = 0.01 represents an average value to give maximum conductivity over the relevant energy range. Comparing Fig. 27.3 with Fig. 27.2 the maximum specific power is lower and, at high reactor operating pressures, ϕ is greater for argon-cesium than for helium-cesium, because of the smaller electron-argon atom collision cross section. However, even with non-equilibrium ionization, the specific power at 10 ata for helium-cesium is greater than for argon-cesium, primarily on account of the lower velocity for a given flow Mach number in argon.

It has been assumed that the fractional ionization (n_e/n_a) is small, allowing electron-ion collisions to be neglected and adoption of the simplified form of Saha's equation (27.11). The regions for which $n_e/n_a > 0.01$ are indicated in Figs. 27.2 and 27.3 and it is probable that specific powers attainable in practice are lower.

27.4.2 Variable Mach number

The effect of varying the generator inlet Mach number is indicated for helium-cesium and argon-cesium for reactor operating pressures of 1, 3 and 10 ata; for all pressures the maximum specific power for equilibrium conductivity occurs at a flow Mach number of about 0.5.

In Fig. 27.4, at the lowest pressure, non-equilibrium ionization has considerable effect, and up to a Mach number of 1.4 the specific power increases monotonically with Mach number. At 10 ata and low Mach numbers the non-equilibrium curve is close to the equilibrium but at Mach 1.4 the specific power for non-equilibrium is about seven times greater than for equilibrium, although the

absolute magnitude is less than the maximum both for equilibrium and non-equilibrium. At intermediate pressure (~3 ata) initially the non-equilibrium curve is close to that for equilibrium (because the static temperature decreases more rapidly than T_e/T increases in equation (27.7) but, at high Mach numbers, non-equilibrium effects become important and the specific power increases rapidly. For 3 ata pressure there is no maximum in the non-equilibrium specific power over the range considered but for $3 < p_o < 10$ ata the non-equilibrium power will follow the maximum in the equilibrium power and then diverge to a greater value at high Mach numbers.

For argon-cesium (Fig. 27.5) there are several significant differences. In the range of parameters being considered ion slip is appreciable, and has the effect that greater specific power is achievable with p_o = 3 ata than with 1 or 10 ata for equilibrium ionization (also apparent in Fig. 27.3). With non-equilibrium ionization at p_o = 1 and 3 the specific power initially increase rapidly with Mach number. For p_o = 1 the rate of increase of specific power falls at high Mach number, eventually showing a maximum. The maximum arises for two reasons: as the Mach number increases the static gas pressure and temperature in the MPD generator decreases but ratio T_e/T increases; at low Mach numbers (for p_o = 1 ata) T_e/T increases sufficiently rapidly to produce an overall increase in electron temperature, whereas at high Mach numbers the static gas temperature becomes very low and the rate of increase of T_e/T is restricted by ion slip. For p_o = 10 ata a maximum and a minimum occur in the non-equilibrium power. At Mach 1.4 the specific power is approximately the same as for the maximum at ~Mach 0.5, but is continuing to increase with Mach number. The actual magnitude of specific power is in this case greater than that for helium at 10 ata, even though the flow velocity is considerably smaller.

27.5 CONCLUSIONS

1 In helium-cesium mixtures at typical reactor operating pressures (10 ata) magnetically-induced extra-thermal ionization will not be of consequence in a typical subsonic segmented-electrode MPD generator unless magnetic fields of greater than 5T are used. Lower reactor operating pressures would enable greater specific powers to be achieved with the same, or lower, magnetic field strengths.

2 In argon-cesium mixtures considerable non-equilibrium effects will occur; typically, for p_o = 10 ata, B = 5T, the non-equilibrium specific power is approximately twice the equilibrium specific power. The actual magnitude of the specific power in argon-cesium is less than that in helium-cesium at a given Mach number, because of the low attainable

flow velocity in argon.

3 As the operating Mach number of the MPD generator is increased non-equilibrium effects become increasingly important, but for helium-cesium mixtures the effects are not significant for a reactor operating pressure of 10 ata even with a Mach number of 1.4. For argon-cesium mixtures the specific power at Mach numbers greater than 1.4 increases beyond the maximum at M ≈ 0.5, and the actual specific power is greater than for helium-cesium. In both cases, if the reactor operating pressure is reduced, for example to 3 ata, the specific power increases very rapdily with Mach number, the effect being most significant in argon-cesium mixtures.

REFERENCES

1 KERREBROCK, J.L. Conduction in gases with elevated electron temperature. Second Symposium on the Engineering Aspects of Magnetohydrodynamics, University of Pennsylvania. March 1961

2 HURWITZ, H, SUTTON, G.W., and TAMOR, S. Electron heating in magnetohydrodynamic power generators. ARS Journal., 32,1237,1962

3 SAHA, M.N. and SAHA, H.K. A treatise on modern physics. Vol. 1. The Indian Press Limited. Allahabad and Calcutta, 1934

4 McNAB, I.R. The electrical properties of a cesium-helium plasma. C.A. Parsons and Company Research Report. NRC 61-12, March 1961

5 BRODE, R.B. Revs. Modern Phys. 5,257,1933

6 CHANIN, L.M. and BIONDI, M.A. Phys. Rev. 107,1219,1957

7 CHANIN, L.M. and STEEN, R.D. Phys. Rev. 132,2554,1963

TABLE 27.1

DATA (MKS UNITS)

Universal constants

$m_e = 9.108.10^{-31}$

$e = 1.601.10^{-19}$

$h = 6.625.10^{-34}$

$k = 1.38.10^{-23}$

All calculations

$\eta_L = 0.85$

$K = 0.80$

$\delta = 1$

$\frac{\varepsilon_e \varepsilon_i}{\varepsilon_a} = 1$

$V_i = 3.893$

$T_o = 2000^{\circ}K$

$T_2/T_4 = 1.3$

$q_{e-Cs} = 300.10^{-20}$

Fig. 27.2, 27.3 and 27.6

$B = 5,3,2,1,0.5$

$M_2 = 0.6$

$p_o = 0.01 \rightarrow 20$ ata (helium-cesium)

$p_o = 0.05 \rightarrow 20$ ata (argon-cesium)

Helium-cesium

$\gamma = 1.658$

$R = 2.075.10^3$

$\chi = 0.02$

$\mu_i = 1.73.10^{22}/n_{He}$

$q_{e-He} = 6.10^{-20}$

Argon-cesium

$\gamma = 1.668$

$R = 2.079.10^2$

$\chi = 1.10^{-2}$

$\mu_i = 5.92.10^{22}/n_A$

$$q_{e-A} = \begin{cases} 1.12.10^{-22}\ \epsilon^{-2.64} & (0.1 < \epsilon < 0.37) \\ 1.2.10^{-20}\ \epsilon^{2} & (0.37 < \epsilon < 1.0) \end{cases}$$

Fig. 27.4 and 27.5

$B = 3$

$p_o = 1,3,10$ ata

$M_2 = 0.2 - 1.4$

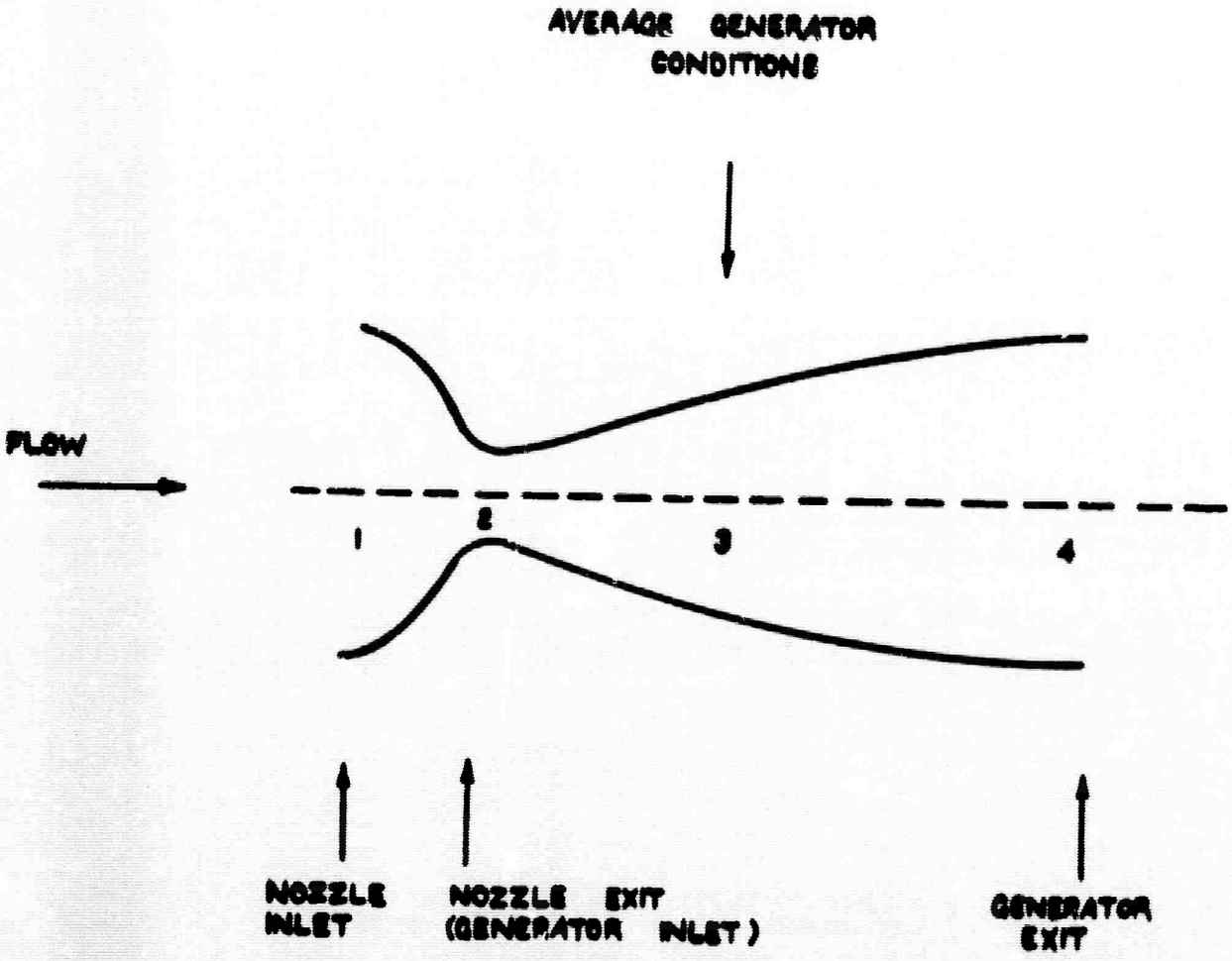

MPD GENERATOR AND NOZZLE STATIONS

FIG 27·1

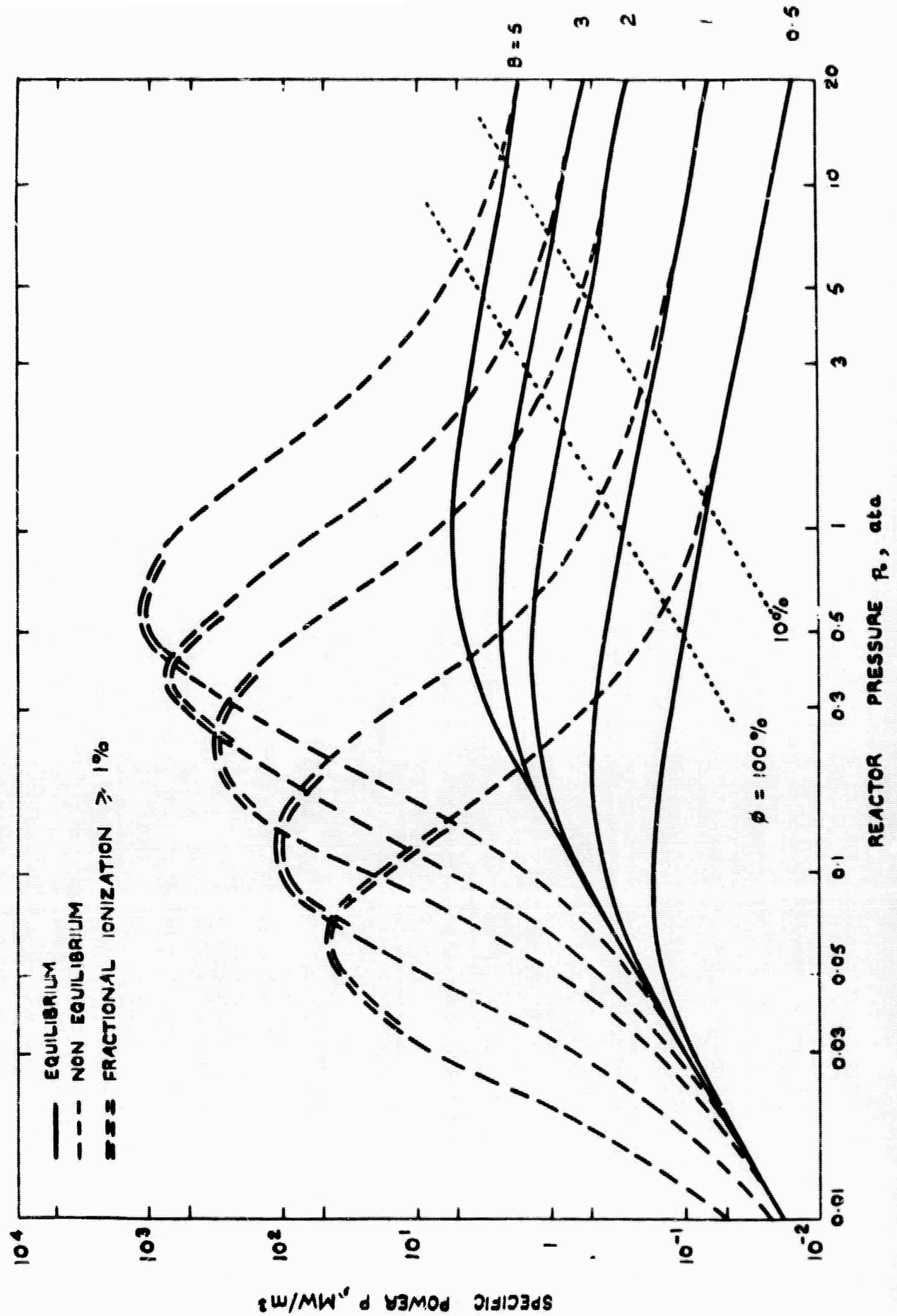

SPECIFIC POWER OF A SUBSONIC $(M = 0{\cdot}6)$, SEGMENTED ELECTRODE HELIUM CESIUM MPD GENERATOR AS A FUNCTION OF REACTOR OPERATING PRESSURE

FIG 27.2

SPECIFIC POWER OF A SUBSONIC (M=0·6) SEGMENTED ELECTRODE ARGON CESIUM MPD GENERATOR AS A FUNCTION OF REACTOR OPERATING PRESSURE

FIG27·3

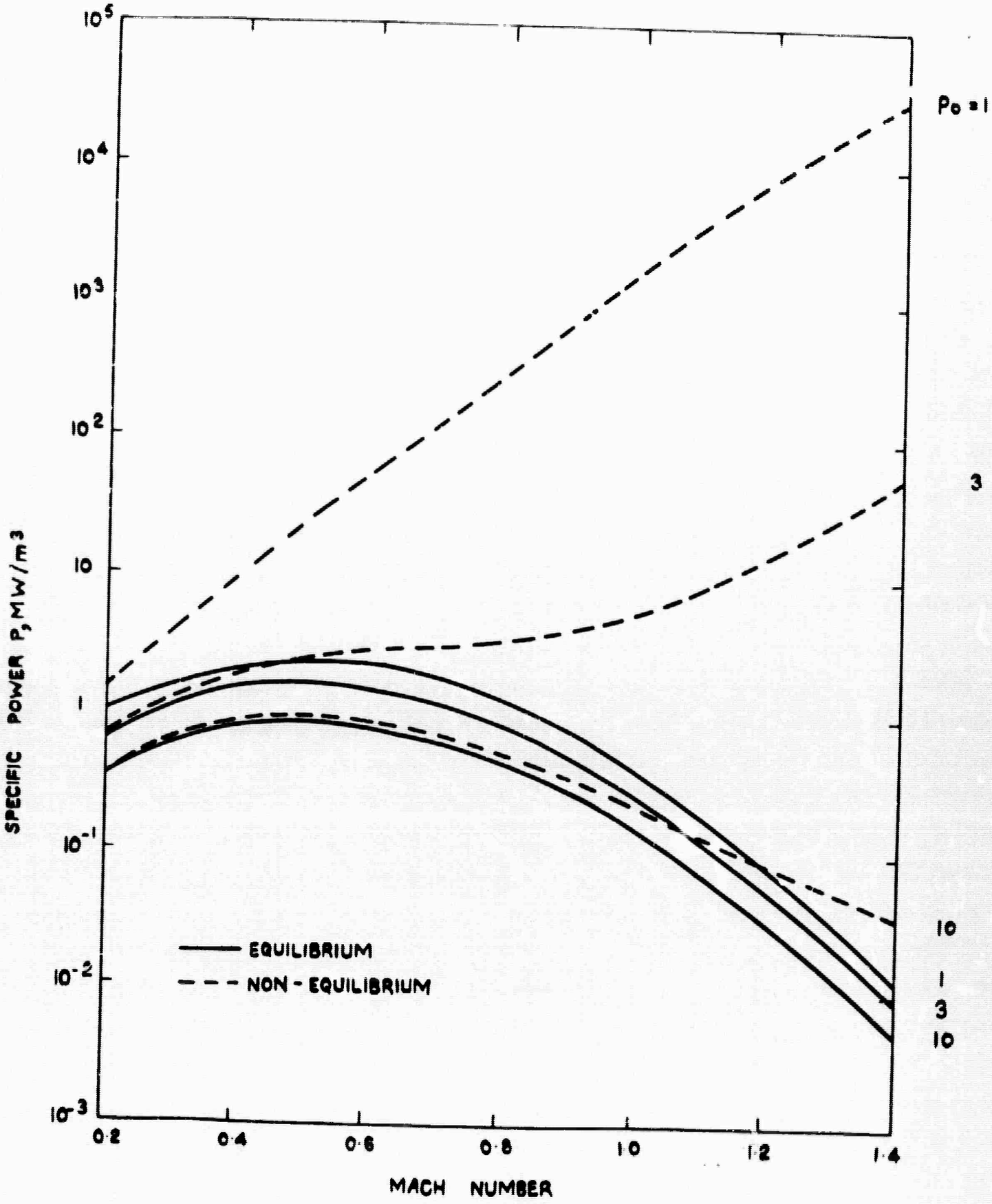

SPECIFIC POWER OF A SEGMENTED ELECTRODE HELIUM CESIUM MPD GENERATOR AS A FUNCTION OF GENERATOR INLET MACH NUMBER

FIG 27.4

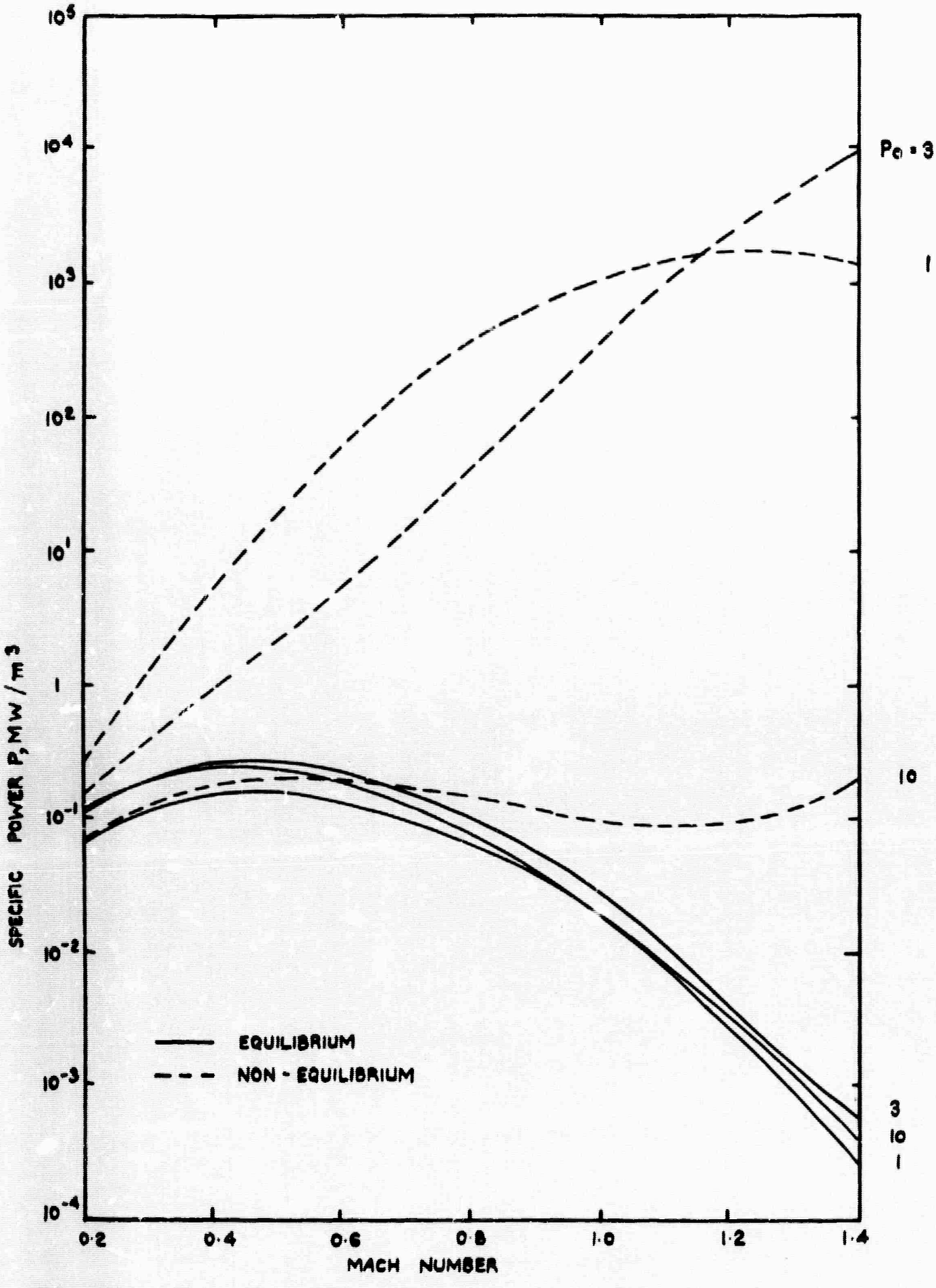

SPECIFIC POWER OF A SEGMENTED ELECTRODE ARGON CESIUM MPD GENERATOR AS A FUNCTION OF GENERATOR INLET MACH NUMBER

FIG 27·5

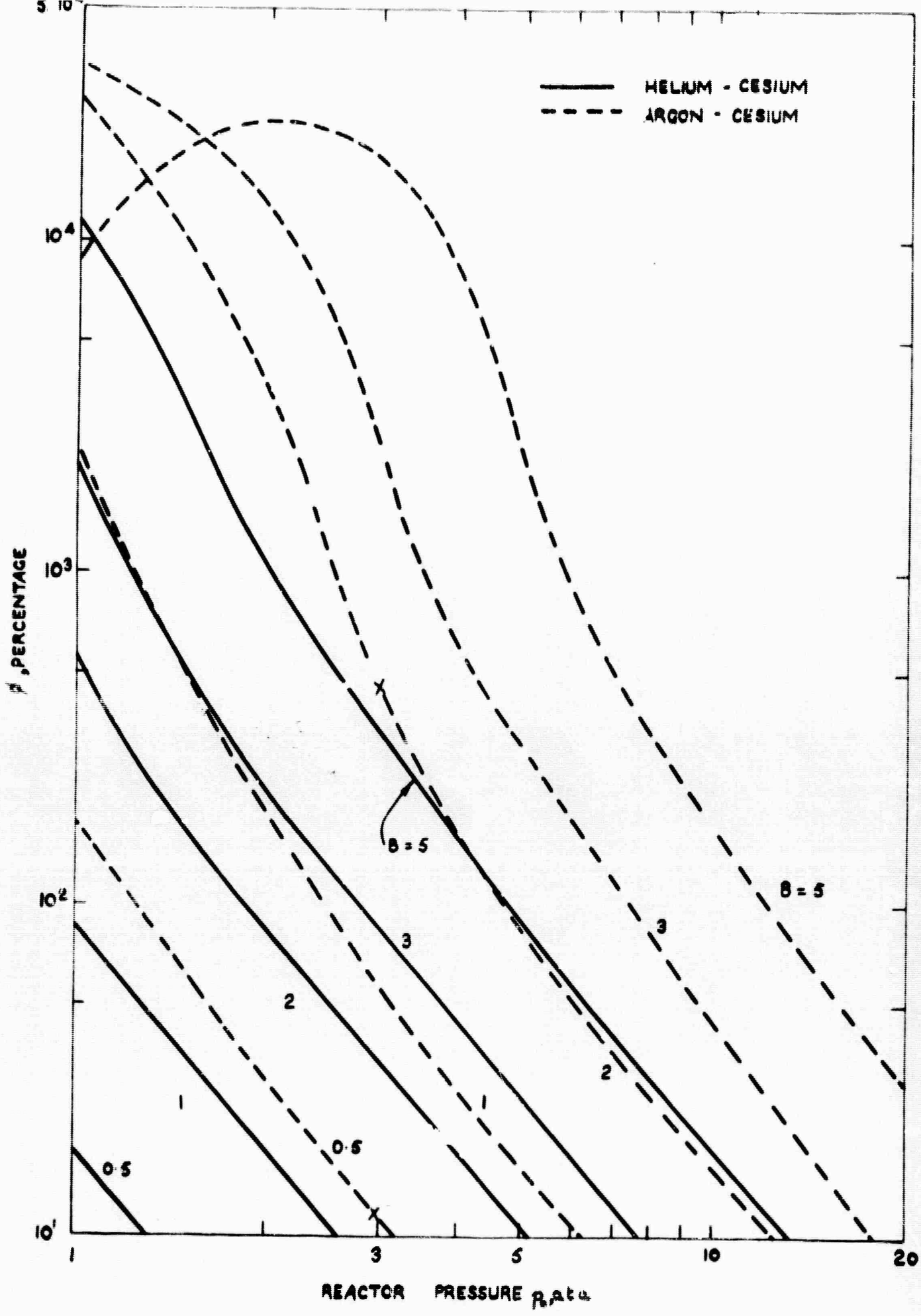

ø AS A FUNCTION OF REACTOR OPERATING PRESSURE

FIG 27·6

NOMENCLATURE (CHAPTER 27)

B	magnetic field strength
e	electronic charge
g_{eia}	statistical weight of electron, ion, atom
h	Planck's constant
k	Boltzmann's constant
K	load factor
m_e	electronic mass
M	Mach number
n_a	atom concentration of seed gas
n_e	electron concentration
n_p	atom concentration (of parent gas)
p	static pressure
p_o	stagnation pressure
P	specific power
q	collision cross section
R	gas constant
T	static gas temperature
T_o	stagnation gas temperature
T_e	electron temperature
V	flow velocity
V_i	ionization potential
β_e	electronic Hall coefficient
β_i	ionic Hall coefficient
γ	ratio of specific heats
δ	inelastic collision factor
ϵ	$T_e/11605$
η_L	local isentropic efficiency
ϕ	$\dfrac{P(T_e) - P(T)}{P(T)}$
ν_e	electronic collision frequency
μ_i	ionic mobility
σ	electrical conductivity
χ	seeding fraction

Subscripts

o	stagnation conditions
1	nozzle inlet conditions
2	MPD generator inlet conditions
3	average MPD generator conditions
4	MPD generator exit conditions

CHAPTER 28

POWER CONVERSION IN SPACE *†

by

I.R. McNab

28.1 INTRODUCTION

Electrical power is undoubtedly the most important single subsystem of any space vehicle, being vital to communications, data gathering and processing, life support and, directly or indirectly, to propulsion. In many cases the constraints imposed on the vehicle design and operation by the power system are severe. For example, the power system can account for a large fraction of the payload weight, it can influence the thermal control system and it may introduce crew hazards. In addition it may also require solar attitude control, involve complicated prelaunch procedures and directly limit the missions the vehicle can perform.

Criteria to be considered in the selection and operation of space power systems include the power to weight ratio, reliability, compatibility and degree of integration with the spacecraft, launch and operation techniques, resistance to space environment and, for manned spacecraft, the possible crew hazards.

Present and past power requirements for satellites, spaceprobes and manned missions have been filled by the use of solar cells and batteries, either separately or together, and radioisotope-thermoelectric devices; the power levels generally being much less than 1 kWe. While such systems have performed satisfactorily they become less attractive when more advanced missions are considered, mainly because of power to weight ratio considerations. Estimated power requirements for space vehicles over the next few years[3,4], (Fig. 28.1) show that electrical propulsion systems will eventually require large amounts of power. Missions utilizing electric propulsion may be arbitrarily divided into four classes, typical examples of which are, in probable order of occurrence:

(A) earth satellite attitude control and station keeping, and earth satellite orbit transfer;

(B) solar, non-ecliptic, planetary and interplanetary probes;

---

* I.R. McNab. International Research and Development Company, Newcastle upon Tyne, 6.
(Paper presented at the I.E.E. Colloquium on 'Electrical Methods of Propulsion in Space', London, February 13th, 1964.)

† It must be emphasized that, in the absence of a British space programme, most of the information contained herein has been obtained from American sources, particularly references 1, 2 and 3.

(C) large spacecraft, manned or unmanned, of the lunar ferry type; and

(D) manned planetary missions.

The electrical power supply requirements for these missions are typically 3 - 30 kWe, 50 - 300 kWe, 1 - 3 MWe and 20 - 40 MWe respectively. Mission durations are unlikely to be less than a week and will generally be several months. (It is mainly this condition which leads to superiority of electrical propulsion compared with chemical or chemical/nuclear propulsion systems for interplanetary missions.) Flight tests of electric propulsion systems, and possibly of Class A missions, are likely to occur during 1964. The early introduction of electric propulsion for Class B missions (by about 1970) is currently anticipated, although this is dependent to a considerable extent on the availability of electric power supplies.

At present a great diversity of space power systems are under investigation, covering many different power levels and mission times. Fig. 28.2 shows approximately the power levels and mission times for different power systems[5]; for electric propulsion systems with high power levels and long mission durations the mid and upper right hand region of this figure is of greatest importance.

To give the background to the development of the advanced conversion systems currently under consideration a brief review of some of the systems shown in Fig. 28.2 will now be made; some of the advantages and disadvantages of each system will be mentioned.

28.2 PRESENT POWER CONVERSION SYSTEMS AND ASSOCIATED RESEARCH

28.2.1 Solar cell systems

Solar cells, with or without associated storage batteries, have been the most widely used power systems to date. These have grown rapidly from the small wattage devices used in early satellites to arrays such as that for the OAO satellite (Orbiting Astronomical Observatory) which, if deployed so that all cells were simultaneously illuminated would generate about 1.5 kWe, the average power being about 600 We.

The main problem of solar cells is the performance degradation occurring due to the nuclear particle radiation associated with the earth radiation belts and solar flares. A change has recently been made from the diffused boron P/N silicon cells originally used in U.S. Satellites to the more radiation resistant diffused phosphorous N/P cells. The most probable method of increasing performance will arise from the development of new materials. One possible method of increasing the power level of present systems is to use reflectors to

increase the amount of light striking the cells. At present however the higher cost of such a panel and the increased operating temperature of the solar cells offset the advantages gained.

28.2.2 Battery systems

Batteries will undoubtedly continue to be of importance for auxiliary power requirements although the introduction of fuel cells may well reduce the number of applications of batteries. Fuel cells are scheduled for the Gemini and Apollo spacecraft. Attractive features of these self-contained systems include their high efficiency, availability of water as a by-product (for hydrogen/oxygen cells) and lack of need for attitude control or shielding. Regenerative fuel cells and batteries will undoubtedly be important in lunar and planetary exploration for life support and vehicle power. Used in conjunction with a main energy depot involving a nuclear or solar power plant, these systems will provide high mobility and efficiency[3,5].

28.2.3 Radioisotope systems

Radioisotope thermoelectric generators have been used and are planned for several space missions. A 2.7 W plutonium 238 fuelled thermoelectric generator (SNAP 3) was launched in Transit 4A in June, 1961, and was still operating satisfactorily two years later. A larger generator (SNAP 9A; 25 We) was launched in September, 1963, in Transit 5; this has a design lifetime of five years. Larger devices (200 - 500 We) are planned for Voyager and Nimbus missions and design studies for 3 - 5 kW systems for use in manned space stations are under way. Most, if not all, of the radioisotope systems require the relatively scarce and expensive α emitters, because of spacecraft and handling considerations. In view of their high cost isotope systems will probably only be considered where their special attributes - invulnerability to external radiation, long life and potential reliability - are important. Isotope systems currently use lead telluride or germanium-bismuth telluride conversion elements, operating at 450^{0} - 500^{0}C. Future converter technology will be devoted towards the more efficient use of isotope heat sources through the development of thermoelectric systems having higher working temperatures and efficiencies (such as germanium-silicon alloys); ultimately thermionic conversion will be employed.

28.2.4 Solar-dynamic systems

The use of reflectors to increase the efficiency of solar cells has been mentioned. A more efficient use of reflectors is for solar-thermionic or solar-dynamic conversion systems. In solar-thermionic systems a mirror is used to focus the solar energy into a small cavity formed by the emitters of a group of

thermionic diodes. Devices of this type have been ground tested and have yielded efficiencies of about 7%.

In solar-dynamic systems a mirror is used to focus the solar energy into a cavity containing the working fluid. Rankine cycle systems are generally considered for such devices, thus the working fluid is evaporated, produces electricity in a turbo-alternator and is then condensed in a condenser/radiator. Considerable effort is currently being put into such systems in the United States, particularly on the NASA "Sunflower" and USAF "Astec" systems, the power outputs being about 15 kWe. The Sunflower system, which is based largely on SNAP 2 turbo-alternator technology, uses a 32.5 ft diameter petal-type mirror and mercury as the working fluid. Some of the major components of the system have already been tested.

To date the accurate focussing required for solar-thermionic and solar-dynamic systems is only available with precise, one piece, rigid mirrors. Considerable effort is presently being made on the development of foamed, inflatable and unfurlable petal systems which can be launched without difficulty. Table 28.1 summarises the advanced mirror development programmes in the U.S.[1]. While mirrors probably eliminate the radiation damage problem of solar cells, little is known at present of their performance characteristics in a space environment, although it may be anticipated that micrometeorite damage will have a significant effect on long term mirror efficiency.

For power systems up to about 100 kWe solar dynamic systems have potentially higher power to weight ratios and lower costs than other systems. The absence of radiation and shielding problems make these solar powered systems attractive for manned space stations. The energy conversion equipment for the solar-dynamic systems is similar to that under investigation for nuclear-dynamic systems and thus offers opportunity for in-flight demonstration and testing without the costs and hazards associated with reactors.

28.2.5 Reactor systems

Reference to the categorisation of electric propulsion missions in the Introduction to this report and to Fig. 28.2 shows that, of the systems this far discussed, only solar collectors are likely to provide the power levels and long lifetimes required for electric propulsion, and then only for Class A or lower power Class B missions. For long term missions of more than 50 - 100 kWe, nuclear power sources are required.

Several power conversion systems for use with nuclear reactors are currently under consideration. Probably the most advanced systems, in terms of the expected

flight test times, are reactor-conversion systems of the SNAP (Systems for Nuclear Auxiliary Power) series. Table 28.2 shows the current status of several SNAP development programmes[4]. The early SNAP reactors such as SNAP 3 and 9A (already launched) and SNAP 10A use thermoelectric conversion. The larger SNAP units use dynamic conversion based on the Rankine cycle, the power output being a.c. The cycle for the SNAP 2 system (Fig. 28.3)[6] uses two fluid loops: the NaK (78% Na, 22% K) reactor coolant loop which remains liquid, and the power conversion loop in which mercury is vaporised, expanded through a turbine, condensed and recycled. Only one moving part, the combined rotating unit (CRU) is used, thus both pumps, the turbine and the alternator are supported on one shaft. The two fluids are completely separated, hermetic sealing being employed. Several problems follow from the use of the CRU, for example, the lubricating ability of the mercury, the balance of component efficiencies at a common shaft speed, thermal distribution, shaft alignment and balance, and protection of sensitive parts from the hot mercury vapour. The start-up procedure is complex and orbital operation will be further complicated by the zero-gravity condition and the effects this will have on the processes in the boiler, and to a greater extent, the radiator/condenser. The SNAP 2 system is about 13 ft long and 5 ft diameter at the base, and the weight with a fully shielded reactor is about 1500 lb.

The more powerful SNAP 8 system can be considered as a logical successor to the SNAP 10A/2 systems. Several components of the smaller systems and much of the accumulated data will be incorporated in the design and construction of SNAP 8. The aim of the programme is the development of a long-life generating system capable of providing at least 35 kW to meet anticipated needs for large amounts of auxiliary power and, possibly, for early electrical propulsion. The basic design is similar to SNAP 2, thus the heat produced by the reactor is removed by liquid NaK and transferred to mercury in the boiler. The mercury is evaporated, drives the turbo-alternator and is then condensed and recycled. An additional NaK loop is provided to transfer the heat from the mercury to the radiator.

Many problems have been encountered in the development programme for SNAP 8 and the current design emphasizes reliability of performance at the expense of weight. One severe problem is that of turbine operation. Because of the requirement of low specific weights for space power systems the rotating speed must be very high. This condition, together with the low viscosity of liquid metal lubricants, creates a condition of bearing operation in the turbulent region, which is not well understood at present. In SNAP 8 the problem of turbulent lubrication by liquid metals has been exchanged for that of seal development and

the use of anti-friction bearings lubricated from a fourth loop circulating an organic fluid. The shaft speed has been dropped from the original 40000 rpm to 12000 rpm.

While SNAP 8 will provide an early nuclear-electric capability, much higher powers and lower specific weights are required to realize the potential of electric propulsion for advanced missions.

SNAP 50 (for which some data are given in Table 28.2) is one approach currently under investigation in the U.S. to the problem of power generation in the power range up to about 350 kWe. The system is basically similar to the SNAP 2 and 8 projects in that a condensing Rankine cycle is used with a turboelectric power conversion system. The reactor power to weight ratio is however vastly increased by using a uranium carbide fuelled lithium cooled fast reactor and as a consequence the overall power to weight ratio is expected to be far better than that of the previous SNAP systems. If the design and performance predictions are fulfilled the SNAP 50 system will enable many useful missions to be carried out using electric propulsion in the Class B missions previously given, although the cost of such a system may be very large.

28.3 HIGH POWER (MEGAWATT) SYSTEMS

For power levels in the several magawatt (electrical) range, it is by no means clear at present which power conversion system will be best. Present hardware commitments for nuclear electric spacecraft powerplants in the megawatt range are limited to liquid metal Rankine cycles. This arises from early comparisons of such cycles with Brayton closed gas cycle power systems[2]. These early comparative studies were based on the weights of the components involved and also to a large extent on the weight and type of radiator. The radiator represents a major portion of the weight of the power conversion system and is also the largest component, being therefore difficult to launch and decreasing the system reliability due to meteoroid penetration. (If armour is provided to decrease the probability of penetration the radiator weight increases.) Thus it is desirable to minimise the radiator area. Calculations performed for Rankine and Brayton turboelectric cycles (Fig. 28.3 and 28.4 respectively show typical cycles) show the superiority of Rankine cycles compared on the basis of radiator area (for the same maximum cycle temperature) or on the basis of the maximum working temperature for the same area. (Table 28.3 shows results due to Sutton[7] which illustrate this, although these relate specifically to power conversion by magnetoplasmadynamic generators.)

These cycle studies have spurred the development of practical Rankine cycle

systems, initially using mercury and eventually alkali metals. However, in view of the many difficult problems encountered in the development of alkali metal devices some attention is being given to the Brayton cycle. Gas cooled reactors and turbo-machinery have been proved reliable over several years of operation whereas alkali metal systems have yet to demonstrate long life performance. In addition, while Table 28.3 indicates that gas cycles require higher maximum temperatures than alkali metal cycles for the same radiator area, gas turbines can almost certainly operate at higher temperatures than alkali metal turbines. Further advantages of the single phase gaseous working fluid are the avoidance of flow problems occurring in two phase systems in zero or low gravity operation and the elimination of freezing during shut-down periods[2].

It is interesting to note that the conventional steam cycle has been proposed as an alternative to the liquid metal Rankine cycle. While steam is limited to low cycle temperatures by vapour pressure considerations, its high heat capacity and the possibility of using aluminium construction results in a low radiator weight per unit area and a reasonable power to weight ratio of the overall system.

If full advantage is to be taken of the high reactor powers available for either gas or alkali metal cycles it is necessary to use one, or more, of the methods of direct conversion of heat to electricity presently under investigation. The two methods of greatest applicability are thermionic diodes and magnetoplasma-dynamics (MPD). Both these methods have the advantage of operation at higher temperatures than turbogenerators, which are limited by stresses in the rotating machinery. While both systems are currently in the research and development stage it is probable that in neither case will the efficiency be very high. For ground based power stations, both diodes and MPD are currently under consideration only as 'topping' devices, working in conjunction with a conventional steam turboalternator plant. However for space power plants the ability of these systems to work at high temperatures, and thus to reject heat at high temperatures may reduce the radiator size to such an extent that thermionics and/or MPD become competitive as the main power conversion system.

Several different cycle arrangements covering different diode locations and working fluids have been suggested for thermionic systems. Probably the most general categorization of thermionic diodes is into 'in-pile' and 'out-of-pile' systems[2]. In the in-pile configuration the heat supplied to the cathode (electron emitter) surface comes directly from the reactor fuel and heat rejected by the anode (electron collector) is removed by the coolant passing through the reactor. In the out-of-pile systems the reactor coolant heats the cathode and the rejected heat is either removed by a second fluid or radiated directly into

space.

Thermionic cell performance is currently temperature limited with typical realistic long-life values of 1750°C at the cathode surface and a corresponding optimum anode temperature of about 700°C. Thus the in-pile systems can use reactor coolant temperatures of about 1000°C less than the out-of-pile systems, for similar diode performance[2]. This results in a considerably different choice of coolants for the two systems. Inert gases, liquid metals and boiling or superheated steam can be considered for in-pile systems. For out-of-pile systems the high temperatures necessitate the use of inert gases in view of the corrosion problems involved with alkali metals. Several possible cycles are discussed below.

Fig. 28.5 shows a typical single stage liquid metal vapour system employing in-pile thermionic diodes. This configuration appears capable of producing a rather better specific weight than a turbo-electric cycle operating at the same temperature. The main problems are the production of a reactor cooled by metal vapour, thermionic diode reliability in the radiation environment and the complex reactor construction required to contain the cells and their associated electrical connections[2]. (Note that, although a single stage two phase cycle is shown in Fig. 28.5, a practical system would probably use a two stage system with a heat exchanger.)

An out-of-pile liquid metal cycle would eliminate the disadvantages of in-pile diode performance and reactor design, but the very high temperatures required would undoubtedly cause severe corrosion problems.

In-pile gas thermionic systems of the type shown in Fig. 28.6 suffer from the same problems of diode reliability and reactor construction as the liquid metal vapour systems[2]. However the use of inert gases minimizes corrosion effects on the cycle components and may enable the anode surface to serve directly as the coolant wall. (With liquid metal vapour or steam coolants an electrical insulator which is also a good heat conductor is required between the anode and the coolant channel.)

To avoid some of the problems inherent in the in-pile cycle the cycles shown in Fig. 28.7 and 28.8 have been investigated[2]. These out-of-pile gas thermionic systems have many advantages (for example, fissionable fuel need not be used, the reactor design is improved, electrical connection problems are simplified) but a very high temperature reactor is required since the coolant must heat the diode cathodes to about 1750°C. For the cycle shown in Fig. 28.7 the overall efficiency is improved by employing a turbine to drive the compressor. The results of a recent theoretical analysis[2] comparing various liquid metal and gas turboelectric

and thermionic systems are shown in Table 28.4. The temperatures considered in the analysis are

liquid metal	(maximum)	1130°C
gas	(maximum)	1730°C
	(turbine)	1280°C
diode, $T_{cathode}-T_{anode}$		840°C

The criterion on which the systems have been compared is the specific radiator weight, which is the single item of greatest weight for a system producing more than 1 MWe. The results show that for a thermionic cell efficiency of more than about 13% the in-pile thermionic gas system will be superior. It is possible, even if advances are made in the efficiency of turboelectric liquid-metal systems, that if corrosion problems cannot be solved, gas systems will be preferred from a reliability viewpoint, even though less efficient.

The second direct conversion system for power levels above 1 MWe is magnetoplasmadynamic (MPD); this system holds promise of generating larger amounts of power with better efficiencies than thermionic diodes. MPD generators may be divided into two main categories, combustion and nuclear reactor powered; combustion devices are usually open cycle and nuclear devices closed cycle systems. Direct current generating combustion devices are the most advanced at the present time so far as power output is concerned. Substantial amounts of power have been generated by several systems, for example the AVCO Mark 2 generator has given an output of over 1 MWe with an efficiency of about 7%. Larger devices are expected to have a higher efficiency and it is likely that land based MPD stations generating several tens of megawatts will be operational within the next few years. However for space missions of several weeks open cycle combustion systems are not attractive in view of the large fuel supplies required.

Closed cycle nuclear fuelled MPD systems, while conserving the working fluid, suffer from the temperature limitations of present and foreseeable reactor developments. The main consideration is to increase the electrical conductivity of the working fluid to a high level ($\gtrsim 30$ mho/m). In both combustion and nuclear reactor heated MPD systems the main working fluid is seeded with an alkali metal to enhance conductivity. Generally only a few atomic percent of the seed is used since the electrical conductivity has a maximum with respect to seed concentration in this regime. Thus pure alkali metals are not usually considered for land based MPD generators; however, radiator size and weight requirements may alter this picture in the space field, as shown in Table 28.3.

Even with the optimum amount of alkali metal seeding it is unlikely that reactor temperatures will be high enough to make MPD conversion feasible if the electrical conductivity takes its thermal equilibrium value. Consequently several methods of producing extra-thermal ionization in MPD generators are currently under investigation. These methods include:

ionization by high voltage electron beams[8];
ionization by high current arcs[8];
ionization by r.f.[9];
photoionization[10];
magnetically induced ionization[11];
ionization by β rays from fission products[8]; and
the use of high acceleration to produce non-equilibrium flows in which the electron density does not decay significantly during the expansion process[12,13].

At present none of these methods has been conclusively demonstrated in an MPD generator producing substantial amounts of power, although several devices are under construction.

Fig. 28.9 shows a typical seeded inert gas nuclear MPD system for space purposes. For this system the problem of corrosion due to alkali metals is lessened by the low percentage of seed present and the fact that the alkali metal need not enter the reactor, however as with other gas cycles the radiator area will be large compared to the metal vapour system.

The main problem of MPD generators may well be the weight of the magnetic field coils. Even if superconducting magnets are available the weight of the associated cryogenic equipment will be high and there is the additional problem of radiating away the excess heat[7].

To overcome the weight disadvantages of the large compressors required for gas MPD cycles, two phase liquid-vapour systems are currently under consideration in which the reactor is cooled by a liquid metal which then mixes with metal vapour and expands the latter into the MPD channel[14]. It seems probable that the overall efficiency of this system will be lower than that of the usual MPD gas cycle, although the power to weight ratio may be similar since compressors are avoided.

28.4 CONCLUSIONS

For power levels up to about 100 kWe, solar or isotope powered systems will probably provide the necessary power for space vehicles; power levels of about

50 kWe will enable early interplanetary missions to be accomplished using electric propulsion systems. For power levels ranging from 50 kWe to several tens of MWe, several alternative conversion systems based on nuclear reactors are under consideration. Of these, alkali metal Rankine cycle turboelectric systems are receiving the most attention at present, although many problems beset the development programmes. Several other systems, based on the Brayton gas cycles, show promise of greater efficiencies and reliabilities, thermionic and MPD systems being particularly interesting above one megawatt. It is possible that the ultimate choice of system will be based on reliability (particularly for manned missions) and the use of hybrid systems involving two, or more, of the conversion methods mentioned above, should not be discounted.

REFERENCES

1 TEEM, J.A., and SZEGO, G.C. Electric propulsion and power, Astronautics and Aerospace Engineering, November 1963, p.98

2 GREY, J., and WILLIAMS, P.M. Re-examination of gas-cycle nuclear electric space power-plants. A.I.A.A. Journal, Vol. 1, No. 12, p.2801. 1963

3 SCOTT, W.C., and SCHULMAN, F. Space electrical power. Astronautics and Aerospace Engineering, p.48. May 1963.

4 BERNATOWICZ, D.T., GUENTERT, D.C., and KLANN, J.L. Space power-plant needs and selection, loc. cit. p.22

5 SZEGO, G.C., and COHN, E.M. Fuel cells for aerospace application, loc. cit. p.107

6 ANDERSON, G.M. Nuclear reactor systems, loc. cit. p.27

7 SUTTON, G.W. The theory of magnetohydrodynamic power generators. G.E. Report R62SD990. December, 1962

8 STERNGLASS, E.J., TSU, T.C., GRIFFITH, G.L., and WRIGHT, J.H. MHD power generation by non-thermal ionization and its application to nuclear energy conversion. Third Symposium on the Engineering Aspects of MHD. Rochester, March 28th, 1962

9 GOURDINE, M.C. Non-equilibrium r.f. plasmas for MPD energy conversion. Magnetoplasmadynamic electrical power generation conference, Newcastle, September 6th, 1962. I.E.E. Conference series No. 4, 1963

10 MAITLAND, A. A criterion for assessing methods of producing non-equilibrium ionization, loc. cit.

11 KERREBROCK, J.L. Conduction in gases with elevated electron temperature. Second symposium on the engineering aspects of MHD. Philadelphia, March 9th, 1961. Columbia U.P. New York and London, 1962

12 ESCHENROEDER, A.Q., and DAIBER, J.W. Ionization non-equilibrium in expanding flows. Paper presented at A.R.S. meeting, December, 1960, Washington D.C.

13 McNAB, I.R. A non-equilibrium electron mode for kilowatt range MPD space power. Paper presented at the 6th AGARD combustion and propulsion colloquium, Cannes 16-20th March, 1964

14 ELLIOTT, D.G. Two-fluid magnetohydrodynamic cycle for nuclear-electric power conversion. A.R.S. Journal, Vol. 32, p.924. 1962

BLANK PAGE

TABLE 2

CURRENT U.S. ADVANCED MIRROR-DEVELO

Type	Diam, ft	Contractor	Po ap
Mylar foam-rigidized mirror	44.5	Goodyear	15 kW dynam
Electroformed unfurlable petal mirror	44.5	EOS	15 kW dynam
Large high-performance one-piece mirror	20-30	EOS	Solar syste
Large high-performance one-piece mirror	20-30	TRW	Solar syste
Inflatable rigidized mirror	9.5	Hughes	Low t syste
High precision mirror master	-	GE	Solar syste
High precision, high temperature rigid mirror	5	EOS, TRW, BOEING	Solar syste

E 28.1

ELOPMENT PROGRAMS (Teem and Szego[1])

Power system application	Status
kWe Astec solar namic system	Hardware development; form for front skin completed
kWe solar namic systems	Six petals completed and optically and structurally tested
lar Brayton cycle stem	Study program in progress emphasizing electroforming
ar Brayton cycle stem	Study program in progress emphasizing stretch-forming of aluminium
w temperature stems	Analytical and experimental research on predistributed rigidization materials
lar thermionic stem	Hardware development; fabrication complete; evaluation to be performed
lar thermionic stem	Hardware development and evaluation; electroformed nickel, stretch-formed aluminium, epoxy fibreglass

TABLE 28.2

CURRENT SNAP DEVELOPMENT PROGRAM STATUS (Teem and Szego[1])

Characteristic	SNAP 10A	SNAP 2	SNAP 8	SNAP 50
Power output, kWe	0.5	3	35	350
Reactor power, kWt	30	50	600	-
Efficiency, %	1.6	6	8	-
Reactor	U-Zr H_x Thermal	U-Zr H_x Thermal	U-Zr H_x Thermal	UC Fast
Reactor outlet temp., °C	540	650	700	1100
Primary coolant	NaK 78	NaK 78	NaK 78	Lithium
Power conversion	Ge Si Thermoelectric	Hg Rankine	Hg Rankine	K Rankine
Turbine inlet temp., °C	-	600	650	1050
Radiator area, ft^2 ft^2/kWe	62.6 125	120 40	1400-1800 45	- -
System unshielded weight, lb lb/kWe	650 1300	1200 400	4500 130	5000 15
Available	1964	1966	1970	1975/80

TABLE 28.3

RADIATOR AREAS AND MAXIMUM WORKING TEMPERATURES FOR VARIOUS CYCLES (Sutton[7])

Cycle	Component efficiency	Overall thermal efficiency	Radiator area parameter	Working fluid max. temp. for same area, ^{o}K
Rankine	0.66	15%	16	1360
Brayton (a)	0.80	15%	145	2370
Brayton (b)	0.85	15%	84	2070
Intercooled Brayton	0.80	15%	220	2690
Tri-cycle	0.90	10%	144	2350
Regenerative Brayton	0.85	25%	48	1800

TABLE 28.4

SPECIFIC RADIATOR WEIGHTS FOR SEVERAL TURBOELECTRIC AND THERMIONIC POWER SYSTEMS AT DIFFERENT THERMIONIC CELL EFFICIENCIES

(Grey and Williams[2])

Thermionic cell efficiency	0.05	0.10	0.15	0.20
System	Specific radiator weight (lb/kWe)			
Out-of-pile gas (radiation cooled)	>> 10	>> 10	> 10	4.5
Gas turboelectric	3.4	3.4	3.4	3.4
Out-of-pile gas (split radiator)	7	4.2	2.8	2
Liquid metal turboelectric	1.3	1.3	1.3	1.3
In-pile liquid metal	4.1	2.1	1.4	0.9
In-pile gas	~10	2	1.0	0.6

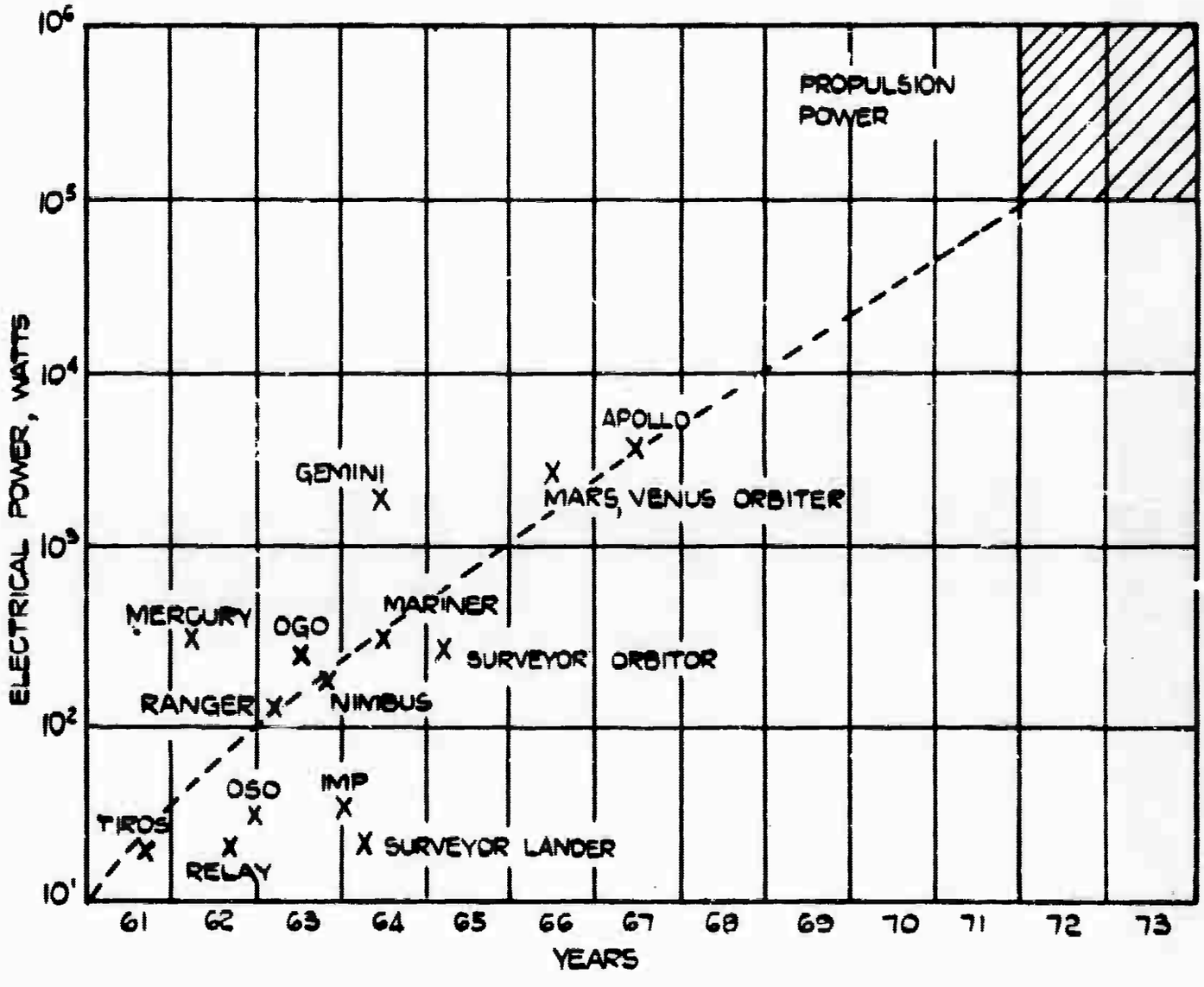

ELECTRIC POWER REQUIREMENT FOR SPACECRAFT

FIG28·1

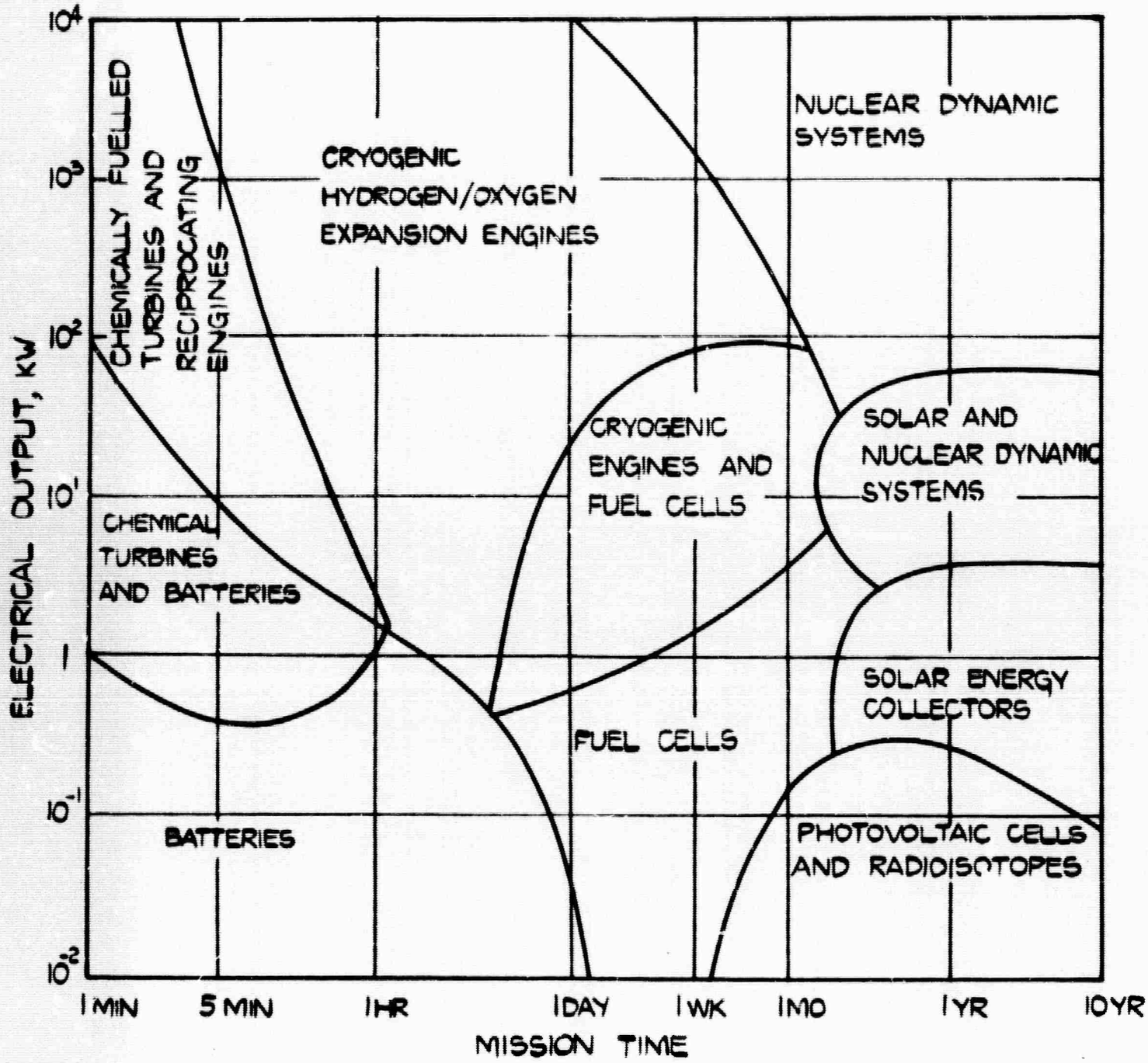

ELECTRIC POWER SYSTEMS

FIG 28·2

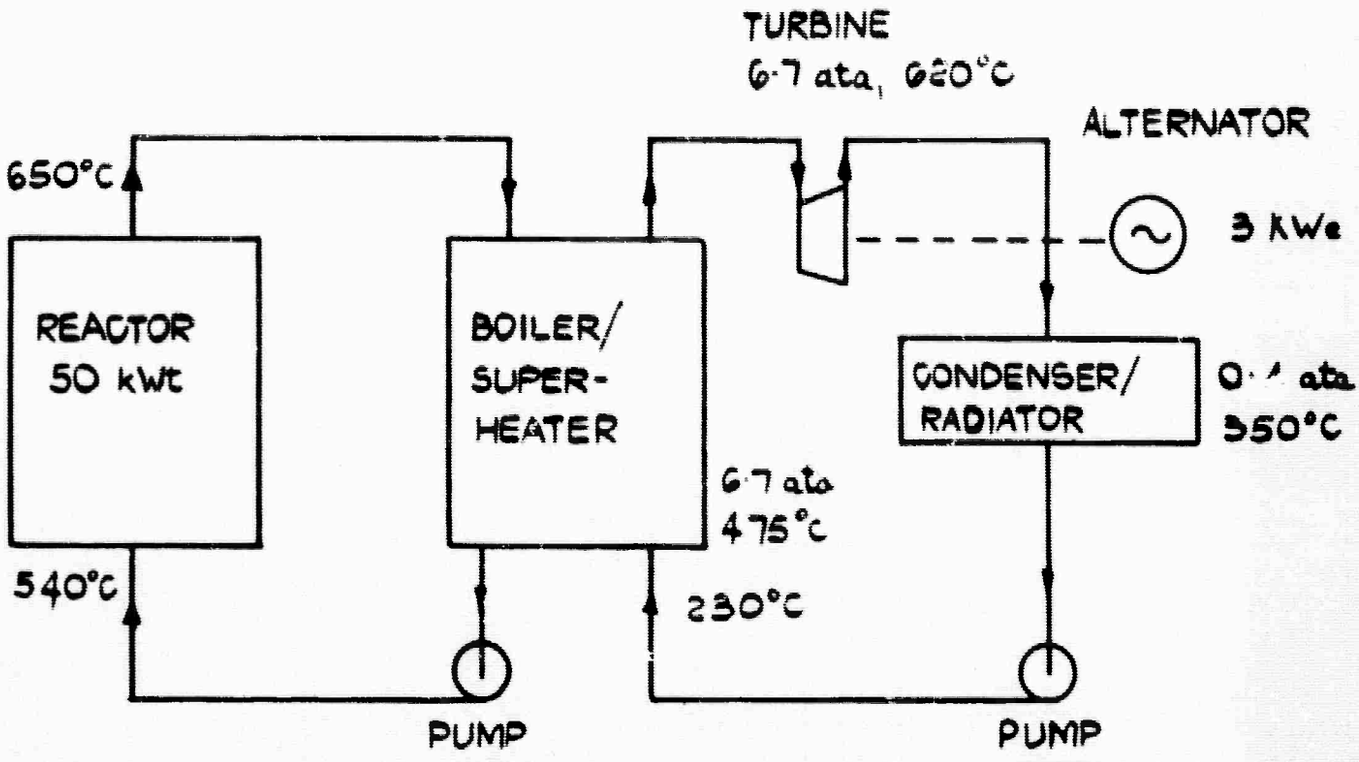

SNAP 2 TWO STAGE LIQUID METAL TURBOELECTRIC POWERPLANT CYCLE CONDITIONS

FIG 28·3

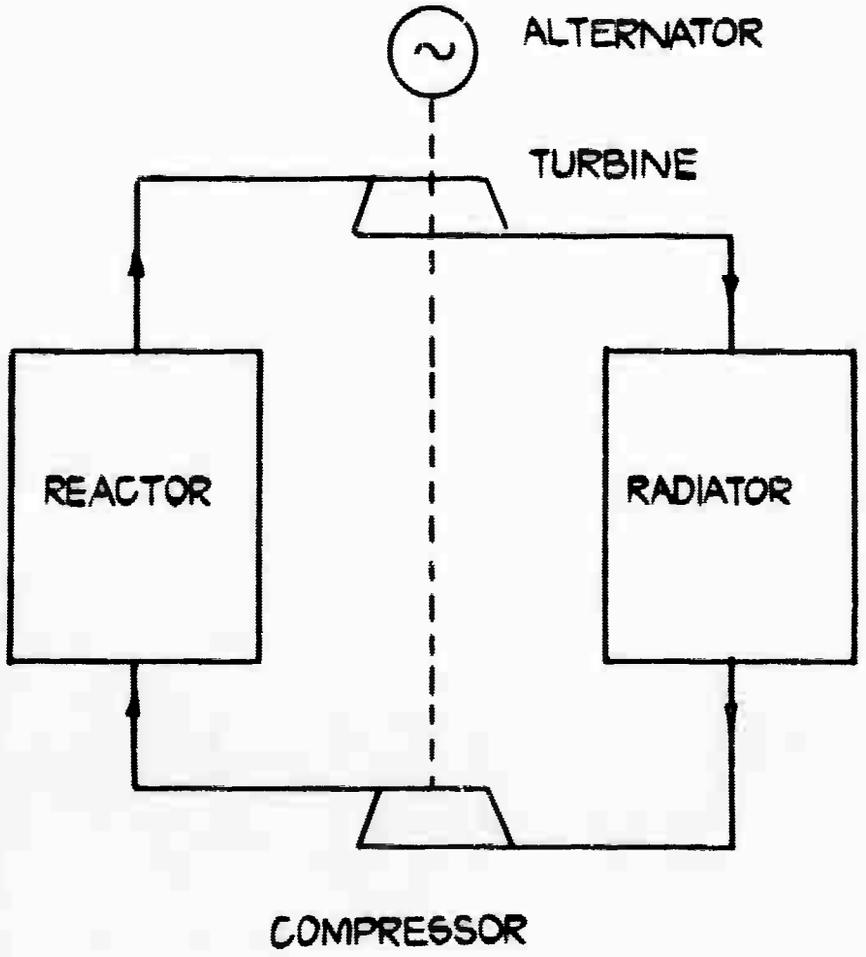

CLOSED CYCLE GAS TURBOELECTRIC POWERPLANT

FIG 28·4

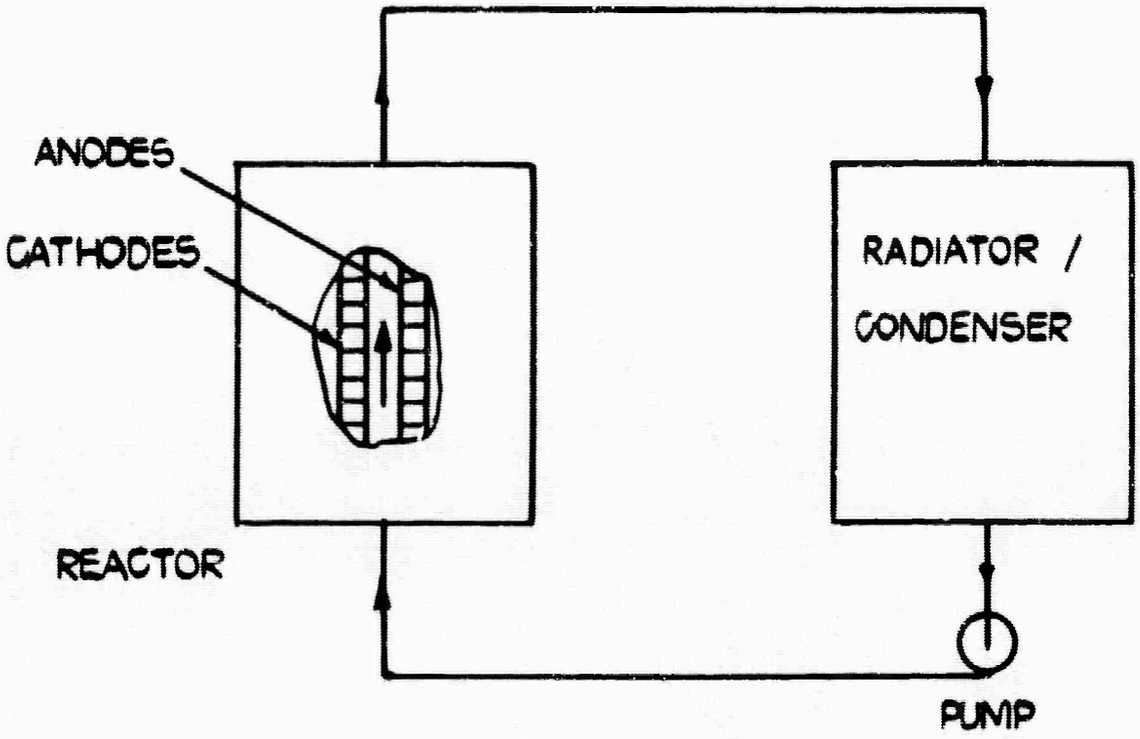

SINGLE STAGE LIQUID METAL VAPOUR IN-PILE THERMIONIC POWERPLANT

FIG 28·5

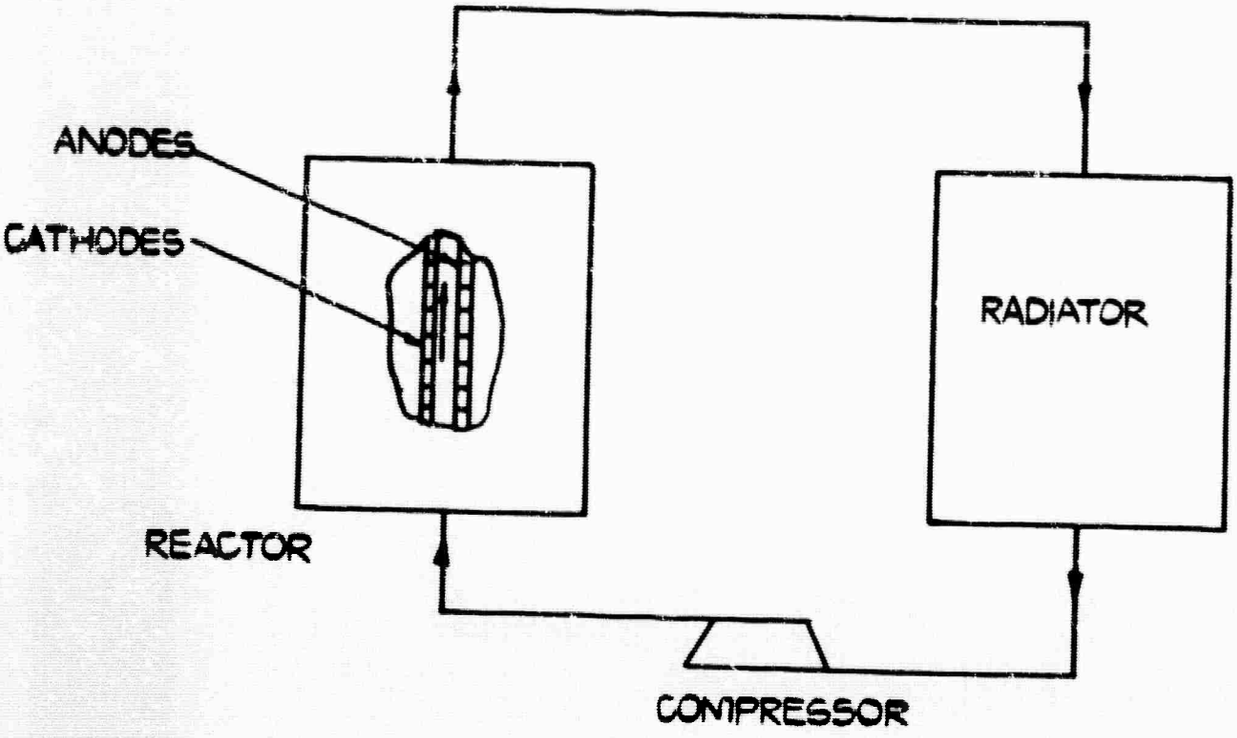

CLOSED CYCLE IN-PILE GAS THERMIONIC POWERPLANT

FIG 28·6

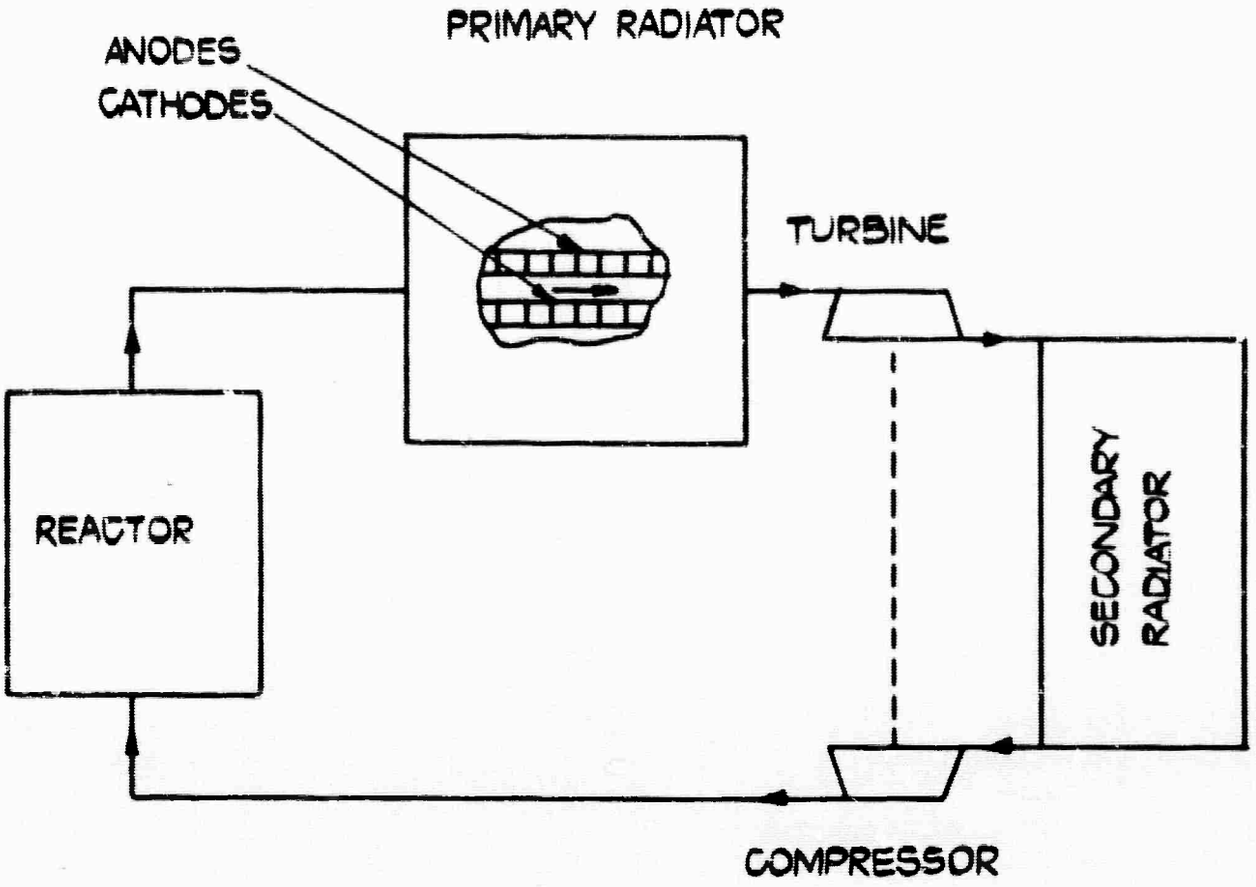

OUT-OF-PILE SPLIT RADIATOR GAS THERMIONIC POWERPLANT

FIG 28·7

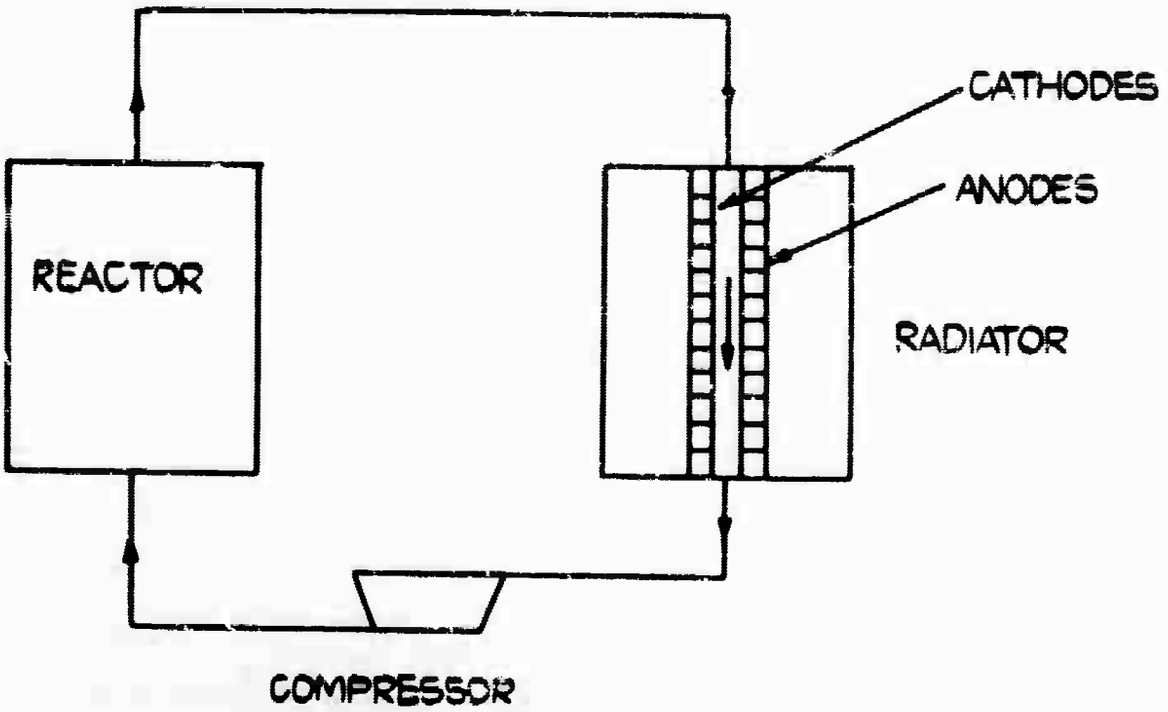

OUT-OF-PILE RADIATION COOLED GAS THERMIONIC POWERPLANT

FIG 28·8

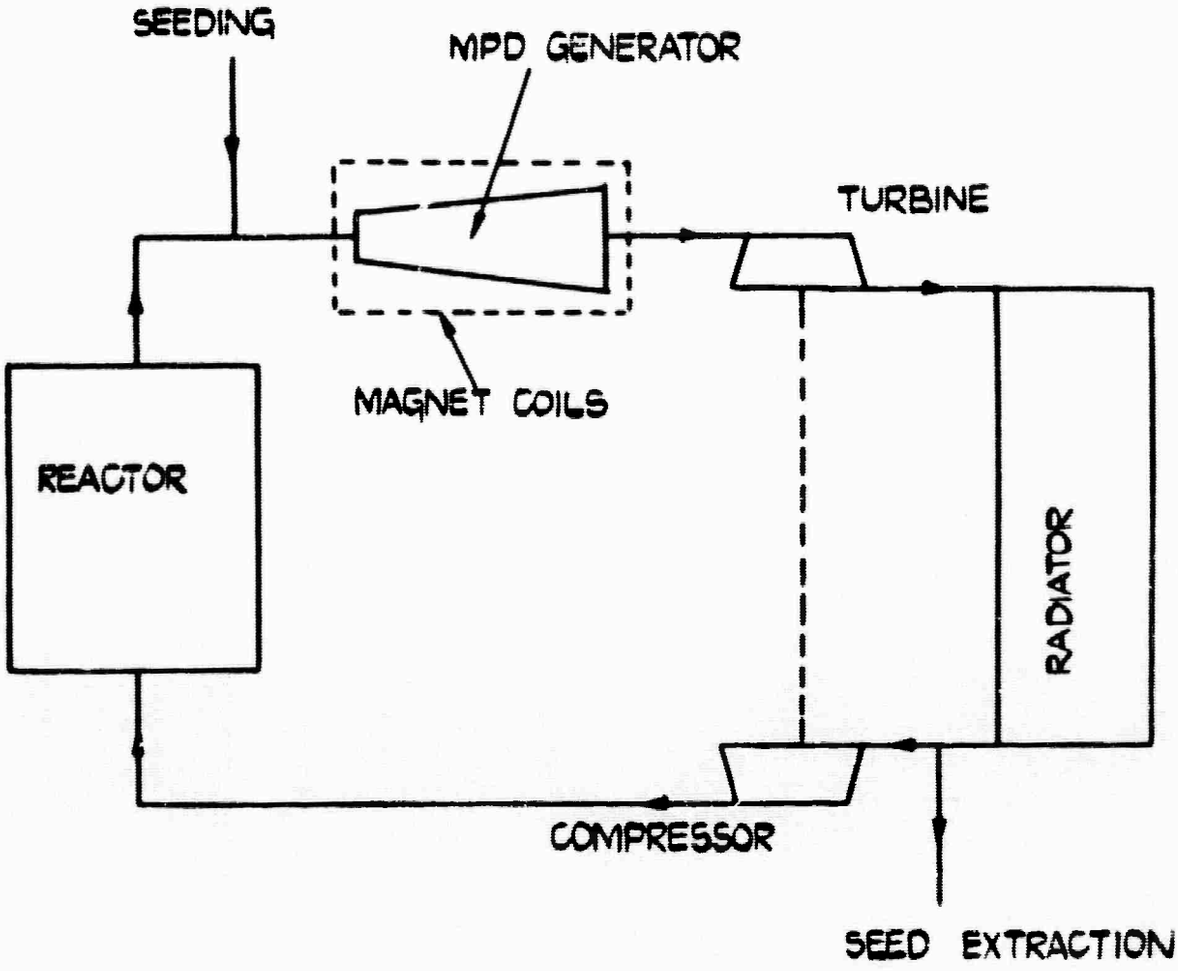

CLOSED CYCLE ALKALI METAL SEEDED GAS-NUCLEAR POWERPLANT

FIG 28·9

BLANK PAGE

CHAPTER 29

A NON-EQUILIBRIUM ELECTRON MODE FOR KILOWATT-RANGE MPD SPACE POWER*

by

I.R. McNab

29.1 INTRODUCTION

The demand for electrical power sources for terrestrial and space purposes is increasing rapidly and many techniques are presently under investigation in efforts to increase the efficiency of conventional equipment and to provide alternative systems. The problems associated with space power systems are severe so far as the power-to-weight ratio, reliability, and operating conditions are concerned; it is these systems which will be considered here.

Present and postulated space power systems include: solar cells, solar collectors (Brayton or Rankine cycle and thermoelectric), nuclear reactor - thermoelectric, nuclear reactor - turbogenerator, nuclear reactor - condensing fluid, radioisotopes, fuel cells, and magnetoplasmadynamic (MPD) generators. While several of these systems (for example solar cells) are already well proven, others hold promise of generating much larger amounts of power with higher efficiencies: one such system is MPD generation.

MPD generators may be divided into two main categories: combustion and nuclear reactor powered. Combustion devices are usually open cycle and nuclear devices closed cycle. Direct current generating combustion devices are the most advanced at the present time so far as power output is concerned. Substantial amounts of power have been generated by several systems, for example, the AVCO Mark 2 generator has given an output of over 1 MWe with an efficiency of about 7 per cent. Larger devices are expected to have a higher efficiency and it is likely that land-based MPD stations generating several tens of megawatts output will be operational within the next few years. However, for a space mission of duration greater than about one week, it is unlikely that open cycle combustion systems will be attractive in view of the large fuel supplies required. At present the prospects of developing closed cycle combustion devices are remote.

* Sixth AGARD Combustion and Propulsion Colloquium, Cannes, March 1964

Closed cycle nuclear-fuelled MPD systems, while conserving the working fluid, suffer from the temperature limitations of present and foreseeable reactors, thus limiting the Saha electrical conductivity and consequently the maximum attainable power output. Development of nuclear reactors to yield high working temperatures, while resulting in a higher electrical conductivity and power output, will introduce more severe materials problems which are only capable of long term solution. The solution to this paradox is to increase the electrical conductivity of the working fluid in the generator without increasing the gas temperature. High power outputs could then be obtained without severe materials problems.

Several methods of obtaining this extra-thermal ionization in MPD generators have been suggested and a few have been tried experimentally.

Karlovitz and Halasz[1], who started work on MPD in 1938, investigated several modes of extra-thermal ionization in their natural gas-fuelled combustion generator. Most attention was paid to ionization by high voltage electron beams, but glow discharges, arcs and r.f. were also tried. These attempts were unsuccessful mainly because of the effects of dissociative recombination which rapidly removed the electrons created by the ionization process. This fast recombination mechanism will not be as severe in a monatomic gas.

Kerrebrock[2] has suggested and investigated, theoretically and experimentally, magnetically-induced ionization in MPD generators. In these processes the electrons in the plasma gain energy from the electric field induced by the magnetic field through which they pass. The energy gained in this manner is lost through collisions with the gas particles, but if the parent gas is monatomic, there are no molecular energy losses and an elevated electron temperature can result. Since electron-atom collisions are the dominant ionization mechanism under MPD generator conditions, the electrical conductivity is considerably enhanced. The success of this method depends, amongst other factors, on the degree of purity of the gases present, as may be seen from the following expression[3]:

$$\frac{T_e}{T} - 1 = \frac{\beta_e^2 \gamma M^2}{3\delta(1+\beta_e^2)} \left[\frac{\beta_e^2 K_H^2}{(1+\beta_e\beta_i)^2} + (1-K)^2 \right]$$

where δ is a factor accounting for the effects of inelastic collisions (other than ionizing ones) and non-Maxwellian electron energy distributions. In general, δ is a function of temperature but typical values for MPD generators are $\delta \approx 1$ for monatomic gases and $\delta \approx 10^3$ for molecular gases. The theory has been verified

experimentally by Kerrebrock[2] with an electric field and tentatively by Robben[4] with both electric and magnetic fields. Devices under construction to investigate and utilize this effect include those at IRD and Martin-Marietta. Recently it has been reported[5] that the device at Martin has proved extra-thermal ionization, but no details are available. Rosa[6] has shown that the production of extra-thermal ionization by this means is quite sensitive to the degree of uniformity of the gas; it is possible therefore that the effect may prove more difficult to achieve experimentally than originally anticipated.

Sternglass et al[7] have discussed theoretically extra-thermal ionization for closed cycle nuclear powered MPD systems by electron beams, by β rays from fission products and by d.c. arcs. Of these methods electron beams appear the most promising in view of the high efficiency of generation of beams, continuous application, ease of adjustment of energy spectrum and lack of contamination caused by their use. The main disadvantage appears to be the technical complexity of the system. Fission product ionization is less efficient and leads to radiation hazards, although this may not be a severe limitation for space systems. D.C. arcs, while giving high conductivities, cause severe heating of the electrodes (which must be cooled) in addition to Joule heating of the gas stream.

A novel extra-thermal ionization method suggested by Maitland[8] is to utilize photoionization caused by a high energy light beam. Initially a laser was suggested as the light source, although this has a low basic efficiency but the recent development of high intensity ultra-violet lamps may make this a more interesting suggestion.

Gourdine[9] is presently investigating the production of non-equilibrium plasmas by r.f. discharges. The main difficulties are associated with the low density of the plasma, the difficulty of coupling into it, and diffusion losses. The technique has the advantage of providing high flow velocity and high conductivity independently - a useful condition for high efficiency MPD conversion, bearing in mind the temperature limitations associated with materials.

29.2 PROPOSED NEW MODE

Although, as is apparent from the above, many methods of producing extra-thermal ionization in closed cycle MPD generator systems are being actively examined at present, to date no MPD generator producing substantial amounts of power has yet utilized such an effect. It is the purpose of this paper to examine another mode of operation which may permit high power outputs to be

obtained from MPD generators. This method, suggested independently by Lindley[10] and Eschenroeder and Daiber[11], consists of rapidly expanding a high enthalpy gas through a large area ratio nozzle, so that the rate of fall of gas temperature is very large. When the temperature falls rapidly in a gas many internal adjustments must be made by molecular collisions. For example, the energy of molecular vibrations must be reduced, a new balance must be found between atoms and molecules, chemical reactions must take place at a different rate, and ions and electrons must recombine to form neutral particles. All these adjustments require a large number of collisions between particles before a new equilibrium is established. If the temperature changes faster than the equilibrium is established then non-equilibrium flow results.

Many studies, both theoretical[12-19] and experimental[20-23], on non-equilibrium flows have been published recently, most are concerned primarily with molecular gases or gas mixtures where vibrational and dissociative non-equilibrium are the dominant factors. This interest arises because the main domains in which such flows are encountered relate to real or simulated (shock tube and wind tunnel) high altitude hypersonic and missile re-entry conditions in air and similar conditions in combustion gases. In general the theoretical solution of such problems is complicated since, in addition to solving the quasi-one-dimensional flow equations, the population densities of the (many) species present must be determined from the rate equations governing the appropriate reactions. In many cases the required rate coefficients are not fully tabulated. Solution of the flow equations is generally complicated since the changes of energy during the relaxation phenomena usually form a significant fraction of the total enthalpy of the gas.

The flow of a monatomic recombining gas is more amenable to analysis since valid simplifying assumptions can be made concerning the number of species present and, consequently, fewer rate equations are required to characterize the flow. For example, the recombination mechanism may be assumed to be controlled by only one excited state. One significant difference between a recombining atomic gas and a relaxing molecular gas is that the electron temperature may be considerably higher than the temperature of the heavy particles in the atomic gas. This leads to reduced recombination, amongst other effects.

Bray and Wilson[24] (following the methods outlined in references 25 and 26) have described the flow of an atomic recombining gas in terms of the equations of mass, momentum and energy, the thermodynamic equations of state and enthalpy, the rate equation for production and loss of electrons and the electron temperature equation. Even such a simple model is difficult to solve and again requires detailed knowledge of the rate coefficients.

To examine the consequences of non-equilibrium nozzle flow on the design and power output of an MPD generator a much simplified model has been constructed which retains the essential features of a non-equilibrium flow.

29.3 THEORETICAL MODEL AND RESULTS

In concepts of closed cycle nuclear reactor MPD generators the working fluid is usually selected to be an inert gas seeded with small amounts of an alkali metal. This may not be the final form of an MPD space power supply (for example, a completely condensing cycle may be superior on a power-to-weight basis) but such a system will probably be the first to yield experimental data and it is this type of generator which will be considered here. The assumption of small fractional seeding, which is generally valid, enables considerable simplification to be made in the analysis since the energy involved in the ionization and recombination processes in the seed element form only a small fraction of the total enthalpy of the working fluid and thus may be neglected. Consequently, neglecting boundary layers and shock phenomena the quasi-one-dimensional flow equations for the parent gas only can be assumed to approximate the real flow system.

To simplify the model further the isentropic flow of a perfect gas has been considered so that the relation between area ratio and Mach number in the nozzle is

$$\frac{A}{A^*} = \frac{1}{M}\left[\frac{2}{\gamma+1}\left(1+\frac{\gamma-1}{2}M^2\right)\right]^{\frac{\gamma+1}{2(\gamma-1)}} ,$$

which, for $\gamma = 5/3$, is

$$\frac{A}{A^*} = \frac{1}{M}\left[\frac{1}{4}(3+M^2)\right]^2 \qquad \ldots\ (29.1)$$

To avoid discontinuities in the theoretical flow caused by a discontinuous throat area the nozzle shape has been assumed hyperbolic, of the form

$$A = A^* + K_N^2 x^2 \qquad \ldots\ (29.2)$$

where x is the distance along the nozzle axis measured from the throat and where the half-angle of the nozzle at infinite distance from the throat is given by

$$\tan\theta = K_N/\sqrt{\pi} \quad .$$

Using the non-dimensional quantities $\hat{A} = A/A^*$ and $\hat{x} = K_N x/\sqrt{A^*}$, and combining equations (29.1) and (29.2) yields an expression for Mach number in terms of the

dimensionless distance through the nozzle

$$\hat{x}^2 = \frac{1}{11}\left[\frac{1}{4}(3+M^2)\right]^2 - 1 \qquad \ldots. (29.3)$$

which has the form shown in Fig. 29.1 The temperature, velocity etc. at any point in the nozzle may then be obtained from the usual isentropic flow relations.

The electrical conductivity at any point in the nozzle is determined from the flow, rate and electron energy equations. In view of the difficulties associated with the values of the rate coefficients and the solution of these equations it is assumed that the electrical conductivity at the exit of the nozzle is related to the throat value by an exponential function of the form:

$$\sigma_{ex} = \sigma_{thr} \exp(-ct_f) \qquad \ldots. (29.4)$$

where c is a coefficient depending on the rate coefficients of the various processes occurring and the electron temperature, and t_f is the time of flight through the nozzle.

The exit conductivity is related to the throat conductivity rather than the inlet conductivity since, in general, the gas is not accelerated sufficiently rapidly in the subsonic region of a nozzle to cause non-equilibrium flow. The throat conductivity may be obtained from the inlet parameters through the use of the isentropic relations, which, for a perfect monatomic gas, are

$$T_{thr} = 0.75\, T_o \qquad \ldots. (29.5)$$

$$p_{thr} = \frac{9\sqrt{3}}{32}\, p_o \qquad \ldots. (29.6)$$

T_o and p_o being the stagnation temperature and pressure respectively.

The time of flight between two points (x_1, x_2) in the nozzle is

$$t_f = \int_{x_1}^{x_2} \frac{1}{V}\, dx = \frac{\sqrt{A^*}}{K_N} \int_{\hat{x}_1}^{\hat{x}_2} \frac{1}{V}\, d\hat{x}$$

For the isentropic flow of a perfect gas with $\gamma = 5/3$

$$V = M\left[\frac{2C_pT_o}{3+M^2}\right]^{\frac{1}{2}}$$

and thus

$$t_f = \left[\frac{A^*}{2K_N^2 C_p T_o}\right]^{\frac{1}{2}} \int_{\hat{x}_1}^{\hat{x}_2} \frac{(3+M^2)^{\frac{1}{2}}}{M}\, d\hat{x} \qquad \ldots. (29.7)$$

Evaluation of the integral enables the time of flight and hence conductivity to be calculated at any point for given inlet conditions.

The power output per unit length of channel for an MPD generator when Hall effects and ion slip are neglected is

$$P = \sigma V^2 B^2 K(1-K)A$$

If the MPD generation section joins smoothly on to the exit of the nozzle this expression gives the power output per unit length at the inlet of the channel when σ, V and A are the exit values for the nozzle, so that

$$\frac{P}{B^2 K(1-K)} = \sigma_{ex} V^2_{ex} A_{ex} \qquad \ldots\ (29.8)$$

For a family of hyperbolic nozzles with constant expansion angle and $\hat{x}_{in} = -\hat{x}_{ex} =$ constant, the values of temperature, velocity, etc., are identical at each value of $\hat{x}$ (for the same inlet conditions) provided the mass flow is adjusted appropriately.

Examining such a family of nozzles for constant magnetic field and load factor shows that if the electrical conductivity were determined only by the Saha (equilibrium) equation, the exit conductivity would be the same for each nozzle, and thus the power output per unit length of channel would increase linearly with cross sectional area.

If, however, extra-thermal conductivity occurs owing to the non-equilibrium effects of a rapid expansion this conclusion will no longer hold. The conductivity will decrease as the nozzle dimensions increase, owing to the increased time-of-flight, while the cross sectional area will increase; consequently, a optimum nozzle size can be expected for any given set of inlet conditions.

To examine this optimum nozzle size for the family of nozzles with $\hat{x}_{in} = -\hat{x}_{ex}$ = constant, equation (29.8) is used; V_{ex} is constant, σ_{ex} is determined from equations (29.4) to (29.7) and A_{ex} from

$$\hat{A}_{ex} = 1 + \hat{x}_{ex}^2 \ . \qquad \ldots\ (29.9)$$

Combining these equations yields

$$\frac{P}{P_c} = \hat{P} = A^* \exp(-c_1 I A^{*\frac{1}{2}}) \ , \qquad \ldots\ (29.10)$$

where $$P_e = \sigma_{thr} V_{ex}^2 B^2 K(1-K)(1+\hat{x}_{ex}^2) \quad \ldots\ldots (29.11)$$

$$c_1 = c(2K_N^2 C_p T_o)^{-\frac{1}{2}} \quad \ldots\ldots (29.12)$$

$$I = \int_o^{\hat{x}_2} \frac{(3+M^2)^{\frac{1}{2}}}{M} \, d\hat{x} \, . \quad \ldots\ldots (29.13)$$

The variation of I with $\hat{x}_2 = \hat{x}_{ex}$ (that is, from the nozzle throat to the exit) is shown in Fig. 29.2.

Differentiation of equation (29.10) yields the result that the maximum value of P occurs when

$$A^*_{opt} = \frac{4}{c_1^2 I^2} \quad \ldots\ldots (29.14)$$

The value of A^*_{opt} for a hyperbolic nozzle with $\hat{x}_{ex} = 2$ (that is, $A_{ex} = 5A^*$), $\theta = 10^\circ$ and C_p for pure helium is shown in Fig. 29.3 as a function of T_o and c. The values of T_o used, 1000° - 2500°K, lie in the range of interest for MPD generators. There is little information available at present which permits accurate evaluation of the coefficient c in the above expressions. Tentative calculations carried out at IRD indicate that, for a helium plasma seeded with one atomic percent of cesium, c will be $\approx 10^5$/sec; thus the range of c shown in Fig. 29.3 should adequately cover the error in the independent calculations.

When the value of $\hat{x}_{ex}$ is altered the value of A^*_{opt} is shifted owing to the change in time of flight through the nozzle which causes a decrease in conductivity as $\hat{x}_{ex}$ is increased; this effect is partially offset by the increase in exit velocity. The effect is shown in Fig. 29.4 for $T_o = 2000^\circ$K and $c = 10^5$/sec, where A^*_{opt} is seen to decrease as $\hat{x}_{ex}$ increases.

The power output per unit length of the MPD channel when A* is optimized is

$$\hat{P}_{opt} = \frac{1}{e^2} A^*_{opt} \quad \ldots\ldots (29.15)$$

The actual power output per unit channel length for

$T_o = 2500^\circ$K
$p_o = 1$ ata
$c = 10^5$/sec
$\hat{x}_{ex} = 2$
$B = 3$ Wb/m^2
$K = 0.5$

for helium seeded with one atomic percent cesium is ~ 32 kW/m. The actual power output in a metre long channel will be less than this since power extraction will cause a rapid drop in the total enthalpy of the gas. This will reduce the velocity, leading to a reduction in power output through the V^2 term and also a reduction in conductivity because of increased recombination. Nevertheless this calculation does show that the power output of an MPD generator using a non-equilibrium nozzle expansion will lie in a range of interest for space power purposes.

29.4 DISCUSSION AND CONCLUSIONS

Although many methods of producing extra-thermal ionization in closed cycle MPD generators have been suggested and tried experimentally none has yet been utilized in a device producing substantial amounts of power. An alternative method of gaining a high electrical conductivity is to use the (already proven) methods of producing a non-equilibrium flow. The non-equilibrium expansion through a hyperbolic nozzle of a plasma with small fractional seeding has been examined here using a simple theoretical model. The investigation shows that the nozzle exit conductivity will be high compared with the equilibrium value. If such a nozzle immediately precedes an MPD generator section this high conductivity enables high power outputs to be achieved with relatively small devices, for example, for the case quoted in the previous section, an initial power output per unit channel length of ~ 32 kW/m for a channel of 7 cm^2. A power source producing such an output is certainly of interest for space purposes; more refined calculations including the loss mechanisms neglected here (heat transfer, wall friction, boundary layers, shock waves, Hall effects, ion slip) will be worthwhile.

The optimum throat area for a hyperbolic nozzle expansion has been evaluated and shown to depend on the inverse square of the coefficient c. This coefficient depends on the electron temperature throughout the expansion and the rate coefficients for all the atomic processes occurring. In order that it might be accurately evaluated the complete solution of the non-equilibrium flow must be found. While there is at present some doubt concerning the rate coefficients, independent calculations carried out at IRD indicate that, for a helium-1 $^a/_o$ cesium plasma, c will be ~ 10^5/sec for a nozzle inlet stagnation temperature of 2000°K. Under these conditions the optimum throat area is ~ 1.5 cm^2, a size which falls into the range of interest for space purposes.

It may be concluded that the effect outlined here is certainly of interest for space power sources and is worthy of a more accurate evaluation than so far performed. It should be noted that other methods of producing extra-thermal

ionization in the MPD generator channel (for example, electron beams, magnetically-induced ionization, etc.) are not precluded by the use of a non-equilibrium flow.

REFERENCES

1 KARLOVITZ, B. and HALASZ, D. History of the K and H generator and conclusions drawn from the experimental results. Third Symposium on the Engineering Aspects of MHD. University of Rochester, March 28, 1962.

2 KERREBROCK, J.L. Conduction in gases with elevated electron temperature. Second Symposium on Engineering Aspects of MHD, Philadelphia March 9, 1961. Columbia U.P. New York and London, 1962.

3 HURWITZ, H., SUTTON, G.W. and TAMOR, S. Electron heating in Magnetohydrodynamic Power Generators. ARS Journal Vol 32, p 1237, 1962

4 ROBBEN, F. Non-equilibrium ionization in an MHD Generator. Am. Phys. Soc. Bull. Vol 7, p 371, 1962

5 Martin-Marietta Co. Press Release, December 22, 1963.

6 ROSA, R.J. Hall and ion slip effects in a non uniform gas. Physics of Fluids, Vol 5, p 1081, 1962.

7 STERNGLASS, E.J, TSU, T.C., GRIFFITHS, G.L. and WRIGHT, J.H. MPD power generation by non-thermal ionization and its application to nuclear energy conversion. Third Symposium on the Engineering Aspects of MHD. Rochester, March 28, 1962.

8 MAITLAND, A. A criterion for assessing methods of producing non-equilibrium ionization. Magnetoplasmadynamic electrical power generation conference, Newcastle, 6 September, 1962. I.E.E. Conference Series No. 4, 1963.

9 GOURDINE, M.C. Non-equilibrium r.f. plasmas for MPD energy conversion. loc. cit.

10 LINDLEY, B.C. Magnetohydrodynamic Power Generation Experiment. C.A. Parsons and Co. NRC Report 60-92, September 1960

11 ESCHENROEDER, A.Q. and DAIBER, J.W. Ionization non-equilibrium in expanding flows. Paper presented at ARS meeting December 5-8, 1960. Washington D.C.

12 LIGHTHILL, M.J. Dynamics of a dissociating gas. J. Fluid Mech. Vol 2, p 1, 1957.

13 FREEMAN, N.C. J. Fluid Mech. Vol 4, p 4, 1958.

14 ESCHENROEDER, A.Q., BOYER, D.W. and HALL J.G. Non-equilibrium expansions of air with coupled chemical reactions. Phys. Fluids, Vol 5, p 615, 1962.

15 TREANOR, C.E. and MARRONE, P.V. Effect of dissociation on the rate of vibrational relaxation. Phys. of Fluids, Vol 5, p 1022, 1962.

16 STOLLERY, J.L. and SMITH, J.E. A note on the variation of vibrational temperature along a nozzle. J. Fluid Mech. Vol 13, p 225, 1962.

17 BLYTHE, P.A. Non-equilibrium flow through a nozzle. J. Fluid Mech. Vol 17, p 126, 1963.

18 APPLETON, J.P. Structure of a Prandtl-Meyer expansion in an ideal dissociating gas. Phys. Fluids Vol 6, p 1057, 1963.

19 ESCHENROEDER, A.Q. Entropy changes in non-equilibrium flows. Physics of Fluids, Vol 6, p 1408, 1963.

20 PETSCHEK, H. and BYRON, S. Approach to equilibrium ionization behind strong shock waves in Argon. Ann. of Phys. Vol 1, p 270, 1957.

21 WILSON, J. An experiment to measure the recombination rate of oxygen. J. Fluid Mech. Vol 15, p 497, 1963.

22 CLAYDEN, W.A. and COLEMAN, P.L. Distribution of electron density and temperature in an arc heated low density wind tunnel. RARDE Report 57/63, October 1963.

23 CURTIS, J.T., BURKE, A.F. and HAYMAN, R.A. An analytical and experimental study of the ionized flow field about a hemisphere cylinder and its effect on the radiation patterns of a slot antenna. Cornell Aeronautical Lab. Inc. Report AFCRL 63-339, August, 1963.

24 BRAY, K.N.C. and WILSON, J.A. Electron-ion recombination in argon. Magnetoplasmadynamic electrical power generation conference. Newcastle upon Tyne. 6 September 1962. I.E.E. Conference Series No.4, 1963.

25 BRAY, K.N.C. Atomic recombination in a hypersonic wind tunnel nozzle. J. Fluid Mech. Vol 6, p 1, 1958.

26 WILSON, J.A. University of Southampton, Ph.D. Thesis, 1962.

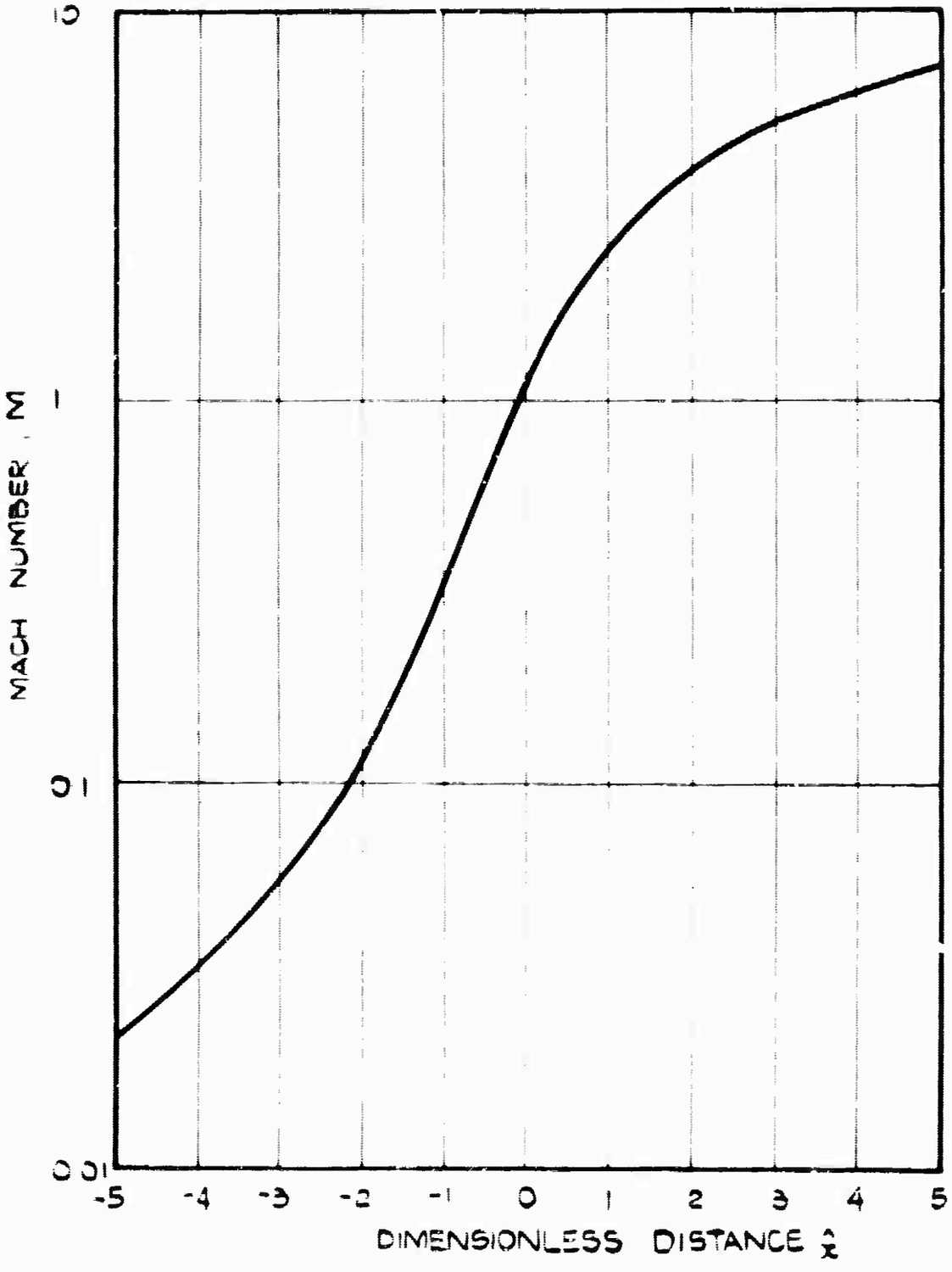

MACH NUMBER AS A FUNCTION OF DIMENSIONLESS AXIAL DISTANCE FOR A HYPERBOLIC NOZZLE

FIG. 29.1

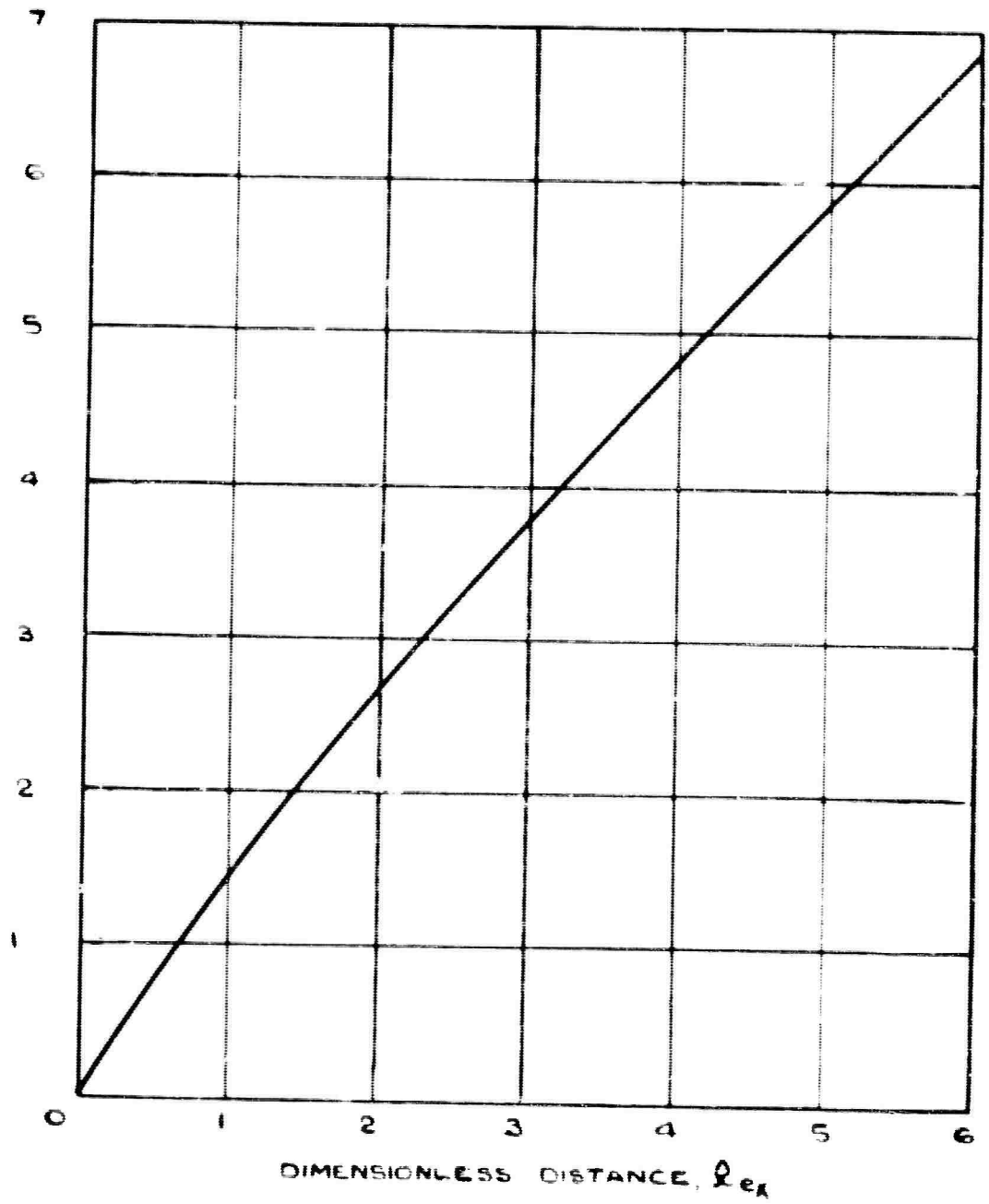

NTEGRAL, I, AS A FUNCTION OF THE DIMENSIONLESS NOZZLE EXIT DISTANCE

FIG 22-2

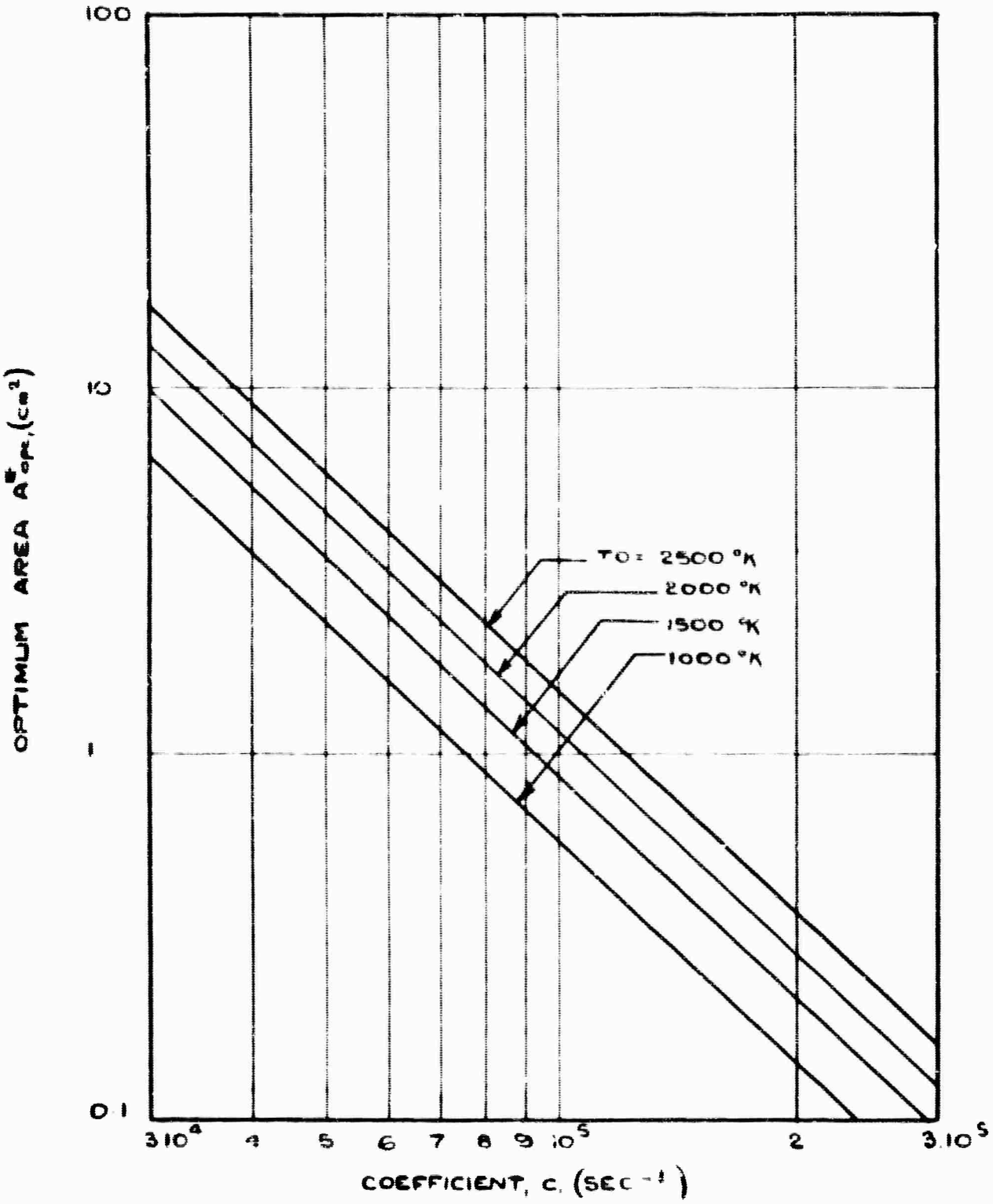

OPTIMUM NOZZLE THROAT AREA AS A FUNCTION OF THE COEFFICIENT C AND NOZZLE STAGNATION TEMPERATURE

FIG 29.3

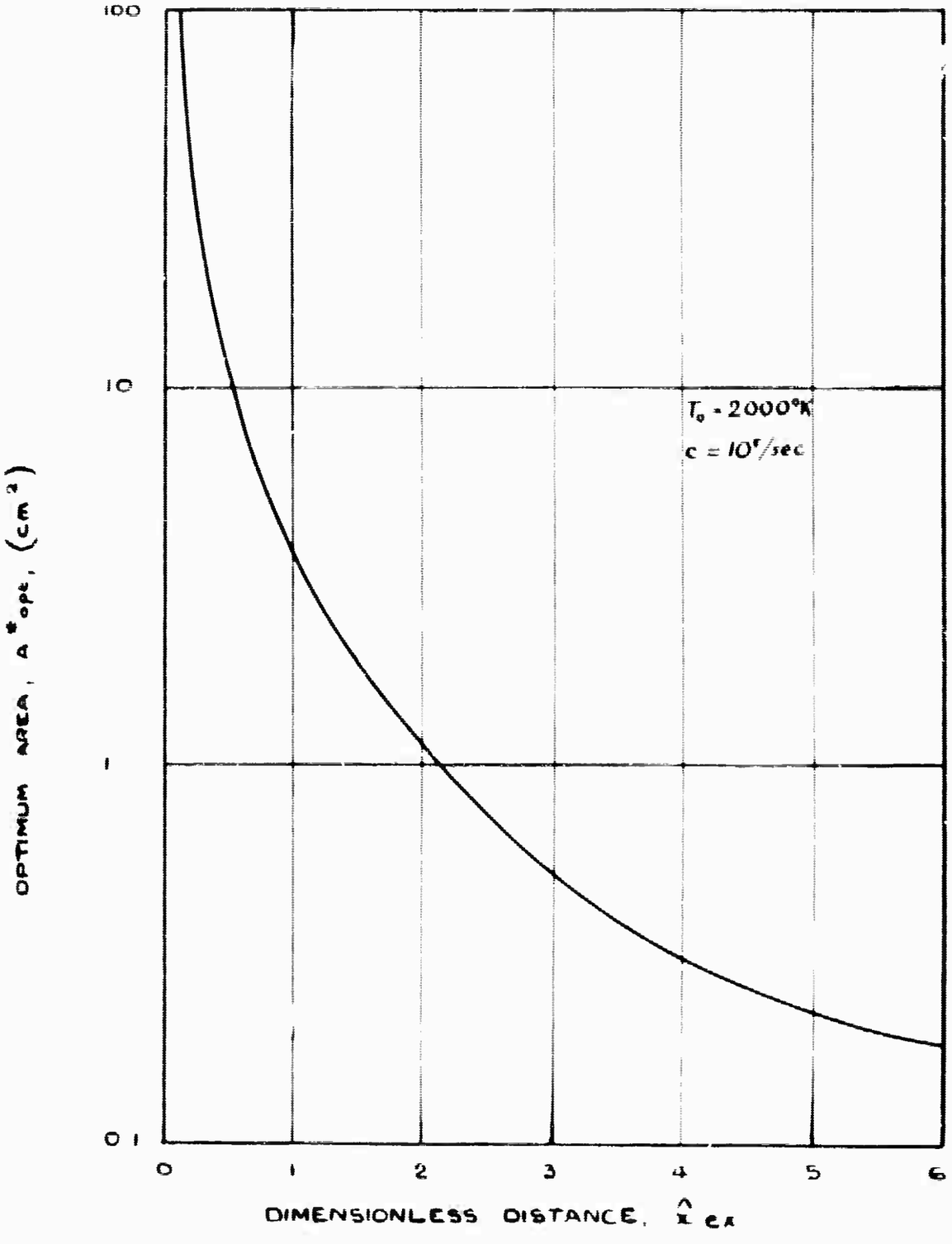

OPTIMUM NOZZLE THROAT AREA AS A FUNCTION OF THE DIMENSIONLESS NOZZLE EXIT DISTANCE

FIG 29.1

NOMENCLATURE (Chapter 29)

A - area of nozzle or channel

B - magnetic field strength

c - coefficient in electrical conductivity equation (29.4)

c_1 - coefficient defined by equation (29.10)

C_p - specific heat at constant pressure

I - integral defined by equation (29.11)

K - transverse MPD generator load factor

K_H - axial MPD generator load factor

K_N - nozzle constant

M - Mach number

p - pressure

P_o - stagnation pressure

P - power output per unit channel length

P_c - characteristic power output

t_f - time of flight in nozzle

T - gas temperature

T_e - electron temperature

T_o - stagnation temperature

V - flow velocity

x - axial distance

β_e - electronic Hall coefficient

β_i - ionic Hall coefficient

γ - ratio of specific heats

δ - factor accounting for inelastic energy losses

θ - hypersonic nozzle angle

σ - electrical conductivity

Subscripts

ex - nozzle exit

in - nozzle inlet

opt - optimum value

thr - nozzle throat

Superscripts

* - value at sonic speed

$\hat{}$ - non-dimensionalised quantity

CHAPTER 30

NON-EQUILIBRIUM PLASMAS

by

I.R. McNab

30.1 INTRODUCTION

For a plasma in thermal equilibrium (that is, in a steady state of equilibrium with its surroundings and having no interaction with them) the Saha equation[1], which is derived on a purely thermodynamic basis, serves to give the particle concentrations of the various constituents present (atoms in ground and excited states electrons and ions). If however, for any reason, the plasma is disturbed from this equilibrium state the particle concentrations cannot be obtained from the Saha equation but must be found by investigating the appropriate particle creation and annihiliation mechanisms. This situation applies if a plasma is momentarily disturbed from the thermal equilibrium state and then relaxes back to it, or if the plasma is maintained in the non-thermal equilibrium state by a continuous disturbance. In the first case the rate at which the plasma returns to thermal equilibrium, and the particle concentrations during this period, must be obtained from the appropriate rate equations for the various mechanisms involved; in the second case the non-thermal equilibrium particle concentrations are obtained by setting the appropriate rates equal to zero.

At present it appears likely that if closed cycle gas nuclear MPD systems are to prove economically feasible, non-thermal equilibrium plasmas must be used in some form. Two typical non-equilibrium plasma conditions presently under investigation at IRD are: non-equilibrium flow during a rapid expansion, and photoionization-induced non-equilibrium. In both these cases evaluation of, for example, the electron concentration, requires solution of the appropriate rate equations.

To study recombination and ionization mechanisms it is necessary to consider the rates at which all these processes can occur in all the energy levels of an atom. While in principle this requires an infinite set of simultaneous differential rate equations it can be shown in practice that convergence can be obtained with a finite set. Thus Bates et al[2] used sets of about twenty simultaneous rate

equations in the calculation of recombination and ionization coefficients.

An alternative approach, particularly useful as many of the required rate coefficients are not accurately known, is to simulate the many energy level system of an atom by a simpler model. For example, BenDaniel and Tamor[7] have investigated a four level model of the cesium atom containing the ground state, two excited states and the continuum. While this model is not completely accurate, in many respects it closely resembles the many level system.

Three separate lines of investigation have been conducted at IRD (it must be stressed that these are merely of a preliminary nature), these are:

(i) a three level model of a cesium plasma in which only electronic and radiative processes are considered;

(ii) a many level system of a cesium plasma in which only electronic and radiative processes are considered; and

(iii) a three level model of a cesium-helium plasma in which atomic processes are included in addition to electronic and radiative processes.

The aims of these three investigations are, respectively:

(i) to evaluate the deviation from Saha's equation in an equilibrium (non-thermal) plasma at low electron concentrations, with and without resonance trapping;

(ii) to investigate a more accurate model of a cesium plasma than (i) and to consider its application to a plasma not in equilibrium (thermal or otherwise); and

(iii) to investigate the influence of atomic processes on recombination and ionization in plasma mixtures where the fraction of inert gas atoms is high.

Only the first of these investigations is reported here since the remainder have not reached the stage where definite conclusions can be formed.

30.2 THREE LEVEL MODEL

For a three level model for pure cesium (ground state, excited state, continuum) in which electronic and radiative processes only are considered, the ionization and recombination mechanisms investigated are:

$$a(1) + e \rightleftharpoons a(2) + e \qquad A\binom{1,2}{2,1} \qquad \ldots\ldots (30.1)$$

$$a(1) + e \rightleftharpoons a^{+} + e \qquad A\binom{1,c}{c,1} \qquad \ldots\ldots (30.2)$$

$$a(2) + e \rightleftarrows a^+ + e \qquad A\binom{2,c}{c,2} \qquad \ldots\ldots (30.3)$$

$$c(1) + h\nu \rightleftarrows a(2) \qquad B\binom{1,2}{2,1} \qquad \ldots\ldots (30.4)$$

$$a(1) + h\nu \rightleftarrows a^+ + e \qquad B\binom{1,c}{c,1} \qquad \ldots\ldots (30.5)$$

$$a(2) + h\nu \rightleftarrows a^+ + e \qquad B\binom{2,c}{c,2} \qquad \ldots\ldots (30.6)$$

where A and B are the collisional and radiative ionization and recombination rate coefficients respectively.

The equations giving the rate of change of the particle densities in each of the three levels are:

$$\frac{du(1)}{dt} = -A(1,2)n(1)n(c) + A(2,1)n(2)n(c) - A(1,c)n(1)n(c) + A(c,1)^1 n(c)^3$$
$$-B(1,2)n(1) + B(2,1)n(2) - B(1,c)n(1) + B(c,1)n(c)^2 \qquad \ldots\ldots (30.7)$$

$$\frac{du(2)}{dt} = A(1,2)n(1)n(c) - A(2,1)n(2)n(c) - A(2,c)n(2)n(c) + A(c,2)^1 n(c)^3$$
$$+B(1,2)n(1) - B(2,1)n(2) - B(2,c)n(2) + B(c,2)n(c)^2 \qquad \ldots\ldots (30.8)$$

$$\frac{du(c)}{dt} = A(1,c)n(1)n(c) - A(c,1)^1 n(c)^3 + A(2,c)n(2)n(c) - A(c,2)^1 n(c)^3$$
$$+B(1,c)n(1) - B(c,1)n(c)^2 + B(2,c)n(2) - B(c,2)n(c)^2 \qquad \ldots\ldots (30.9)$$

and the conservation equation is:

$$N = n(1) + n(2) + n(c) \qquad \ldots\ldots (30.10)$$

(N.B. In equations (30.7), (30.8) and (30.9), $A(c,1)^1$ and $A(c,2)^1$ are not functions of $n(c)$.)

In equilibrium the rates of change of particle concentration with time are zero. Making $dn(2)/dt$ and $du(c)/dt$ equal to zero in equations (30.8) and (30.9), $n(2)$ may be eliminated (after some manipulation) and a relation between $n(1)$ and $n(c)$ obtained:

$$n(1) = -\frac{n(c)^2\left[n(c)^2K_1 + n(c)K_2 + K_4\right]}{n(c)^2K_3 + n(c)K_5 + K_6} \qquad \ldots\ldots (30.11)$$

where $K_1 = -A(2,c)A(c,1)^1 - A(2,1)A(c,1)^1 - A(2,1)A(c,2)^1$

$K_2 = -A(2,c)B(c,1) - A(2,1)B(c,1) - A(2,1)B(c,2) - B(2,c)A(c,1)^1$
$-B(2,1)A(c,1)^1 - B(2,1)A(c,2)^1$

$K_3 = A(1,2)A(2,c) + A(2,c)A(1,c) - A(2,1)A(1,c)$

$K_4 = -B(2,c)B(c,1) - B(2,1)B(c,1) - B(2,1)B(c,2)$